

21st Day of Clinical Research

Neue Immunotherapien am USZ

Donnerstag, 19. Mai 2022, 8.15 – 17.45 Uhr
Grosser Hörsaal OST, Universitätsspital Zürich

Verleihung Day of Clinical Research Preis 2022
18. Hartmann Müller Gedächtnisvorlesung 2022
Georg-Friedrich-Götz-Preisverleihung 2022

Wir wissen weiter.

Committee Day of Clinical Research

Aguzzi Adriano, Prof. Dr.
Cinelli Paolo, PD Dr.
Distler Oliver, Prof. Dr.
Katan Kahles Mira, PD Dr.
Moch Holger, Prof. Dr.
Schneider Robin, MBA
Senti Gabriela, Prof. Dr.
Speck Roberto, Prof. Dr.
Van den Broek Maries, Prof. Dr.
von Eckardstein Arnold, Prof. Dr.
Weller Michael, Prof. Dr.
Zinkernagel Annelies, Prof. Dr.

Table of contents

Program	
List of Abstracts	3 - 18
Abstracts	19 - 186

Cover Figure:

Spheroid of MB-MDA-231 cells, infiltrated by macrophages

Roberto Speck, Prof. Dr. med., Clinic for Infectious Diseases and Hospital Hygiene, University Hospital Zurich

Neue Immunotherapien am USZ

08.15 Uhr Begrüssung

Gregor Zünd, Prof. Dr. med., Vorsitzender der Spitaldirektion, USZ

08.20 Uhr Begrüssung

Frank Rühli, Prof. Dr. Dr. med., Dekan der Medizinischen Fakultät der Universität Zürich

08.25 Uhr Begrüssung, Einführung und Moderation durch

Gabriela Senti, Prof. Dr. med. und Chairman Roberto Speck, Prof. Dr. med.

Block 1: Input Referate

08.35 Uhr Immunsystem einfach erklärt

Miro Räber, Dr. sc. nat., Klinik für Immunologie, USZ

08.55 Uhr Übersicht Immuntherapien

Alexander Theocharides, PD. Dr. med., Klinik für medizinische Onkologie und Hämatologie, USZ

Block 2: Rheuma Patient*in

09.15 Uhr Gezielter Einsatz von Immuntherapien bei Rheumatoider Arthritis

Adrian Ciurea, Prof. Dr. med., Klinik für Rheumatologie, USZ

09.35 Uhr Diagnostik und Therapie der kardialen Inflammation – Myokarditis-Sprechstunde

Dörthe Schmidt, PD Dr. med., Klinik für Kardiologie, USZ

09.55 Uhr Coffee Break

Block 3: Melanom Patient*in

10.10 Uhr Mit dem Immunsystem gegen Hautkrebs

Reinhard Dummer, Prof. Dr. med., Dermatologische Klinik, USZ

10.30 Uhr Nebenwirkungen von Immuntherapien

Antonios Kolios, PD Dr. med., Dermatologische Klinik, USZ

10.50 Uhr Darmbakterien zur Immuntherapie? – Mikrobiom Sprechstunde

Michael Scharl, Prof. Dr. med., Klinik für Gastroenterologie und Hepatologie, USZ

Block 4: Neurologie Patient*in

11.10 Uhr Immuntherapien bei Multipler Sklerose und anderen neuroimmunologischen Erkrankungen

Ilijas Jelcic, Dr. med., Klinik für Neurologie, USZ

11.30 Uhr Diagnostik und Schutz vor Infektionen unter Immuntherapien durch Impfen – Impfsprechstunde

Nadia Eberhard, Dr. med., Klinik für Infektionskrankheiten und Spitalhygiene, USZ

11.50 Uhr Roundtable mit den Ärzt*innen der Patient*innen Blöcke 2/3/4

12.20 Uhr Lunch

- 13.50 Uhr** **Verleihung Day of Clinical Research Preis**
Gabriela Senti, Prof. Dr. med., Direktorin Forschung und Lehre, USZ
- 14.00 Uhr** **Session 1: Cardiovascular/Metabolism/Endocrinology**
Acetate Reverses the Gut Microbiota Metabolite Phenylacetyl Glutamine (PAG)-induced Endothelial Senescence by Epigenetic and SASP Modulation
Sayed Soheil Saeedi Saravi, Center for Molecular Cardiology, University Zurich
- 14.10 Uhr** **Session 2: Hematology/Oncology**
CITE-seq for Liquid and Solid tissues: Customization towards Clinical Biomarker Discovery
Aizhan Tastanova, Department of Dermatology, USZ
- 14.20 Uhr** **Session 3: Head Region/Neuroscience**
Robust and Versatile Arrayed Libraries for Human Genome-Wide CRISPR Activation, Deletion and Silencing
Jiang-An Yin, Institute of Neuropathology, USZ
- 14.30 Uhr** **Session 4: Infection/Immunity/Inflammation/Systemic Diseases**
CD26-inhibition Correlates with the Absence of Chronic Lung Allograft Dysfunction and Decreases Fibroblast Activity in Vitro
Isabelle Moneke, Department of Thoracic Surgery, USZ
- 14.40 Uhr** **Session 5: Mixed Topics**
A Macrophage-based Drug Delivery Platform for Glioma Treatment
Miaomiao Sun, Department of Neurology and Clinical Neuroscience Center, USZ
- 18. Hartmann Müller Gedächtnisvorlesung und Preisverleihung**
- 15.00 Uhr** **Einführung und Preisverleihung**
Michael Scharl, Prof. Dr. med., Präsident der Hartmann Müller-Stiftung, Klinik für Gastroenterologie und Hepatologie, USZ und Universität Zürich
- 15.10 Uhr** **Vorlesung des Preisträgers «Auf der Suche nach der verlorenen Evidenz»**
Josef Smolen, Prof. em. Dr. med., Klinik für Innere Medizin 3, Klinische Abteilung für Rheumatologie, Medizinische Universität Wien
- 15.50 Uhr** **Coffee Break / Pause**
- Verleihung des Georg Friedrich Götz-Preis 2022**
- 16.30 Uhr** **Begrüßung der Gäste**
Beatrice Beck Schimmer, Prof. Dr. med., Direktorin Universitäre Medizin Zürich
- 16.35 Uhr** **Einführung und Würdigung des Preisträgers Karl J. Frontzek, Dr. med. Dr. sc. nat.**
Frank Rühli, Prof. Dr. Dr. med., Dekan der Medizinischen Fakultät der Universität Zürich
- 16.40 Uhr** **Kurzreferat «Rationales Therapiedesign gegen Prionenkrankheiten»**
Karl J. Frontzek, Dr. med. Dr. sc. nat., Institut für Neuropathologie, USZ
- 17.00 Uhr** **Preisverleihung**
Beatrice Beck Schimmer, Prof. Dr. med., Direktorin Universitäre Medizin Zürich
- 17.10 Uhr** **Einführung und Würdigung der Preisträgerin Susanne Wegener, Prof. Dr. med.**
Frank Rühli, Prof. Dr. Dr. med., Dekan der Medizinischen Fakultät der Universität Zürich
- 17.15 Uhr** **Kurzreferat «Neutrophilen-induzierte Verstopfungen der Hirnkapillaren sind eine wichtige Ursache von Reperfu-sionsversagen beim akuten ischämischen Schlaganfall»**
Susanne Wegener, Prof. Dr. med., Klinik für Neurologie, USZ
- 17.35 Uhr** **Preisverleihung**
Beatrice Beck Schimmer, Prof. Dr. med., Direktorin Universitäre Medizin Zürich

Cardiovascular / Metabolism / Endocrinology

Basic Research

315

D. Voci, S. Zbinden, E. Micieli, N. Kucher, S. Barco
Fixed-dose ultrasound-assisted catheter-directed thrombolysis for acute pulmonary embolism associated with COVID-19

316

D. Voci, U. Fedeli, L. Valerio, E. Schievano, M. Righini, N. Kucher, D. Spirik
Mortality rate related to peripheral artery disease: a retrospective analysis of epidemiological data (years 2008 - 2019)

320

E. Micieli, D. Voci, S. Barco, A. Grigorean, A. Lecler
Transient Perivascular Inflammation of the Carotid artery (TIPIC) syndrome: an updated multinational analysis of 72 patients

322

Y. Gong, R. Renikunta, K. Lazarow, P. Shukla, H. Giral, A. Kratzer, V. Nageswaran, L. Opitz, F. Engel, A. Haghikia, J. Kries, F. Paneni, K. Streckfuss-bömeke, U. Landmesser, P. Jakob
A Large-scale MicroRNA Functional High-throughput Screening Identifies Mir-515 and Mir-519e as Potent Inducers of Human iPSC-cardiomyocyte Proliferation

342

T. Diteepeng, Y. Puspitasari, S. Ministrini, D. Vdovenko, A. Akhmedov, F. Ruschitzka, J. Beer, G. Camici, M. Luciani
Protein misfolding: an additional mechanism in the heart-brain communication after ischemic stroke

359

C. Gil-Cruz, C. Perez-Shibayama, M. Nägele, H. Cheng, M. Lütge, K. Frischmann, A. Joachimbauer, D. Parianos, A. Flammer, F. Ruschitzka, D. Schmidt, B. Ludewig
Dissecting the immune cell landscape in myocarditis

373

T. Papisotiropoulos, I. Martínez López, F. Schläpfer, S. Ulrich, I. Opitz, M. Kirschner
MicroRNA expression in Chronic Thromboembolic Pulmonary Hypertension

424

S. Ambrosini, F. Montecucco, D. Koljin, A. Akhmedov, S. Mohammed, G. Liuzzo, A. Beltrami, F. Crea, F. Ruschitzka, T. Lüscher, N. Hamdani, S. Costantino, F. Paneni
The methyltransferase SETD7 drives myocardial ischemic injury by modulating the Hippo pathway: a study in mice and humans

425

I. Martinez Lopez, M. Haberecker, M. Kirschner, F. Schläpfer, V. Orłowski, JH. Rüschoff, I. Opitz
Analysis of surgery-derived specimens and primary cell cultures for the study of Chronic Thromboembolic Pulmonary Hypertension

428

K. Gegenschatz-Schmid, S. Buzzi, J. Grossmann, B. Roschitzki, R. Urbanet, R. Heuberger, D. Glück, A. Zucker, M. Ehrbar
A surface treatment of nitinol implants reduces blood activation by altered protein adsorption

443

SS. Saeedi Saravi, G. Karsai, P. Lee, J. Beer
Acetate reverses the gut microbiota metabolite phenylacetyl glutamine (PAG)-induced endothelial senescence by epigenetic and SASP modulation

444

Y. Trinh, S. Frank, E. Schlumpf, J. Robert, A. von Eckardstein
Endothelial lipase and its endogenous inhibitor Angiotensin-like protein 3 regulate binding and uptake of both low and high-density lipoproteins by aortic endothelial cells

Clinical Trials

354

K. Furrer, D. Bettex, T. Horisberger, I. Inci, O. Schmid, N. Nagaraj, H. Morselli, B. Battilana, R. Schuepbach, S. Ulrich, M. Hebeisen, A. Matter, I. Opitz
The choice of priming solution for cardiopulmonary bypass during pulmonary endarterectomy for CTEPH has important impact

355

K. Furrer, J. Welsch, D. Bettex, T. Horisberger, I. Inci, R. Schuepbach, M. Kirschner, S. Ulrich, A. Matter, I. Opitz
Carbon dioxide and alveolar dead space as a prognostic marker for patients undergoing pulmonary endarterectomy

360

Y. Butscheid, S. Barco, T. Sebastian, D. Voci, R. Spescha, N. Kucher, on behalf of the SirPAD Investigators
The "SirPAD" randomized controlled trial in patients with peripheral artery disease requiring percutaneous transluminal angioplasty: study design and experience from the first year of recruitment

366

S. Barco, D. Voci, H. Held, T. Sebastian, S. Roth, R. Spescha, R. Bingisser, G. Colucci, D. Duerschmied, A. Frenk, B. Gerber, S. Konstantinides, F. Mach, M. Righini, T. Rosemann, S. Stortecky, S. Windecker, N. Kucher
Enoxaparin for primary thromboprophylaxis in ambulatory patients with coronavirus disease-2019: the investigator-initiated OVID randomized controlled trial

408

R. Erlebach, L. Wild, B. Seeliger, A. Rath, R. Andermatt, D. Hofmaenner, C. Ganter, C. Putensen, T. Welte, P. Wendel Garcia, S. David, C. Bode, K. Stahl
Outcomes of patients with initial acute respiratory failure on venovenous extracorporeal membrane oxygenation (ECMO) requiring additional circulatory support by VVA-ECMO

437

D. Müller Vizentini, T. Haider, M. Cavusoglu, G. Pathare, I. Sudano, J. Loffing, C. Wagner, D. Schmidt, P. Suter, C. Rossi
The impact of 3 days dietary salt load on skin sodium content, intravascular volume and blood pressure in healthy men

448

I. Krizanovic-Grgic, S. Anwer, C. Spengler, A. Breitenstein, F. Tanner
3D Atrial Strain for Prediction of Atrial Fibrillation Recurrence

452

N. Winkler, A. Shehab, F. Tanner
Right and left ventricular strain for outcome prediction in severe aortic stenosis

459

S. Nussbaum, S. Anwer, L. Erhart, D. Zurcher, A. Walther, G. Tsiourantani, F. Tanner
Association of left ventricular myocardial work with all-cause mortality after transcatheter aortic valve implantation

460

S. Anwer, F. Guastafierro, L. Erhart, S. Costa, D. Akdis, M. Schuermann, S. Hosseini, N. Kuzo, A. Gasperetti, C. Brunckhorst, F. Duru, A. Saguner, F. Tanner
Right atrial strain and cardiovascular outcome in arrhythmogenic right ventricular cardiomyopathy

461

T. Ziswiler, M. Luciani, C. Vanetta, A. Springer, T. Diteepeng, A. von Eckardstein, D. Müller, M. Barbagallo, D. Conen, C. Aubert, N. Rodondi, T. Sinnecker, G. Moschovitis, A. Auricchio, S. Osswald, M. Kühne, L. Bonati, J. Beer, on behalf of the Swiss-AF Investigators
Association of Trimethylamine N-Oxide with Impaired Cognitive Function in Patients with Atrial Fibrillation: A Swiss-AF Cohort Study

463

K. Valkova, L. Matter, T. Schachtner, M. Huellner, D. Mueller, V. Luyckx, T. Mueller
Development of a protocol for the dynamic measurement of renal functional reserve

471

M. Hänzel, K. Steigmiller, A. Luft, C. Gebhard, U. Held, S. Wegener
10-year trends in cardiovascular risk factors in Switzerland: non-traditional risk factors are on the rise in women more than in men

Hematology / Oncology

Basic Research

323

V. Vetter, B. Sobottka, A. Banaei-Esfahani, M. Nowak, L. de Leval, A. Lorch, K. Mertz, A. Kahraman, V. Koelzer, H. Moch
Immune phenotype-genotype associations in primary and matched metastatic clear cell renal cell carcinoma

326

T. Do, C. Lohoff, J. Lu, W. Huber, T. Zenz
High-throughput transcriptional profiling of ex-vivo drug effects in patients with leukemia and lymphoma

328

A. Tastanova
CITE-seq for liquid and solid tissues: customization towards clinical biomarker discovery

336

R. Schimmer, L. Kovtonyuk, N. Klemm, J. Fullin, SM. Stolz, J. Mueller, F. Caiado, K. Kurppa, B. Ebert, M. Manz, S. Boettcher
TP53 mutations confer resistance to hypomethylating agents and BCL-2 inhibition in myeloid neoplasms

338

J. Müller, F. Schneiter, R. Schimmer, N. Russkamp, T. Schröder, S. Böttcher, M. Manz
TP53-mutant acute myeloid leukemia cells are relatively resistant against CAR T cell-mediated killing

344

L. Bankel, R. Wegmann, K. Dedes, D. Franzen, P. Bode, M. Zoche, F. Arnold, M. Manz, H. Moch, C. Britschgi, B. Snijder
Updated results of pharmacoscopy on fluid samples from patients with solid tumors

345

D. Villars, L. Hänsch, M. Silginer, T. Weiss, M. Weller, P. Roth
Integrin-specific CAR T cells for the treatment of glioblastoma

362

C. Porcheri, C. Meisel, T. Mitsiadis
The Notch ligand Dll4 orchestrates the initiation and maintenance of undifferentiation in a mouse model of squamous cell carcinoma

368

L. Planas-Paz, A. Pliego-Mendieta, C. Hagedorn, F. Arnold, C. Pauli
Investigating HRDness in sarcoma

375

N. Klemm, N. Konrad, J. Fullin, R. Schimmer, S. Stolz, E. Topcu, S. Böttcher
Elucidating the molecular mechanism of the dominant-negative effect of the p53 missense variant R248Q

377

J. Fullin, N. Klemm, R. Schimmer, S. Stolz, E. Topcu, C. Koch, S. Böttcher
The Divergent Roles of Mono- and Biallelic TP53 Mutations in Leukemogenesis

379

F. Lehner, C. Kündig, S. Salemi, D. Eberli
Impact of pharmacological inhibition of human kallikrein 2 in prostate cancer in vitro

388

A. Laure, A. Rigutto, M. Kirschner, S. Hiltbrunner, A. Curioni
Comparative transcriptomics of inVivo and exVivo Mesothelioma samples

400

V. Haunerding, J. Sarabia del Castillo, L. Pelkmans, M. Levesque
Trametinib selectively increases susceptibility to immune-mediated cell death in the M130219 melanoma cell line while having the opposite effect on M130429 cells

401

T. Look, E. Puca, R. De Luca, T. Hemmerle, P. Roth, D. Neri, M. Weller, T. Weiss
Lomustine and the immunocytokine L19TNF display promising anti-tumor activity against glioblastoma

412

M. Gassner, S. Tanadini-Lang, R. Braun, N. Andratschke, J. Barranco-García
Interpretability-Guided Content-Based Image Retrieval in Dermatology Imaging

417

S. Changkhong, P. Lithanatudom, I. Opitz, M. Meerang
Role of CD147 (Basigin) in Malignant Pleural Mesothelioma

418

J. Jang, S. Itani, M. Dobler, M. Honegger, I. Opitz, W. Jungraithmayr
Targeting lung cancer by CD26/DPP4 inhibition in combination with an immune-checkpoint inhibitor

419

M. Meerang, J. Kreienbühl, V. Orlowski, S. Müller, M. Kirschner, I. Opitz
Importance of Cullin4 Ubiquitin Ligase in Malignant Pleural Mesothelioma

423

A. Hariharan, W. Qi, H. Rehrauer, M. Ronner, M. Wipplinger, J. Kresoja-Rakic, S. Sun, M. Sculco, L. Oton-Gonzalez, J. Rüschoff, I. Schmitt-Opitz, E. Felley-Bosco
RNA editing landscape in mesothelioma and the role of editing enzyme ADAR2 in growth, chemotherapy response and interferon signaling

429

M. Kirschner, Y. Zhang, F. Schläpfer, V. Orlowski, M. Meerang, I. Opitz
MicroRNAs contribute to the chemotherapy response of malignant pleural mesothelioma

445

A. Kraft, M. Meerang, M. Kirschner, V. Boeva, I. Opitz
Screening for extracellular vesicle-derived biomarkers for early detection of malignant pleural mesothelioma

451

H. Gabrys, L. Basler, S. Burgermeister, S. Hogan, M. Ahmadsei, M. Pavic, M. Bogowicz, D. Vuong, S. Tanadini-Lang, R. Förster, K. Kudura, M. Huellner, R. Dummer, M. Guckenberger, M. Levesque
PET/CT radiomics for prediction of hyperprogression in metastatic melanoma patients treated with immune checkpoint inhibition

456

E. Cannizzaro, G. Forestieri, A. Brusca, M. Roncador, D. Rossi, T. Zenz
Liquid biopsy for genomic profiling of circulating tumor DNA (ctDNA) in lymphoma through CAPP-seq.

457

P. Brasier-Lutz, M. De Marco Zompit, S. Adam, D. Durocher, M. Stucki
Targeting CIP2A as a potential alternative or complementary treatment strategy to PARP Inhibitor therapy

465

H. Lakshminarayanan, D. Rutishauser, S. Pfammatter, P. Schraml, H. Bolck, H. Moch
Liquid biopsy-based protein biomarkers as a tool for disease monitoring in clear cell renal cell carcinoma

Clinical Trials

341

B. Nguyen-Sträuli, H. Frauchiger-Heuer, J. Talimi-Schnabel, J. Loesch, D. Vorburger, K. Dedes
Single-incision approach for breast-conserving surgery and sentinel node biopsy - feasibility of round block technique

357

K. Furrer*, R. Werner* (*contributed equally), A. Curioni, S. Hillinger, D. Schneiter, I. Inci, I. Opitz
Salvage surgery in patients with locally advanced non-small cell lung cancer

367

T. Thavayogarah, G. Nair, D. Balabanov, M. Manz, D. Müller, U. Schanz
Optimization of fludarabine pharmacokinetics to reduce the relapse incidence in AML patients after allogeneic stem cell transplantation

422

G. Forgo, N. Kucher, S. Barco, E. Micieli, W. Ageno, L. Castellucci, G. Gabriela, H. Ddungu, V. Erich, M. Dumantepe, M. Guillermo Esposito, S. Konstantinides, C. McLintock, F. Ní Áinle, A. Spyropoulos, T. Urano, B. Hunt
An update on the global use of risk assessment models and thromboprophylaxis in hospitalized patients with medical illnesses from the World Thrombosis Day steering committee: systematic review and meta-analysis

427

H. Bischoff-Ferrari, W. Willett, J. Manson, B. Dawson-Hughes, M. Manz, R. Theiler, K. Brändle, B. Vellas, R. Rizzo, R. Kressig, H. Staehelin, J. da Silva, G. Armbrecht, A. Egli, J. Kanis, E. Orav, S. Gängler
Combined Vitamin D, omega-3 fatty acids and a simple home strength exercise program may reduce cancer risk among active adults age 70 and older: a randomized clinical trial

466

E. Breuer, L. Roth, L. Russo, V. Kepenekian, G. Passot, P. Gertsch, O. Glehen, K. Lehmann
Hematogenous, but not locoregional recurrence is controlled by systemic chemotherapy following cytoreductive surgery & HIPEC for colorectal cancer

Head Region / Neuroscience

Basic Research

309

S. Neupane

High-throughput whole genome-wide CRISPR activation screening for the identification of potential modifiers of alpha-synuclein aggregates.

313

V. Dimakopoulos, J. Gotman, W. Stacey, C. Bénar, F. Bartolomei, N. von Ellenrieder, J. Jacobs, J. Cimbalk, G. Worrell, M. Sperling, M. Zijlmans, L. Imbach, B. Frauscher, J. Sarnthein
Protocol for multicenter comparison of interictal high frequency oscillations as a predictor of seizure freedom.

325

R. Reimann, S. Litinov, A. Reuss, A. Economides, B. Schreiner, A. Aguzzi

Tissue clearing enhances accuracy of intraepidermal nerve fibre quantification

330

J. Yin, L. Frick, A. Aguzzi

Robust and Versatile Arrayed Libraries for Human Genome-Wide CRISPR Activation, Deletion and Silencing

331

T. Liu

Deciphering Prion Toxicity via Genome-Wide CRISPR Activation Synthetic Lethality Screening

337

K. Burelo, F. Costa, G. Ramantani, G. Indiveri, J. Sarnthein

A neuromorphic spiking neural network detects epileptic high frequency oscillations in the scalp EEG

356

B. Thomson, H. Richter, K. Akeret, R. Buzzi, N. Schwendinger, V. Anagnostakou, K. Kulcsar, P. Kronen, L. Regli, J. Fierstra, D. Schaer, M. Hugelshofer
Cerebrovascular Reactivity Measured by BOLD-fMRI as Imaging Strategy to Monitor CSF-Hemoglobin Toxicity

389

K. Akeret, R. Buzzi, B. Thomson, N. Schwendinger, D. Schaer, M. Hugelshofer

Multimodal spatiotemporal analysis identifies a dominant MyD88/TLR4 dependent role of the choroid plexus in intracerebral hemorrhage related neuroinflammation

420

E. De Cecco

CRISPR screen to identify modulators of prion transfer

421

A. Lakkaraju, A. Aguzzi

Gpr133 ablation delays onset of prion disease

431

C. Trevisan

Arrayed CRISPR activation screening of human transcription factors to identify modifiers of PrPC

432

S. Sellitto

Investigate the genetic and molecular landscape of the hnRNP K cellular essentiality by performing unbiased CRISPR screens

Clinical Trials

406

N. Lohaus, R. Reichen, R. Reimann, I. Abela, I. Jelcic, M. Huellner
A case of SARS-CoV-2-associated acute disseminated encephalomyelitis

439

N. Schwendinger, B. Thomson, H. Richter, J. Fierstra, M. Hugelshofer
Near-Infrared Spectroscopy Based Bedside Monitoring for Cerebrovascular Disease

472

P. Baumgartner, M. Zahn, H. Handelsmann, K. Geier, S. Petrus, M. Hänsel, A. Luft, S. Wegener
Optic Nerve Sonography to monitor Intracranial pressure afTer large vessel ischemic strokE – The
ONSITE Study

473

M. Zahn, B. Lafci, A. Steiner, P. Baumgartner, F. Fierz, J. Gunzinger, A. Luft, A. Boss, D. Razansky,
S. Wegener
Multispectral optoacoustic imaging of cerebrovascular disease

Infection / Immunity / Inflammation / Systemic Diseases

Basic Research

304

T. Schweizer, S. Mairpady Shambat, C. Vulin, S. Hoeller, C. Acevedo, M. Huemer, A. Gomez-Mejia, C. Chang, J. Baum, S. Hertegonne, E. Hitz, T. Scheier, D. Hofmaenner, P. Buehler, H. Moch, R. Schuepbach, S. Brugger, A. Zinkernagel
Blunted sFasL signaling exacerbates TNF-driven neutrophil necroptosis in critically ill COVID-19 patients

307

J. Bär, M. Boumassoud, S. Mairpady Shambat, C. Vulin, M. Huemer, T. Schweizer, A. Gómez-Mejia, N. Eberhard, Y. Achermann, P. Zingg, C. Mestres, S. Brugger, R. Schuepbach, R. Kouyos, H. Barbara, A. Zinkernagel
Quantification of within patient Staphylococcus aureus phenotypic heterogeneity as a proxy for presence of persisters across clinical presentations

310

I. Heggli, T. Mengis, N. Herger, R. Hove, R. Schüpbach, N. Farshad-Amacker, C. Laux, F. Wanivenhaus, M. Betz, J. Spirig, F. Brunner, M. Farshad, O. Distler, S. Dudli
Infectious and autoinflammatory etiologies of Modic type 1 changes have different cytokine profiles

314

T. Schweizer, F. Andreoni, C. Acevedo, T. Scheier, I. Heggli, E. Marques Maggio, N. Eberhard, S. Brugger, S. Dudli, A. Zinkernagel
Intervertebral disc cell chondroptosis elicits neutrophil response in Staphylococcus aureus spondylodiscitis

317

D. Voci, U. Fedeli, I. Farmakis, L. Hobohm, K. Keller, L. Valerio, E. Schievano, C. Barbiellini Amidei, S. Konstantinides, N. Kucher, S. Barco
Deaths related to pulmonary embolism and cardiovascular events before and during the 2020 COVID-19 pandemic: an epidemiological analysis of data from an Italian high-risk area

319

S. Mairpady Shambat, A. Gómez-Mejia, T. Schweizer, M. Huemer, C. Chang, C. Acevedo, J. Bergada-Pijuan, C. Vulin, D. Hofmaenner, T. Scheier, S. Hertegonne, E. Parietti, N. Miroshnikova, P. Wendel Garcia, M. Hilty, P. Buehler, R. Schuepbach, S. Brugger, A. Zinkernagel
Hyperinflammatory environment drives dysfunctional myeloid cell effector response to bacterial challenge in COVID-19

332

C. Steinack, A. Gaspert, J. Rüschoff, F. Gautschi, R. Hage, T. Gaisl, M. Schuurmans, D. Franzen
Transbronchial cryobiopsy compared to forceps biopsy for diagnosis of acute cellular rejection in lung transplant recipients

333

C. Steinack, P. Saurer, F. Gautschi, R. Hage, G. Ortmanns, M. Schuurmanns, T. Gaisl
Influence of mycophenolate mofetil dosage and plasma levels on the occurrence of chronic lung allograft dysfunction in lung transplants

346

R. Wolfensberger, E. Sarti, P. Sander, M. Meuli, S. Bredl, R. Speck, J. Nemeth
Clofazimine affects macrophage activity in vitro and in vivo

350

E. Sarti, R. Wolfensberger, R. Speck, P. Sander, S. Bredl, J. Nemeth
The sequence of activation and infection determines outcomes of macrophage infections with Mycobacterium tuberculosis

352

A. Hukara, T. Tabib, M. Rudnik, O. Distler, P. Blyszczuk, R. Lafyatis, G. Kania
FOSL-2 transcription factor as a regulator of macrophage polarization and function in systemic sclerosis

361

L. Jungblut, A. Euler, J. Von Spiczak, T. Sartoretti, V. Mergen, A. Landsmann, V. Englmaier, O. Distler, H. Alkadhi, T. Frauenfelder, K. Martini
Potential of Photon-Counting Detector CT for Radiation Dose Reduction for the Assessment of Interstitial Lung Disease in Patients with Systemic sclerosis

364

C. Pasin, I. Abela, D. Garcia Nuñez, K. Kusejko, K. Aebi-Popp, H. Buvelot, M. Cavassini, L. Damonti, C. Fux, A. Hachfeld, B. Martinez de Tejada, P. Vernazza, A. Trkola, H. Günthard, R. Kouyos
Hormone intake differentially affects the immune system of HIV-positive cis and trans women

365

N. Keller, M. Boumasmoud, F. Andreoni, A. Tarnutzer, T. Scheier, A. Gomez-Mejia, M. Huemer, E. Marques Maggio, R. Schuepbach, S. Mairpady Shambat, S. Brugger, A. Zinkernagel
Group A Streptococcus persists in necrotizing fasciitis resulting in antibiotic tolerance

370

C. Jünger, F. Imkamp, S. Balakrishna, M. Gysin, K. Haldimann, R. Kouyos, S. Hobbie, H. Günthard, D. Braun
Phenotypic and genotypic characterization of *N. gonorrhoeae* strains in a men who have sex with men population with high-risk sexual behavior in Zurich Switzerland

374

I. Abela, C. Pasin, M. Schwarzmüller, S. Epp, M. Sickmann, M. Schanz, P. Rusert, J. Weber, S. Schmutz, A. Audigé, L. Maliqi, A. Hunziker, M. Hesselman, C. Niklaus, J. Gottschalk, E. Schindler, A. Wepf, U. Karrer, A. Wolfensberger, S. Rampini, P. Meyer Sauter, C. Berger, M. Huber, J. Böni, D. Braun, M. Marconato, M. Manz, B. Frey, H. Günthard, R. Kouyos, A. Trkola
Multifactorial seroprofiling dissects the contribution of pre-existing human coronaviruses responses to SARS-CoV-2 immunity

376

S. Klinnert, A. Chemnitzer, P. Rusert, K. Metzner
Systematic HIV-1 promoter targeting with CRISPR/dCas9-VPR reveals optimal region for activation of the latent provirus

378

L. Baroncini, T. Mlambo, R. Speck
Do macrophages have any antiviral activity in HIV infection?

382

M. Maane, G. Kullak-Ublick, S. Hobbie, M. Visentin
Biochemical characterization of membrane transport and mitochondrial electron transport chain inhibitory effect of the aminoglycoside apramycin: side-by-side comparison with gentamicin

385

M. Paolucci, N. Wuillemin, C. Arena, Y. Wäckerle-Men, V. Homère, M. Träxler, Y. Severin, T. Kündig, D. Bieli, T. Sonati, P. Johansen
Allergen-specific profiling of serum antibodies from patients with peanut allergy

386

Z. Marti, J. Ruder, R. Martin
Characterization of Antibody-Secreting Cells in Multiple Sclerosis Patients and Healthy Controls Using an In Vitro Expansion System

393

L. Jingya, D. Abegg, L. Malinowska, M. Rudnik, O. Distler, P. Błyszczuk, P. Picotti, G. Kania
Protein conformational changes and functional alterations in dermal fibroblasts from patients with systemic sclerosis

395

K. Becker, M. Gysin, D. Verma, K. Haldimann, N. Müller, M. Schuurmans, D. Ordway, B. Schulthess, S. Hobbie
Preclinical profiling of apramycin as a possible drug candidate for the treatment of mycobacterial lung infections

411

M. Spalinger, R. Sanchez Alvarez, C. Gottier, A. Montalban-Arquez, M. Schwarzfischer, A. Niechcial, S. Lang, M. Scharl
Loss of PTPN23 in the intestinal epithelium results in epithelial hyperproliferation and lethal diarrhea in a microbiota dependent manner

434

D. Werner, W. Faigle, J. Ruder, V. Kana, R. Martin
Assessing the antioxidative and immunomodulatory capacity of hydroxytyrosol in lymphocytes

440

M. Paolucci, V. Homère, N. Wuillemin, D. Bieli, Y. Wäckerle-Men, T. Kündig, N. Pengo, T. Sonati, A. Barberis, P. Johansen
Pre-clinical evaluation of fully human anti-peanut monoclonal antibodies: protection against anaphylaxis in mice

441

J. Tschumi, L. Jörimann, A. Ciuffi, J. Fellay, M. Battegay, E. Bernasconi, A. Calmy, M. Cavassini, A. Rauch, S. Kuster, T. Klimkait, R. Kouyos, H. Günthard, K. Metzner, . SHCS
No Evidence of Low-Level Replication in 40 HIV-1 Infected Individuals on Suppressive Antiretroviral Therapy

442

L. Jörimann, J. Tschumi, C. Leemann, C. Schenkel, S. Chaudron, M. Zeeb, K. Neumann, H. Kuster, D. Braun, C. Grube, R. Kouyos, K. Metzner, H. Günthard, . SHCS
Absence of HIV-1 Evolution in early treated patients switching to DTG monotherapy for 48 weeks

449

M. Mirrahimi, K. Klein, M. Houtman, M. Frank-Bertoncelj, M. Macukiewicz, O. Distler, C. Ospelt
Homeobox D transcription factors shape differential joint environment between anterior finger joints and thumb

454

Z. Kotkowska, Y. Waeckerle-Men, A. Duda, I. Kolm, A. Høgset, T. Kündig, C. Halin, P. Sander, P. Johansen
Photochemically-delivered antigens of Mycobacterium bovis BCG induce strong T-cell response in mice

464

O. Evrova, E. Müller, L. Fabbella, M. Hartmann, I. Dedes, P. Imesch, J. Metzler, G. Schär, M. Shilaih, V. Vongrad, B. Leeners
Isolation and characterization of primary human cells from eutopic and ectopic endometrium and endometriosis associated adhesions.

467

I. Moneke, M. Haberecker, J. Jang, E. Faccioli, I. Opitz, W. Jungraithmayr
CD26-inhibition correlates with the absence of Chronic Lung Allograft Dysfunction and decreases fibroblast activity in vitro

Clinical Trials

311

K. Kusejko, L. Salazar-Vizcaya, C. Shah, M. Stöckle, C. Beguelin, P. Schmid, M. Ongaro, K. Darling, E. Bernasconi, A. Rauch, R. Kouyos, H. Günthard, J. Böni, J. Fehr, D. Braun
Sustained effect on hepatitis C elimination among men who have sex with men in the Swiss HIV Cohort Study: A systematic re-screening for hepatitis C RNA two years following a nation-wide elimination program

324

A. Ring, B. Balakrishna, F. Imkamp, S. Burkhard, F. Triet, F. Brunschweiler, C. Grube, R. Kouyos, R. Bodmer, H. Günthard, D. Braun
High rates of asymptomatic Mycoplasma genitalium infections with high proportion of genotypic resistance to first-line treatment azithromycin among men who have sex with men initially presenting with a primary HIV-infection

327

V. Kufner, C. Frey, S. Schmutz, M. Zaheri, S. Burkhard, A. Plate, A. Trkola, M. Huber, N. Mueller
Etiology of upper respiratory tract infection in outpatients before and during the SARS-CoV-2 pandemic

347

C. Pasin, A. Huang, C. Cicin-Sain, S. Epp, A. Audigé, A. Bankova, N. Wolfensberger, O. Vilirovski, G. Nair, P. Hockl, U. Schanz, J. Nilsson, R. Kouyos, B. Hasse, A. Zinkernagel, A. Trkola, M. Manz, I. Abela, A. Müller
Antibody Response to SARS-CoV-2 Vaccination in Patients Following Allogeneic Hematopoietic Cell Transplantation

351

I. Abela, M. Marconato, A. Hauser, M. Schwarzmüller, R. Katzensteiner, D. Braun, S. Epp, A. Audigé, J. Weber, P. Rusert, E. Schindler, C. Pasin, E. West, J. Böni, V. Kufner, M. Huber, M. Zaheri, S. Schmutz, B. Frey, R. Kouyos, H. Günthard, M. Manz, A. Trkola
Contribution of endogenous and exogenous antibodies to clearance of SARS-CoV-2 during convalescent plasma therapy

396

C. Zhao, A. Chirkova, R. Palma Villar, S. Rosenborg, J. Lindberg, L. Friberg, S. Hobbie
Apramycin first-in-human trial to determine population pharmacokinetics in plasma and urine to guide efficacious dose finding predictions

402

P. Wendel-Garcia, R. Erlebach, D. Hofmaenner, G. Camen, R. Schuepbach, C. Jüngst, B. Müllhaupt, J. Bartussek, P. Buehler, S. David, R. Andermatt
Effect of long-term ketamine infusion on cholangiopathy in COVID-19 associated acute respiratory distress syndrome

407

D. Hofmaenner, B. Seeliger, M. Doebler, P. Wendel-Garcia, R. Schuepbach, J. Schmidt, T. Welte, M. Hoepfer, H. Gillmann, C. Kuehn, S. Ehrentraut, J. Schewe, C. Putensen, K. Stahl, C. Bode, S. David
Intracranial Hemorrhages on Extracorporeal Membrane Oxygenation: Differences Between COVID-19 and Other Viral Acute Respiratory Distress Syndrome

469

I. Jelcic, A. Müller, M. Hilty, I. Reichen, K. Jordan, N. Wolfensberger, J. Ruder, B. Vlad, S. Ferrer, K. Ritter, M. Foegel, L. Andreas, U. Schanz, R. Martin
Efficacy and safety of autologous hematopoietic stem cell transplantation in multiple sclerosis (aHSCT-in-MS) in Zurich

Mixed Topics

Basic Research

305

K. Ging, C. Trevisan, L. Frick, J. Yin, D. Böck, P. Gilormini, A. Aguzzi, B. Züllig
An arrayed CRISPR activation screen to identify genetic modifiers of acid beta-glucosidase activity

308

J. Buschmann, S. Andreoli, J. Jang, O. Gröninger, W. Stark, K. Spanaus, C. Opelz, G. Meier Bürgisser, M. Calcagni, W. Jungraithmayr
Hybrid nanocomposite as a chest wall graft with improved vascularization by copper oxide nanoparticles

312

S. Dudli, A. Karol, L. Guidici, I. Heggli, C. Laux, J. Spirig, F. Wanivenhaus, M. Betz, C. Germann, N. Farshad-Amacker, F. Brunner, O. Distler, M. Farshad
Histomorphometry of Modic changes

318

E. Köksal, A. Levin, I. Condado-Morales, L. Madrigal, S. Neupane, E. De Cecco, A. Aguzzi, T. Knowles, S. Hornemann
Digital microfluidics for absolute quantification of α -synuclein propagons for Parkinson disease diagnosis

334

A. La Greca, C. Marchiori, M. Bogowicz, J. Barranco-García, E. Konukoglu, O. Riesterer, P. Balermipas, C. Malossi, M. Guckenberger, J. van Timmeren, S. Tanadini-Lang
Explainability of deep learning-based HPV status prediction in oropharyngeal cancer

340

I. Miescher, P. Wolint, C. Opelz, J. Snedeker, P. Giovanoli, M. Calcagni, J. Buschmann
Impact of hyaluronic acid on rabbit Achilles tenocytes in vitro with respect to proliferation and gene expression

349

N. Jarzebska, J. Frei, T. Weiss, T. Holzinger, M. Mellett, M. Diken, R. Speck, T. Kundig, U. Sahin, S. Pascolo
RNA with chemotherapeutic base analogues as a superlative dual-functional anti-cancer drug

353

P. Wallimann, M. Mayinger, M. Bogowicz, M. Guckenberger, N. Andratschke, S. Tanadini-Lang, J. van Timmeren
Comparison of methods for T1-w brain MRI intensity normalization for quantitative MRI analysis

369

S. Salemi, L. Schori, G. Gerwin, M. Horst, D. Eberli
Influence of myostatin inhibitor on smooth muscle cells regeneration

371

W. Baumgartner, P. Wolint, S. Hofmann, C. Nüesch, M. Calcagni, M. Brunelli, J. Buschmann
Impact of fiber mesh structure and tensile stretching of coaxial electrospun scaffolds on tenogenic and inflammatory gene expression in human adipose-derived stem cells

381

A. Korczak, B. Carrara, K. Gegenschatz-Schmid, Q. Vallmajó Martín, M. Ehrbar
Functional characterization of human bone marrow stromal cells in vivo with increased throughput

383

D. Rutishauser, S. Krackow, A. Batavia, P. Schraml, N. Wey, H. Moch
The Merge of Synoptic Reports and Molecular Data from Renal Cancer Clinical Cohort Studies

390

L. Krattiger, B. Simona, M. Tibbitt, M. Ehrbar
An in vitro model to study the recovery of therapeutically ablated vascular networks

391

M. Wiplinger, A. Abukar, A. Hariharan, S. Sun, M. Ronner, M. Sculco, A. Okonska, J. Kresoja-Rakic, H. Rehrauer, W. Qi, V. van Beusechem, E. Felley-Bosco
Double-stranded RNA structural elements holding the key to translational regulation in cancer: the case of editing in RNA Binding Motif Protein 8A

392

B. Carrara, Q. Vallmajó Martín, P. Papageorgiou, M. Ehrbar
3D in vivo Bone Marrow Organoids to dissect Mesenchymal Stromal Cells Chaos

394

R. Odabasi, L. Krattiger, B. Emiroglu, M. Ehrbar, M. Tibbitt
Lymphatic endothelial cell vascular structure formation

399

E. Avilla-Royo, L. Vonzun, J. Monné Rodriguez, M. Weisskopf, F. Famos, R. Zimmermann, U. Ueli, N. Ochsenbein-Kölbl, M. Ehrbar
Healing-triggering biomaterials for fetal membrane repair

405

M. Sun, M. Bialasek, M. Król, M. Weller, T. Weiss
A macrophage-based drug delivery platform for glioma treatment

409

E. Lattmann, T. Deng, M. Walser, P. Widmer, C. Rexha-Lambert, V. Prasad, O. Eichhoff, M. Daube, R. Dummer, M. Levesque, A. Hajnal
A DNA replication-independent function of pre-replication complex genes during cell invasion in *C. elegans*

413

K. Kostopanagiotou, R. Costa, M. Kirschner, A. Curioni, H. Moch, M. Rechsteiner, I. Opitz
Technical aspects of selective pulmonary vein plasma sampling in liquid biopsy for lung cancer in translational research.

414

S. Kakava, E. Schlumpf, A. von Eckardstein, J. Robert
Differential trafficking of high-density lipoproteins containing or lacking apolipoprotein E in brain endothelial cells

430

S. Sun, W. Qi, M. Ronner, A. Hariharan, M. Wiplinger, I. Opitz, H. Rehrauer, E. Felley-Bosco
Endogenous Retrovirus expression and type-I interferon signaling in human mesothelioma

433

S. La Cioppa, L. Krattiger, B. Emiroglu, L. Moser, J. Kartenbender, M. Tibbitt, M. Ehrbar
A microfluidic osteogenesis-on-a-chip device

436

J. Frej, N. Jarzebska, A. Reichmuth, M. Mellett, S. Pascolo
Synthetic mRNA platform

447

V. Baumgartner, S. Salemi, D. Eberli
Targeting Mitochondria: A Link between Prostate Cancer Metabolism and Novel Therapeutic Approaches

453

R. Fritze, M. Hilty, C. Ganter, R. Schüpbach, J. Bartussek
Can we trust what we measure? Analysis of blood oxygenation levels obtained by fingertip sensors and arterial blood gas using classical statistics and machine learning techniques.

458

M. Jacobs, O. Krupkova, A. Barbero, M. Ehrbar
Development of a bioinspired engineered ovary to restore fertility in cancer patients

462

E. Breuer, D. Birrer, S. Da Silva Guerra, A. Gupta, P.-A. Clavien, B. Humar
Division of tasks in the regenerating liver: proliferation, hypertrophy & metabolic functions

468

Z. Khodabakhshi, P. Wallimann, H. Gabrys, M. Guckenberger, N. Andratschke, S. Tanadini-Lang
The Impact of Image Preprocessing and Harmonization Methods on Magnetic Resonance Image Radiomic Features Stability

Clinical Trials

303

S. Halvachizadeh, R. Pfeifer, Y. Kalbas, S. Schürle-Finke, P. Cinelli, HC. Pape
Physical properties of soft tissue injury during the decision making of surgical treatment in ankle fractures

321

S. Zbinden, D. Voci, P. Philippe, N. Kucher, S. Barco
Catheter-directed thrombolysis for the treatment of pulmonary embolism: Experience at a University Hospital

358

K. Furrer, M. Schuurmans, M. Hebeisen, S. Schulte, D. Schneiter, W. Weder, I. Opitz, S. Hillinger
Smoking prevention intervention with school classes in university hospital by thoracic surgeon und pulmonologist. The Zurich prevention project.

384

A. Bauer, A. Eskat, A. Ntekim, C. Wong, D. Eberle, E. Hedayati, F. Tay, H. Yau, L. Stockley, d. María, S. Şen, S. Egert-Schwender, Y. Üresin, R. Grossmann
How COVID-19 changed clinical research strategies: a global survey

387

D. Eberle
Patient and Public Involvement in Clinical Research – an Overview and Outlook for Switzerland

397

L. Zurfluh, T. Hothorn, R. Zimmermann, C. Haslinger, A.P. Simões-Wüst
Study protocol: Bryophyllum pinnatum treatment of anxiety related to preterm labour – a randomized, double-blind, placebo-controlled trial, as IIT

398

H. Bischoff-Ferrari, G. Freystätter, B. Vellas, B. Dawson-Hughes, R. Kressig, J. Kanis, W. Willett, J. Manson, R. Rizzoli, R. Theiler, L. Hofbauer, G. Armbrecht, J. da Silva, M. Blauth, C. de Godoi Rezende Costa Molino, W. Lang, U. Siebert, A. Egli, E.J. Orav, M. Wiczorek for the DO-HEALTH Research group
Effects of vitamin D, omega-3 fatty acids and a simple home strength exercise program on fall prevention: the DO-HEALTH randomized clinical trial

404

K. Slankamenac, J. Müller, D. Keller

Unplanned Re-visits of Seniors in the Emergency Department

426

M. Gagesch, M. Wieczorek, B. Vellas, R. Kressig, R. Rizzoli, J. Kanis, W. Willett, A. Egli, W. Lang, E. Orav, h. Bischoff-Ferrari

Effects of vitamin D, omega-3 fatty acids and a simple home exercise program on pre-frailty prevention among generally healthy and robust adults age 70 and older: The DO-HEALTH randomized clinical trial

438

H. Bischoff-Ferrari, S. Gängler, T. Muenzer, B. Dawson-Hughes, W. Lang, R. Theiler, A. Egli, G. Freystätter

Effects of transdermal testosterone and/or monthly vitamin D on fall risk in pre-frail hypogonadal men age 65 and older: a double blind 2x2 factorial design randomized placebo-controlled trial

446

A. Joachimbauer, C. Gil-Cruz, K. Frischmann, R. Büchel, D. Schmidt, F. Ruschitzka, B. Ludewig
Investigating the immunologic pathways involved in the progression of acute myocarditis to inflammatory cardiomyopathy

450

F. Haslbeck, L. Schmidli, M. Adams, H. Bucher, D. Bassler, G. Natalucci

Creative music therapy and long-term neurodevelopmental outcomes in preterm infants at age two and five years: Results of a controlled, feasibility trial

S. Halvachizadeh², R. Pfeifer², Y. Kalbas², S. Schürle-Finke¹, P. Cinelli², HC. Pape²

Physical properties of soft tissue injury during the decision making of surgical treatment in ankle fractures

*Institute of Translational Medicine, Department of Health Science & Technology, ETH Zurich¹,
University Hospital Zurich, Department of Trauma²*

Introduction:

The local soft tissue status (STS) guides surgical treatment strategies of fractures fixation and distinguished temporary stabilization from definitive surgical strategies. The aim of this study was to assess the physical properties of STS in lateral malleolar fractures that led to either temporal (TEMP) or definitive surgical strategy.

Methods:

This study was designed as a prospective double-blinded cohort study. Adult patients admitted between February 1st, 2019 and December 31st, 2020 presenting with closed lateral malleolar fracture were eligible, if they required surgical treatment. Exclusion criteria: Previous injuries to the lower extremity, acute deep venous thrombosis, skin diseases, delayed presentation (admission > 24 hours after injury). The primary outcome was the treatment strategy (temporal vs. definitive) as decided by the treating trauma surgeon. Examination included clinical measurements: circumference and bone-skin distance on plain radiograph. Physical properties assessment of the STS included optical measures of local perfusion (O2C, Lea Inc. Germany) and tactile measures of mechanical characteristics (Myoton® tensiometer AS, Estonia). Measurements were taken on admission and prior decision of treatment strategy. The contralateral not-injured ankle served as control. Quality of assessment tools were quantified by calculating the smallest detectable change (SDC).

Results:

Forty patients at a mean age of 41 (± 17.6) years were included. The SDC for local blood flow was 3.2% (95%CI 2.5 to 3.8) and for soft tissue stiffness 1.1% (95%CI 0.4 to 1.7). The circumference at admission was significantly higher when compared with the healthy site (28.6 ± 3.6 cm versus 24.3 ± 2.7 cm, $p < 0.001$). The local perfusion (blood flow 109.6, SD 39.8 A.U. vs. 81.9, SD 15.5 A.U., $p = 0.0051$), and local dynamic stiffness of the skin (679.4 N/m, SD 147 N/m vs 469.9N/m, SD 117.9 N/m, $p < 0.001$) were significantly higher at the injured site. During TEMP, the local blood flow was significantly higher when compared with definitive surgery (109.6, SD 39.8 vs. 94.5, SD 13.0, $p = 0.023$). The dynamic stiffness of the soft tissue was significantly higher during TEMP (679.4 N/m, SD 147.0 N/m vs. 573.0 N/m, SD 93.8 N/m, $p < 0.001$). The physical properties of STS were not associated with fracture classification.

Conclusion:

Altered physical properties of the STS following injury include optical perfusion and dynamic stiffness at the surface. These changes might be indicative for the treatment strategy. The assessment tools could be implemented in routine clinical practice guiding decision making for either temporal or definitive surgical treatment strategies.

T. Schweizer¹, S. Mairpady Shambat¹, C. Vulin¹, S. Hoeller², C. Acevedo¹, M. Huemer¹, A. Gomez-Mejia¹, C. Chang¹, J. Baum¹, S. Hertegonne¹, E. Hitz¹, T. Scheier¹, D. Hofmaenner³, P. Buehler³, H. Moch², R. Schuepbach³, S. Brugger¹, A. Zinkernagel¹

Blunted sFasL signaling exacerbates TNF-driven neutrophil necroptosis in critically ill COVID-19 patients

Department of Infectious Diseases and Hospital Epidemiology, University Hospital of Zurich, University of Zurich, Zurich 8091, Switzerland¹, Department of Pathology and Molecular Pathology, University Hospital of Zurich, University of Zurich, Zurich 8091, Switzerland², Institute for Intensive Care Medicine, University Hospital of Zurich, University of Zurich, Zurich 8091, Switzerland³

Introduction:

Critically ill coronavirus disease 2019 (COVID-19) patients are characterized by a severely dysregulated cytokine profile and elevated neutrophil counts, impacting disease severity. However, it remains unclear how neutrophils contribute to pathophysiology during COVID-19. Here, we assessed the impact of the dysregulated cytokine profile on the regulated cell death (RCD) program of neutrophils.

Methods:

RCD phenotype of neutrophils isolated from critically ill COVID-19 patients or healthy donors and stimulated with COVID-19 or healthy plasma *ex vivo* was assessed by flow cytometry, time-lapse microscopy and cytokine multiplex analysis. Immunohistochemistry of COVID-19 patients and control biopsies were performed to assess the *in situ* neutrophil RCD phenotype. Plasma cytokine levels of COVID-19 patients and healthy donors were measured by multiplex analysis. Clinical parameters were correlated to cytokine levels of COVID-19 patients.

Results:

COVID-19 plasma induced a necroptosis-sensitive neutrophil phenotype, characterized by cell lysis, elevated release of damage associated molecular patterns (DAMPs), increased receptor interacting serine-threonine protein kinase (RIPK) 1 levels and mixed lineage kinase domain-like pseudokinase (MLKL) involvement. Occurrence of neutrophil necroptosis was further confirmed in COVID-19 thrombus and lung biopsies. Necroptosis was induced via the tumor necrosis factor receptor 1 (TNFR1)/TNF- α axis. Moreover, reduction of soluble Fas-Ligand (sFasL) levels in COVID-19 patients and hence decreased signaling to Fas directly increased RIPK1 levels, exacerbated TNF-driven necroptosis and correlated with disease severity, which was abolished in patients treated with glucocorticoids.

Conclusion:

Our results suggest a novel role for sFasL signaling in TNF- α -induced RCD program in neutrophils during COVID-19 and a potential therapeutic target to curb inflammation and thus influence disease severity and outcome.

K. Ging¹, C. Trevisan¹, L. Frick¹, J. Yin¹, D. Böck³, P. Gilormini², A. Aguzzi¹, B. Züllig¹

An arrayed CRISPR activation screen to identify genetic modifiers of acid beta-glucosidase activity

Neuropathology USZ¹, Sam Fraser University, CA², University of Zürich³

Introduction:

β -Glucocerebrosidase (GCase) is a lysosomal enzyme crucially involved in the turnover of cell membranes and in sphingolipid metabolism. Homozygous mutations in GBA, the gene encoding GCase, are causative of Gaucher disease (GD), the most frequent lysosomal storage disorder. Although the majority of patients suffer from visceral symptoms, around 10% show nervous system involvement. In the last two decades, the distinction between these two phenotypes has been blunted when it became clear that GD patients show an increased risk to develop Parkinson disease (PD). Today, mutations in GBA are considered the most prevalent genetic risk factor for the development of PD also in people not suffering from GD.

Genotype-phenotype correlation in GD is limited. Patients with identical genotypes can have vastly different clinical manifestations and severity, even between siblings. This observation strongly suggests that additional factors such as genetic modifiers contribute to disease development and phenotype. The discovery of modifiers is important to gain a deeper understanding of disease pathophysiology. This may yield new or improved treatment approaches and allow to better stratify the risk to develop PD in GBA mutation carriers in general.

Methods:

We performed an arrayed CRISPR activation screen in a 384-well plate format using sgRNAs targeting 1,644 human transcription factors. A human glioblastoma cell line (LN229) harboring a homozygous mutation in GBA associated with GD (pL444P) and stably expressing dCas9-VPR was used as a cellular model. Enzymatic activity of GCase was determined using a fluorescent artificial substrate.

Results:

We identified 27 transcription factors regulating GCase enzymatic activity (17 up- and 10 downregulators) according to our cut-off criteria (fold-change >1.25 as compared to non-targeting controls and p-value <0.05). Validation of these candidate genes is ongoing. After confirmation of our results in LN229 pL444P and LN229 GCase wt cells, we will validate our candidate genes in fibroblasts and iPSC-derived dopaminergic neurons of Gaucher patients.

Conclusion:

By performing an arrayed CRISPR activation screen, we aim at identifying genetic modifiers of GCase activity in an unbiased manner. With this approach, we hope to identify currently unknown regulators of enzymatic activity and describe novel pathways involved in the regulation of this important lysosomal protein. Our findings might translate into new treatment avenues for neurological involvement of Gaucher disease as well as Parkinson disease

J. Bär³, M. Boumasmoud³, S. Mairpady Shambat³, C. Vulin³, M. Huemer³, T. Schweizer³, A. Gómez-Mejía³, N. Eberhard³, Y. Achermann³, P. Zingg¹, C. Mestres², S. Brugger³, R. Schuepback⁴, R Kouyos³, H. Barbara³, A. Zinkernagel³

Quantification of within patient *Staphylococcus aureus* phenotypic heterogeneity as a proxy for presence of persisters across clinical presentations

Balgrist University Hospital, University of Zurich, Zurich, Switzerland¹, Clinic for Cardiovascular Surgery, University Hospital Zurich, University of Zurich, Zurich, Switzerland², Department of Infectious Diseases and Hospital Epidemiology, University Hospital Zurich, University of Zurich, Zurich, Switzerland³, Institute for Intensive Care Medicine, University Hospital Zurich, University of Zurich, Zurich, Switzerland⁴

Introduction:

Difficult-to-treat infections caused by antibiotic susceptible strains have been linked with the occurrence of persisters, a subpopulation of dormant bacteria that tolerate antibiotic exposure despite lacking genetic resistance. They can be identified phenotypically upon plating on nutrient agar because of their altered growth dynamics, resulting in colony size heterogeneity. The occurrence of within-patient bacterial phenotypic heterogeneity in various infections and clinical determinants of persister formation remains unknown.

Methods:

We plated bacteria derived from 132 patient-samples of difficult-to-treat infections directly on nutrient-rich agar and monitored colony growth by time-lapse imaging. Of these, we retained 36 *Staphylococcus aureus* mono-cultures for further analysis. We investigated clinical factors potentially associated with increased colony growth-delay with regression analyses. Additionally, we corroborated the clinical findings using in vitro grown static biofilms, exposed to distinct antibiotics.

Results:

The extent of phenotypic heterogeneity of patient-derived *S. aureus* varied substantially between patients. Increased heterogeneity coincided with increased median colony growth-delay. Multivariable regression showed that rifampicin treatment was significantly associated with increased median growth-delay. *S. aureus* grown in biofilms and exposed to high concentrations of rifampicin or a combination of rifampicin with either clindamycin or levofloxacin exhibited prolonged growth-delay, correlating with a strain-dependent increase in antibiotic tolerance.

Conclusion:

Colony size heterogeneity upon direct sampling of difficult-to-treat *S. aureus* infections was common, with growth-delays of more than two days observed in the most extreme cases. Future studies are needed to assess the potential benefit of bacterial phenotypic heterogeneity quantification for staphylococcal infection prognosis and treatment guidelines.

J. Buschmann³, S. Andreoli³, J. Jang⁴, O. Gröniger², W. Stark², K. Spanaus¹, C. Opelz³, G. Meier Bürgisser³, M. Calcagni³, W. Jungraithmayr⁴

Hybrid nanocomposite as a chest wall graft with improved vascularization by copper oxide nanoparticles

Clinical Chemistry, USZ¹, Institute for Chemical and Bioengineering, Department of Chemistry and Applied Biosciences, ETH Zurich², Plastic Surgery and Hand Surgery, USZ³, Thoracic Surgery, USZ⁴

Introduction:

Synthetic tissues often include composite materials with an organic and an inorganic component to reflect physiological conditions. On the basis of previously reported hybrid nanocomposite poly lactic-co-glycolic acid amorphous calcium phosphate nanocomposite (PLGA/aCaP), a CuO component was incorporated to give a novel material PLGA/aCaP/CuO (60%/ 35%/ 5%).

The CuO was used because copper supports angiogenesis. Vascularization of novel scaffold materials is an important feature because real tissue integration is based on an adequate vascular network to provide oxygen and nutrients to the cells invading the implanted material. Growth factors have been used to support angiogenesis in that sense, for example, vascular endothelial growth factor (VEGF). One problem with application of growth factors is that they are prone to deteriorate in the wound secretome due to enzymatic degradation and thus may lose their efficacy. Hence, more stable angiogenic stimuli, such as inorganic nanoparticles, may offer a viable option to provide an increased vascularization over longer periods of time. Nanoparticles containing copper may be the first choice as copper stimulates angiogenesis.

Methods:

PLGA/aCaP/CuO was tested in vitro by seeding with murine adipose-derived stem cells (ASCs) for cell attachment and migration. The graft was compared to PLGA/CaCO₃ and PLGA/hydroxyapatite, two further nanocomposites providing the inorganic phase as nanoparticles. Characterization of the graft was performed using scanning electron microscopy.

Furthermore, PLGA/aCaP/CuO was implanted as a chest wall graft in a murine model. After 4 weeks, total cell density, graft integration, extracellular matrix components, such as fibronectin and collagen I, inflammatory response (macrophages (F4/80) and lymphocytes (CD3)) as well as vascularization (CD31) were quantitatively assessed.

Results:

The nanocomposite PLGA/aCaP/CuO showed a good cell attachment – and cells migrated well into the pores of the electrospun meshes. Cell densities did not differ between PLGA/aCaP/CuO and PLGA/CaCO₃ or PLGA/hydroxyapatite, respectively. When applied as a chest wall graft in mice, adequate stability for suturing into the thoracic wall could be achieved. Four weeks post-implantation, there was an excellent tissue integration without relevant fibrotic changes and a predominating collagen I matrix deposition within the graft. Slightly increased inflammation, reflected by increase infiltration of macrophages could be observed. Vascularization of the graft was significantly enhanced when compared with PLGA/aCaP (no CuO).

Conclusion:

We conclude that the hybrid nanocomposite PLGA/aCaP/CuO is a viable option to be used as a chest wall graft. Surgical implantation of the material is feasible and provides stability and enough flexibility. Proper tissue integration and an excellent vascularization are characteristics of this biodegradable material.

S. Neupane¹

High-throughput whole genome-wide CRISPR activation screening for the identification of potential modifiers of alpha-synuclein aggregates.

Institute of Neuropathology, University Hospital Zurich, Schmelzbergstrasse 12 8091 Zürich¹

Introduction:

The progressive accumulation of misfolded α -synuclein proteins in the nervous system is the key histopathological hallmark of neurodegenerative diseases, including Parkinson's Disease, Multiple System Atrophy, and Dementia with Lewy body, which are collectively referred to as synucleinopathies. α -Synuclein is a small (14 kDa) soluble acidic protein which is mainly localized in presynaptic nerve terminals associated with synaptic vesicles. Although the normal physiological function is not fully understood, α -synuclein contributes to the maintenance of synaptic homeostasis, vesicle recycling, and synaptic plasticity by enhancing neurotransmitters release. Under pathophysiological conditions, the native unfolded α -synuclein monomers assemble into the highly ordered β -sheet rich structure. During the progression, the misfolded α -synuclein species forms dimers, trimers, and oligomeric structures i.e. neurotoxic protofibrils which are phosphorylated at Ser 129 residue. The oligomers further aggregate to form higher-order amyloid structures via a nucleated polymerization mechanism. These amyloid fibrils give rise to the formation of intracellular inclusions known as Lewy bodies and cause the clogging of the endogenous protein degradation pathways, oxidative stress, synaptic dysfunction, and mitochondrial dysfunction eventually leading to neurodegeneration.

Methods:

Here, in our study by utilizing the CRISPR/Cas-9 based technology we are activating all the protein-coding genes in HEK293 cells overexpressing the human SNCA followed by preformed fibrils treatments. The screening will be carried out in 384 well plates in an arrayed format. Utilizing the anti-Ser-P 129 antibodies, the newly formed aggregated will be stained and imaging will be done using a high-throughput microscope. The identified hits will be further studied in neuronal models and in vivo models for the validation of the hits.

Results:

We have optimized PFFs (Preformed Fibrils) assay in 384 well plates by treating the cells with different concentrations of PFFs and monomeric α -synuclein. We have successfully established the protocol to produce and sonicate the fibrils in a reproducible way. The development and validity of the assay pilot study were carried out using positive and negative controls. Activation of *RAB8B*, *RAB13*, *CAMK1*, *ITPKB* showed to decrease α -synuclein aggregates will be used as control.

Conclusion:

The identified novel key genetic players help in understanding the pathways underlying α -Synuclein aggregation which would contribute in the development of new therapeutic strategies against synucleinopathies.

I. Hegglj^{1,3}, T. Mengis^{1,3}, N. Herger^{1,3}, R. Hove^{1,3}, R. Schüpbach⁵, N. Farshad-Amacker⁴, C. Laux², F. Wanivenhaus², M. Betz², J. Spirig², F. Brunner³, M. Farshad², O. Distler^{1,3}, S. Dudli^{1,3}

Infectious and autoinflammatory etiologies of Modic type 1 changes have different cytokine profiles

Center of Experimental Rheumatology, Department of Rheumatology, University Hospital, University of Zurich, Zurich, Switzerland¹, Department of Orthopaedic Surgery, Balgrist University Hospital, University of Zurich, Zurich, Switzerland², Department of Physical Medicine and Rheumatology, Balgrist University Hospital, University of Zurich, Zurich, Switzerland³, Department of Radiology, Balgrist University Hospital, University of Zurich, Zurich, Switzerland⁴, Unit of Clinical and Applied Research, Balgrist University Hospital, University of Zurich, Zurich, Switzerland⁵

Introduction:

Modic changes are vertebral bone marrow (BM) edema that associate with low back pain (LBP). Two etiologies have been described. In the infectious etiology *Cutibacterium acnes* (*C. acnes*) invade damaged intervertebral discs (IVDs) resulting in disc infection and endplate damage. In the autoinflammatory etiology disc and endplate damage lead to the exposure of immune privileged disc cells and matrix to leukocytes. In both etiologies, an immune response in the BM is triggered. It has been shown that discs adjacent to MC secrete more pro-inflammatory cytokines and maintain a pro-inflammatory and- fibrotic crosstalk with the MC BM possibly through endplate damages. However, it remains unknown if these cytokines are also increased in MC BM and whether etiology-specific cytokine profiles exist. This is the first study that quantifies cytokines directly in Modic type 1 change (MC1) BM and shows that etiology-specific cytokine profiles exist.

Methods:

BM aspirates were obtained from LBP patients with MC1 undergoing spinal fusion. From each patient, a MC1 and an intra-patient control aspiration from the adjacent vertebral level was taken. BM plasma fraction was obtained by centrifugation. Using Meso Scale Discovery biomarker assays, quantitative protein levels of IL-1 β , GM-CSF, ENA-78, TNF- α , M-CSF, CCL2, IL-4, IL-6, IL-8, and IL-13 were measured (n=12+12). To test if different cytokine profiles existed among patients, protein concentrations were visualized using UMAP dimensionality reduction technique. To identify whether the resulting clusters represented MC1 of different etiologies, *C. acnes* genome copies/gram IVD tissue were quantified with 16S qPCR in IVDs adjacent to MC1 lesions (n=8 of 12) and median copy numbers per cluster were evaluated. To identify cluster/etiology specific pathomechanisms, RNA was isolated from CD45+CD66b+ sorted neutrophils from BM aspirates (n=7+7) and bulk RNA sequencing was performed. According to the cytokine clustering, patients were assigned to the infectious or autoinflammatory etiology (inf.=4+4, auto=3+3) and etiology-specific gene ontology (GO) enrichment analysis was performed separately.

Results:

UMAP dimensionality reduction identified two cytokine clusters (1A). We found that IVDs of patients in cluster 1 had much lower *C. acnes* genome copies/gram IVD tissue (n=2, median=351 copies/g, IQR=325,378) than IVDs in cluster 2 (n=6, median=2848 copies/g, IQR=1355, 3339) (1B). Based on the cluster analysis, we assigned patients of cluster 1 to the autoinflammatory and patients of cluster 2 to the infectious etiology. Without distinguishing the two etiologies (n=12+12), cytokine concentrations were similar in MC1 and intra-patient control BM plasma. However, when stratifying for the two etiologies, we found that the pro-inflammatory cytokine IL-8 was significantly upregulated in MC1 BM from the infectious etiology (p=0.04) and down-regulated in the autoinflammatory etiology (p=0.07), resulting in a significant difference between the two etiologies (p=0.004). Similar results were found for M-CSF (inf.: p=0.07, auto: p=0.02, inf. vs auto: p=0.004), IL-1 β (inf: p=0.18, auto: p=0.13, inf. vs. auto: p=0.004), and ENA-78 (inf: p=0.18, auto:p=0.13, inf. vs. auto: p=0.048) (1C). GO enrichment analysis of biological processes (BP) revealed an upregulated response to bacterium in MC1 neutrophils of patients assigned to the infectious (cluster 2), but not in MC1 neutrophils of patients assigned to the autoinflammatory etiology (cluster 1) (1D).

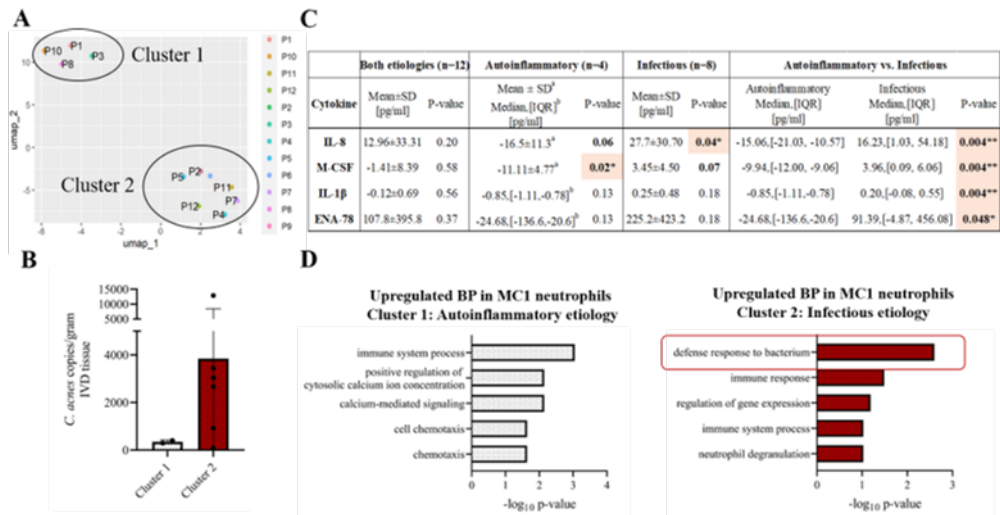


Figure 1: (A) UMAP dimensionality reduction of cytokine profiles resulted in 2 clusters. (B) Higher *C. acnes* genome copies in cluster 2. (C) Upregulated pro-inflammatory cytokines in infectious etiology (Values: MC1-control (D) Cluster/etiology specific GO enrichment analysis: MC1 neutrophils from the infectious (but not autoinflammatory) etiology make a defense response to bacterium. * $p < 0.05$, ** $p < 0.01$

Conclusion:

Autoinflammatory and infectious etiologies of MC1 have different cytokine profiles, suggesting different pathomechanisms. Increased pro-inflammatory cytokines and an upregulated defense response to bacterium of MC1 neutrophils indicates an acute pro-inflammatory process with potential contribution of neutrophils in the infectious MC1 etiology. This study shows the importance to distinguish the two etiologies, because different pathomechanisms require different treatments.

K. Kusejko^{7,8}, L. Salazar-Vizcaya¹, C. Shah⁸, M. Stöckle⁵, C. Beguelin¹, P. Schmid², M. Ongaro⁶, K. Darling³, E. Bernasconi⁴, A. Rauch¹, R. Kouyos^{7,8}, H. Günthard^{7,8}, J. Böni⁸, J. Fehr^{7,8}, D. Braun^{7,8}

Sustained effect on hepatitis C elimination among men who have sex with men in the Swiss HIV Cohort Study: A systematic re-screening for hepatitis C RNA two years following a nationwide elimination program

Bern University Hospital¹, Cantonal Hospital St Gallen², Lausanne University Hospital³, Regional Hospital Lugano⁴, University Hospital Basel⁵, University Hospital Geneva⁶, University Hospital Zurich⁷, University of Zurich⁸

Introduction:

The WHO elimination targets for hepatitis C (HCV) in 2030 are to achieve 80% reduction in new HCV infections. The Swiss HCVfree Trial (NCT 02785666) was conducted in 2015-2017 with the goal of implementing a population-based systematic HCV micro-elimination program among men who have sex with men (MSM) living with HIV in Switzerland. The trial led to a 91% and 77% decline of HCV prevalence and incidence, respectively. However, the long-term effect of this HCV micro-elimination program is uncertain.

Methods:

All MSM enrolled in the Swiss HIV Cohort Study (SHCS) with a plasma sample available from 2019 were screened for HCV-RNA. All blood samples were tested in pools of five using the Cobas Roche HCV test. The point-prevalence in 2019 of HCV infections was determined, where we distinguished: 1) Primary incident infections: No or a negative HCV test (HCV-RNA and/or anti-HCV-IgG) documented in the SHCS database before 2019 with a positive HCV-RNA result in this screening project, 2) Incident re-infections: Positive anti-HCV-IgG test but negative HCV-RNA test documented in the SHCS database before 2019 with a positive HCV-RNA test obtained in the screen, 3) Prevalent infections: Positive HCV test documented in the SHCS database before 2019 with a positive HCV-RNA result obtained in the screen. Patient charts were used to clarify uncertain cases. Basic characteristics between patients with replicating and non-replicating HCV screening results were compared.

Results:

In total, 4641 participants were screened for HCV RNA, the median age was 54 (IQR = 42-58). In 2019, the point-prevalence of replicating HCV was 28/4641 (0.60%). We observed 9 (32.1%) primary incident infections, 2 (7.0%) re-infections and 17 (60.7%) prevalent infections. Compared to the HCVfree Trial, this indicates a further decline, as there were 177/3715 (4.8%) replicating HCV infections 2015 and 36/3107 (1.2%) in 2017. Looking at characteristics of patients with replicating HCV RNA, we found that patients with replicating HCV reported more often previous intravenous drug use as compared to patients without replicating HCV RNA.

Conclusion:

A systematic HCV-RNA-based screening among MSM living with HIV conducted two years after the Swiss HCVfree elimination program revealed a sustained effect on the point-prevalence of replicating HCV. This indicates that the HCVfree Trial was successful in curbing the HCV epidemic among MSM living with HIV. In addition, Switzerland is on the right track to reach the WHO HCV elimination goals in this population.

S. Dudli¹, A. Karol², L. Guidici⁶, I. Heggli¹, C. Laux³, J. Spirig³, F. Wanivenhaus³, M. Betz³, C. Germann⁵, N. Farshad-Amacker⁵, F. Brunner⁴, O. Distler¹, M. Farshad³

Histomorphometry of Modic changes

Center of Experimental Rheumatology¹, Department of Molecular Mechanisms of Disease², Department of Orthopedic Surgery³, Department of Physical Medicine and Rheumatology⁴, Department of Radiology, Balgrist University Hospital⁵, Institute of Pathology and Molecular Pathology⁶

Introduction:

Modic changes (MC) are vertebral bone marrow lesions seen on MRI, that associate with disc degeneration and low back pain (LBP). Few studies described MC histopathology qualitatively based on a few patient samples. This study provides the first semi-quantitative histomorphometric analysis of MC bone marrow and compares findings to bone marrow oedema in other joint diseases.

Methods:

Human biopsies from Modic type 1 changes (MC1: n=8), Modic type 2 changes (MC2, n=6), and control biopsies (MC0, n=8) from adjacent vertebrae were obtained from 14 LBP patients during lumbar spinal fusion. Biopsies were processed for histology/immunohistochemistry. Inflammatory changes (oedema, inflammatory infiltrates), fibrotic changes (connective tissue, type I and III collagen, fibronectin, α -smooth muscle actin), and amount of bone marrow stromal cells (CD90, CD105) were scored (0-6). Scores for MC0, MC1, and MC2 were compared with non-parametric tests. Pairwise correlations, hierarchical clustering, and principal component analysis of histological readouts were calculated to identify most important histomorphometric MC characteristics.

Results:

Compared to MC0, MC1 had more connective tissue, oedema, inflammatory infiltrates, and CD90+ cells. MC2 compared to MC0 had more oedema and CD90+ cells. Scores of CD90 correlated and clustered with inflammatory and fibrotic changes. Amount of connective tissue correlated with LBP. Fibrotic changes were found in MC1 and MC2 and are typical for bone marrow oedema in osteoarthritic joints. Mononuclear infiltrates were found in MC1 and are typical for bone marrow edema in rheumatoid arthritis and axial spondylarthritis.

Conclusion:

Accumulation of CD90+ cells is a major characteristic of MC and associates with inflammatory and fibrotic changes. MC share characteristics with bone marrow oedema of other joint diseases but are not identical. MC1 are not pure degenerative changes and suggests that MC1 locate on the degenerative-inflammatory axis between osteoarthritis and rheumatoid/spondylo-arthritis. Therefore, MC-specific studies are required to understand MC pathomechanisms and to develop MC-specific treatments.

V. Dimakopoulos⁶, J. Gotman⁷, W. Stacey³, C.G. Bénar¹, F. Bartolomei¹, N. von Ellenrieder⁷, J. Jacobs², J. Cimbalnik⁹, G. Worrell⁵, M. Sperling⁴, M. Zijlmans¹⁰, L. Imbach⁸, B. Frauscher⁷, J. Sarnthein⁶

Protocol for multicenter comparison of interictal high frequency oscillations as a predictor of seizure freedom.

Aix Marseille Univ, INSERM, INS, Inst Neurosci Syst, and APHM, Timone hospital, Epileptology and cerebral rythmology, Marseille, France¹, Alberta Children's Hospital, University of Calgary, Calgary, Canada², Department of Neurology and Department of Biomedical Engineering, University of Michigan, USA³, Department of Neurology, Jefferson University Hospitals, Philadelphia, PA, USA⁴, Department of Neurology, Mayo Clinic, Rochester, MN, USA⁵, Klinik für Neurochirurgie, UniversitätsSpital Zürich, Universität Zürich, Switzerland⁶, Montreal Neurological Institute & Hospital, McGill University, Montreal Quebec, Canada⁷, Schweizerisches Epilepsie Zentrum, Zurich, Switzerland⁸, St. Anne's University Hospital, Brno, Czech Republic⁹, University Medical Center, Utrecht, and Stichting Epilepsie Instellingen Nederland (SEIN), The Netherlands¹⁰

Introduction:

In drug-resistant focal epilepsy, interictal high frequency oscillations (HFO) recorded from intracranial EEG (iEEG) may provide clinical information for delineating epileptogenic brain tissue. The iEEG electrode contacts that contain HFO are hypothesized to delineate the epileptogenic zone; their resection should then lead to postsurgical seizure freedom.

Methods:

We test whether our prospective definition of clinically relevant HFO is in agreement with postsurgical seizure outcome. The algorithm is fully automated and is equally applied to all datasets. The aim is to assess the reliability of the proposed detector and analysis approach.

We use an automated data-independent prospective definition of clinically relevant HFO that has been validated in data from two independent epilepsy centers. In this study, we combine retrospectively collected datasets from 9 independent epilepsy centers. The analysis is blinded to clinical outcome. We use iEEG recordings during NREM sleep with a minimum of 12 epochs of 5 minutes of NREM sleep. We automatically detect HFO in the ripple (80-250 Hz) and in the fast ripple (250-500 Hz) band. There is no manual rejection of events in this fully automated algorithm. The type of HFO that we consider clinically relevant is defined as the simultaneous occurrence of a fast-ripple and a ripple. We calculate the temporal consistency of each patient's HFO rates over several data epochs within and between nights. Patients with temporal consistency < 50% are excluded from further analysis. We determine whether all electrode contacts with high HFO rate are included in the resection volume and whether seizure freedom (ILAE 1) was achieved at ≥2 y follow-up. We estimate the 95% confidence intervals for the confusion matrix of the classification according to pilot studies.

Results:

The lower limit for the number of patients that must be included before publication is N = 255. The expected 95% confidence interval for the size of the expected multicenter cohort size for N = 255 and N = 300 patients are above chance level.

Conclusion:

Applying a previously validated algorithm to a large cohort from several independent epilepsy centers may advance the clinical relevance and the generalizability of HFO analysis as essential next step for use of HFO in clinical practice.

T. Schweizer², F. Andreoni², C. Acevedo², T. Scheier², I. Heggli¹, E. Marques Maggio³, N. Eberhard², S. Brugger², S. Dudli¹, A. Zinkernagel²

Intervertebral disc cell chondroptosis elicits neutrophil response in *Staphylococcus aureus* spondylodiscitis

Center of Experimental Rheumatology, University Hospital Zurich and Balgrist University Hospital, University of Zurich, Zurich 8008, Switzerland¹, Department of Infectious Diseases and Hospital Epidemiology, University Hospital of Zurich, University of Zurich, Zurich 8091, Switzerland², Department of Pathology and Molecular Pathology, University Hospital of Zurich, University of Zurich, Zurich 8091, Switzerland³

Introduction:

The incidence of vertebral bone and intervertebral disc (IVD) infection, termed spondylodiscitis, has doubled over the last two decades, in particular in the elderly. *Staphylococcus aureus* is the most frequent pathogen isolated in spondylodiscitis. In order to achieve cure, patients receive long-term antibiotics as well as surgical debridement, when indicated. Interestingly, the IVD usually is an immune-privileged site and hence the initial immune reaction has to be orchestrated by IVD cells. However, it remains largely unknown how IVD cells initiate an immune response upon *S. aureus* challenge. Here, we aimed at understanding the pathophysiology of spondylodiscitis due to *Staphylococcus aureus*, by combining clinical insights and experimental approaches.

Methods:

Clinical data and histological material of patients suffering from *S. aureus* spondylodiscitis were collected. To mirror the clinical findings experimentally, we developed a novel porcine *ex vivo* model mimicking acute *S. aureus* spondylodiscitis and assessed the interaction between *S. aureus* and IVD cells within their native environment. In addition, the inflammatory features underlying this interaction were assessed in primary human IVD cells. Finally, we went one step further and assessed primary human neutrophils for their ability to respond to secreted inflammatory modulators of IVD cells upon *S. aureus* challenge.

Results:

Acute *S. aureus* spondylodiscitis in patients was characterized by tissue necrosis and neutrophil infiltration. Additionally, the presence of empty IVD cells' lacunae was observed. This was mirrored in the *ex vivo* porcine model, where *S. aureus* induced extensive IVD cell death, leading to empty lacunae. Concomitant engagement of the apoptotic and pyroptotic cell death pathways was observed in primary human IVD cells, resulting in cytokine release. Among the released cytokines, functionally intact neutrophil-priming as well as broad pro- and anti-inflammatory cytokines known for their involvement in IVD degeneration were found.

Conclusion:

In patients as well as *ex vivo*, *S. aureus* spondylodiscitis infection caused IVD cell death, resulting in empty lacunae, which was accompanied by release of inflammation markers and recruitment of neutrophils. These findings offer valuable insights into the important role of inflammatory IVD cell death during the onset of spondylodiscitis and potential future therapeutic approaches.

D. Vocj¹, S. Zbinden¹, E. Micieli¹, N. Kucher¹, S. Barco¹

Fixed-dose ultrasound-assisted catheter-directed thrombolysis for acute pulmonary embolism associated with COVID-19

University Hospital Zurich - Department of Angiology¹

Introduction:

In patients with acute pulmonary embolism (PE), fixed-dose ultrasound-assisted catheter-directed thrombolysis (USAT) rapidly improves hemodynamic parameters and reverses right ventricular dysfunction. The effectiveness of USAT for acute PE associated with coronavirus disease 2019 (COVID-19) is unknown.

Methods:

Our study population consisted of 36 patients with an intermediate-high or high-risk PE, who were treated with a fixed low-dose USAT protocol (r-tPA 10-20 mg/15 hours). Of these, 9 patients were tested positive for COVID-19 and age-sex matched to 27 patients without COVID-19. The USAT protocol included anti-Xa-activity-adjusted unfractionated heparin (target 0.3-0.7U/L). The study outcomes were (i) the invasively measured mean pulmonary arterial pressure (mPAP) before and at completion of USAT and (ii) the National Early Warning Score (NEWS), according to which more points indicate greater hemodynamic severity.

Results:

Twenty-four (66.7%) patients were men; the mean age was 67±14 years. Mean±standard deviation mPAP decreased from 32.3±8.3 to 22.4±7.0 mmHg among COVID-19 patients and from 35.4±9.7 to 24.6±7.0 mmHg among unexposed, with no difference in the relative improvement between groups (p=0.84). Within 12 hours of USAT start, the median NEWS decreased from 6 (Q1-Q3:4-8) to 3 (Q1-Q3:2-4) points among COVID-19 patients and from 4 (Q1-Q3:2-6) to 2 (Q1-Q3:2-3) points among unexposed (p=0.29). One COVID-19 patient died due to COVID-19-related complications 14 days after acute PE. No major bleeding events were recorded.

Conclusion:

Among COVID-19 patients with acute PE, mPAP and hemodynamic parameters rapidly improved during USAT. The improvement was similar to that of control group.

D. Vocj⁵, U. Fedeli¹, L. Valerio², E. Schievano¹, M. Righini³, N. Kucher⁵, D. Spirk⁴

Mortality rate related to peripheral artery disease: a retrospective analysis of epidemiological data (years 2008 - 2019)

Azienda Zero - Padova¹, Center for Thrombosis and Hemostasis, Johannes Gutenberg University Mainz, Mainz, Germany², Division of Angiology and Hemostasis, Department of Medical Specialties, Geneva University Hospital and Faculty of Medicine, Geneva, Switzerland³, Institute of Pharmacology, University of Bern, Bern, Switzerland⁴, University Hospital Zurich - Department of Angiology⁵

Introduction:

Peripheral artery disease (PAD) is one of the most prevalent cardiovascular diseases with more than 230 million people being affected worldwide. As highlighted by the recent guidelines of the European Society of Cardiology, data on the epidemiology of PAD is urgently needed.

Methods:

We accessed the vital registration data of the Veneto region (Northern Italy, approximately five millions inhabitants) covering the period 2008-2019. We computed annual age-standardized rates for PAD reported as the underlying cause of death (UCOD) or as one of multiple causes of death (MCOD). Age-adjusted odds ratios (OR) served to study the association between PAD and cardiovascular comorbidities.

Results:

The age-standardized mortality rate for PAD as MCODE slightly declined from 20.4 to 18.3 in men and from 10.4 to 10.0 deaths per 100,000 population-years in women during the study period. The age-standardized PAD-related mortality rate declined from 4.7 to 4.6 in men and increased from 3.2 to 3.6 deaths per 100,000 population in women. These trends were not statistically significant. PAD contributed to 1.6% of all deaths recorded in the region. Ischemic heart disease, diabetes mellitus, and neoplasms were the most prevalent UCOD among PAD patients. PAD was strongly associated with diabetes mellitus (OR 3.79, 95%CI 3.55-4.06) and chronic kidney diseases (OR 2.73, 95%CI 2.51-2.97) in men and with atrial fibrillation (OR 2.26, 95%CI 2.10-2.44) in women.

Conclusion:

PAD remains a substantial cause of death in the general population of this high-income region of Western Europe with marked sex-specific differences.

D. Voci³, U. Fedeli¹, I. Farmakis², L. Hobohm², K. Keller², L. Valerio², E. Schievano¹, C. Barbiellini Amidei¹, S. Konstantinides², N. Kucher³, S. Barco³

Deaths related to pulmonary embolism and cardiovascular events before and during the 2020 COVID-19 pandemic: an epidemiological analysis of data from an Italian high-risk area

Azienda Zero - Padova¹, Center for Thrombosis and Hemostasis, Johannes Gutenberg University Mainz, Mainz, Germany², University Hospital Zurich - Department of Angiology³

Introduction:

Pulmonary embolism (PE) is a known complication of coronavirus disease 2019 (COVID-19). Epidemiological population data focusing on PE-related mortality is limited.

Methods:

Veneto is a region in Northern Italy counting 4,879,133 inhabitants in 2020. All ICD-10 codes from death certificates (1st January 2018 to 31st December 2020) were examined. Comparisons were made between 2020 (COVID-19 outbreak) and the average of the two-year period 2018-2019. All-cause, COVID-19-related and the following cardiovascular deaths have been studied: pulmonary embolism, hypertensive disease, ischemic heart disease, atrial fibrillation/flutter, and cerebrovascular diseases.

Results:

In 2020, a total of 56,412 deaths were recorded, corresponding to a 16% (n=7,806) increase compared to the period 2018-2019. The relative percentage increase during the so-called first and second waves was 19% and 44%, respectively. Of 7,806 excess deaths, COVID-19 codes were reported in 90% of death certificates. The percentage increase in PE-related deaths was 27% (95%CI 19-35%): this was more evident among men (+45%) than in women (+14%), and primarily driven by deaths recorded during the second wave (+91% between October and December). An excess of deaths, particularly among men and during the second wave, was also observed for other cardiovascular diseases, notably hypertensive disease, atrial fibrillation, cerebrovascular disease, and ischemic heart disease.

Conclusion:

We observed a considerable increase of all-cause mortality during the year 2020. This was mainly driven by COVID-19 and its complications. The relative increase in the number of PE-related deaths was more prominent during the second wave, suggesting PE underdiagnosis during the first wave.

E. Köksal¹, A. Levin², I. Condado-Morales¹, L. Madrigal¹, S. Neupane¹, E. De Cecco¹, A. Aguzzi¹, T. Knowles², S. Hornemann¹

Digital microfluidics for absolute quantification of α -synuclein propagons for Parkinson disease diagnosis

University Hospital of Zürich¹, University of Cambridge²

Introduction:

Parkinson's disease (PD) is associated with the misfolding of the α -synuclein (α Syn) protein resulting in the accumulation of pathological protein aggregates. The diagnosis of PD is based on clinical assessment, because reliable biochemical tests, in particular for the early diagnosis, are still missing. Recent progress has been made by the development of seed amplification assays (SAA). These assays are based on the amplification of signals derived from aggregates, also termed propagons, that seed monomeric α Syn in bulk solutions. Although SAAs allow the detection of α Syn aggregates in body fluids at minute concentrations, an absolute and precise quantitation is limited due to a restriction in the number of replicas. We therefore aim to use digital microfluidics to develop a diagnostic assay for the absolute and accurate quantification of single α Syn propagons in clinical samples of PD patients.

Methods:

We have set-up a microfluidics platform to generate thousands of picoliter sized water-in-oil microdroplets that act as microreactors and contain recombinant α Syn monomers mixed with a sample to be analysed. To identify specific and sensitive amplification conditions, several parameters were optimized in terms of monomer concentration, temperature and buffer composition using synthetic α Syn preformed fibrils (PFFs). Growth and proliferation of propagons inside up to 5,000 droplets were monitored simultaneously through Thioflavin T, a fluorescent probe that specifically detects amyloid aggregates. Obtained epifluorescence microscopy images were analyzed by counting fluorescent positive, propagon containing, and negative microdroplets. Poisson statistics was applied for absolute quantification.

Results:

Growth and proliferation of α Syn aggregates was optimized in bulk samples using a microplate SAA and in microdroplets. While a minimum of 72 hours was required for signal development in the bulk reactions of the SAA, less than 24 hours were sufficient for the detection in microdroplets. The testing of the Hofmeister ion series revealed several anions such as $\text{Na}_3\text{Citrate}$ and NaCl that enhanced the seeding activity of synthetic PFFs, while suppressing unspecific reactions in the unseeded reactions. Detection of PFFs was achieved in picomolar range. In the future, results obtained with synthetic PFFs will be validated with CSF samples from PD patients and healthy controls.

Conclusion:

Our digital microfluidic assay would allow for sensitive and rapid detection of α Syn aggregates in CSF samples of PD patients at early stages. Quantification at single aggregate level would enable monitoring disease progression and success of therapeutic strategies on preventing aggregation in PD patients.

S. Mairpady Shambat¹, A. Gómez-Mejía¹, T. Schweizer¹, M. Huemer¹, C. Chang¹, C. Acevedo¹, J. Bergada-Pijuan¹, C. Vulin¹, D. Hofmaenner², T. Scheier¹, S. Hertegonne¹, E. Parietti¹, M. Hilty², N. Miroshnikova¹, P. Wendel Garcia², P. Buehler², R. Schuepbach², S. Brugger¹, A. Zinkernagel¹

Hyperinflammatory environment drives dysfunctional myeloid cell effector response to bacterial challenge in COVID-19

Department of Infectious Diseases and Hospital Epidemiology, University Hospital of Zurich, University of Zurich, Zurich, Switzerland¹, Institute of Intensive Care, University Hospital of Zurich, University of Zurich, Zurich, Switzerland²

Introduction:

COVID-19 displays diverse disease severities and symptoms including acute systemic inflammation and hypercytokinemia, with subsequent dysregulation of immune cells. Bacterial superinfections in COVID-19 can further complicate the disease course and are associated with increased mortality. However, there is limited understanding of how SARS-CoV-2 pathogenesis and hypercytokinemia impede the innate immune function against bacterial superinfections.

Methods:

For this purpose, luminex-based and proteomic-based functional assays were established for the determination of cytokine and inflammatory mediator levels in plasma. A specific flow-cytometry based panel was developed for the phenotypic and functional characterization of both neutrophils and monocytes isolated from severely-ill COVID-19 acute and recovery patients. Finally, the microbicidal capacity and the impact of a specific cluster of cytokines in the functional response of both neutrophils and monocytes was evaluated in vitro using *Staphylococcus aureus* and *Streptococcus pneumoniae* as secondary bacterial superinfection agents

Results:

Neutrophils and monocytes derived from COVID-19 patients in their acute-phase showed an impaired intracellular microbicidal capacity upon bacterial challenges. The impaired microbicidal capacity was reflected by abrogated MPO and reduced NETs production in neutrophils along with reduced ROS production in both neutrophils and monocytes. Moreover, we observed a distinct pattern of cell surface receptor expression on both neutrophils and monocytes, in line with suppressed autocrine and paracrine cytokine signaling. This phenotype was characterized by a high expression of CD66b, CXCR4 and low expression of CXCR1, CXCR2 and CD15 in neutrophils and low expression of HLA-DR, CD86 and high expression of CD163 and CD11b in monocytes. Furthermore, the impaired antibacterial effector function was mediated by synergistic effect of the cytokines TNF- α , IFN- γ and IL-4. COVID-19 patients receiving dexamethasone showed a significant reduction of overall inflammatory markers in the plasma as well as exhibited an enhanced immune response towards bacterial challenge ex vivo. Finally, broad anti-inflammatory treatment was associated with a reduction in CRP, IL-6 levels as well as length of ICU and hospital stay in critically ill COVID-19 patients.

Conclusion:

Our data provides insights into the transient functional dysregulation of myeloid immune cells against subsequent bacterial infections in COVID-19 patients and describe a beneficial role for the use of dexamethasone in these patients, which improves the antibacterial effector functions of neutrophils and monocytes.

E. Micieli², D. Voci², S. Barco², A. Grigorean², A. Lecler¹

Transient Perivascular Inflammation of the Carotid artery (TIPIIC) syndrome: an updated multinational analysis of 72 patients

Department of Neuroradiology, A. Rothschild Foundation Hospital, Paris, France¹, USZ²

Introduction:

The Transient Perivascular Inflammation of the Carotid artery (TIPIIC) syndrome is presumably a very rare disease characterized by a local transient inflammation of the tissue around the carotid artery. Its pathophysiology remains unknown. We performed a large, updated study of TIPIIC syndrome cases in the setting of a multinational collaborative study.

Methods:

This study was conducted as an observational multinational retrospective individual patient level cohort study. Information from all known cases diagnosed with TIPIIC syndrome in the literature (2005-2020) was collected after a semi-structured literature search of PubMed and Web of Science. We also collected unpublished information of patients from French, Swiss, and Italian Vascular Medicine or Radiology departments.

Results:

A total of 72 patients were included and served for data analysis: 42 (58.3%) were women; the mean age was 47.9 (SD 11.4) years. Symptoms were unilateral in 92% of patients and 81.4% required pain killers. At baseline, irrespective of the imaging method used, the median thickness of the carotid lesions was 5 (Q1-Q3: 4-7; range 2-11) mm and the median length of the lesion was 20 (Q1-Q3: 10-30; range 3-50) mm. We found a positive linear correlation between thickness and length. At follow-up, the thickness of the carotid lesions decreased to a median of 2 (Q1-Q3: 1-3; range 0-6) mm; the length decreased to a median 10 (Q1-Q3: 5-15; range 0-41) mm. A linear correlation between baseline and follow-up values was observed for both thickness and length measurements. Symptoms disappeared after a median of 14 (Q1-Q3: 10-15) days. Thirteen patients experienced a recurrence after a median follow-up of 6 (Q1-Q3: 2-12) months.

Conclusion:

The present analysis elucidates clinical and sonographic characteristics of TIPIIC syndrome, indicating the benign nature of this condition. A future international registry will study the long-term course of the disease.

S. Zbinden¹, D. Voci¹, P. Philippe¹, N. Kucher¹, S. Barco¹

Catheter-directed thrombolysis for the treatment of pulmonary embolism: Experience at a University Hospital

Department of Angiology, University Hospital Zurich¹

Introduction:

Systemic thrombolysis for acute hemodynamically stable intermediate-risk pulmonary embolism (PE) reduced early decompensation and death, but was associated with an unacceptable rate of major and intracranial bleedings. Catheter-directed (ultrasound-assisted) thrombolysis (EKOS-lysis) is potentially effective to reverse right ventricular dysfunction without increasing the risk of bleeding

Methods:

We studied the course of hemodynamic improvement in consecutive acute PE patients treated at a University Hospital, 2018-2020. Patients with intermediate-high or high-risk acute PE were included and underwent EKOS-lysis with a standard regimen of 10 mg alteplase/catheter over 15 hours. Early and late clinical and hemodynamic outcomes were studied: (i) mean pulmonary arterial pressure (mPAP) before and after treatment; (ii) early death, hemodynamic decompensation within 7 and 30 days of treatment; (iii) early major and minor bleeding complications (ISTH definition) or device-related complications within 7 days of treatment.

Results:

A total of 149 patients were identified. Data collection was completed for 142 patients. 86 patients (60.6%) were men and the mean age was 61.4 (SD 15.6) years. All patients received anti-Xa activity-adjusted unfractionated heparin. mPAP decreased from a mean of 35.5 (SD 8.9) to 25.8 (SD 6.9) mmHg (absolute difference 10 mmHg; 95%CI 6.6-13.5). One major, non fatal, bleeding (0.7%) and three minor bleedings (2.1%) were observed.

Conclusion:

Catheter-directed ultrasound-assisted thrombolysis rapidly reduced the mean pulmonary arterial pressure in intermediate-high or high-risk acute PE with an acceptable rate of major bleeding events.

Y. Gong², R. Renikunta^{4, 5}, K. Lazarow¹⁰, P. Shukla^{4, 11}, H. Giral⁴, A. Kratzer⁴, V. Nageswaran^{4, 5}, L. Opitz³, F. Engel⁷, A. Haghikia^{1, 4, 5}, J. Kries¹⁰, F. Paneni², K. Streckfuss-Bömeke^{3, 6, 9}, U. Landmesser^{1, 4, 5}, P. Jakob^{1, 2, 4, 5}

A Large-scale MicroRNA Functional High-throughput Screening Identifies Mir-515 and Mir-519e as Potent Inducers of Human iPSC-cardiomyocyte Proliferation

Berlin Institute of Health (BIH) at Charité – Universitätsmedizin Berlin, Charitéplatz 1, 10117 Berlin, Germany¹, Center for Molecular Cardiology, University of Zürich, Wagistrasse 12, 8952 Schlieren and University Heart Center, Cardiology, University Hospital Zurich, 8091 Zürich, Switzerland², Clinic for Cardiology and Pneumology, University Medical Center Göttingen, Robert-Koch-Strasse 40, 37075 Göttingen, Germany³, Department of Cardiology, Charité University Medicine Berlin, Campus Benjamin Franklin, Hindenburgdamm 30, Berlin 12203, Germany⁴, DZHK (German Center for Cardiovascular Research), partner site Berlin, Hindenburgdamm 30, Berlin, Germany⁵, DZHK (German Center for Cardiovascular Research), partner site Göttingen, Robert-Koch-Strasse 42a, 37075 Göttingen, Germany⁶, Experimental Renal and Cardiovascular Research, Department of Nephropathology, Institute of Pathology, Friedrich-Alexander-Universität Erlangen-Nürnberg (FAU), Schwabachanlage 12 (TRC), 91054 Erlangen, Germany⁷, Functional Genomics Center Zurich UZH/ETH, ETH Zurich and University of Zurich, 8057, Switzerland⁸, Institute of Pharmacology and Toxicology, Würzburg University, Versbacher str. 9, 97078 Würzburg, Germany⁹, Leibniz-Institute for Molecular Pharmacology (FMP), Campus Berlin-Buch, Robert-Rössle-Strasse 10, 13125 Berlin, Germany¹⁰, School of Medical Science and Technology, Indian Institute of Technology, Kharagpur 721302, West Bengal, India¹¹

Introduction:

Ischemic cardiomyopathy, driven by loss of cardiomyocytes and inadequate proliferative response, persists to be a major global health problem. Experimental studies have shown that miRNAs may be used as a therapeutic option to reinduce adult cardiomyocyte proliferation. This study thought to evaluate proliferative potential in human cardiomyocytes after overexpression and inhibition of 2019 microRNAs (miRNAs).

Methods:

To identify miRNAs that regulate cardiomyocyte proliferation, we performed functional high-throughput screenings in human iPSC-derived cardiomyocytes (hiPSC-CM) after transient hypoxia. Herein, 2019 miRNA-mimics for overexpression and 2019 anti-miRs for inhibition were individually transfected to examine EdU-incorporation in hiPSC-CM. MiR-mimic-515 and miR-mimic-519e that induced the highest EdU-uptake, were further assessed by immunostaining and molecular methods for markers indicative of early and late mitosis. In addition, RNA-Sequencing in hiPSC-CM after overexpression of miR-515 and miR-519e was performed to examine differential gene expression and miRNA-modulated pathways involved in cardiomyocyte proliferation.

Results:

Whereas miR-inhibitors failed to enhance EdU-uptake, overexpression of 28 miRNAs substantially induced proliferative activity in hiPSC-CMs, with an overrepresentation of miRNAs belonging to the primate-specific microRNA cluster on chromosome 19 (C19MC) and adjacent miR-371-373 family. Two of these miRNAs, miR-515 and miR-519e, increase markers of early and late mitosis, indicative of cell division, and substantially alter signaling pathways and transcription factors relevant for cardiomyocyte proliferation.

Conclusion:

Collectively, these results support a critical role of miR-515 and miR-519e for induction of proliferation in human cardiomyocytes under hypoxic conditions and therefore represent a potential novel therapeutic option in ischemic cardiomyopathy.

V. Vetter⁴, B. Sobottka⁴, A. Banaei-Esfahani⁴, M. Nowak⁴, L. de Leval², A. Lorch³, K. Mertz¹, A. Kahraman⁴, V. Koelzer⁴, H. Moch⁴

Immune phenotype-genotype associations in primary and matched metastatic clear cell renal cell carcinoma

Cantonal Hospital Baselland, Institute of Pathology¹, Institut universitaire de pathologie, Centre hospitalier universitaire vaudois (CHUV)², University Hospital Zurich, Department of Medical Oncology and Haematology³, University Hospital Zurich, Institute of Pathology and Molecular Pathology⁴

Introduction:

Metastatic disease is the main cause of cancer-related mortality. In clear cell renal carcinoma (ccRCC) one third of patients present with synchronous metastases, while another third will develop metachronous metastases. Adjuvant immunotherapy and VEGF-targeted therapy have been recommended for high risk or metastatic ccRCC, but there are no tissue biomarkers to predict treatment response. Potential predictive biomarkers are mainly assessed in primary tumors, whereas metastases remain understudied.

Methods:

To explore differences between genomic alterations and immune phenotypes in primary tumors and their matched metastases, we analyzed ccRCC primary tumors (PTs) of 47 patients and their inpatient matched distant metastases (METs) by digital and molecular pathology. We quantified the spatial distribution of tumor-infiltrating CD8⁺ T cells, including their co-expression of TOX, indicating T-cell-exhaustion, and measured tertiary lymphoid structures.

Results:

Inflamed, pathologically “hot” PTs were associated with a decreased disease-free survival (DFS), worst for patients with high levels of CD8⁺TOX⁺ T cells. Most METs were pathologically “cold”. Interestingly, inflamed METs showed a relative increase of exhausted, CD8⁺TOX⁺ T cells compared to PTs. Remarkably, integrative analysis of molecular and immune phenotyping results revealed BAP1 and CDKN2A/B deficiency to be associated with an inflamed immune phenotype.

Conclusion:

Our results highlight the importance of integrating molecular alterations and immunoprofiling results, preferably of the metastatic site.

A. Ring¹, B. Balakrishna¹, F. Imkamp¹, S. Burkhard¹, F. Triet¹, F. Brunschweiler¹, C. Grube¹, R. Kouyos¹, R. Bodmer¹, H. Günthard¹, D. Braun¹

High rates of asymptomatic *Mycoplasma genitalium* infections with high proportion of genotypic resistance to first-line treatment azithromycin among men who have sex with men initially presenting with a primary HIV-infection

University of Zurich¹

Introduction:

Mycoplasma genitalium (Mg) is an emerging sexually transmitted pathogen among men who have sex with men (MSM). Resistance to recommended antimicrobial agents are of public health concern. Few data exist on Mg infections in MSM diagnosed with HIV during primary HIV infection.

Methods:

Participants of the Zurich Primary HIV Study (NCT 00537966) were systematically offered a screening for sexually transmitted infections (STI) between April 2019 and September 2020. Screening was performed using an in-house PCR panel comprising Mg including genotypic resistance testing for macrolides and quinolones, *Chlamydia trachomatis* including serovars L1-L3, *Neisseria gonorrhoeae*, *Treponema pallidum* and *Hemophilus ducreyi*.

Results:

We screened 148/266 (55.6%) participants with overall 415 follow-up visits. 91% were MSM. The incidence rate for all STI was 47.0 (95% CI [32.2, 68.6]) per 100 person-years. Mg was the most detected pathogen: Thirty participants (20%) presented with at least one Mg infection, corresponding to a period prevalence of 20.3% and incidence rate of 19.5 Mg infections (95% CI [11.8, 32.4]). Most Mg infections (93%) were asymptomatic, and 9 (30%) participants showed spontaneous clearance. We detected high rates of antibiotic resistance: 73.3% to macrolides, 3.3% to quinolones, and 13.3% resistance to both antibiotics.

Conclusion:

The high prevalence of mostly asymptomatic Mg infections and high rate of spontaneous clearance support cautious initiation for treatment. The high proportion of macrolide-resistant strains suggests that a genotypic determination of resistance should be standard of care. Moxifloxacin should be the preferred treatment option for symptomatic Mg infections among MSM if resistance testing is unavailable.

R. Reimann³, S. Litinov¹, A. Reuss³, A. Economides¹, B. Schreiner², A. Aguzzi³

Tissue clearing enhances accuracy of intraepidermal nerve fibre quantification

CSElab Harvard University¹, Institute of neurology USZ², Institute of neuropathology USZ³

Introduction:

The quantification of intraepidermal nerve fiber density (IENFD) in human skin punch biopsies is a standard diagnostic technique for patients with small fiber neuropathies (SFN). SFN is a disabling chronic condition with an annual incidence of 11.7 cases/100,000 that is characterized by distal burning pain, numbness, paresthesias, and autonomic symptoms. Currently, IENFD is evaluated on 50 µm thick 2D sections and involves visual quantification of all fibers that cross the dermal epidermal interface. Following immunolabeling with the PGP9.5 antibody, the standard protocol calls for counterstaining with Epidermal-dermal boarder is displayed in conventional histology with haematoxylin or periodic acid Schiff (PAS). The procedure is subject to technical artifacts due to cutting and mounting of tissue sections that can lead to underestimation of nerve fiber density. The goal of this project is to improve diagnostic accuracy by quantifying IENFD with an automated system using 3D histology of the entire 3 mm skin punch biopsy. Our initial aim is the establishment of an IENFD3D protocol for routine diagnosis.

Methods:

Entire human skin punches were stained and cleared using an adapted DISCO, an acronym for 3D imaging of solvent-cleared organs. After clearing, intraepidermal nerve fibers were labeled with the PGP9.5 antibody and then analysed with confocal imaging.

Results:

In the search for an appropriate marker of the epidermal dermal on 3D punches, we identified tomato lectin as a suitable stain for the stratum basale of human skin. Applying a higher order polynomial function, we can use this staining in order to fit an area on our dataset. Further we prototyped a script to segment the PGP9.5 labeled nerve fibers. We now plan to validate the new method versus the established standard 2D method on an adequate number of skin samples.

Conclusion:

Clearing techniques have the potential of increasing the accuracy of quantifying IENFD in routine skin punch biopsies. Here we present preliminary data on an IENFD3D protocol that relies on an automated process with staining, imaging and computational assessment. This procedure not only facilitates objective assessment of IENFD, but expands the diagnostic armamentarium for evaluating other markers in peripheral neuropathies in skin punch biopsies.

T. Do¹, C. Lohoff², J. Lu^{2,3}, W. Huber², T. Zenz¹

High-throughput transcriptional profiling of ex-vivo drug effects in patients with leukemia and lymphoma

Department of Medical Oncology and Hematology, University Hospital Zurich¹, Genomic Biology Unit, EMBL Heidelberg², Institute for Computational Biomedicine, University Hospital Heidelberg³

Introduction:

Chronic lymphocytic leukemia (CLL) is a lymphoproliferative disorder of mature B cells and the most common type of leukemia in adults. It is characterized by a heterogeneous genetic landscape which contributes to the differences in disease biology and response to treatment. Based on the concept of the *Connectivity Map* by the NIH LINCS consortium, where gene expression signatures can be used to “connect” to disease states, molecular features and perturbations, we leverage transcriptional profiling of *ex-vivo* treated patient samples to reveal downstream signaling events after drug inhibition of specific pathways. Furthermore, screening drug effects across a large representative cohort allows us to characterize and compare the impact of pathway inhibition between molecular subgroups in CLL, e. g. IGHV mutational status or trisomy 12.

Methods:

Samples from 116 CLL and B cell lymphoma patients were each treated *ex-vivo* with 9 small-molecule inhibitors targeting members of important B cell signaling pathways (BTK, PI3K, AKT, mTOR, MEK, IRAK4, XPO1, MDM2, BRD4, combination of BTK and IRAK4, as well as DMSO as negative control) for 48h. Sample viability before and after drug treatment was determined by flow cytometry. Transcriptional profiling was performed by shallow depth 3'-end bulk RNA sequencing with a median of 9 million reads per sample. Raw reads were mapped and quantified using the alignment-free salmon algorithm. Transcriptional profiles were explored using unsupervised dimensionality reduction and clustering methods. Differentially expressed genes (DEGs) were calculated with the R package DESeq2 by comparing drug- against DMSO-treated conditions after controlling for patient-to-patient variation. Stratified analyses were performed according to available *ex-vivo* drug screening as well as DNA, RNA and proteome information on baseline characteristics.

Results:

So far, 90 out of 116 patients have been profiled (85 CLL, 5 B cell lymphoma patients). Unsupervised clustering revealed patient-to-patient variation as major determinant of the variance in gene expression which is mainly driven by sample viability, IGHV and trisomy 12 status. Consistent with the position of the targets within the respective pathways, DEGs were among others enriched in B cell receptor (BTK, PI3K), Toll-like receptor and chemokine (MEK), or P53 signaling (MDM2) pathways. In total, 8741 genes were found to be differentially expressed when treated with either drug condition (FDR 10%). While PI3K and BTK inhibition led to the most changes (4695 and 4538 DEGs, respectively), the large overlap among these DEGs points to a similar mechanism of action for these drugs (61.7% shared downregulated and 48.5% shared upregulated genes). As a contrary example, MDM2 inhibition compared to the remaining treatments induced a unique gene expression signature reflecting the activation of the P53 pathway.

Conclusion:

Concordant with the *Connectivity Map*, we can show that our transcriptional screening approach is able to “connect” samples to different molecular disease subgroups and pathway perturbations based on the respective gene expression profiles. Further analyses will focus to dissect and stratify differences of drug effects in the light of the heterogeneous genomic landscape. Taking advantage of the large sample cohort, our goal is to construct pathway activity maps for different groups of leukemia and lymphoma samples.

V. Kufner¹, C. Frey², S. Schmutz¹, M. Zaheri¹, S. Burkhard², A. Plate², A. Trkola¹, M. Huber¹, N. Mueller²

Etiology of upper respiratory tract infection in outpatients before and during the SARS-CoV-2 pandemic

Institute of Medical Virology, University of Zurich, Switzerland¹, University Hospital Zurich, Division of Infectious Diseases and Hospital Epidemiology, University Zurich, Zurich, Switzerland²

Introduction:

Acute upper respiratory tract infections (URTIs) are among the most common reasons for consultations in primary care and frequently result in unnecessary antibiotic treatment. In order to improve the clinical decision making, the distinction between viral and bacterial infections is crucial. Here, we investigated the utility of viral metagenomic next generation sequencing (mNGS) in an outpatient setting. By providing a comprehensive viral detection, mNGS may allow for an adjustment of the clinical diagnosis, less antibiotic use and thus impacting antibiotic resistance development.

Methods:

Viral mNGS was applied in a prospective cross-sectional study aimed at investigating the potential of mNGS in immunocompetent patients suffering from an acute URTI. Pharyngeal swabs were collected by GPs and analyzed using viral mNGS. Demographic and medical data were obtained by questionnaire. The detected pathogen(s) were subsequently communicated to both the GPs and the patients. EC approval was obtained (2019-01120).

Results:

A total of 281 patients (mean age 42.5 years, 58% female) were recruited by 21 GPs between 10/2019 and 12/2020. In 209 patients, mNGS identified one or more viral species. In 91% of patients a viral etiology was suspected by the GP. Only 23 patients received antibiotic treatment, of which in four cases mNGS revealed a possible viral cause. Rhinoviruses were the most frequently detected respiratory viral species (20% of all patients). The study showed the seasonal occurrence of influenza viruses in early 2020 and the arrival of the SARS-CoV-2 pandemic in Switzerland in March 2020. During the lockdown, with hygienic measures in place, respiratory viruses other than SARS-CoV-2 continued to be recorded.

Conclusion:

In the case of URTI, viral mNGS analysis enables the re-evaluation of the GPs presumed diagnosis. In certain cases, this may reduce inappropriate antibiotic use. Given future reduction in turnaround time, this method could prospectively influence URTI treatment. On an epidemiological level, mNGS allows to anticipate circulating viruses in a population, guiding informed choices on prevention. Retrospectively, such data could provide essential information on implemented hygiene measures, particularly during a pandemic.

A. Tastanova¹

CITE-seq for liquid and solid tissues: customization towards clinical biomarker discovery

*University of Zurich, University of Zurich Hospital, Department of Dermatology*¹

Introduction:

While great efforts are being made to establish single-cell transcriptomics profiling of clinical material, protein expression of clinically relevant biomarkers has been harder to integrate into existing pipelines. CITE-seq bridges the RNA-protein gap, but has so far primarily been applied to liquid biopsies, which do not require tissue dissociation. Processing of solid biopsies to characterize the tumor microenvironment is an essential next step in applying single-cell technologies to translational studies.

Methods:

Optimization of high dimensional single cell profiling techniques such as CITE-seq (cellular indexing of epitopes and transcriptome by sequencing) and application of multiplex Immunohistochemistry for biomarker discovery and validation in oncology.

Results:

Here, we demonstrate CITE-seq performance and protocol customizations on dissociated tissues such as human skin and primary and metastatic melanoma biopsies on a total of 52,672 cells from 11 solid and 6 liquid primary samples. Analogous to fluorescently activated cell sorting (FACS), we describe gating of cell populations based on transcriptome signatures and setting thresholds for protein expression using cell type-specific ridge plot visualization. For a panel of 97 antibodies, we report on gene and protein expression correlation in liquid and solid sample cohorts. Using peripheral blood mononuclear cells (PBMCs) as a model, we show the effect of enzymatic digestion on transcriptome and epitope expression in immune cell populations. Additionally, we optimized digestion protocols for healthy skin and tumor tissues that yield various cell populations within a given tissue type. Finally, we demonstrate the applicability of CITE-seq for biomarker discovery on metastatic melanoma.

Conclusion:

Our work provides a blueprint and pipeline for CITE-seq to a broad range of clinically relevant samples, thus allowing for an increasingly detailed resolution of solid tissue specimens and enabling translational studies where protein biomarker profiling could provide better functional descriptions of cell states. We believe that the described protocol will find wide-ranging applications for basic and clinical research.

J. Yin¹, L. Frick¹, A. Aguzzi¹

Robust and Versatile Arrayed Libraries for Human Genome-Wide CRISPR Activation, Deletion and Silencing

Institute of Neuropathology¹

Introduction:

CRISPR (clustered regularly interspaced short palindromic repeats)-mediated gene perturbations have enormously expanded the toolkits of genetic screening, and now allow for gene ablation (CRISPRo), activation (CRISPRa), suppression (CRISPRi) and silencing (CRISPRoff). Pooled CRISPR guide RNA (sgRNA) libraries are powerful tools for identifying lethality phenotypes and, to some extent, modifiers of cell-surface markers. Arrayed CRISPR libraries extend the territory of CRISPR to cell-nonautonomous, biochemical, and morphological genetic screens. Yet, very limited resources for arrayed CRISPR screens are available.

Methods:

Here we devise APPEAL (Automated liquid-phase Plasmid assEmbly And cLoning) for massively parallel liquid-phase plasmid cloning and generate two human genome-wide arrayed libraries termed T.spiezzo (CRISPRo, 19'820 plasmids) and T.gonfio (CRISPRa/CRISPRoff, 22'326 plasmids). APPEAL assembles 4 sgRNAs (driven by four different promoters) into a single lentiviral vector, and eliminates the necessity for colony-picking, enabling the automation of high-throughput liquid-phase cloning of libraries in a cost-effective manner. Our sgRNA design algorithm considers common DNA polymorphisms and selects highly specific and non-overlapping sgRNAs to maximize the synergistic activity and versatility of the libraries.

Results:

This 4sgRNA-vector achieves maximal gene-perturbation efficacy while retaining high lentiviral titers. Well-by-well PacBio Single Molecule Real-Time (SMRT) long-read (2.2-kilobase) sequencing of the library confers that ~90% of the plasmid population of each well contained ≥ 3 intact sgRNAs. Furthermore, in a proof-of-concept arrayed screen using CRISPRa sublibrary targeting human transcription factor (1,634 plasmids), several interesting genes, for the first time, were identified could restore the activity of the L444P mutation in lysosome enzyme beta-glucocerebrosidase (GCase), which is the most common risk factor for Parkinson disease and Gaucher diseases. Currently, we are benchmarking our libraries via genome-scale comparison with widely-used pooled libraries.

Conclusion:

Our T.spiezzo and T.gonfio libraries present the next-generation efficacy and versatility and provide a powerful resource for the individual perturbation of each human protein-coding gene.

T.L. Liu¹

Deciphering Prion Toxicity via Genome-Wide CRISPR Activation Synthetic Lethality Screening

Institute of Neuropathology¹, University Hospital Zurich

Introduction:

Protein aggregates are thought to be toxic and major drivers of the devastating neurodegenerative diseases including Alzheimer's, Parkinson's, Huntington's, amyotrophic lateral sclerosis, and prion diseases. However, the underlying mechanism for the toxicity of these protein depositions remains largely unknown. Prion diseases, unlike other neurodegenerative disorders, can be faithfully modeled both in vivo (mouse) and in vitro (eg GT1-7 mouse hypothalamic GnRH neuronal cell line), proving us an ideal system to address the question. Tuning (via CRISPR activation or ablation) mediators of prion toxicity in principle will affect the survival of prion infected cells. Thus, a genome-wide synthetic lethality screening in chronic prion infected cells via CRISPR activation (CRISPRa) or ablation (CRISPRo) pooled libraries will provide us a global understanding of prion toxicity.

Methods:

To conduct the primary screening, we used the mouse CRISPR SAM (Synergistic Activation Mediator) pooled sgRNA library. Firstly, we generated RML6 (Rocky Mountain Laboratory scrapie strain, passage 6)-chronically infected or NBH (non-infected brain homogenate)-treated GT1-7 cell lines, and further stably express dCas9 on these cells. Followed by pooled lentiviral sgRNA library infection, these cells were passaged 2, 4, 8 passages and their genomic DNA were collected respectively and subjected to NGS sequencing.

Results:

In the NGS data, we found both dropout and enriched hits in RML6 infected cells compared to NBH treated cells for all cell passages. We then selected the top 96 dropout hits overlapped in different cell passages for the followed hits. Taking advantage of our self-designed highly efficient 4sgRNA-expressing plasmid cloning method for generating CRISPRa/ko human arrayed libraries in our lab, now we have finished the plasmid cloning for 96 hits and related lentivirus packaging. We will firstly validate hit genes in RML6-infected GT1-7 cell line and further confirm on ME7 prion-infected GT1-7 cell line and COCS prion model.

Conclusion:

Our genome-wide pooled CRISPR screening provides a global understanding and unbiased investigation on prion toxicity. Currently, the CRISPR activation screening is still poorly utilized in the field of neurodegeneration. Thus, our innovative trial using the CRISPR activation screening could greatly extend our understanding on prion toxicity, as some interesting and crucial hits could be discovered that may not be displayed in the CRISPR knockout screening. In addition, both suppressor or mediators of neuronal death, PrPC replication, PrPSc aggregates formation/clearance, or vacuolation could be identified in this screening system. Thus, our project will provide a landscape for the mechanisms underlying prion toxicity.

C. Steinack², A. Gaspert¹, J. Rüschoff¹, F. Gautschi², R. Hage², T. Gaisl², M. Schuurmans², D. Franzen²

Transbronchial cryobiopsy compared to forceps biopsy for diagnosis of acute cellular rejection in lung transplant recipients

University Hospital Zurich (USZ), Department of Pathology and Molecular Pathology¹, University Hospital Zurich (USZ), Department of Pulmonology²

Introduction:

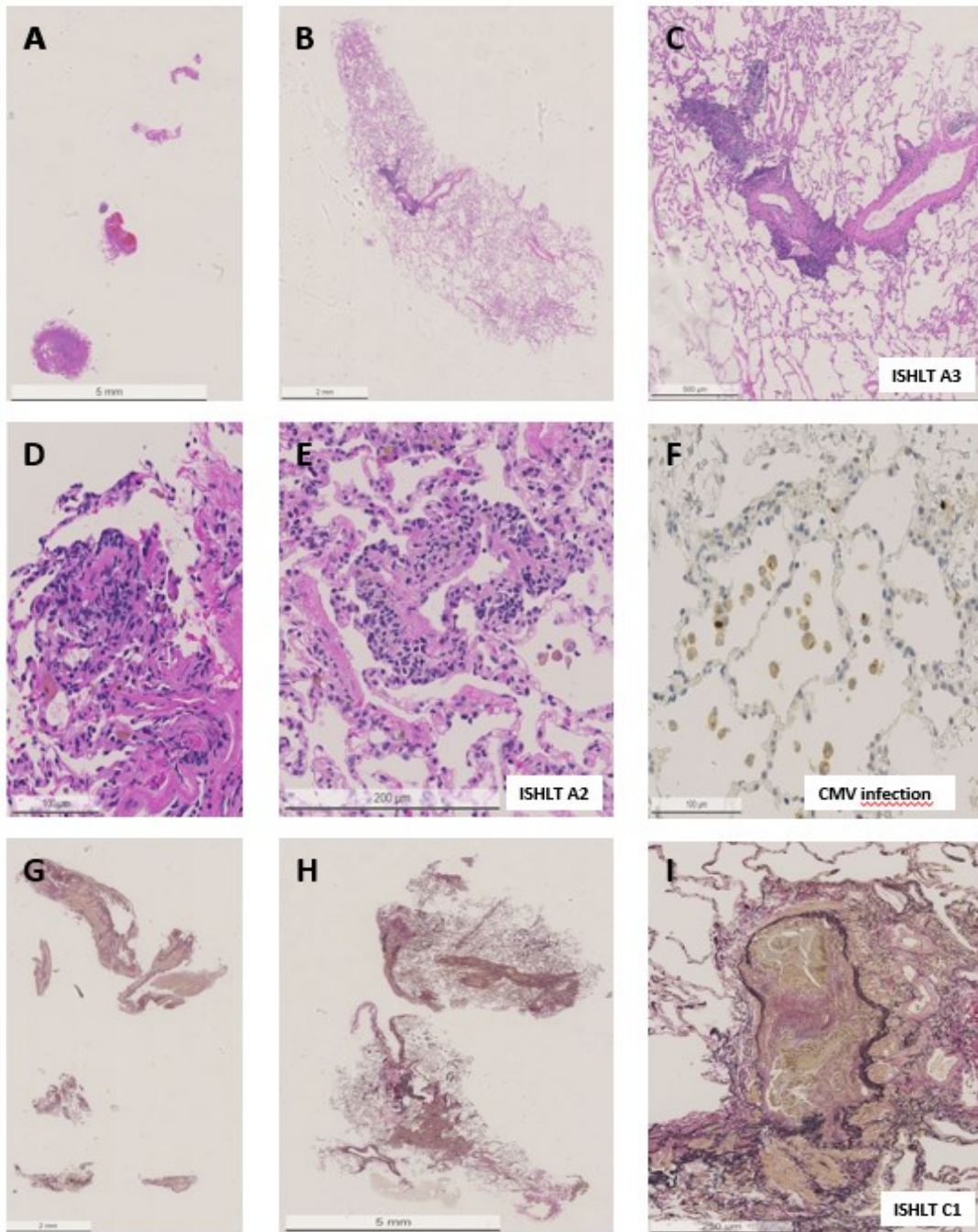
Acute cellular rejection (ACR) is a frequent complication in the first year after lung transplantation (LTx) and an important risk factor for chronic allograft dysfunction (CLAD) and mortality. Diagnosis of ACR is based on histologic findings using lung biopsies primarily by transbronchial forceps biopsy (FB). However, its diagnostic yield (DY) is limited due to the small biopsy size and crush artifacts. Transbronchial lung cryobiopsy (CB) is a more recent technique for diagnosis of interstitial lung diseases with improved DY compared to FB. Yet, there is insufficient evidence for CB in the diagnosis of ACR. This study aims to provide data on DY, safety, and impact on treatment decisions after CB in lung transplant recipients (LTRs).

Methods:

Between December 2019 and January 2021, both FB and CB were obtained serially in LTRs during the same bronchoscopy session. According to our protocol, after 5 FB samples, 2 samples by CB were taken from different lung segments. The biopsies were scored according to the recent ISHLT criteria (A0 - A4) by a dedicated transplant pathologist, assessing FB and CB samples independently. We assessed the severity of bleeding with the Nashville Bleeding Scale (grade 1 – 4), and presence of pneumothorax was assessed by chest radiography.

Results:

Figure 1. FB (A, D, G) are smaller and contain less alveoli and small airways than CB (B, C, E, F, H, I). Patient 1 (A, B, C) shows moderate acute cellular rejection ISHLT Grade A3, Patient 2 (D, E, F) mild acute cellular rejection ISHLT Grade A2 and cytomegalovirus infection and patient 3 (G, H, I) obliterative bronchiolitis ISHLT C1 classified as chronic airway rejection. (A-E: hematoxylin-eosin, F: immunohistochemistry for CMV, G-I: Elastica van Gieson)



Totally, 52 consecutive procedures in 32 LTRs (29 males, median age 58) were performed either as routine surveillance bronchoscopy (n = 41) or as clinically indicated bronchoscopy (n = 11). A retrospective analysis of 260 FB and 103 CB samples was performed. ACR (A1 – A3, minimal – moderate acute rejection) was detected in 17 cases (33%) by CB resulting in a change of immunosuppressive strategy, compared to 6% by FB. CB showed obliterative bronchiolitis in 2 and cytomegalovirus (CMV) infection in 1 case. The biopsy procedures were complicated by moderate (grade 2) bleeding in 19 (36%) cases requiring repeat wedging or installation of diluted vasoactive agents and tranexamic acid. In one procedure bleeding grade 3 was observed demanding introduction of an endobronchial balloon blocker. Pneumothorax occurred in 4 (8%) cases.

Conclusion:

CB provided improved DY of ACR diagnosis with an acceptable safety profile, leading to reclassification and a change of treatment strategy in one third of cases.

C. Steinack¹, P. Saurer¹, F. Gautschi¹, R. Hage¹, G. Ortmanns¹, M. Schuurmanns¹, T. Gaisl¹

Influence of mycophenolate mofetil dosage and plasma levels on the occurrence of chronic lung allograft dysfunction in lung transplants

University Hospital Zurich (USZ), Department of Pulmonology¹

Introduction:

Development of chronic lung allograft dysfunction (CLAD) is a limiting factor for post-lung transplant survival. We evaluated, whether the dose of the immunosuppressant mycophenolate mofetil (MMF) or the active metabolite of MMF, mycophenolic acid (MPA) plasma concentrations, affect the development of CLAD in patients with lung transplantation.

Methods:

In this retrospective, controlled cohort study we recruited 71 patients with a lung transplantation between 2010 and 2014 who provided a consent and did not develop complications within a year after transplantation. The observation period ranged to July 01, 2021. An event-time-analytical Cox proportional-hazards regression model with time-dependent covariates was used to estimate the association of MMF dose, MPA plasma concentrations and CLAD, with adjustment for sociodemographic factors and coexisting conditions.

Results:

Figure 1: Kaplan-Meier failure estimate. Almost 50% of the patients developed CLAD by the 5th post-transplant year.

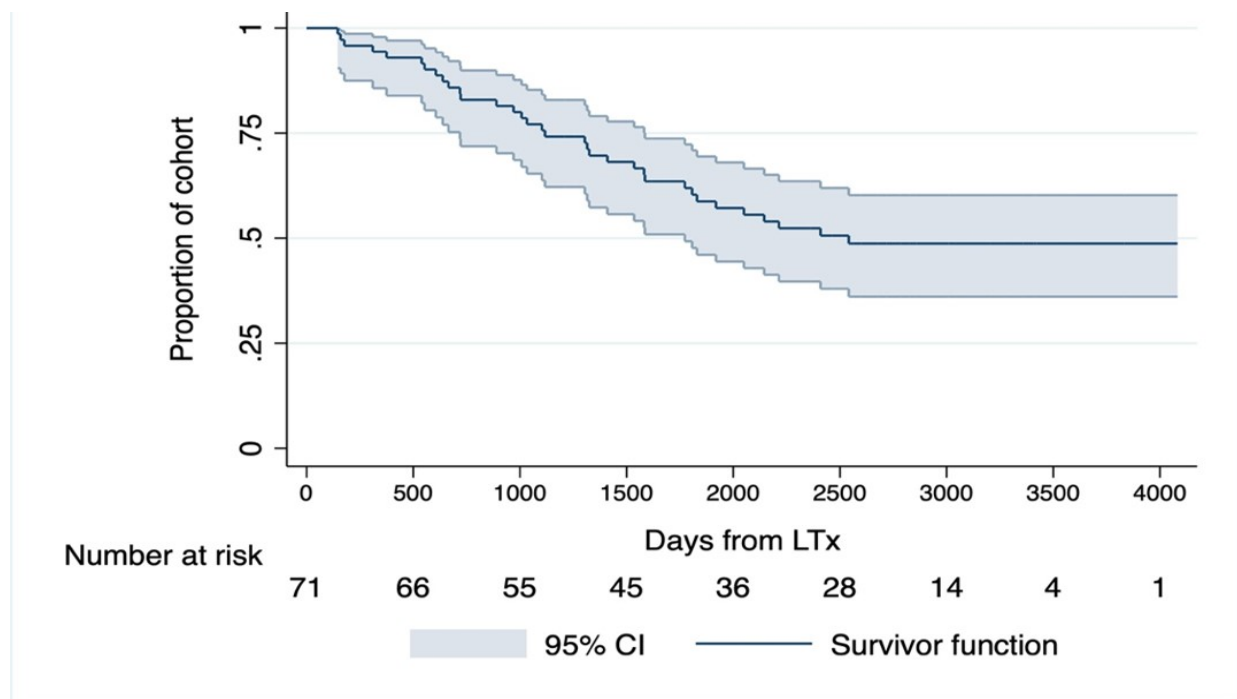


Table 1: Average MMF characteristics by groups. No association could be established between MPA0 or MMF dosage and the occurrence of CLAD.

Variables	Patients without CLAD (n=37)	Patients with CLAD (n=34)	p-value
Average MPA0-level, mg/l	2.8 ± 1.7	3.0 ± 2.3	0.724
Average MMF-dosage, mg	1828 ± 533	1731 ± 676	0.511

37 patients did not develop CLAD (41.3±15.6 years, FEV1 95.5±19.1% predicted) and 34 patients developed CLAD (age 50.9±13.3 years, FEV1 102.2±25.4% predicted). The mean plasma MPA concentration did not differ significantly between the groups without and with CLAD (2.8±1.7 mg/L and 3.0±2.3mg/L; p=.724). While there was a dose-effect relationship between MMF dosage, plasma MPA concentrations, as well as lymphocyte levels, traditional risk factors (age, lung-function, radiological features) predicted CLAD. Continuously measured MPA plasma concentration did not predict CLAD (period of 382.97 patient-years) nor death (period of 472.8 patient-years).

Conclusion:

MMF dosage and MPA plasma concentration were not associated with CLAD development or death. Thus, the MMF dose or MPA plasma concentration are not a primary factor related to chronic organ rejection. CLAD may be influenced by other components of immunosuppression or other factors.

A. La Greca⁵, C. Marchiori³, M. Bogowicz⁴, J. Barranco-García⁵, E. Konukoglu², O. Riesterer¹, P. Balermipas⁵, C. Malossi³, M. Guckenberger⁵, J. van Timmeren⁵, S. Tanadini-Lang⁵

Explainability of deep learning-based HPV status prediction in oropharyngeal cancer

Cantonal Hospital Aarau¹, ETH Zurich², IBM Research Zurich³, Maastrro Clinic⁴, University Hospital Zurich⁵

Introduction:

Patients with human papilloma virus (HPV)-positive oropharyngeal tumors present a more favorable prognosis when compared to their negative counterparts and, thus, hold the potential for treatment de-escalation. In clinical practice, HPV diagnosis requires the analysis of biopsy samples, while medical image analysis tools have been proposed in literature as complementary non-invasive methods. In this study, we aimed to assess the diagnostic accuracy and explainability of deep learning (DL) for HPV status prediction in computed tomography (CT) images of oropharyngeal cancer (OPC).

Methods:

One internal (n1=96) and two public cohorts (n2=498; n3=146) of oropharyngeal cancer patients were employed. The dataset was split in a stratified fashion based on HPV status into training (60%), validation (20%) and test (20%) sets. All CT scans were resampled to a cubic resolution of 2 mm³ and a sub-volume of 96x96x96 pixels was cropped. In the axial direction, the sub-volume spanned from the nasal columella to 96 pixels below, i.e., approximately the start of the lungs. On the axial plane, the crop was centered around the center of mass of the first cranial slice. ModelsGenesis, a publicly available 3D model pre-trained on lung CT, was fine-tuned to perform the classification task. The model with the highest F1-score on the validation set was selected and applied to the test set. Class activation maps (CAMs) of those test subjects belonging to the internal dataset (n=25) were obtained post-hoc by means of two explainability methods, Grad-CAM and Score-CAM. CAMs were posteriorly thresholded using the 70th and 90th percentile values to select the most important regions (CAM70th and CAM90th) and their volumetric overlap with the gross tumor volume (GTV) was calculated using Szymkiewicz–Simpson formula for the primary tumor (GTV_{pt}) and the affected lymph nodes (GTV_{ln}), separately and together (GTV_{all}).

Results:

The model achieved an AUC/accuracy/F1-score of 0.89/0.82/0.78, 0.83/0.77/0.70 and 0.87/0.79/0.74 on the training, validation, and test cohorts, respectively. Figure 1 shows the visual explanation obtained after applying Grad-CAM for two test subjects. Among the 25 internal test cases, 19 were correctly classified. An overlap between GTV_{all} and Grad-CAM70th of at least 0.8 was observed in 21 cases, while the same was true for 24 cases using Score-CAM70th. The overlap coefficients of GTV_{all} with Grad-CAM90th and Score-CAM90th were at least 0.5 for 13 subjects. The mean overlap coefficients of the GTV_{pt}, GTV_{ln} and GTV_{all} with the different CAMs are shown in Table 1.

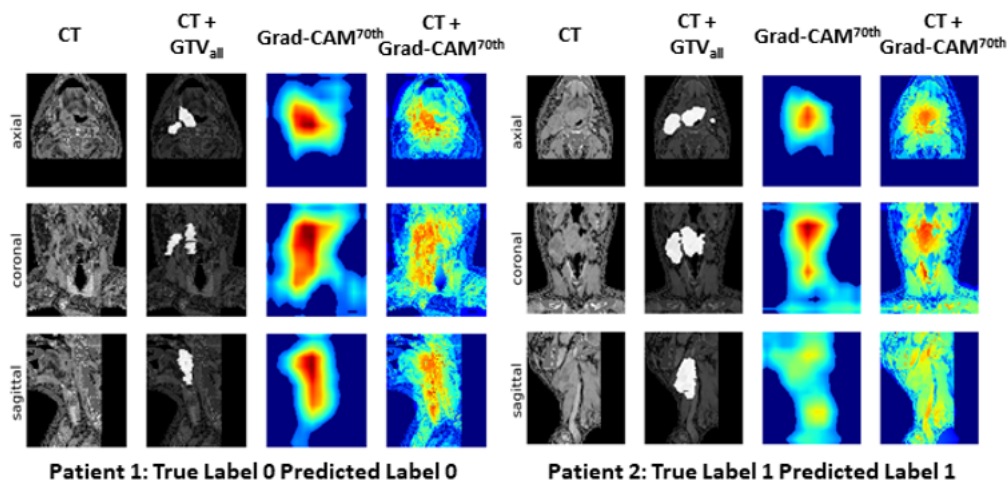


Figure 1 Visual explanation of the HPV status prediction by the deep learning model for two patients from the test set. CT: computed tomography; GTV_{all}: Gross Tumor Volume all (primary tumor and affected lymph nodes); Grad-CAM^{70th}: grad-class activation map thresholded at the 70th percentile value.

	Grad-CAM ^{70th}	Grad-CAM ^{90th}	Score-CAM ^{70th}	Score-CAM ^{90th}
<i>GTV_{pt}</i>	0.88	0.55	0.95	0.60
<i>GTV_{ln}</i>	0.77	0.35	0.96	0.50
<i>GTV_{all}</i>	0.89	0.54	0.94	0.53

Table 1 Mean overlap coefficients among the 70th-percentile- and 90th-percentile-thresholded heatmaps of the 25 internal test subjects and their corresponding primary tumor and affected lymph nodes.

Conclusion:

Two explainability methods were employed to explore which CT regions were the most relevant in HPV status prediction by a 3D DL model. Our study showed a promising classification performance and volumetric overlap between the resulting heatmaps and the *GTV_{pt}* and *GTV_{ln}*.

R. Schimmer³, L. Kovtonyuk³, N. Klemm³, J. Fullin³, S. Stolz³, J. Mueller³, F. Caiado³, K. Kurppa², B. Ebert¹, M. Manz³, S. Boettcher³

TP53 mutations confer resistance to hypomethylating agents and BCL-2 inhibition in myeloid neoplasms

Department of Medical Oncology, Dana-Farber Cancer Institute, Boston, MA, United States¹, Institute of Biomedicine and MediCity Research Laboratories, University of Turku, and Turku Bioscience Centre, University of Turku and Åbo Akademi University, Turku, Finland², University of Zurich & University Hospital Zurich³

Introduction:

TP53 mutations are found in up to 5-10% in acute myeloid leukemia (AML) and myelodysplastic syndrome (MDS), further enriched in patients with therapy-related myeloid neoplasms. *TP53*-mutant AML/MDS have inferior response rates and extremely poor survival with standard induction chemotherapy, even after allogeneic hematopoietic stem cell transplantation. The hypomethylating agents (HMAs) decitabine and azacitidine +/- the BCL-2 inhibitor venetoclax have recently emerged as promising therapeutics for patients with *TP53*-mutant myeloid neoplasms. However, due to so far conflicting results from various clinical studies, it remains unclear whether *TP53* mutations are predictive of outcomes to treatment with HMAs. We therefore set out to clarify the impact of *TP53* mutational status on treatment efficacy with HMAs +/- venetoclax.

Methods:

We made use of CRISPR-Cas9-engineered isogenic human AML cell lines harboring the six most frequent *TP53* missense mutations (R175H, Y220C, M237I, R248Q, R273H and R282W), null (KO) and wildtype (WT) alleles. Drug sensitivity assays measuring cell viabilities in response to monotherapies with HMAs and venetoclax as well as combinatorial therapies with HMAs + venetoclax were performed using the various cell lines. To demonstrate clonal expansion, *in vitro* competition assays were performed in which fluorescently-labeled isogenic MOLM13-*TP53* cell lines were seeded in a 1:1 ratio with MOLM13-*TP53*^{WT} cells and co-cultured in the continuous presence of DMSO, HMAs, venetoclax or HMAs + venetoclax. To validate results *in vivo*, we performed xenograft experiments by engrafting NOD/SCID/IL2R γ null (NSG) mice with a 1:1 mixture of fluorescently-labeled *TP53* WT and *TP53* KO or *TP53* R248Q/- MOLM13 cells followed by treatment with vehicle, venetoclax, HMAs, or HMA + venetoclax, ultimately assessing relative contributions of *TP53* WT and *TP53* mutant MOLM13 cells to the leukemia burden in bone marrow. Lastly, we performed survival analysis of NSG mice engrafted with either *TP53* WT, *TP53* KO or *TP53* R248Q/- MOLM13 cells expressing luciferase and consequently treated with either vehicle, HMAs, or azacitidine + venetoclax.

Results:

Isogenic cell lines with *TP53* mutations demonstrated significantly increased resistance to all drug monotherapies. Combining venetoclax with HMAs resulted in an additive but no synergistic drug effect irrespective of the *TP53* genotype. This increased resistance of *TP53*-mutant cells towards HMAs +/- venetoclax translated into a strong competitive advantage with statistically significant outgrowth over *TP53* wildtype cells in *in vitro* competition assays. The addition of venetoclax to HMAs did not prevent clonal expansion of *TP53*-mutant AML cells but led to a significantly accelerated outgrowth. *In vivo*, all treatment regimens with HMAs +/- venetoclax favored selective outgrowth of MOLM13 AML cells carrying *TP53* mutations. Ultimately, *TP53* mutations were associated with decreased survival of leukemic mice when treated with HMAs +/- venetoclax.

Conclusion:

Using multiple independent isogenic, CRISPR/Cas9-engineered, *TP53*-mutant human AML cell line models, we demonstrate that the efficacies of monotherapy with the HMAs and venetoclax, as well as combination therapies of HMAs + venetoclax depend on the *TP53* mutational status of AML cells. *TP53* mutations confer resistance towards HMAs +/- venetoclax *in vitro* and *in vivo* that translates into clonal expansion of *TP53*-mutant over *TP53* WT cells as well as decreased survival of leukemic mice. Our preclinical data strongly support the emerging clinical observation that although HMAs +/- venetoclax retain clinically meaningful activity in *TP53*-mutant AML patients, *TP53* mutations still predict inferior responses and survival compared to AML patients with a wildtype *TP53* status. Thus, to overcome the negative impact of *TP53* mutations in AML, novel therapeutic approaches are urgently needed.

K. Burelo^{3,4}, F. Costa^{3,4}, G. Ramantani^{2,4}, G. Indiveri^{1,4}, J. Sarnthein^{3,4}

A neuromorphic spiking neural network detects epileptic high frequency oscillations in the scalp EEG

ETH¹, Universitäts-Kinderspital Zurich², UniversitätsSpital Zurich³, University of Zurich⁴

Introduction:

Interictal High Frequency Oscillations (HFO) are measurable in scalp EEG. This development has aroused interest in investigating their potential as biomarkers of epileptogenesis, seizure propensity, disease severity, and treatment response. The demand for therapy monitoring in epilepsy has kindled interest in compact wearable electronic devices for long-term EEG recording. Spiking neural networks (SNN) have emerged as optimal architectures for embedding in compact low-power signal processing hardware.

Methods:

We analyzed 20 scalp EEG recordings from 11 pediatric focal lesional epilepsy patients. We designed a custom SNN to detect events of interest (Eol) in the 80-250 Hz ripple band and reject artifacts in the 500-900 Hz band.

Results:

We identified the optimal SNN parameters to detect Eol and reject artifacts automatically. The occurrence of HFO thus detected was associated with active epilepsy with 80% accuracy. The HFO rate mirrored the decrease in seizure frequency in 8 patients ($p = 0.0047$). Overall, the HFO rate correlated with seizure frequency ($\rho = 0.90$ CI [0.75 0.96], $p < 0.0001$, Spearman's correlation).

Conclusion:

The fully automated SNN detected clinically relevant HFO in the scalp EEG. This study is a further step towards non-invasive epilepsy monitoring with a low-power wearable device.

TP53-mutant acute myeloid leukemia cells are relatively resistant against CAR T cell-mediated killing*Clinic of Medical Oncology and Hematology¹, ETH Zürich, D-BSSE²***Introduction:**

Acute myeloid leukemia (AML) is a neoplastic disease characterized by rapidly proliferating hematopoietic progenitor cells, often with myeloid lineage differentiation. With current treatment regimens only <30% of all patients with newly diagnosed disease are alive 5 years after initial diagnosis. This constitutes a major unmet clinical need. About 10% of de novo AML and 30% of therapy-related AML cases carry TP53 mutations, which are associated with a particularly bad prognosis.

CAR T-cell therapy is a new form of cancer treatment, mostly shown to be effective in hematological malignancies arising from the more mature B-cell compartment. Developing effective and safe CAR T-cell therapies for myeloid malignancies like AML is currently a major effort in research.

Methods:

Isogenic MOLM-13 AML cell lines with TP53 wildtype, knockout and the six most common miss-sense mutations were used in this study. In vitro cellular killing assays were analyzed using an LSR II Fortessa 4L equipped with a high throughput sampler (BD Biosciences). For in vivo assays, NSG mice were engrafted with MOLM-13 cells expressing luciferase and treated with 2-10Mio CD33-directed CAR T-cells and T-cell controls. Quantification was performed by in vivo D-luciferin bioluminescence imaging (PerkinElmer). Fluorescent live-cell imaging and single-cell tracking and quantification were performed using a Nikon-Ti Eclipse equipped with a motorized stage (Orca Flash 4.0 V2, Hamatsu) and a culture chamber and using a custom-made tracking and analysis software.

Results:

We performed a series of in vitro and in vivo experiments, to analyze whether the TP53-status of AML cells influences the resistance to CAR T-cell killing. When we co-incubated CAR T-cells together with isogenic MOLM-13 cells differing only in TP53-status, observable differences started upon 3 days of co-culture: CAR T-cells co-incubated with MOLM-13 cells harboring a TP53 knockout miss-sense mutation proliferated less, upregulated exhaustion markers and were not able to eradicate target cells in vitro. We did not observe significant differences in target antigen expression or in expression of the immune checkpoint molecule PD-L1 between knockout and wildtype AML cells. Higher effector-to-target ratios were needed to overcome this relative resistance. To explore further the underlying mechanistic difference between TP53 knockout and wildtype target cell killing, we imaged the CAR T-cell killing of target cells in microwells by fluorescence live-cell microscopy and could observe a significantly longer duration of the immunological synapse between CAR T-cells and knockout than wildtype AML cells before CAR T-cell killing. Finally, in a therapeutic in vivo model, NSG mice engrafted with MOLM-13 harboring wildtype TP53 were cured by the infusion of 2Mio CD33-directed CAR T-cells on day 7 after leukemia-cell transfer, whereas mice engrafted with MOLM-13 with a TP53 knockout succumbed to leukemic disease within 4 weeks. Consistent with our in vitro results, this relative resistance could be overcome by increasing the effector-to-target ratio by infusion of up to 10Mio CAR T-cells.

Conclusion:

Taken together, our results show a relative resistance of AML cells harboring a TP53 knockout or a miss-sense mutation to CAR T-cell killing leading to increased exhaustion and decreased proliferation of effector cells starting on day 3 of co-incubation. As we could not observe antigen loss or increased immune checkpoint expression on target cells, we hypothesize that this relative resistance is due to an intrinsic apoptosis defect of TP53-deficient AML cells leading to prolonged antigen exposure, activating intracellular signaling and ultimately exhaustion of CAR T-cells. To challenge our working hypothesis and elucidate the mechanism behind the observed resistance we are currently further characterizing both the effector (CART) and target (MOLM-13) cells using mRNA sequencing, live-cell imaging and functional assays.

I. Miescher², P. Wolint², C. Opelz², J. Snedeker¹, P. Giovanoli², M. Calcagni², J. Buschmann²

Impact of hyaluronic acid on rabbit Achilles tenocytes in vitro with respect to proliferation and gene expression

Balgrist Campus and ETH Zurich¹, Plastic Surgery and Hand Surgery, USZ²

Introduction:

Tendon injuries go ahead with a long healing time because of the poor regenerative capacity of the tissue. Re-rupture, scarring, adhesion to the surrounding tissue and joint stiffness are common clinical problems. Despite progress in the treatment options, tendon repair remains difficult and methods to improve tendon healing are of big interest.

In our study, we focus on high molecular weight (HMW) hyaluronic acid (HA), a lubricating biomolecule present in the synovial fluid. We plan to use HA incorporated into an anti-adhesion implant in a rabbit Achilles tendon full laceration model to reduce adhesion due to its inherent barrier function. Before starting the in vivo experiments, we studied the effects of HMW HA supplementation on rabbit Achilles tenocytes in vitro regarding cell proliferation and gene expression.

Methods:

Achilles tenocytes from three New Zealand White rabbits were isolated by the migration method and cultivated in culture medium, before seeding into 6-well plates. Growth curves \pm HA were performed by AlamarBlue™ assay. Medium containing HA was supplemented each day over a period of 14 days (control: no HA). RNA-Isolation was performed on days 3, 7 and 14, followed by cDNA-transcription and qPCR analysis, assessing matrix turnover, proliferation, fibrosis, remodelling, inflammation and resolution markers. Furthermore, rabbit tenocytes were exposed to Lipopolysaccharides (LPS) to mimic inflammation, to Lipoxin A4 to mimic resolution, or subsequently to both chemicals to assess inflammatory and pro-resolving markers by qPCR.

Results:

AlamarBlue Assay did not show any differences in proliferation. This result was confirmed by the qPCR data with the proliferation marker ki67. Moreover, a downregulation of collagen 1 and collagen 3 was observed. Expression of Lysil oxidase (LOX), a collagen cross-linking enzyme, was as well reduced. However, MMP-2, a metalloproteinase, which degrades collagen fragments, was slightly upregulated. Expression of IL-6, a pro-inflammatory marker, was increased over time. The expression of the pro-resolving marker ALOX15 remained at the same level except on day 3, when the expression was slightly, but significantly lower than in the control group. LPS significantly induced expression of IL-6. Addition of Lipoxin A4 after LPS treatment reduced the upregulation, but expression was still significantly higher than in the control group. Cells with HA supplementation showed a somewhat lower IL-6 expression level in both treatments. Expression of ALOX15 was not affected by the LPS supplementation or by the combination of LPS and Lipoxin A4. However, the expression level of ALOX15 in cells without HA treatment was slightly lower than in the control group. Cells cultured with HA expressed moderately higher but not statistically different ALOX15 levels.

Conclusion:

Gene expression of matrix components was downregulated by HMW HA supplementation in vitro. This result is important regarding the incorporation of HA into a planned anti-adhesion implant material because it has been reported that less matrix components favors anti- in vivo. In addition, the observed slight upregulation of MMP-2 might influence the anti-adhesive effect positively as well because collagen fragments could be degraded to a higher extent. On the other hand, it has been shown that IL-6 enhances collagen synthesis in dermal fibroblast and the observed higher levels of IL-6 could therefore promote adhesion. It has been shown that IL-6 is important in the acute phase. The effect of HA regarding inflammation reactions in vivo remains to be investigated because on the one hand, IL-6 induces pro-inflammatory reactions, but on the other hand, is involved also in processes resolving inflammation. Overall, HMW HA is a promising material to fabricate an anti-adhesive implant. After degradation, the dissolved HA molecules influence tenocytes in a way that is compatible with our anti-adhesion strategy.

B. Nguyen-Sträuli¹, H. Frauchiger-Heuer¹, J. Talimi-Schnabel¹, J. Loesch¹, D. Vorburger¹, K. Dedes¹

Single-incision approach for breast-conserving surgery and sentinel node biopsy - feasibility of round block technique

University Hospital Zurich, Department of Gynecology¹

Introduction:

Breast-conserving therapy (BCT) has become the standard of care for most patients with early breast cancer. Similarly, sentinel lymph node biopsy (SLNB) has proven to be as effective as axillary lymph node dissection in early breast cancer. As a result, breast surgery has become less radical in favour of improved cosmetic outcomes and minimal functional deficiency over time. Reconstruction algorithms for oncoplastic breast-conserving surgery (OPS) have been described with the purpose to overcome breast asymmetry and to improve the quality of life for women. With OPS techniques, BCT has become an equal alternative to mastectomy also in larger and multifocal tumours. The round block technique (RBT) was first described by Louis Benelli in 1990 and has found a key place as an oncoplastic technique used in periareolar lesions since then, particularly in breasts with moderate ptosis or hypertrophy. Conventional BCS contains one incision for the tumour resection and another incision in the axilla for sentinel lymph node (SLN) retrieval. As a result, phenomena such as axillary retraction, impaired shoulder movement, lymphoedema, or axillary neuralgia are not uncommonly observed and impair cosmetic outcome and quality of life. Recently, minimal-access breast surgery (MABS) has been promoted by several authors using a lateral, radial, inframammary, periareolar or axillary incision for both tumour resection and SLN retrieval. The primary objective of this study was to evaluate the single-incision RBT for tumour resection of breast cancer and SLN retrieval, with this focusing on oncological safety regarding local control and feasibility of SLN retrieval through round block incision. The secondary objective was to determine feasibility of tumour resection located in medial upper and lower quadrants using single-incision RBT.

Methods:

A retrospective observational case-control study was conducted from January 2017 to October 2021. The study population consisted of two groups. In both groups, breast-conserving surgery was carried out through the round-block technique. SLN retrieval was performed using the round-block incision in the study group, while in the control group, SLN retrieval was achieved as the standard by a second skin incision in the axilla. The decision to perform conventional BCT with two incisions or the single-incision approach was made according to the four physicians' choice concerning breast size, shape, and tumour localization. Patient and tumour characteristics, surgical characteristics, complications, and reoperation rates were analyzed in both groups using the clinical information system. The local ethical committee KEK approved the study in Zurich. Data were analyzed using SPSS 26.0.

Results:

Overall, 134 patients met the inclusion criteria, of whom 86 patients underwent breast-conserving surgery and SLN retrieval using the single-incision approach and 48 patients had a second skin incision in the axilla for SLN retrieval. SLN retrieval was successful in 97.7% of patients in the single-incision group, with most of the tumours located in the upper outer (47.7%) and upper inner quadrant (27.9%). Axillary neuralgia and axillary skin retraction were significantly more often observed in the control group. We observed a greater tendency towards breast seroma in the study group and axillary seroma in the control group. Both groups showed no differences regarding reoperations due to complications, revisions due to positive margins, locoregional recurrence, or death. The mean follow-up was 11 months.

Conclusion:

The single-incision approach through the round-block technique is as safe and effective as the standard approach regarding lymph node staging and complete tumour resection and seems to be suitable for all quadrant tumours.

T. Diteepeng¹, Y. Puspitasari¹, S. Ministrini^{1, 5}, D. Vdovenko⁶, A. Akhmedov¹, F. Ruschitzka², J. Beer^{1, 3}, G. Camici^{1, 2, 4}, M. Luciani^{1, 3}

Protein misfolding: an additional mechanism in the heart-brain communication after ischemic stroke

Center for Molecular Cardiology, University of Zurich, Schlieren, Switzerland¹, Department of Cardiology, University Heart Center, University Hospital Zurich, Zurich, Switzerland², Department of Internal Medicine, Cantonal Hospital of Baden, Baden, Switzerland³, Department of Research and Education, University Hospital Zurich, Zurich, Switzerland⁴, Internal Medicine, Angiology and Atherosclerosis, Department of Medicine and Surgery, University of Perugia, Perugia, Italy⁵, Maisonneuve-Rosemont Hospital Research Center, Département de Microbiologie, Infectiologie et Immunologie, Université de Montréal, Montréal, Quebec, Canada⁶

Introduction:

Acute ischemic stroke is associated with a high risk of non-neurological complications which include cardiovascular dysfunction, reinforcing the biological paradigm of the heart-brain crosstalk on an etiological level. Although it has been widely accepted that protein misfolding occurs in the setting of local ischemic damage in the suffering milieu of the brain after a stroke, little is known about the possible systemic effects occurring in light of the physio-chemical properties of misfolded proteins (MPs). In the present study, we aim to evaluate the occurrence, the magnitude, the origin and the possible traffic routes for MPs elicited by an acute ischemic event. Particular attention will be given to the biological and functional response of the heart under these pathologic conditions.

Methods:

In order to induce acute cerebral ischemic injury, transient-left middle cerebral artery occlusion (tMCAO) with 45 minutes of ischemia followed by 24 hours of reperfusion was performed using 3 months-old C57BL/6J wild type males; sham-operated wild type males were employed as control. After 24-hours post-ischemia, the morpho-functional assessment was applied. Heart, brain, blood and lymph nodes along with other tissues were harvested for transcriptional and translational analysis for the localization and semi-quantification of misfolded protein aggregates (oligomers) and the biological response of the myocardium.

Results:

Our preliminary results showed that acute ischemic stroke was associated with a significantly increased presence of oligomers in the myocardial tissue, compared to sham ones. In addition, increased oligomers were detected in axillary lymph nodes harvested from stroke mice, suggesting a possible MPs' pathophysiological route. Concerning the myocardium, transcriptional and translational analyses showed an alteration of protein homeostasis including protein folding (heat shock protein 90; HSPA5), unfolded protein response (UPR) (ATF6 and CHOP) and oxidative stress response (catalase; Cat) after an ischemic stroke indicating a relevant role of the ATF6 axis.

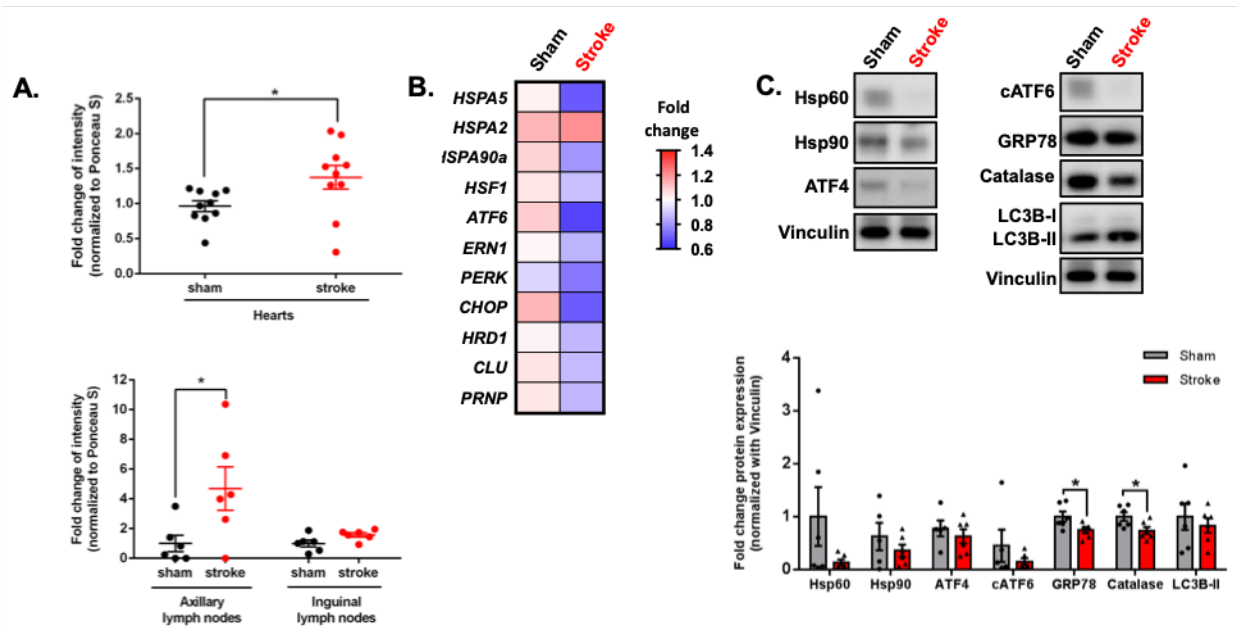


Figure 1: Acute ischemic stroke increases the presence of oligomers and impairs the protein homeostasis in the heart. Dot blot assay shows an increased relative level of misfolded oligomers in the heart, similar to axillary lymph nodes after ischemic stroke (A). qPCR (B) and western blot assay (C) show the alteration of protein homeostasis in the myocardium after ischemic stroke

Conclusion:

Obtained preliminary data suggest an increased production of oligomers in acute ischemic events not only locally but also in distant organs possibly due to the spreading of MPs and to the reduced resistance against proteotoxicity in the setting of acute stress. Further experiments will be conducted in order to understand the cardiac functional response to acute ischemic stroke and provide a deeper insight into MPs pathophysiology.

L. Banke^{2, 5}, R. Wegmann⁵, K. Dedes¹, D. Franzen⁴, P. Bode³, M. Zoche³, F. Arnold³, M. Manz², H. Moch³, C. Britschgi², B. Snijder⁵

Updated results of pharmacoscopy on fluid samples from patients with solid tumors

Department of Gynecology, Comprehensive Cancer Center Zurich, University Hospital Zurich¹, Department of Medical Oncology and Hematology, Comprehensive Cancer Center Zurich, University Hospital Zurich², Department of Pathology and Molecular Pathology, Comprehensive Cancer Center Zurich, University Hospital Zurich³, Department of Pulmonology, Comprehensive Cancer Center Zurich, University Hospital Zurich⁴, Institute of Molecular Systems Biology, ETH Zurich⁵

Introduction:

In patients with metastatic solid tumors there is an urgent need for predictive biomarkers. Fluids containing malignant cells, like pleural effusion or ascites, are easily accessible and could potentially provide information on drug sensitivities *ex vivo*.

Methods:

Image-based single-cell drug response testing (pharmacoscopy) on fluid samples containing tumor cells is used to investigate drug response variability on an intra- and interpersonal level. A population of malignant and healthy cells is incubated with a drug panel (24 hours). After staining with fluorescent antibodies, cells are imaged using automated microscopy and then classified using convolutional neural networks. Multiplexed transcriptomic data is then correlated with the *ex vivo* drug responses. At a later stage, genomic and transcriptomic data from baseline RNAseq and targeted next generation sequencing will be matched with clinical and drug response data.

Results:

The clinical cohort currently includes 205 samples from 142 patients. 70% of included patients had a sample with sufficient viability and cancer cell content permitting pharmacoscopy. 79 of those are samples from lung adenocarcinoma (LUAD), comprising the largest subcohort. In 21 patients, pharmacoscopy was repeated on specimens taken within a short period of time, for which we observed a high intra-individual reproducibility of the drug response profiles.

In a patient with LUAD harboring a BRAF p.V600E mutation, pharmacoscopy was able to predict clinical response to targeted treatment with dabrafenib/trametinib. Multiplexed RNAseq under multiple drug conditions (DRUGseq) revealed downregulation of genes associated with MAPK pathway activity upon *ex vivo* treatment with Dabrafenib + Trametinib. This observation was consistent with decreased phospho-ERK levels measured in pharmacoscopy.

So far, 76 samples underwent comprehensive genomic profiling (Foundation One CDx) and on 114 samples bulk RNAseq was performed for baseline expression.

Conclusion:

Pharmacoscopy on fluid samples is feasible to explore drug responses in solid tumors. Further integration of drug response profiles with molecular measurements including transcriptomic and genomic profiling will provide comprehensive insights into the molecular mechanisms underlying drug response variability and will help to develop clinical predictive relevance.

D. Villars¹, L. Hänsch¹, M. Silginer¹, T. Weiss¹, M. Weller¹, P. Roth¹

Integrin-specific CAR T cells for the treatment of glioblastoma

*Molecular Neurooncology*¹, University Hospital Zurich

Introduction:

With limited efficacy of existing therapies for glioblastoma, hope lies in innovative treatment strategies. Chimeric antigen receptor (CAR) T cells have shown therapeutic success in patients with hematological malignancies and are now also investigated for different solid tumor types, including glioblastoma. αv integrins are overexpressed in glioma cells and have already been used as targets for small molecule inhibitors and antibodies. Here, we propose that these molecules serve as an ideal target structure for CAR T cell-based immunotherapy.

Methods:

Integrin-specific CAR T cells targeting all αv integrins or specific heterodimers (pan- αv , $\alpha v\beta 3$, $\alpha v\beta 5$ and $\alpha v\beta 8$) were generated by transducing primary human T cells from healthy donors with a lentiviral vector expressing a second generation CAR. Activity and specificity of CAR T cells was determined by co-culture assays with different glioma cells. Efficacy of CAR T cells to control tumor growth in vivo was investigated in clinically relevant orthotopic xenograft glioma mouse models.

Results:

All integrin-targeting CAR T cells showed strong anti-glioma activity in vitro. Long-term killing assays, repetitive killing assays and cytokine-release measurements showed highest activity of $\alpha v\beta 5$ and $\alpha v\beta 8$ integrin-specific CAR T cells. Antigen specificity of these cells was confirmed as target cells with a CRISPR/Cas9-mediated knockout of the target antigen were resistant to CAR T cell-mediated cytotoxicity. Additionally, intratumoral injection of $\alpha v\beta 5$ or $\alpha v\beta 8$ CAR T cells significantly prolonged the survival and cured a substantial fraction of glioma-bearing NOD Scid mice in two different xenograft models.

Conclusion:

We show strong and integrin-specific anti-glioma activity of the newly generated CAR T cells in vitro. Furthermore, $\alpha v\beta 5$ and $\alpha v\beta 8$ CAR T cells exerted strong therapeutic activity in two different xenograft glioma models in vivo. These data support the evaluation of integrin-specific CAR T cells as a therapeutic strategy in clinical neuro-oncology.

Clofazimine affects macrophage activity *in vitro* and *in vivo*

Universität Zürich¹, Universitätsspital Zürich²

Introduction:

Combined antibiotic treatment of *Mycobacterium tuberculosis* (MTB) infection has saved millions of patients over the last century. However, the global rise of multidrug resistant MTB (MDR-MTB) necessitates novel treatment strategies. One of the re-purposed drugs for the treatment of MDR-MT is Clofazimine (CLO), which is mostly effective in the late phase of treatment, which aims to clear persisting bacteria. We know that besides the anti-mycobacterial effects, CLO has immune-modulatory effects on the host. How exactly CLO acts, which pathways are being altered and to which extent this contributes to mycobacterial clearing is not yet understood. We hypothesize, that contrary to previous findings, CLO is a significant immune system modulator and a very potent booster-tool and should not be primarily considered an antibiotic drug per se. The immune-modulatory effects may contribute as much to the overall treatment efficacy of CLO as direct anti-mycobacterial activity.

Methods:

To assess the effects of CLO on macrophages *in vitro*, we incubated mouse bone marrow derived macrophages (BMDM) over a range of clinically relevant doses of CLO and assessed phenotypical changes as gauged by the expression of cell surface markers as well as the phagocytic capacity using pHrodo labelled *E. coli* cells. Next, we assessed the *in vitro* changes in the transcriptome of CLO treated and untreated BMDMs after 48h incubation by bulk RNAseq. To assess the *in vivo* effects of CLO, we subjected C57Bl/6 mice to oral application of CLO (25 mg/kg for 6 weeks), and measured differences in the expression of activation markers in myeloid cells in the lymphatic tissue. To assess the impact of CLO treatment on macrophage functionality *in vivo*, we harvested peritoneal macrophages from treated mice and assessed their phagocytic capacity.

Results:

In vitro CLO significantly downregulated CD206, a surface marker associated with cell homeostasis in a dose dependent way and increased the phagocytic activity of BMDM by 1.3 fold (24h) or 3.3 fold (48h) following exposure to 1 µg/ml CLO. Additionally, the transcriptome revealed that CLO treated BMDM upregulated a pro-inflammatory transcriptional program. We found 1061 significantly up- or down-regulated genes (Log2 fold threshold = 1.5, p-value threshold = 0.05) and 82 significantly up- or down-regulated pathways (Log2 Ratio = 1, Input DEG P-value = 0.01). Strikingly, the Tumor necrosis factor (TNF) pathway, which has been repeatedly linked to play a central role in controlling MTB infection, was repeatedly found to be highly enriched in GSEA, KEGG and GO enrichment analyses. In line with our *in vitro* data, phagocytic activity of peritoneal macrophages significantly increased by 2.2 fold in mice exposed to CLO. Notably, the proportion of myeloid cells in all organs analysed (liver, blood, lymph nodes, spleen, lung and peritoneal macrophages) were similar irrespective of CLO treatment.

Conclusion:

In summary, CLO has marked effects on the macrophage phenotype as well as on their functionality as evidenced by *in vitro* and *in vivo* experiments. Future experiments with a CLO-resistant MTB strain will assess the contribution of the immune modulatory effects on treatment outcomes.

C. Pasin^{3,4}, A. Huang², C. Cicin-Sain², S. Epp⁴, A. Audigé⁴, A. Bankova², N. Wolfensberger², O. Viliñovszki², G. Nair², P. Hockl², U. Schanz², J. Nilsson¹, R. Kouyos^{3,4}, B. Hasse³, A. Zinkernagel³, A. Trkola⁴, M. Manz², I. Abela^{3,4}, A. Müller²

Antibody Response to SARS-CoV-2 Vaccination in Patients Following Allogeneic Hematopoietic Cell Transplantation

Department of Immunology, University Hospital Zurich, Switzerland¹, Department of Medical Oncology and Hematology, University Hospital Zurich, Switzerland², Division of Infectious Diseases and Hospital Epidemiology, University Hospital Zurich, Switzerland;³, Institute of Medical Virology, University of Zurich, Switzerland⁴

Introduction:

Vaccines against SARS-CoV-2 have been rapidly approved. While pivotal studies were conducted in healthy volunteers, little information is available on safety and efficacy of mRNA vaccines in immunocompromised patients, including recipients of allogeneic hematopoietic cell transplantations (allo-HCT).

Methods:

Here, we used a novel assay to analyze patient- and transplant-related factors and their influence on immune responses over an extended period of time (up to 6 months) to the SARS-CoV-2 vaccination in a large and homogenous group of allo-HCT recipients at a single center in Switzerland.

We examined longitudinal antibody responses to SARS-CoV-2 vaccination with BNT162b2 (BioNTech/Pfizer) or mRNA-1273 (Moderna) in 110 allo-HCT recipients and 86 healthy controls. Seroproliling recording IgG, IgA, and IgM reactivities against SARS-CoV-2 antigens (receptor-binding domain (RBD), spike glycoprotein subunits S1 and S2, and nucleocapsid protein (N)) was performed prior to vaccination, prior to the 2nd dose, and 1, 3, and 6 months (m) after the 2nd dose. Patients were stratified to three groups (A) 3-6m post HCT; (B) 6-12m post HCT; and (C) >12m post HCT.

Results:

Individuals early post allo-HCT (3-6 and 6-12m post HCT) developed significantly lower antibody titers after vaccination compared to patients >12m post allo-HCT and healthy controls ($p < 0.001$). Within the cohort of HCT recipients, patients >65 years ($p = 0.030$), those under immunosuppression for prevention or treatment of graft-vs-host disease (GVHD) ($p = 0.033$), and/or with relapsed disease ($p = 0.014$) displayed poor humoral immune response to the vaccine. In contrast, the intensity of the conditioning regimen, underlying disease (myeloid/lymphoid/other), and presence of chronic GVHD had no impact on antibody levels. Antibody titers achieved the highest levels 1m after the 2nd dose of the vaccine but substantially waned in all transplanted groups and healthy controls over time.

Conclusion:

This analysis of long-term vaccine antibody response is of critical importance to allo-HCT recipients and transplant physicians to guide treatment decisions regarding re-vaccination and social behavior during the SARS-CoV-2 pandemic.

N. Jarzebska^{2, 5}, J. Frei², T. Weiss³, T. Holzinger⁵, M. Mellett^{2, 5}, M. Diken¹, R. Speck⁴, T. Kundig^{2, 5}, U. Sahin¹, S. Pascolo^{2, 5}

RNA with chemotherapeutic base analogues as a superlative dual-functional anti-cancer drug

BioNTech AG¹, Department of Dermatology, University Hospital Zürich², Department of Neurology and Brain Tumor Center, University Hospital Zurich³, Division of Infectious Diseases and Hospital Epidemiology, University Hospital of Zurich⁴, University of Zurich⁵

Introduction:

RNA-based therapies hold great promise for cancer treatment as they can be used to block oncogenes (using siRNA), or express proteins of interest (by mRNA) or activate the innate immune system (isRNA). Formulating immunostimulating (is)RNA with the pharmaceutical compound Protamine, a natural cationic histone, enables the generation of nanoparticles that induce IFN α release and limit tumour growth in mice.

To augment therapeutic, anti-tumour effects of Protamine-RNA nanoparticles, we incorporated the chemotherapeutic pyrimidine 5-fluorouracil (5FU) into RNA in place of uracil. We found that the modified 5FU-RNA is as potently chemotherapeutic as free 5FU. In addition, we could show that this substitution does not interfere with the capacity of the RNA to trigger TLR7 and induce production of type I interferons. Thereby 5FU-RNA exhibits dual-functionality and is immuno-chemotherapeutic (icRNA).

Methods:

Cytotoxicity of icRNA was evaluated in vitro on CT26 murine colon carcinoma cells. The cells were incubated with increasing concentrations of Protamine-RNA/5FU nanoparticles (PR 5FU) or Protamine-mRNA (PR Luc) or free 5FU and proliferation was measured. Therapeutic capacities of icRNA was assessed in mice implanted with CT26 colon carcinoma murine cell line. On Day 4 and 11-post tumour cell implantation, mice were administered with two intravenous injections (10 μ g of RNA each) of PR 5FU (i.e. immunochemotherapeutic) or PR Luc (i.e. immunostimulating only) particles.

Results:

Proliferation of CT26 cells in vitro was reduced in the presence of increasing concentrations of PR 5FU even more than in cells treated with standard free 5FU. This corresponds to a higher chemotherapeutic activity of the modified ribonucleoside versus the free base. PR 5FU particles retained their immunostimulatory effects on human PBMCs and induced IFN α secretion. Mice receiving PR 5FU showed a greater control of subcutaneous tumour volume compared to mice receiving PR Luc. This difference was dependent on the cytotoxic effect of 5FU, as both PR 5FU and PR Luc nanoparticles induced similar levels of IFN α 4 h after I.V. injection.

Conclusion:

We observed that substituting uracil with the chemotherapeutic pyrimidine 5FU bestowed the RNA oligo with a dual mechanism of action; they retained their ability to stimulate the innate immune response but now also exerted potent cytotoxic effects against rapidly dividing cells. These immunochemotherapeutic RNA (icRNA) nanoparticles demonstrate more effective killing of tumour cells in vitro and in vivo. Therefore, we demonstrated that icRNAs are promising cancer therapies, which warrants their further validation for use in the clinic.

E. Sarti¹, R. Wolfensberger¹, R. Speck¹, P. Sander², S. Bredl¹, J. Nemeth¹

The sequence of activation and infection determines outcomes of macrophage infections with *Mycobacterium tuberculosis*

University Hospital Zürich¹, University of Zürich²

Introduction:

Mycobacterium tuberculosis (MTB) rewires the infected macrophages following phagocytosis, resulting in the inhibition of anti-mycobacterial effectors, antigen presentation and response to cytokines including IFN- γ (IFN- γ). In vivo experiments in the contained MTB infection (CMTB) mouse model suggest that immunity induced by a primary, asymptomatic infection is sufficient to induce close to sterilizing protection against re-exposure. However, the primary response remains unaffected. Mechanistically, IFN- γ released from the primary infection results in activation of distant macrophages and resistance to secondary infection. However, IFN- γ appears to be ineffective for already infected macrophages. Therefore, we hypothesize that the sequence of activation with IFN- γ and infection with MTB is a crucial determinant of outcome.

Methods:

We explored major biological phenotypes (mycobacterial viability, host cell viability, host cell activation) in mouse bone marrow-derived macrophages (BMDM) infected in vitro with either H37Rv or the MTB Live/Dead H37Rv reporter strain. Macrophages were stimulated with IFN- γ for 24h either prior or after infection. We analyzed the resulting phenotypes with flow cytometry, plating of bacteria and bulk RNAseq.

Results:

Activation of macrophages with IFN- γ for 24h prior to infection significantly increased anti-mycobacterial activity of macrophages and decreased the number of live and transcriptionally active bacteria by 45% (+/-12%). Also, activation increased expression of MHCII and CD80. Additional activation with IFN- γ after the infection did not increase antibacterial effectivity. In contrast, macrophages activated with IFN- γ for 24 h directly after infection, allowed increased bacterial growth and increased MTB transcriptional activity. This phenotype was associated with reduced expression of activation markers on macrophages. The transcriptional response comparing infected/activated versus activated/infected macrophages showed substantial differences in proinflammatory pathways and transcriptional self-renewal programs. On a transcriptional level, infected/activated cells expressed genes associated with immune privilege including PD1-L and CD47, all of which are known to be controlled by c-MYC. We therefore blocked c-MYC, a key regulator of self-renewal in macrophages using a chemical inhibitor. In BMDM infection experiments, c-MYC blockade decreased MTB transcriptional activity and MTB survival with an effect comparable to the activation with IFN- γ .

Conclusion:

Taken together, our data suggest that the activation state of the macrophage prior to MTB infection is the key determinant of outcome in vitro, complementing our observations from the CMTB mouse model in vivo. C-MYC signaling appears to play a significant role in macrophage MTB infections in vitro.

I. Abela^{3,4}, M. Marconato², A. Hauser⁴, M. Schwarzmüller⁴, R. Katzensteiner³, D. Braun³, S. Epp⁴, A. Audigé⁴, J. Weber⁴, P. Rusert⁴, E. Schindler¹, C. Pasin^{3,4}, E. West³, J. Böni⁴, V. Kufner⁴, M. Huber⁴, M. Zaheri⁴, S. Schmutz⁴, B. Frey¹, R. Kouyos^{3,4}, . Huldrych F. Günthard^{3,4}, M. Manz², A. Trkola⁴

Contribution of endogenous and exogenous antibodies to clearance of SARS-CoV-2 during convalescent plasma therapy

Blood Transfusion Service Zurich, Switzerland¹, Department of Medical Oncology and Hematology, University Hospital Zurich, Switzerland², Division of Infectious Diseases and Hospital Epidemiology, University Hospital Zurich, Switzerland³, Institute of Medical Virology, University of Zurich, Switzerland⁴

Introduction:

Neutralizing antibodies are considered a key correlate of protection by current SARS-CoV-2 vaccines. The ability of antibody-based therapies, including convalescent plasma therapy (CPT), to affect established disease remains to be elucidated.

Methods:

Here, we conducted a proof-of-principle study of CPT based on a phase I trial in thirty hospitalized COVID-19 patients with a median interval between the onset of symptoms and the first transfusion of 9 days (IQR, 7-11.8 days). A comprehensive longitudinal monitoring of the virologic, serologic, and disease status of recipients allowed deciphering of parameters on which plasma therapy efficacy depends.

Results:

In the context of this trial CPT was safe as evidenced by the absence of transfusion related adverse events and a low mortality (3.3%). Treatment with highly neutralizing plasma was significantly associated with faster virus clearance, as demonstrated by Kaplan-Meier analysis ($p = 0.034$) and confirmed in a parametric survival model including viral load and comorbidity (adjusted hazard ratio (HR) = 3.0 [95% confidence interval (CI) 1.1;8.1], $p = 0.026$). The onset of endogenous neutralization had a noticeable effect on viral clearance but, importantly, even after adjusting for their endogenous neutralization status recipients benefitted from plasma therapy with high neutralizing antibodies (HR= 4.0 [95% CI 1.3;13], $p = 0.017$).

Conclusion:

In summary, our data demonstrate a clear impact of exogenous antibody therapy on the rapid clearance of viremia in the early stages of infection and provide directions for improved efficacy evaluation of current and future SARS-CoV-2 therapies beyond antibody-based interventions.

A. Hukara¹, T. Tabib², M. Rudnik¹, O. Distler¹, P. Blyszczuk¹, R. Lafyatis², G. Kania¹

FOSL-2 transcription factor as a regulator of macrophage polarization and function in systemic sclerosis

Center of Experimental Rheumatology, Department of Rheumatology, University Hospital Zurich, University of Zurich, Switzerland¹, Division of Rheumatology and Clinical Immunology, Department of Medicine, University of Pittsburgh, Pittsburgh, Pennsylvania, USA²

Introduction:

Pathological effects of the AP-1 transcription factor Fos-related antigen 2 (FOSL-2) have been associated with systemic sclerosis (SSc). Macrophages play a crucial role in the development and progression of SSc. In this study, we aim to assess the role of FOSL-2 in macrophage polarization and function in SSc.

Methods:

Peritoneal macrophages were isolated from *FOSL2* overexpressing transgenic (*FOSL2* tg), *Csf1R^{Cre}FOSL2^{fl/fl}*, wild-type (wt) and *FOSL2^{fl/fl}* mice. Human peripheral CD14⁺ blood-derived monocytes were isolated from healthy controls and SSc patients and differentiated to human monocytes-derived macrophages (hMDM). Murine and human macrophages were polarized with LPS (10 ng/ml) or remained untreated. Expression of macrophage polarization markers was assessed by flow cytometry using mouse or human antibody-designed panels. Phagocytic activity in hMDM was detected using pHrodo Red *E.coli* particles by flow cytometry. Secretion of pro-inflammatory markers was measured by ELISA. FOSL-2 protein expression was detected by Western Blot. Single cell RNA sequencing (scRNAseq) of human explanted lung tissue from SSc-ILD patients was conducted using the 10X Genomics Chromium Instrument. Further analyses for this study were performed using the R package Seurat V2.3.4.

Results:

Peritoneal macrophages isolated from *FOSL2* tg mice, an immunofibrotic animal model of SSc, showed increased expression of M(IL-4) alternative CD206 (p=0.0591) and PD-L2 (p<0.05) polarization markers compared to wt cells (n=5-9). *Csf1R^{Cre}FOSL2^{fl/fl}* peritoneal macrophages revealed lower expression of CD206 (p<0.05) and PD-L2 (p<0.01) compared to *FOSL2^{fl/fl}* control macrophages (n=5-9). After in vitro LPS polarization, we found lower secretion of pro-inflammatory TNF- α (p<0.01) and IL-6 (p<0.05) in *FOSL2* tg peritoneal macrophages compared to wt cells (n=9-18). *Csf1R^{Cre}FOSL2^{fl/fl}* peritoneal macrophages did not show a significant difference in the secretion of TNF- α and IL-6 (n=4-5), indicating no involvement of *FOSL2* in the polarization of classically-activated M(LPS) macrophages. Our human data revealed enhanced protein expression of FOSL-2 in untreated (p<0.01) and LPS stimulated (p<0.01) SSc hMDM (n=18-25) compared to healthy hMDM (n=11-18). Phagocytic activity was increased in SSc hMDM (n=29-34) compared to untreated (p<0.01) and LPS stimulated (p<0.05) healthy hMDM (n=12-16). Phenotypical characterization of untreated SSc hMDM (n=17) showed an increased percentage of CD40⁺CD86⁺CD206⁺PD-L2⁺CD163⁺ cells (p<0.05) compared to healthy hMDM (n=7), with no expression of the M(LPS)-associated markers CD38 and PD-L1. To investigate the role of *FOSL2* in other macrophage types, scRNAseq analysis of the SSc-ILD lung dataset was performed and identified differentially expressed macrophage polarization (*CD206*) and phagocytosis-associated genes (*MARCO*, *C1QA*, *C1QB* and *C1QC*) in SPP1^{hi} lung macrophages from SSc-ILD patients when comparing *FOSL2^{hi}* and *FOSL2^{null}* cells (p.adj. \leq 0.05; log₂ ratio \geq 0.5).

Conclusion:

In this study, we showed an involvement of FOSL-2 in the regulation of the M(IL-4) alternative macrophage phenotype, rather than in driving macrophages into classically-activated M(LPS) phenotypes. Moreover, for the first time, we demonstrated increased expression of the profibrotic transcription factor FOSL-2 with an increased phagocytic activity in SSc hMDM. Therefore, targeting this alternative/pro-phagocytic phenotype could serve as an effective tool to counteract disease progression.

P. Wallimann¹, M. Mayinger¹, M. Bogowicz¹, M. Guckenberger¹, N. Andratschke¹, S. Tanadini-Lang¹, J. van Timmeren¹

Comparison of methods for T1-w brain MRI intensity normalization for quantitative MRI analysis

Department of Radiation Oncology, University Hospital Zürich and University of Zürich¹

Introduction:

The quantitative comparison of MRI intensities between sessions, patients, and machines requires a normalization. There is currently no consensus about the optimal normalization approach. Here we compared the consistency of normalized intensity values within different tissue types in brain MRI for three commonly used intensity normalization techniques and a newly developed method.

Methods:

We analyzed the publicly available dataset CC-359, containing 359 T1-w brain MRI of different healthy individuals from 6 different scanners. Preprocessing of the images consisted of brain extraction and N4 bias field correction. Using the FSL FAST algorithm, all images were automatically segmented into three tissue types, forming the three regions of interest (ROI): cerebrospinal fluid (CSF), gray matter (GM) and white matter (WM). Voxels were assigned to a region if the algorithm reported 100% certainty. The evaluated normalization techniques were: piecewise linear normalization known as Nyul, z-score transformation on all brain intensities, normalization based on the WM intensity peak known as WhiteStripe, and a custom normalization method. The custom method isolates the homogeneous parts of the image by excluding voxels whose local surroundings have a high change in intensity. In the remaining image, the two peak intensities are detected and interpreted as CSF and WM. Then, the intensities of the entire image are linearly transformed, mapping the CSF peak intensity to 0 and the WM peak intensity to 100. For each normalization method and ROI, the Jensen-Shannon distance (JSD) was calculated between each subject's histogram and the average histogram among all subjects. A lower JSD across subjects correspond to less variability between subjects and thus a more consistent normalization of the intensities in the ROI.

Results:

For each normalization method and each ROI, the histograms of each subject, along with the average histogram of all subjects, are shown in figure 1. All normalization methods resulted in more consistent intensity values than no normalization (figure 2). Nyul normalization achieved the lowest median JSD for each ROI. Among the other techniques, the lowest median JSD for WM was achieved in WhiteStripe and for CSF and GM in z-score. For each ROI, all pairwise comparisons of JSD values between normalizations were statistically significant ($p < 0.05$; Wilcoxon), except for CSF between the custom method and z-score ($p = 0.83$).

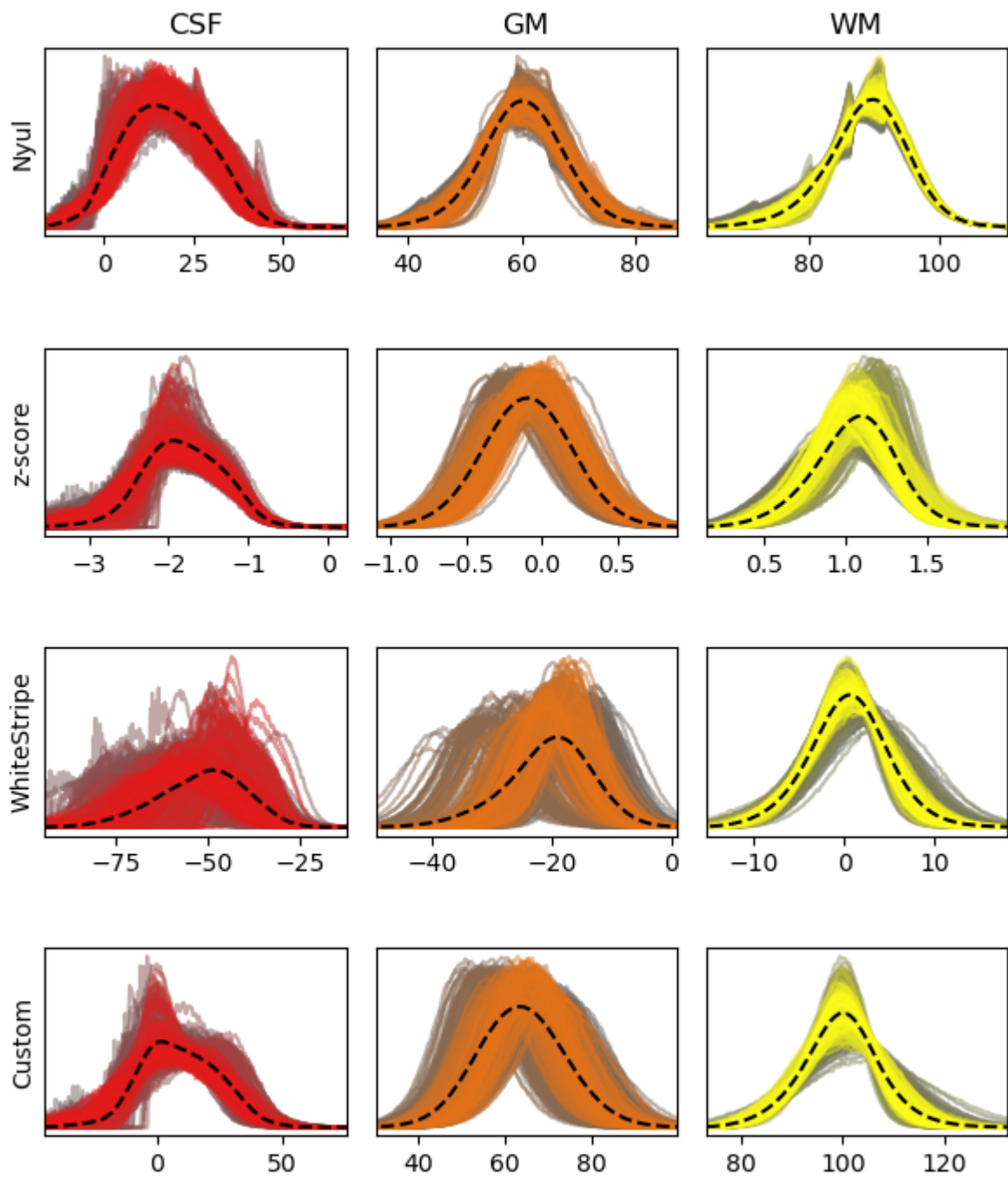


Figure 1: For each ROI and each normalization method: Normalized histograms of normalized images for all subjects overlaid. The dashed black line represents the average histogram in each plot.

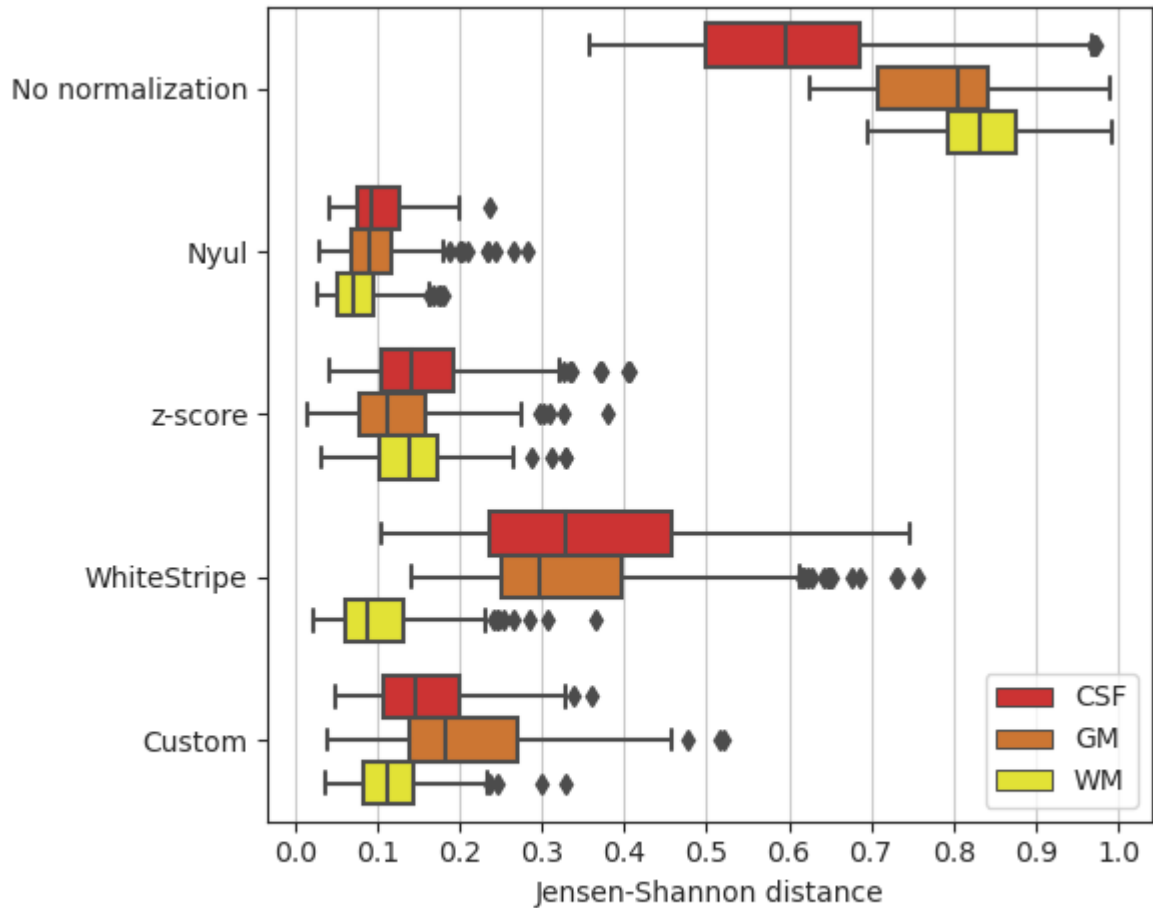


Figure 2: Box plot of the Jensen-Shannon distances calculated for all subjects for each normalization method and each ROI.

Conclusion:

Nyul normalization performed best in each ROI. However, it has caveats not addressed in this evaluation, e.g. it affects the image texture. The normalization methods which are based on known tissue characteristics (WhiteStripe and custom) performed well in at most 2 out of 3 ROI. The same was observed for z-score. This suggests that a nonlinear normalization is necessary to achieve consistent intensities for all brain tissue types. This knowledge will be used to further develop the methods.

K. Furrer¹, D. Bettex¹, T. Horisberger¹, I. Inci¹, O. Schmid¹, N. Nagaraj¹, H. Morselli¹, B. Battilana¹, R. Schuepbach¹, S. Ulrich¹, M. Hebeisen², A. Matter¹, I. Opitz¹

The choice of priming solution for cardiopulmonary bypass during pulmonary endarterectomy for CTEPH has important impact

University Hospital Zurich¹, University of Zurich²

Introduction:

Pulmonary endarterectomy (PEA) is the treatment of choice for chronic thromboembolic pulmonary hypertension (CTEPH). In recent decades, a refined surgical technique of PEA using a cardiopulmonary bypass (CPB) has achieved a significant reduction in mortality. The hemodilution caused by priming solutions in general heart surgery causes a number of disadvantages, and no standard for PEA is described. We aim to assess the outcome of CTEPH patients after protocol change for CPB with adding 5% albumin to the priming solution during PEA.

Methods:

Since changing the CPB protocol in 2018, 28 CTEPH patients were retrospectively compared to a historical control by 1:1 propensity score matching gender, age, PVR (pulmonary vascular resistance) before PEA surgery. The resulting two cohort groups were analysed for intraoperative fluid balance, vasoactive-inotropic score (VIS), operative time and their influence on outcome. Regression models of hospitalization-, ICU (intensive care unit) and intubation time considered the total blood volume balance as a mediator of the effect of the new protocol.

Results:

Lower CPB-balance ($p < 0.001$), VIS score ($p = 0.04$), shorter operative time ($p = 0.03$) and hospitalization ($p = 0.008$) were observed in the cohort operated with the new protocol. Postoperative 30- and 90 day mortality and morbidity were similar between the two groups. Shorter operative time (mean change (mc) 1.4, 95% CI [0.8, 2.0], $p < 0.0001$) and new protocol (mc -3.68, 95% CI [-5.22, -2.14], $p < 0.0001$) are independently associated with lower CPB balance, resulting in a beneficial effect on the ICU-, intubation and hospitalization time and the VIS score (mean ratio (mr) 1.11, 1.14, 1.05, 1.12, $p = 0.0011$, 0.0013, 0.008, $p < 0.0001$, respectively). The protocol change shows a clear positive trend with significance reached for hospitalization time ($p = 0.02$).

Conclusion:

Priming protocol for CBP with addition of 5% albumin had a beneficial effect on the CPB balance and improved outcome after PEA for CTEPH patients.

K. Furrer¹, J. Welsch¹, D. Bettex¹, T. Horisberger¹, I. Inci¹, R. Schuepbach¹, M. Kirschner¹, S. Ulrich¹, A. Matter¹, I. Opitz¹

Carbon dioxide and alveolar dead space as a prognostic marker for patients undergoing pulmonary endarterectomy

University Hospital Zurich¹

Introduction:

In patients with chronic thromboembolic pulmonary hypertension (CTEPH) partial pressure of carbon dioxide (PCO₂) at rest and exercise is reduced in proportion to disease severity and reflect the abnormality in ventilatory efficiency by increase in physiologic alveolar dead space. Our aim was to determine the value of the delta in PCO₂ and the alveolar dead space (AVDSf) as prognostic marker after pulmonary endarterectomy (PEA) in CTEPH patients.

Methods:

Between 2013 and 2020, 51 CTEPH patients undergoing PEA with 2-year follow-up time were retrospectively analysed including cardiopulmonary exercise testing and hemodynamic measurements before and 1 year after PEA. PCO₂ and AVDSf were analysed before and after PEA.

Results:

PCO₂ values before PEA measured during induction are lower compared to the values at the end of PEA (mean 4.47, SD 0.653 vs 5.66, SD 0.83, $p=0.000$) and at postoperative day 1 (POD1) (mean 4.47, SD 0.65 vs 4.82, SD 0.73, $p=0.000$). Delta PCO₂ values (between before and after surgery) (mean 1.183, SD 1.18) as well as the delta pCO₂ between the end of surgery and POD 1 (mean 0.354, SD 1.14) correlates significantly with postoperative NYHA improvement and mPAP-decrease at one year postoperative ($p=0.19$; $p=0.00$ and $p=0.000$; $p=0,000$, respectively). PEA resulted in increase of Vo₂max (mean 17.68mL/kg/min, SD 6.14 vs 13.47mL/kg/min, SD 5.13, $p=0.000$), oxygen uptake at aerobic threshold (mean 12.92 mL/kg/min, SD 5.14, vs 10.03mL/kg/min, SD 4.12, $p=0.001$), decrease of mPAP at one year postoperative (mean 26.37mmHg, SD 8.64 vs 40.22mmHg, SD 8.67, $p=0.000$), pulmonary vascular resistance (mean 3.193 WU, SD 1.69 vs 6.13 WU, SD 2.69, $p=0.000$) and improvement of NYHA functional class ($p=0.000$) in comparison to preoperative values. AVDSf values before PEA at induction (mean 0.055, SD 0.166), to the end of surgery (mean 0.336, SD 0.12) and at POD1 (mean 0.152, SD 0.15) was observed and correlated significantly with postoperative NYHA improvement and mPAP decrease at one year postoperative ($p=0.000$; $p=0.000$; $p=0.000$ and $p=0.000$; $p=0,000$, $p=0.000$ respectively)

Conclusion:

In patients with CTEPH undergoing PEA, markers for alveolar dead space and ventilation/prefusion mismatch may predict longterm outcome after surgery. If confirmed in a prospective way, these markers can support indicating and early start of additional treatment modalities such as ballon angioplasty or medication.

B. Thomson^{4, 5}, H. Richter^{1, 2}, K. Akeret⁴, R. Buzzi⁵, N. Schwendinger⁴, V. Anagnostakou⁴, K. Kulcsar³, P. Kronen^{1, 6}, L. Regli⁴, J. Fierstra⁴, D. Schaer⁵, M. Hugelshofer⁴

Cerebrovascular Reactivity Measured by BOLD-fMRI as Imaging Strategy to Monitor CSF-Hemoglobin Toxicity

Center for Applied Biotechnology and Molecular Medicine¹, Clinic for Diagnostic Imaging, Department of Clinical Diagnostics and Services, Vetsuisse Faculty, UZH², Department of Neuroradiology, USZ³, Department of Neurosurgery, USZ⁴, Division of Internal Medicine, USZ⁵, Veterinary Anaesthesia Services – International⁶

Introduction:

After aneurysmal subarachnoid hemorrhage (aSAH), patients are at risk to develop secondary brain injury (SAH-SBI), which significantly increases the morbidity and the socioeconomic burden of this disease. One of the main drivers of secondary brain injury is thought to be cell-free hemoglobin in the cerebrospinal fluid (CSF-Hb). CSF-Hb interacts with cerebrovascular nitric oxide signaling and induces arterial vasospasm (aVSP), which may impair regional cerebral blood flow regulation. Digital subtraction angiography (DSA) is the gold-standard to image vascular anatomy of the brain but provides only limited functional parameters to determine brain areas at risk for ischemia. Monitoring of blood oxygenation level dependent (BOLD) fMRI cerebrovascular reactivity (CVR) may close this diagnostic gap and provide additional information about vascular CSF-Hb toxicity.

Methods:

DSA imaging was performed in four anesthetized and ventilated sheep 15, 30, 45 and 60 minutes after infusion of hemoglobin (Hb) into the left lateral ventricle. In the same setup, BOLD-CVR fMRI imaging was performed in an additional 5 anesthetized and ventilated sheep. As a control group, four and 5 sheep for DSA and BOLD fMRI respectively, were co-infused with haptoglobin, which prevents the delocalization of CSF-Hb into the vessel wall of cerebral arteries.

Results:

In the DSA experiment, mean changes in CBF are reported as 0.05 s (+/- 1.98 s), -1.8 s (+/- 1.93 s), -2.62 s (+/- 4.13 s) and -1.4 s (+/- 1.41 s) in the Hb group and 1.68 s (+/- 4.83 s), -2.7 s (+/- 3.06 s), -1.69 s (+/- 3.56 s) and 0.35 s (+/- 4.87 s) in the Hb:Hp group. Mean MTT changes were 0.19 s (+/- 0.39 s), 0.19 s (+/- 0.12 s), 0.11 s (+/- 0.29 s) and 0.34 s (+/- 0.27 s) versus -0.0 s (+/- 0.38 s), 0.08 s (+/- 0.17 s), 0.3 s (+/- 0.41 s) and 0.22 s (+/- 0.27 s) in the Hb and Hb:Hp group respectively. Changes in temporal BOLD-CVR profiles in the Hb group were -0.03 (+/- 0.01), -0.03 (+/- 0.01), -0.03 (+/- 0.01) and -0.03 (+/- 0.02) versus -0.01 (+/- 0.02), 0.0 (+/- 0.01), 0.01 (+/- 0.02) and 0.01 (+/- 0.01) in the controls co-infused with haptoglobin at respectively the pre-infusion, 15-, 30-, 45- and 60-minutes time point.

Conclusion:

BOLD-CVR is able to quantify vascular effects of cell-free Hb infused into the CSF-compartment, prior to macrovascular constriction. This sensitivity allows for earlier adaptive measures and guide therapeutic interventions such as scavenging of CSF-Hb with intracerebroventricular application of Hp. Contrarily, the DSA derived parameters MTT and CBF were not sensitive enough to discriminate between Hb and Hb:Hp coinfusion. Our results contribute to establishing BOLD-CVR as an imaging modality to detect vascular changes after aSAH with a high sensitivity and strengthen the rationale for novel treatment strategies targeting Hb-toxicity after aSAH.

K. Furrer*¹, R. Werner* (*contributed equally)¹, A. Curioni¹, S. Hillinger¹, D. Schneiter¹, I. Inci¹, I. Opitz¹

Salvage surgery in patients with locally advanced non-small cell lung cancer

*University Hospital Zurich*¹

Introduction:

In patients with stage IIIB or IV non-small cell lung cancer (NSCLC), current guidelines recommend a combination of systemic treatment including chemotherapy, targeted- or immunotherapy with definitive radiotherapy. Nevertheless, relapses still occur in >30% within 2 years. In selected patients with local tumor recurrence or residual disease, so-called “salvage resection” can be performed with curative intent. Since previous reports on this approach are scarce and candidate selection remains challenging, we aimed to assess the outcomes of salvage surgery.

Methods:

We retrospectively identified 33 patients with initial stage IIIB or IV NSCLC who underwent salvage lung resection in curative intent between time period from 2001 to 2021 and included only patients if this resection was not part of the first line treatment approach.

Results:

Median age was 62 (38-78) years with 54% of patients were male. 7 patients had stage IIIB and 24 had stage IVA and 2 stage IVB. Anatomical lung resections with 22 lobectomies/bilobectomies (with 8 extended), 1 segmentectomy and 10 extended pneumonectomies were performed and R0 resection was achieved in 93.9% (31/33) patients. The histology revealed 26 adenocarcinomas, 4 squamous carcinomas and 1 large cell carcinoma with pathological complete response in 8/33 cases. Morbidity rate was 33.3% (11/33) with 5/11 minor (Grade II) and 7/11 major (Grade IIIA-V) complications. 30- and 90-day mortality was 0% and 12% (4/33). Median overall survival (OS) were 5 years [95%CI: 3.37; 6.62] respective 69 months [95%CI: 49.4; 94.2] and progression-free survival (PFS) were 2 years [95%CI: 0.0; 4.55] respective 12 months [95%CI: 0.0; 30.42]. R0 resection of the primary tumor was an independent factor influencing OS and PFS (71 months [95%CI; 38.4; 103.6, p=0.033] and 22 months [95%CI; 0.54; 43.46, p=0.000] respectively).

Conclusion:

Salvage surgery is a potentially curative procedure with promising OS and PFS in selected patients with stage IIIB/IV NSCLC.

K. Furrer¹, M. Schuurmans¹, M. Hebeisen², S. Schulte¹, D. Schneiter¹, W. Weder¹, I. Opitz¹, S. Hillinger¹

Smoking prevention intervention with school classes in university hospital by thoracic surgeon and pulmonologist. The Zurich prevention project.

*University Hospital Zurich*¹, *University of Zurich*²

Introduction:

Smoking prevention in schoolchildren to inform and prevent smoking initiation has been widely studied, however the potential effect of interventions provided in a hospital setting is unknown. An intervention programme named "Schoolchildren smoking prevention in the hospital" was developed in which the health aspects of smoking and its individual consequences were presented in an interactive informational event provided by a thoracic surgeon and a pulmonologist. We aimed to assess the feasibility and the short-term effect of smoking-related knowledge improvement in schoolchildren in a hospital setting.

Methods:

Scholars of 45 classes in Canton of Zurich in Switzerland filled in an anonymous 5-item questionnaire with questions on general knowledge about smoking. The answers were evaluated in this prospective observational cohort study. The primary endpoint was to compare the knowledge improvement by interpretation of answers before-and-after the smoking prevention intervention. Additionally, the performance of children was compared after setting up an overall score and specific subgroups according to gender and school-level.

Results:

Between Jan 2010, and Oct 2019, schoolchildren aged 10 to 16 years participated in this intervention programme and completed the questionnaire before (N=1270) and after (N=1264) the intervention. The amount of correctly answered questions increased from 40% (± 20) before to 81% (± 17), $p < 0.0001$ after the educational session.

Conclusion:

An intervention programme on health effects of smoking provided by lung specialists in the hospital is feasible, well received, leads to a substantial increase of knowledge, and hopefully can be further explored in the development of smoking prevention programmes for schoolchildren.

C. Gil-Cruz^{1, 2}, C. Perez-Shibayama¹, M. Nägele², H. Cheng¹, M. Lütge¹, K. Frischmann^{1, 2}, A. Joachimbauer^{1, 2}, D. Parianos², A. Flammer², F. Ruschitzka², D. Schmidt², B. Ludewig^{1, 2}

Dissecting the immune cell landscape in myocarditis

Kantonsspital StGallen¹, University Hospital Zurich²

Introduction:

Myocarditis is the prototypical cardiac inflammatory disease, with an incidence of 20-30 per 100 000 individuals. Acute myocarditis develops into potentially lethal inflammatory cardiomyopathy in a substantial fraction of the patients, rendering myocarditis and its sequelae the underlying reason for approximately half of all heart transplants and 10-20% of cardiovascular sudden deaths in young adults. Different pathological routes had been described to lead to myocardial inflammation (eg. viral, bacterial or parasitic infection, autoimmune processes, toxins). Moreover, genetic predisposition and environmental factors as the microbiome influence the progression of the disease. Therefore, it is plausible that the inherent complexity of the disease hampers the elucidation of effective therapeutic interventions because the molecular mechanisms underlying this severe heart condition are – to a large extent – incompletely understood. Therefore, it is important to elucidate the molecular pathways that govern the interplay between immune cells and stromal cells in the cardiac microenvironment in myocarditis.

Methods:

To analyse the mechanisms involved in cardiac inflammation, we used single cell and single nucleus transcriptomic approaches in conjunction with a T cell receptor transgenic mouse model of spontaneous autoimmune myocarditis (TCRM) and endomyocardial biopsies from myocarditis patients (HeartRNAseq_01 study, USZ); as controls healthy mice and biopsies from heart transplantation patients were used respectively.

Results:

Our analysis shows that dynamic changes occur in the cardiac microenvironment during the course of myocarditis; these changes involve not only the recruitment of immune cells expressing pro-inflammatory signatures to the myocardium (T cells, inflammatory monocytes, neutrophils) but also the alteration of transcriptional programs in non-immune cells including fibroblast and cardiomyocytes. Analysis of endomyocardial biopsies of myocarditis patients and heart-transplanted individuals revealed similar changes in the cardiac cell population's transcriptome.

Conclusion:

Our study reveal that the cardiac landscape is profoundly altered in myocarditis. Moreover, we show that the analysis of endomyocardial biopsies by single-nucleus RNAseq represents a powerful tool to unveil the processes involved in cardiac diseases.

Y. Butscheid¹, S. Barco¹, T. Sebastian¹, D. Voci¹, R. Spescha¹, N. Kucher¹, on behalf of the SirPAD Investigators¹

The “SirPAD” randomized controlled trial in patients with peripheral artery disease requiring percutaneous transluminal angioplasty: study design and experience from the first year of recruitment

Department of Angiology, University Hospital Zurich, Switzerland¹

Introduction:

Peripheral artery disease (PAD) is a progressive atherosclerotic disease with symptoms ranging from intermittent claudication to acute critical limb ischemia that might result in an amputation. Drug-coated balloons and stents were developed to prevent neo-intimal proliferation and restenosis after percutaneous transluminal angioplasty (PTA). Randomized controlled trials showed that paclitaxel-coated devices reduce restenosis, late lumen loss, and the need for target lesion revascularization compared with uncoated ones. However, the limited size of these trials and the restricted patient population did not allow demonstrating superiority for “hard” clinical outcomes like the rate of revascularization and/or amputation. Alternative sirolimus-coated balloons were approved for clinical use in patients with PAD. By encapsulating sirolimus in phospholipid drug nanocarriers, they optimize adhesion properties of sirolimus leading to better bioavailability. Several large-scale clinical trials with sirolimus-coated balloons were recently initiated including the SirPAD trial that we are reporting about.

Methods:

In this investigator-initiated all-comer open-label phase III randomized controlled trial, we will evaluate whether sirolimus-coated balloon angioplasty is non-inferior and eventually superior, according to a predefined hierarchical analysis, to uncoated balloon angioplasty in adults with infra-inguinal peripheral artery disease requiring PTA. A total of 1'200 patients will be enrolled in the trial. Inclusion criteria include signed informed consent, age \geq 18 years and requirement of the PTA for a PAD lesion located below the inguinal ligament. Exclusion criteria include pregnancy/breastfeeding, known intolerance or allergy to sirolimus, and the participation in a clinical trial during the previous 3 months.

The primary efficacy outcome is the composite of two clinically relevant non-subjective “hard” outcomes: unplanned major amputation of the target limb and endovascular or surgical target lesion revascularization for critical limb ischemia occurring within one year of randomization. The primary safety outcomes include death from all causes within 30 days, 180 days, one year, two years, and five years of randomization. A number of predefined secondary efficacy outcomes will be tested.

Results:

Since the study initiation in November 2020 until the 2021 year-end 400 patients have been randomized in the trial. 32 patients did not provide informed consent and 44 patients were considered a screening failure, mainly because of the lesion localization above the inguinal ligament. Of the first 400 participants, 36% were women and the median age was 74 years (range 32-97 years). The most common PAD risk factor was arterial hypertension present in 79% of the participants, followed by smoking history (64%), dyslipidemia (57%), and diabetes mellitus (43%). 65 patients (16%) initially presented with a critical limb ischemia, defined according to the Fontaine classification as the presence of rest pain or ulceration/gangrene.

A second study center (Division of Angiology, Cantonal Hospital Fribourg) will be initiated at the beginning of February 2022.

Conclusion:

By focusing on clinically relevant outcomes, this study aims to provide essential data on the efficacy and safety of sirolimus-coated balloon catheters for infra-inguinal PAD in a representative (all-comer) population of unselected patients.

Trial registration: NCT04238546 (ClinicalTrials.gov).

L. Jungblut², A. Euler², J. Von Spiczak², T. Sartoretti², V. Mergen², A. Landsmann², V. Englmaier², O. Distler¹, H. Alkadhi², T. Frauenfelder², K. Martini²

Potential of Photon-Counting Detector CT for Radiation Dose Reduction for the Assessment of Interstitial Lung Disease in Patients with Systemic sclerosis

Department of Rheumatology, University Hospital Zurich, University of Zurich, Zurich, Switzerland¹, Institute of Diagnostic and Interventional Radiology, University Hospital Zurich, University of Zurich, Zurich, Switzerland²

Introduction:

In interstitial lung disease the detection of small lung changes is crucial. With the era of photon-counting detector CT (PCD-CT) there is a great potential for dose savings without penalties in image quality and diagnostic confidence.

Methods:

In this IRB-approved retrospective study, consecutive patients with SSc receiving a follow up non-contrast chest-examination on a first-generation PCD-CT were included between May 2021 and December 2022. The baseline scans were generated on a dual-source EID-CT by adjusting the tube current time product for each of the two x-ray tubes to obtain a 100% dose image (D100), a 66% dose image (D66) and a 33% dose image (D33) from the same data set. Image noise was measured manually in the subcutaneous fat and defined as the standard deviation of attenuation. Subjective image quality was assessed by two independent readers on a five-point likert-scale for overall subjective image, presence, extent, and diagnostic confidence and accuracy of SSc-ILD. D100 evaluated by an expert radiologist with 22 years of experience served as reference standard. Cohen's κ was used to assess the interobserver agreement. A paired t-test was used to compare mean variables.

Results:

Eighty consecutive patients (mean 56 ± 14 , 64 women) were included. While CTDIvol of PCD-CT was comparable to D33 (0.72 vs. 0.76 mGy, $p=0.091$), mean image noise of PCD-CT was comparable to D100 (131 ± 15 vs. 113 ± 12 , $p>0.05$). Overall subjective image quality of PCD-CT was comparable to D100 (4.72 vs. 4.71; $p=0.874$). Similarly, diagnostic accuracy in PCD-CT was maintained (95% and 98.5%, respectively).

Conclusion:

PCD-CT allowed for a radiation dose reduction of 66% compared to EID-CT without penalty in image quality and diagnostic performance for the detection of SSc-ILD.

C. Porcheri¹, C. Meisel¹, T. Mitsiadis¹

The Notch ligand Dll4 orchestrates the initiation and maintenance of undifferentiation in a mouse model of squamous cell carcinoma

University of Zurich¹

Introduction:

The molecular basics of squamous cell carcinoma are largely unknown and strongly variable depending on the site of the primary tumor. In a chemically-induced murin model of squamous cell carcinoma, we studied the mechanisms of cancer initiation, growth and maintenance at both cellular and molecular level. Previous transcriptomic analyses identified the Notch pathway as one of the major mutated pathway in oral squamous cell carcinoma. We hereby analyse the dynamics of this pathway activation over-time and the cross-talk with other signaling pathways in the regulation of proliferation and differentiation of the tongue epithelium

Methods:

An oral squamous cell carcinoma model was induced on mice by chronic exposure to 4-Nitroquinoline 1-oxide (4NQO). The chemical induces DNA instability and accumulation of mutation in the epithelium of the oral cavity, primarily on the tongue dorsum. We then apply next-generation sequencing and advanced confocal microscopy, to analyse the molecular cascade and the structural changes driving cancer development.

Results:

We identified in the Notch pathway a major player in all stages of the oral cancer progression: initiation, establishment and growth. We then dive into the details of the Notch molecular cascade to identify the specific receptor-ligand interaction and the downstream targets directing cancer development. Similarly to other systems, dysregulation of the Notch pathway alters the expression of the transcription factors of the RUNX family and activation of the Wnt pathway.

Conclusion:

In conclusion, we identified a novel, druggable target crucial for the oral squamous cell carcinoma development. The Notch1-Dll4 interaction is present since the initial phases of cancer emergence, providing an early stage marker for carcinoma detection. The same interaction has been proven essential for the growth of oral carcinoma, revealing a functional role in the maintenance and progression of this type of cancer.

C. Pasin^{8,9}, I. Abela^{8,9}, D. Garcia Nuñez⁶, K. Kusejko^{8,9}, K. Aebi-Popp⁷, H. Buvelot², M. Cavassini⁴, L. Damonti⁵, C. Fux³, A. Hachfeld⁷, B. Martinez de Tejada², P. Vernazza¹, A. Trkola⁹, H. Günthard^{8,9}, R. Kouyos^{8,9}

Hormone intake differentially affects the immune system of HIV-positive cis and trans women

Cantonal Hospital St Gallen¹, Geneva University Hospital², Kantonsspital Aarau³, Lausanne University Hospital⁴, Regional Hospital Lugano⁵, University Hospital Basel⁶, University Hospital Bern⁷, University Hospital Zurich⁸, University of Zurich⁹

Introduction:

Sex and gender differences in immune responses and in pharmacokinetics and pharmacodynamics have been observed in many conditions, including SARS-CoV-2 infection and HIV disease. These differences could be partly due to the modulatory effect of hormones on the immune system. The effect of hormones on the dynamics of HIV immune markers has not been extensively explored. Moreover, concerns regarding drug-drug interactions between antiretroviral treatment (ART) and hormones might limit hormone prescription by physicians in cis women (CW) and trans women (TW). It is also unclear how the sex differences in drug responses translate to TW taking hormones. We aimed to quantify the effect of oestrogen and/or progestogen intake on the immune system by comparing several key HIV biomarkers in different HIV-positive groups: CW under hormone intake (CW-H) or not (CW-NH), and TW under hormone intake (TW-H) or not (TW-NH).

Methods:

The Swiss HIV Cohort Study (SHCS) is a prospective multicenter cohort study enrolling people living with HIV in Switzerland. We considered laboratory measurements from CW and TW after January 1st, 2015, when systemic report of most comedications taken by SHCS patients started. Measurements during pregnancy and those not on ART were excluded. Hormone intake was defined as either oestrogens and progestogens alone or in combination. We classified laboratory measurements into those sampled during hormone intake or not. CD4+ T cell counts, CD8+ T cell counts and CD4:CD8 ratio were estimated using linear mixed effect models with a random effect per patient and adjusted for ethnicity, transmission mode, education level, last center of follow up, age at sample, years on ART, depression status, smoking status, and menopause status. We ensured consistency by using two models: M1 with a single "group" variable (CW-NH, CW-H, TW-NH, TW-H) and M2 with the variables "gender" (CW, TW), "under hormones" (yes, no), and the interaction term.

Results:

We identified 76 TW with 402 TW-H and 695 TW-NH laboratory measurements, and 3038 CW with 2690 CW-H and 41033 CW-NH laboratory measurements. Hormone intake was significantly associated with increased CD4 counts of 22 (13-32, $p=9.10^{-6}$) in CW and 89 (60-118, $p=3.10^{-9}$) in TW (M1: see figure). The increase was significantly higher in TW versus CW (interaction term in M2: $p=3.10^{-5}$). Results were robust when considering the square root of CD4 counts. Only TW-H had significantly higher CD8 counts than TW-NH ($p=0.03$), leading to an unchanged CD4:CD8 ratio in TW-H versus TW-NH, but a significantly higher ratio in CW-H versus CW-NH (0.06 (0.04-0.08), $p=3.10^{-9}$).

Conclusion:

Hormonal intake was associated with statistically significantly higher CD4+T cell counts and CD4:CD8 ratio in CW (in line with comparisons between CW and cis men), and both significantly higher CD4+ and CD8+ T cells counts in TW. This suggests differential effects of hormone intake in CW versus TW, potentially due to differences in doses, combination of hormones taken, and/or mechanisms of actions of hormones on the immune system in CW and TW.

N. Keller¹, M. Boumasmoud¹, F. Andreoni¹, A. Tarnutzer¹, T. Scheier¹, A. Gomez-Mejia¹, M. Huemer¹, E. Marques Maggio¹, R. Schuepbach¹, S. Mairpady Shambat¹, S. Brugger¹, A. Zinkernagel¹

Group A Streptococcus persists in necrotizing fasciitis resulting in antibiotic tolerance

*University Hospital Zurich*¹

Introduction:

Group A Streptococcus (GAS, aka *Streptococcus pyogenes*) is one of the major bacterial pathogens causing life-threatening acute infection such as necrotizing fasciitis (NF). GAS NF is a devastating bacterial infection still associated with high morbidity and mortality despite appropriate antibiotic treatment and extensive surgical debridement. NF is often fueled by the presence of a high bacterial load, biofilm formation and necrosis, necessitating surgery in order to prevent treatment failure. We recently showed that staphylococcal infections and treatment failure were linked to the presence of persister cells. Persisters are a subpopulation of bacterial cells that tolerate antibiotics for a prolonged time, without displaying antibiotic resistance. Whether such antibiotic tolerant persisters are associated with GAS-NF is not known.

Methods:

To investigate GAS persisters in NF, bacteria freshly collected from tissue debrided from GAS NF patients were plated and characterized for their colony appearance time and colony size heterogeneity. In in vitro modelling studies, bacterial isolates derived from the patients were stressed by exposure to acidic pH or nutrient starvation, mimicking the host stress associated with NF. Bacteria were subsequently challenged with antibiotics and persisters formation was assessed in vitro.

Results:

GAS recovered directly from NF patients were characterized by increased colony appearance time resulting in heterogeneity, indicating the presence of persisters. In addition we demonstrated that this heterogeneity was induced in vitro after applying stressors such as low pH or nutrition starvation, resulting in increased antibiotic tolerance.

Conclusion:

We describe the formation of GAS persisters in samples derived directly from GAS NF patients for the first time. These persisters exhibit antibiotic tolerance and contribute to the low success rate of antibiotics in GAS NF treatment.

S. Barco⁴, D. Voci⁴, H. Held⁵, T. Sebastian⁴, S. Roth⁴, R. Spescha⁴, R. Bingisser⁹, G. Colucci¹¹, D. Duerschmied⁷, A. Frenk⁶, B. Gerber³, S. Konstantinides², F. Mach¹, M. Righini⁸, T. Rosemann¹⁰, S. Stortecky⁶, S. Windecker⁶, N. Kucher⁴

Enoxaparin for primary thromboprophylaxis in ambulatory patients with coronavirus disease-2019: the investigator-initiated OVID randomized controlled trial

Cardiology Division, Geneva University Hospital, Geneva¹, Center for Thrombosis and Hemostasis, University Medical Centre of the Johannes Gutenberg University, Mainz², Clinic of Haematology, Oncology Institute of Southern Switzerland, Bellinzona³, Department of Angiology, University Hospital Zurich⁴, Department of Biostatistic and Epidemiology, University of Zurich⁵, Department of Cardiology, Inselspital Bern, University of Bern⁶, Department of Medicine III (Interdisciplinary Medical Intensive Care), Medical Center, Faculty of Medicine, University of Freiburg⁷, Division of Angiology and Haemostasis, Department of Medical Specialties, Geneva University Hospital⁸, Emergency Department, University Hospital Basel⁹, Institute of Primary Care, University of Zurich¹⁰, Service of Haematology, Clinica Luganese Moncucco, Lugano¹¹

Introduction:

It is unknown whether adding antithrombotic therapy with low-molecular-weight heparin may reduce early hospitalisations and thromboembolic events among symptomatic but clinically stable outpatients with COVID-19.

Methods:

The OVID study was conducted as a multicentre multinational investigator-initiated open-label superiority randomised controlled trial. Symptomatic patients aged 50 years or older with a positive test for SARS-CoV2 in the past 5 days and eligible for ambulatory treatment were included. The key exclusion criteria included: (i) any acute or chronic condition posing an indication for anticoagulant treatment, e.g. atrial fibrillation, prior venous thromboembolism (VTE), acute confirmed symptomatic VTE, acute coronary syndrome; (ii) anticoagulant thromboprophylaxis deemed necessary in view of the patient's history, comorbidity or predisposing strong risk factors for thrombosis; (iii) recent major bleeding or use of dual antiplatelet therapy; (iv) haemoglobin < 8 g/dL or severe renal insufficiency. Patients randomized to the intervention group received subcutaneous enoxaparin at the recommended dose of 4,000 IU anti-Xa activity (40 mg/0.4 ml) once daily for 14 days. Patients randomized to the comparator group received no anticoagulation (standard treatment). The primary outcome was a composite of any unplanned hospitalization and all-cause death occurring within 30 days of randomization. A single interim analysis with predefined criteria for early stop (futility or superiority) is planned after the enrolment of 50% of the study population. An independent data and safety monitoring board composed of two physician and one statistician monitored the study. The OVID trial was funded by the Swiss National Science Foundation (SNF) and by the University Hospital Zurich. Study ID: NCT04400799

Results:

From August 2020 to January 2022, a total of 475 patients with symptomatic COVID-19 who were candidate to an ambulatory treatment were randomly assigned to receive either prophylactic-dose enoxaparin or standard treatment. The predefined intention-to-treat interim analysis of the primary study outcome will be conducted on 15 Feb 2022, 30 days after the enrolment of the latest patients.

Conclusion:

The final results of the interim analysis will be presented in occasion of the meeting.

T. Thavayogarah¹, G. Nair¹, D. Balabanov¹, M. Manz¹, D. Müller², U. Schanz¹

Optimization of fludarabine pharmacokinetics to reduce the relapse incidence in AML patients after allogeneic stem cell transplantation

*Departement of Medical Oncology and Hematology, University Hospital and University of Zurich¹,
Institute of Clinical Chemistry, University Hospital Zurich, Switzerland²*

Introduction:

Acute myeloid leukemia (AML) is a hematological, clonal malignancy of the myeloid stem cell precursors, which is proliferative and is characterized by clonal evolution and genetic heterogeneity. For adverse risk acute myeloid leukemias, allogeneic stem cell transplantation (allo HCT) is one of the most potent curative options. Unfortunately, disease relapse is still around 40% in the first year after HSCT. In allo HCT, fludarabine is a frequently used agent, mainly in reduced intensity conditioning regimens. It is often combined with busulfan for which dose individualization based on pharmacokinetics with area under the curve (AUC) determination is used successfully for many years. It has already been shown that fludarabine exposure might be predictive for the survival in allo HCT and it is suggested that individualized dosing can improve the survival after transplantation within the first year. Actually for fludarabine dose calculation in adults, only the body surface area is used, which might either result in too high exposition causing increased toxicity or with too low exposure and increased relapse incidence (RI). With the aim to reduce RI we established pharmacokinetic measurements for fludarabine in addition and combined to the established ones for busulfan.

Methods:

Fludarabine was measured with a validated LC-MS/MS method. The exposure, expressed as AUC, was calculated for each patient using a three-compartmental model (adapted from Langenhorst et al.) in n=19 consecutive patients receiving a conditioning regime with fludarabine being diagnosed with acute myeloid leukemia. Fludarabine was given on days -7 to -2 with a dose calculation based on 30mg/m² infused over 30 minutes. In addition patients received peroral busulfan 4mg/kg bw on days -3 and -2 and ATG 10mg/kg bw (Grafalon®) on days -4 to -1.

Results:

So far, there is no dose individualization based on pharmacokinetic parameters for fludarabine specifically suggested in AML patients. The study published by Langenhorst et al. mixed up benign and malignant hematological malignancies, suggests lower optimal fludarabine AUC than we observed in our patients. We have seen that the fludarabine AUC were higher within our patients. In the analysis of Langenhorst et al. the optimal AUC was postulated to be 20 mg*h/l. In our (n=19) AML patients the median of the AUC was 42.97 (+/- 11.5) mg*h/l, twice as high than the suggested level for an optimal toxicity profile. However, none of our patients experienced any acute toxicity (within 30 days after transplant). Our 1 year TRM is stable for many years with 2-4%. Moreover, there was also no major toxicity (e.g. cytopenias, infections) seen at day 100. So far, we did not see a low retrospective RI (currently 35% at 1 year) despite the AUC was much higher than the suggested optimal levels.

Conclusion:

In a regimen with more (6 vs 4), but lower single fludarabine dosage (30mg/m² vs 40mg/m²) and a shorter infusion duration (30min vs 60min) resulting in higher AUC (40mg*h/l vs 20 mg*h/l) than previously published. Within our small cohort, a low RI or high TRM seem not to be observed compared with a retrospective cohort. Further prospective data within an observational study are needed.

L. Planas-Paz¹, A. Pliego-Mendieta¹, C. Hagedorn¹, F. Arnold¹, C. Pauli¹

Investigating HRDness in sarcoma

Department of Pathology and Molecular Pathology, University Hospital Zürich, Switzerland¹

Introduction:

Sarcomas are rare mesenchymal cancers, accounting for approximately 1 % of all malignancies. They can arise anywhere in the soft tissue in the body as well as in bone and consist of more than 70 distinct subtypes. Standard of care mostly relies on radiation, chemotherapy and surgical resection. Sarcoma often show chemoresistance and metastatic disease is associated with a poor prognosis. There is an increasing emphasis on understanding the cancer biology of individual sarcoma subtypes to inform the development of personalized targeted treatment approaches. Studies performed in distinct sarcoma subtypes have revealed mutational signatures reminiscent of HRDness. The homologous recombination (HR) pathway is essential for high-fidelity DNA double strand break (DSB) repair and involves numerous genes such as BRCA1 and BRCA2. HR deficiency (HRD) due to inactivation of such genes leads to impaired DSB repair and increased levels of genomic alterations. Accurate detection of HRD is of clinical relevance as it is indicative of sensitivity to targeted therapy with poly ADP-ribose polymerase inhibitors (PARPi) as well as to DNA damaging reagents. The prevalence of HRD extends beyond BRCA1/2-deficiency and includes other genes such as ATM, PALB2 and RAD51C that are active in this pathway. Consequently, treatment opportunities are overlooked, and this highlights the need for the development of better biomarkers for HRD.

Methods:

We investigated genomic instability in sarcoma by measuring chromosomal instability (CIN) features as well as the genomic scar signatures LOH, LST and TAI. We cross-validated our findings from different sarcoma subtypes among several data sources. We established and genomically characterized eight patient-derived ex vivo sarcoma cell models. We functionally tested the sensitivity of our models to several targeted therapies and chemotherapies in six point dose response curves either in monotherapy or in combination.

Results:

We showed that a subset of sarcoma entities exhibit high levels of aneuploidies, a complex pattern of chromosomal gains and losses and a high HRDscore. These features of HRDness were accompanied by specific gene expression signatures that correlate with HR repair deficiency in other tumor types. In addition, we found that deficiency in HR repair mechanisms was among the most significant mutational signatures in HRD^{high} sarcoma. At the transcriptomic level, we identified transcriptional signatures and gene sets involved in cell cycle processes and DNA repair mechanisms enriched in HRD^{high} sarcoma. We functionally evaluated the sensitivity of sarcoma to PARP inhibition and showed a significant reduction in cell viability in HRD^{high} patient-derived ex vivo sarcoma cell models compared to HRD^{low} cell models. Combined modality treatment with chemotherapy further enhanced the effect of PARP inhibitors on cell viability. Furthermore, we demonstrate a dependency of other DNA repair pathways for the viability of HRD^{high} sarcoma cell models, thereby highlighting potential new targeting strategies.

Conclusion:

We show that a subset of sarcoma entities exhibit features of HRDness at the genomic and transcriptomic level and highlight the need to characterize sarcoma patients with multiple parameters to better identify those with HRDness. We functionally demonstrate that PARP inhibitors are a promising tool for personalizing the treatment of HRD^{high} sarcoma patients. In addition, we identified other targeted therapies, beyond PARP inhibitors, targeting DNA repair pathways that may also benefit such patients.

S. Salemi², L. Schori², G. Gerwinn¹, M. Horst¹, D. Eberli²

Influence of myostatin inhibitor on smooth muscle cells regeneration

University Children's Hospital Zürich, Department of Pediatric Surgery¹, University Hospital Zürich, Department of Urology²

Introduction:

Cell therapies and tissue engineering approaches using smooth muscle cells may provide alternative treatments for diseases such as bladder dysfunction, urinary incontinence and erectile dysfunction. Myostatin is a negative regulator of muscle growth and development and its inhibitors are used in clinical trials as a therapy for skeletal muscle diseases, but the role of myostatin has not yet been reported within bladder smooth muscle cells (SMCs). Therefore, the ultimate goal of our research is to improve the SMCs quality and quantity by direct inhibition of myostatin using Domagrozumab or indirect inhibition by Suramin. Therefore, we investigated the expression pattern of myostatin gene and protein in bladder biopsies obtained from children with normal and neuropathic bladder dysfunction.

Methods:

Human bladder tissue samples were evaluated histologically and SMCs were isolated and characterized by flow cytometry (FACS). SMCs were cultured in the presence and absence of Domagrozumab (1pg- 10ug/ml) or Suramin (100 ng-50 µg/ml). Cells proliferation was evaluated by WST-1 assay. The impact of Domagrozumab or Suramin on SMCs protein expression was analyzed by FACS, immunoblotting and immunofluorescent staining.

Results:

Histological assessment via H&E staining of the bladder tissue confirmed the described alterations of neuropathic bladder, such as structural changes and decreased muscle to collagen ratios compared to normal bladder. Decreased cell proliferation was observed in neuropathic compared to control bladder SMCs. All contractile proteins; alfa SMA, calponin, smoothelin and myosin heavy chain 11 (MYH11) were expressed in both the groups. However, higher expression of alpha SMA and MYH11 was observed in control compared to neuropathic SMCs. Higher expression of myostatin was detected in neuropathic compared to control SMCs. Myostatin pathway related proteins Smad2 and Follistatin were higher in control SMCs but no differences were observed in phospho- Smad2 protein expression. Treatment with Domagrozumab (1 µg/ml) and Suramin (20 µg/ml) increased the cell proliferation in both groups. Down regulation of myostatin protein expression was observed upon treatment with Domagrozumab (1 µg/ml) and 50 µg/ml of Suramin. Decrease in myostatin led to increase in MYH11 in neuropathic SMCs.

Conclusion:

Our study demonstrates for the first time that myostatin is expressed in bladder SMCs. In addition, Domagrozumab and Suramin improve bladder SMCs proliferation and increase in the expression of late contractile proteins. This study indicates that both myostatin inhibitors may have a tissue engineering therapeutic potential for patients with incontinence and other smooth muscle disorders.

C. Jünger¹, F. Imkamp¹, S. Balakrishna¹, M. Gysin¹, K. Haldimann¹, R. Kouyos¹, S. Hobbie¹, H. Günthard¹, D. Braun¹

Phenotypic and genotypic characterization of *N. gonorrhoeae* strains in a men who have sex with men population with high-risk sexual behavior in Zurich Switzerland

*University Hospital Zurich*¹

Introduction:

The incidence of reported gonorrhoea is increasing worldwide, in particular among men who have sex with men (MSM). *Neisseria gonorrhoeae* can lead to serious sequelae. The growing number of multidrug resistant (MDR) *N. gonorrhoeae* strains has led to ceftriaxone being the sole recommended first-line treatment. Numerous countries report decreased in vitro susceptibility and treatment failures to ceftriaxone, creating an urgent threat and the need for new treatment options. In this study, we analyzed *N. gonorrhoeae* resistance patterns in a high-risk MSM population by phenotypic and genotypic means.

Methods:

Patients included in this study were systematically tested either because of sexual high-risk behaviour or due to symptomatic complaints at the department of infectious diseases and hospital epidemiology at the University Hospital Zurich from January 2019 to December 2021. From the 142 patients tested positive for *Neisseria gonorrhoeae* by polymerase chain reaction (PCR), we analysed clinical data and performed antibiotic susceptibility testing of 23 clinical isolates analysing a panel of twelve antimicrobials. Further, all isolates were subjected to whole genome sequencing (WGS) to gain more detailed insights in mechanisms underlying the different phenotypic resistance patterns.

Results:

Overall, 182 positive PCR tests obtained from 142 participants were analysed, of whom all but one were male and MSM. The median year of birth was 1980 and 118 (84%) of the participants were HIV-positive. 85 (60%), 70 (50%) and 64 (45%), had at least one previous syphilis, *Chlamydia trachomatis* and *N. gonorrhoeae* infection, respectively. 68 patients (87%) acquired the *gonorrhoeae* in Switzerland. Of all 142 participants tested positive for gonorrhoea, 85 (60%) participants were asymptomatic. All participants were treated with ceftriaxone intramuscularly (N= 79), azithromycin orally (N= 2) or a combination of both (N = 61), according to local guidelines and determined resistance patterns. No participant showed lack of microbiological or clinical cure. Of the 142 participants with a positive PCR test for gonorrhoea, 23 isolates were cultured. All isolates demonstrated susceptibility and low minimal inhibitory concentrations (MICs) to ceftriaxone (MIC-range: 0.003-0.03 mg/L), cefixime, cefpodoxime, ertapenem, zoliflodacin and spectinomycin. Cefixime (0.004-0.042 mg/L) and cefpodoxime (0.016-0.19 mg/L) exhibited similar MICs to ceftriaxone (0.004-0.042 mg/L). Resistance to azithromycin and tetracyclines was seen in 43% and 100% respectively. 48% of participants showed resistance towards ciprofloxacin. Analysis of WGS data revealed various combinations of resistance determinants which matched well with phenotypic resistance of the isolates, respectively.

Conclusion:

In our study population consisting of mainly MSM living with HIV diagnosed with gonorrhoea, first-line treatment ceftriaxone showed low MICs in all samples and no treatment failures were observed. The therapeutically useful alternative agents, ertapenem, cefixime, zoliflodacin, spectinomycin and cefpodoxime showed promising results with excellent in vitro activity, representing potential therapeutic candidates in case that ceftriaxone is contraindicated or not available. Azithromycin, which current guidelines recommend as the first alternative among individuals with severe allergy to ceftriaxone, shows high levels of in vitro resistance in our population.

W. Baumgartner², P. Wolint², S. Hofmann², C. Nüesch², M. Calcagni², M. Brunelli¹, J. Buschmann²

Impact of fiber mesh structure and tensile stretching of coaxial electrospun scaffolds on tenogenic and inflammatory gene expression in human adipose-derived stem cells

EMPA St. Gallen¹, Plastic Surgery and Hand Surgery, USZ²

Introduction:

Tendon injuries are among the most occurring musculoskeletal injuries. Due to their low cell densities and low metabolic activity, tendons only heal very slowly. After critical size defects, tendons must be regenerated, at best with a construct that is fast and well integrated into the surroundings and leads to a strong and long-term stable graft. Adipose-derived stem cells (ASC) belong to one of the most popular populations of adult stem cells in regenerative medicine, which also show clinical relevance. It is possible to obtain ASCs from large quantities of lipoaspirates, in the context of plastic surgery procedures. The cells thus obtained are grown under standard tissue culture conditions. By appropriately stimulating through external cues, such as specific substrates or dynamic cell cultivation, the cells can differentiate into the tenogenic lineage. In this study, gene expression of ASCs incubated under either static or dynamic conditions on a novel coaxial electrospun biomaterial was investigated and the two conditions were compared.

Methods:

The coaxially electrospun scaffold based on Polyvinylidene-Fluoride/Hexafluoropropylene-Polydimethylsiloxane (PVDFhfp/PDMS) has been recently developed at EMPA St. Gallen. The core/shell fiber meshes have been fabricated either as aligned or as random fiber meshes. ASCs were seeded onto these scaffolds and either cultivated for one week under static conditions or with subsequent 10% dynamic stretching for 10,800 cycles (1 Hz, 3 h), assessing load elongation curves in a Bose® bioreactor system. Afterwards, RNA of the ASCs was isolated and quantitative real-time PCR was performed for typical tenogenic and inflammation markers, as well for genes of matrix metalloproteases (MMPs).

Results:

Core/shell microfibers of PVDFhfp/PDMS enhanced tenogenic marker genes, such as Tenascin-C (TNC), Tenomodulin (TNMD) and Scleraxis (SCX), of ASCs compared to ASCs cultivated without scaffold. Significantly higher TNMD gene expression was observed under dynamic conditions compared to static culture. As for inflammatory marker genes, IL-8 was upregulated, while IL-6 was downregulated on PVDF/hfp-PDMS compared to ASCs without scaffold. Likewise, pro-inflammatory marker genes were upregulated by dynamic stretching. Regarding ECM markers, collagen III in ASCs showed significantly higher expression on random fibers than on aligned fibers. However, promotion of tenogenic markers was particularly exhibited on random fiber meshes and not on aligned fibers.

Conclusion:

Random core/shell fibers fabricated on the basis of PVDFhfp/PDMS enhanced tenogenic marker gene expression to a higher extent compared to aligned fibers of the same material. Additionally, static cultivation is preferred over dynamic cultivation since dynamic cultivation showed a prominent upregulation of pro-inflammatory markers. Due to the high elasticity of this material and the ability to stimulate the cells towards a tenogenic phenotype, it is qualified as an implant which surrounds the sutured injured tendon as a functional anti-adhesion membrane.

T. Pappasotiropoulos², I. Martínez López², F. Schlöpfer², S. Ulrich¹, I. Opitz², M. Kirschner²

MicroRNA expression in Chronic Thromboembolic Pulmonary Hypertension

Department of Pulmonology, University Hospital Zurich¹, Department of Thoracic Surgery, University Hospital Zurich²

Introduction:

Chronic thromboembolic pulmonary hypertension (CTEPH) is a rare, chronic illness with severe course of disease, characterized by symptomatic pulmonary hypertension and caused by bilateral pathological chronic thickening of the intima layer of the pulmonary arteries (PA). The underlying molecular and pathogenic mechanisms are still largely unexplored. Aiming to understand a possible contribution of microRNAs in CTEPH, we investigated expression levels of two specific microRNAs in pulmonary endarterectomy (PEA)-derived tissue.

Methods:

We analysed the expression of microRNAs let-7b and let-7d in PEA specimens of 45 CTEPH patients and in PA tissue from explanted lungs of 10 patients who underwent lung transplantation (reference PA). Spearman's correlation was performed to investigate possible relationships between microRNA expression and clinical parameters, and Mann-Whitney-U test was used to investigate differences in microRNA expression between CTEPH tissue and reference PA.

Results:

Both let-7b and let-7d were successfully quantified in PEA-derived tissue. Expression levels of let-7b and let-7d were positively correlated between left and right side ($r = 0.403$, $p = 0.016$ and $r = 0.615$, $p < 0.001$, respectively). Moreover, let-7b expression of both sides was positively correlated with let-7d expression of the same side (right: $r = 0.377$, $p = 0.020$; left: $r = 0.615$, $p < 0.001$). There was no significant correlation between microRNA expression levels and clinical parameters. Unlike our observation for two other microRNAs on which we reported previously, in this sample subset, no statistically significant differences of let-7b and let-7d expression levels between CTEPH samples and reference PA samples were found.

Conclusion:

This is one of the first studies evaluating microRNAs in PEA-derived tissue. Our results do not argue in favour of a marked association between expression levels of microRNAs let-7b and let-7d and clinical presentation of CTEPH patients, although such correlations have been observed for other microRNAs. However, based on previous studies, it is possible that these specific microRNAs act more like systemic trait-markers, with elevated plasma expression levels implying a higher susceptibility towards CTEPH. Nevertheless, the successful detection and quantification of let-7b/7d in CTEPH tissue is a first step towards the study of the possible involvement of microRNAs in pathogenic mechanisms leading to CTEPH.

I. Abela^{6, 8}, C. Pasin^{6, 8}, M. Schwarzmüller⁸, S. Epp⁸, M. Sickmann⁸, M. Schanz⁸, P. Rusert⁸, J. Weber⁸, S. Schmutz⁸, A. Audigé⁸, L. Maliqi⁸, A. Hunziker⁸, M. Hesselman⁸, C. Niklaus⁸, J. Gottschalk¹, E. Schindler¹, A. Wepf⁷, U. Karrer⁴, A. Wolfensberger⁶, S. Rampini², P. Meyer Sauter⁵, C. Berger⁵, M. Huber⁸, J. Böni⁸, D. Braun^{6, 8}, M. Marconato³, M. Manz³, B. Frey¹, H. Günthard^{6, 8}, R. Kouyos^{6, 8}, A. Trkola⁸

Multifactorial seroprofiling dissects the contribution of pre-existing human coronaviruses responses to SARS-CoV-2 immunity

Blood Transfusion Service Zurich, Switzerland¹, Department of Internal Medicine, University Hospital Zurich, Zurich, Switzerland², Department of Medical Oncology and Hematology, University Hospital and University of Zurich, Switzerland³, Department of Medicine, Cantonal Hospital Winterthur, Winterthur, Switzerland⁴, Division of Infectious Diseases and Hospital Epidemiology, University Children's Hospital Zurich, Zurich, Switzerland⁵, Division of Infectious Diseases and Hospital Epidemiology, University Hospital Zurich, Switzerland⁶, Institute of Laboratory Medicine, Cantonal Hospital Winterthur, Winterthur, Switzerland⁷, Institute of Medical Virology, University of Zurich, Switzerland⁸

Introduction:

Determination of SARS-CoV-2 antibody responses in the context of pre-existing immunity to circulating human coronavirus (HCoV) is critical to understand protective immunity.

Methods:

We performed a multifactorial analysis of SARS-CoV-2 and HCoV antibody responses using a custom-designed multiplex bead-based assay. Specific IgG, IgA, and IgM responses to SARS-CoV-2 antigens (RBD, S1, S2, and N) and HCoV antigens (S1 of HKU1, OC43, 229E, and NL63) were measured in healthy pre-pandemic (N=825) and SARS-CoV-2-infected donors (N=389).

Results:

Time-matched analysis of antibody responses revealed significantly higher HCoV reactivity in healthy donors (N=653) compared to SARS-CoV-2-positive patients (N=65). In early infected patients (N=204, up to 60 days after infection), high HCoV reactivity was associated with elevated SARS-CoV-2 responses, indicating cross-stimulation of antibody responses. Most importantly, in a subset of SARS-CoV-2-positive patients (N=80), high HCoV reactivity was associated with significantly lower odds to require hospitalization compared to low HCoV reactivity (logistic regression OR=0.16, 95% CI (0.04, 0.67)).

Conclusion:

Uninfected individuals displayed higher HCoV reactivity compared to infected individuals, suggesting that pre-existing HCoV immunity may protect against SARS-CoV-2 acquisition. SARS-CoV-2-infected individuals with high HCoV reactivity developed higher SARS-CoV-2 antibody levels, indicating that HCoV immunity may also have positive effects in SARS-CoV-2 infection. Most notably, we observed an impact of HCoV immunity on disease severity, as SARS-CoV-2-infected individuals with low HCoV reactivity had a higher likelihood of requiring hospitalization. Collectively, this evidence points to HCoV immunity promoting the rapid development of SARS-CoV-2-specific immunity, underscoring the importance of exploring cross-protective responses for comprehensive coronavirus prevention.

N. Klemm¹, N. Konrad¹, J. Fullin¹, R. Schimmer¹, S. Stolz¹, E. Topcu¹, S. Böttcher¹

Elucidating the molecular mechanism of the dominant-negative effect of the p53 missense variant R248Q

Department of clinical oncology and hematology, USZ¹

Introduction:

The transcription factor p53 – encoded by its gene *TP53* – is the most frequently mutated gene in cancer. Unlike other tumor suppressors, most *TP53* mutations are missense mutations clustering in the DNA binding domain and leading to the expression of aberrant p53 variants. It was recently shown that the driving force for the selection of *TP53* missense mutations during tumorigenesis – creating this unusual mutational spectrum – is the ability of missense p53 variants to exert a dominant-negative effect (DNE) over wild-type p53 in a heterozygous genotype. Since the DNE has not been thoroughly studied so far, we aim to characterize the DNE and elucidate its molecular mechanism while focusing on *TP53*^{R248Q} - one of the most common *TP53* missense mutations.

Methods:

To characterize the DNE, isogenic human acute myeloid leukemia (AML) cell lines MOLM13 harboring a full allelic series of *TP53* mutations (*TP53*^{+/+}, *TP53*^{+/-}, *TP53*^{-/-}, *TP53*^{R248Q/+}, *TP53*^{R248Q/-}) generated by CRISPR-mediated genome editing were used to perform competition assays upon treatment with p53-activating agents. Its dependency on p53-regulated pathways was validated by flow cytometry-based analysis of their apoptotic potential and cell cycle progression via Annexin-V and Cytophase Violet staining, respectively. Given that p53 is a tetrameric protein, the dependency of the DNE on heterotetramerization was determined by transient transfection of plasmids encoding oligomerization-deficient p53 variants into reporter cell lines expressing a p53-regulated p21-GFP fusion protein and subsequent flow cytometric analysis. Prior and post cycloheximide treatment, Western Blot (WB) analysis was performed to determine the abundance and stability of p53^{R248Q} versus p53^{WT}. Whether mutant p53 accumulation provokes the DNE was determined (1) by transient transfection of varying ratios of plasmids encoding p53^{R248Q} versus p53^{WT} into p21-GFP reporter cell lines, and (2) by a quantifiable and inducible targeted p53^{R248Q} degradation assay using an artificial degron protein tag.

Results:

We identified a competitive growth advantage of *TP53*^{R248Q/+} over *TP53*^{+/-} cells, but none between *TP53*^{R248Q/+} and *TP53*^{R248Q/-} cells. Upon DNA damage, the apoptotic potential, and the ability to undergo cell cycle arrest in G1 was equally lost in *TP53*^{R248Q/+} and *TP53*^{R248Q/-} cells as compared to *TP53*^{+/-} cells thereby clearly indicating that p53^{R248Q} exerts a DNE over p53^{WT}. Transient expression of tetramerization-deficient p53^{R248Q} variants partially restored p53^{WT} function, whereas it has been fully recovered upon impairment of p53^{R248Q} dimerization, suggesting that heterotetramerization is required to exert the DNE. Surprisingly, transfecting p53^{WT} into p21-GFP reporter cells rescued p53 function in a dose-dependent manner, suggesting that the strength of the DNE depends on p53^{R248Q} protein abundance. This hypothesis was further substantiated by transient expression of varying ratios of p53^{WT} and p53^{R248Q}, and by targeted p53^{R248Q} degradation experiments, both resulting in restoration of p53^{WT} function upon p53^{R248Q} reduction. In line with this assumption, WB analysis of the isogenic cell models showed an accumulation of p53^{R248Q} caused by increased protein half-life.

Conclusion:

Our studies demonstrate that the p53^{R248Q} missense variant exerts a DNE over p53^{WT}, which was shown to be dependent on: (1) Heterotetramerization, and (2) supraphysiological levels of missense mutant protein levels resulting from an increased protein half-life of p53^{R248Q}. Ongoing studies will address the exact mechanism of p53^{R248Q} protein accumulation, and how p53^{R248Q} protein abundance could be pharmacologically targeted – potentially providing a therapeutic window of opportunity for cancer patients with heterozygous *TP53* missense mutations.

S. Klinnert^{1, 2, 3}, A. Chemnitzer^{1, 2}, P. Rusert², K. Metzner^{1, 2}

Systematic HIV-1 promoter targeting with CRISPR/dCas9-VPR reveals optimal region for activation of the latent provirus

Department of Infectious Diseases and Hospital Epidemiology, University Hospital Zurich, University of Zurich, CH-8091 Zurich, Switzerland¹, Institute of Medical Virology, University of Zurich, CH-8091 Zurich, Switzerland², Life Sciences Graduate School, University of Zurich, CH-8091 Zurich, Switzerland³

Introduction:

CRISPR/dCas9-based activation systems (CRISPRa) enable sequence-specific gene activation and are therefore of particular interest for the “shock and kill” cure approach against HIV-1 infections. This approach aims to activate the latent HIV-1 proviruses in infected cells and subsequently kill these cells. Several CRISPRa systems have been shown to specifically and efficiently activate latent HIV-1 when targeted to the HIV-1 5’LTR promoter, making them a promising “shock” strategy.

Methods:

Here, we aimed to evaluate the dCas9-VPR system for its applicability in reversing HIV-1 latency and identify the optimal gRNA target site in the HIV-1 5’LTR promoter leading to the strongest activation of the provirus with this system.

Results:

We systematically screened the HIV-1 promoter by selecting 14 specific gRNAs that cover almost half of the HIV-1 promoter region from the 3’ half of the U3 until the beginning of R. Transfection of TZM-bl and J-Lat 10.6 cells showed high efficiency of HIV-1 activation by dCas9-VPR and revealed an optimal activation region in the HIV-1 promoter, -165 to -106 bp from the transcriptional start site. Moreover, one gRNA target site within this region could be identified as the most effective site for proviral activation with dCas9-VPR.

Conclusion:

Our data demonstrates that the dCas9-VPR system is a powerful tool for HIV-1 activation and could be harnessed for the “shock and kill” cure approach.

J. Fullin¹, N. Klemm¹, R. Schimmer¹, S. Stolz¹, E. Topcu¹, C. Koch¹, S. Böttcher¹

The Divergent Roles of Mono- and Biallelic TP53 Mutations in Leukemogenesis

Department of medical Oncology and Hematology, University Hospital Zurich¹

Introduction:

Mutations in the tumor suppressor gene TP53 affect approximately 50% of tumors across all cancer entities and are commonly associated with an inferior patient survival. While the prognostic value of alterations in TP53 for myeloid malignancies is well established, only recent efforts demonstrated that the allelic configuration of these alterations is of great clinical relevance. In fact, a study in a large cohort of patients with myelodysplastic syndromes showed that the well-established association of TP53 mutations with a complex karyotype and a dismal prognosis is confined to patients with biallelic inactivation of TP53 only. This striking finding implicates divergent roles of mono- and biallelic inactivation of wild-type TP53 regarding both, their functional effects and their clinical consequences. We therefore sought to further study this putative functional divergence and unravel the underlying molecular mechanisms.

Methods:

We have devised a strategy to generate a versatile in vitro model system allowing us to study the functional and molecular consequences of mono- and biallelic TP53 mutations in otherwise genetically stable hematopoietic progenitor cells. To this end, we made use of a recently established knock-in mouse model with inducible expression of Trp53.R245W - the murine equivalent of one of the most common TP53 missense mutations in cancer - linked to a GFP marker. Bone marrow cells from mice with wild-type Trp53, as well as carrying mono- and biallelic missense mutations were isolated and reversibly immortalized by forced expression of estrogen receptor-coupled homeobox b8 (Hoxb8), allowing to keep them in culture indefinitely upon the addition of β -estradiol, while maintaining their genomic integrity. Subsequently, a doxycycline-inducible Cre recombinase was introduced, enabling us to precisely control the timing of induction of Trp53 mutations as well as the proportion of Trp53 mutated cells in the population, which can be traced by their concomitant GFP expression. These cells were then used to characterize the unconfounded effects of the Trp53 allelic state on their propensity for clonal expansion, maintenance of genomic stability and potential for malignant transformation.

Results:

Immunophenotyping indicated that the immortalized cells resemble hematopoietic progenitor cells arrested at the granulocyte-macrophage progenitor stage, retaining their normal differentiation potential upon withdrawal of β -estradiol. P53-dependent functional characterization revealed strong reductions in target gene expression, induction of apoptosis and arrest at G1 stage of the cell cycle in cells with biallelic Trp53 mutations but only an intermediate phenotype in the monoallelic state. Notably, in co-culturing assays, cells with both, mono- and biallelic Trp53 mutations exhibited competitive advantages over their wild-type counterparts upon treatment with various chemotherapeutic agents. In contrast, analysis of γ H2AX signaling after recovery from DNA damage induction suggested a selective persistence of DNA damage in cells with biallelic Trp53 mutations only. While wild-type and monoallelic mutated cells underwent terminal differentiation and cell death upon termination of Hoxb8 overexpression by β -estradiol removal, biallelic mutated cells, pre-treated with DNA damaging agents, formed rare colonies of surviving cells with blocked differentiation - a hallmark of malignant transformation.

Conclusion:

Our data confirm and expand the recent clinical observations suggesting divergent roles of mono- and biallelic Trp53 mutations in leukemogenesis. While monoallelic mutations seem to be sufficient to induce clonal expansion, as it is observed in clonal hematopoiesis of indeterminate potential, inactivation of the second functional allele is necessary to promote genomic instability and provide the potential for transformation into highly aggressive myeloid neoplasms, which are characterized by complex karyotypes and a dismal prognosis.

L. Baroncini¹, T. Mlambo¹, R. Speck¹

Do macrophages have any antiviral activity in HIV infection?

*University Hospital Zurich*¹

Introduction:

Although it is well established macrophages are permissive to HIV infection, it is still unclear what their role in viral infection and disease progression is. The absence of robust pre-clinical models makes the study of these cells *in vivo* troublesome at best. Various *in vitro* models, mostly based on monocyte-derived macrophages, are already available. Nevertheless, these cell culture systems are not always representing patients immune response. We created a new humanized mouse model in which we can selectively deplete human myeloid cells at will, without perturbing any other immune subset. We did perform this depletion during HIV infection to explore if these cells play a role in its progression.

Methods:

In order to develop the mouse model, we generated recombinant CD34⁺ cells via lentiviral transduction. Recombinant cells, harbouring a suicide gene (iCasp9) under the control of a myeloid specific promoter, were transplanted in NSG new-borns. Upon engraftment, the model was validated *ex vivo* and *in vivo*, via dimerizing agent AP1903. Once validated, mice were infected with HIV-1 YU-2. AP1903 treatment was performed on weekly basis, in parallel to viral load evaluation (RT-qPCR). In-depth immunophenotyping of macrophages and dendritic cells was performed via flow cytometry in major organs to evaluate differences in activation between HIV infected and uninfected mice.

Results:

Model characterization showed suicide gene selective macrophage and myeloid cells expression. Furthermore, up to 95% cells expressing the transgene underwent apoptosis upon a single AP1903 treatment, both *ex vivo* and *in vivo*. Prolonged treatment (>4 weeks) was well tolerated by the animals and proved non-toxic. Myeloid cell characterization *in vivo* (HIV+ vs HIV-) showed significant M1 and M2 activation in most tissues analysed of HIV+ animals. These results corroborate with the 8-fold increase in HIV viral load observed upon myeloid cells depletion in HIV infected mice.

Conclusion:

Macrophages play a role in containing HIV-1 replication *in vivo* during HIV chronic infection. To discover the mechanisms by which this happens, next generation sequencing of these macrophages will be necessary. The model we created, based on recombinant hematopoietic stem cells can be used beyond the study of HIV. Applying from cancer research to diabetes.

F. Lehner¹, C. Kündig², S. Salemi¹, D. Eberli¹

Impact of pharmacological inhibition of human kallikrein 2 in prostate cancer in vitro

Department of Urology, University Hospital Zurich, Switzerland¹, Med Discovery SA, Epalinges, Switzerland²

Introduction:

Potent therapy options for castration-resistant prostate cancer (CRPC) are very limited and additionally we are confronted with drug resistance. The few options we have mainly affect the androgen axis. Human Kallikrein 2 (hK2), a serine protease, is a downstream target gene of the androgen receptor (AR) but it is also known to have an AR independent function. HK2 is a promising target for therapy in CRPC because of its high prostate cancer (PCa) specificity and its expression rate correlates to the rising cancer grade and stage. Therefore, we hypothesize that the inhibition of hK2 can lead to a suppression of tumor growth.

Methods:

Different human prostate cancer cell lines (PNT1A, LNCaP, C4-2, CWR1, PC3 and DU145) were cultured in 2D and 3D to test hK2 expression. Immunoblotting (WES) of cell lysates was performed. Cells were then treated with different concentrations of MDPK67b, which is a recombinant protease inhibitor targeting hK2, (0.1, 0.5, 0.75 and 1ug/uL) or vehicle over 7 days. Cell proliferation was measured by CellTiter-Glo. Immunofluorescent staining of hK2 and Ki-67 was performed after treatment.

Results:

Immunoblotting revealed hK2 expression in the LNCaP and C4-2 but not in PNT1A, CWR1 and PC3 cells. DU145 served as a negative control for further experiments. After treatment with MDPK67b a dose- and time-dependent decrease in cell viability was observed in LNCaP cells. The highest significant reduction in cell viability (50%) was achieved with 0.75ug/uL of inhibitor after 5 days compared to control. C4-2 showed significant reduction in cell viability starting at day 4 with all the concentrations tested. Interestingly, compared to LNCaP cells, C4-2 remained proliferative even after 7 days. No statistically significant reduction in cell viability was observed in DU145. Reduction of hK2 and Ki-67 expression was observed by immunofluorescent staining in LNCaP and C4-2 spheroids upon treatment with MDPK67b. In addition, decreased hK2 protein was detected in treated LNCaP and C4-2 cell lysates.

Conclusion:

Our study demonstrates that a pharmacological blockage of hK2 has a potent inhibitory effect in a dose- and time-dependent manner on cell proliferation in the LNCaP cell line. In the androgen independent cell line C4-2 a lower impact of inhibition was achieved. Taken together, hK2 represents an appealing therapeutic target and its inhibition might be an additional therapy option for CRPC to the standard drugs affecting the androgen axis.

A. Korczak², B. Carrara², K. Gengschatz-Schmid², Q. Vallmajó Martín^{1,2}, M. Ehrbar²

Functional characterization of human bone marrow stromal cells in vivo with increased throughput

Gene Expression Laboratory, Salk Institute for Biological Studies, USA¹, Laboratory for Cell and Tissue Engineering, Department of Obstetrics, University and University Hospital Zurich²

Introduction:

The human bone marrow (BM) is home to Hematopoietic Stem Cells (HSCs) and Bone Marrow Stromal Cells (hBMSCs) which are known to contain skeletal stem cell populations. Whereas the HSC compartment is well characterized, the identity and function of the hBMSC populations remain obscure and requires thorough investigation. A better understanding of the BM and the accommodated cells is crucial as changes in the microenvironment homeostasis may cause severe diseases including leukemia. Recent advances in single cell analysis featured hBMSCs as a heterogeneous cell population with only a small fraction of cells having the potential for multilineage differentiation and long-term self-renewal. To unveil the true fate of hBMSCs we perform cell implantations in vivo to reliably verify their function in the complex native environment.

Methods:

To reveal the function and hierarchical organization of distinct hBMSC subpopulations we propose to engineer a multiplexing screening device for efficient in vivo testing. Additionally, using transglutaminase crosslinked poly(ethylene glycol) (PEG) hydrogels we are establishing robust microenvironmental conditions for the osteo-, chondro- and adipogenic differentiation of hBMSCs. Then, we will encapsulate prospectively isolated hBMSC populations in defined microenvironments and place them in the implantable multiplexing device. Finally, multiplexing devices will be implanted in subcutaneous pouches of immune-deficient mice and used to assess the in vivo differentiation capacity of candidate subpopulations of hBMSCs.

Results:

First experiments dedicated to minimize the number of required hBMSCs and increasing the number of test conditions have revealed in vivo differentiation in an osteogenic microenvironment and formation of small bone ossicles containing a hematopoietic niche within the multiplexing device.

Conclusion:

In this project, we develop a multiplexing platform to screen hBMSC behavior in vivo in a higher throughput manner. We will optimize the designs for multiplexed testing of health and disease-related low-abundant hBMSC subpopulations, requiring minimal cell numbers and tiny hydrogel volumes. The results of this project will constitute an important foundation to study human BM stromal hierarchy and elucidate the functional role of individual hBMSC subpopulations.

M. Maane², G. Kullak-Ublick², S. Hobbie¹, M. Visentin²

Biochemical characterization of membrane transport and mitochondrial electron transport chain inhibitory effect of the aminoglycoside apramycin: side-by-side comparison with gentamicin

Institut für Medizinische Mikrobiologie¹, Klinik für klinische Pharmakologie und Toxikologie²

Introduction:

Aminoglycosides are potent broad-spectrum antibiotics whose use is limited by the early onset of nephrotoxicity and ototoxicity. Aminoglycosides bind to prokaryotic ribosomes, thereby inhibiting bacterial protein synthesis, but with lower affinity also to mitochondrial ribosomes, causing inhibition of mitochondrial protein synthesis, reduction of the steady-state level of mitochondrion-encoded proteins and, in turn, alteration of cellular respiration and energetics. One recent study showed that the aminoglycoside gentamicin could also directly inhibit the mitochondrial electron transport chain. Decades of clinical use have given rise to extensive resistance to aminoglycosides, mostly due to aminoglycoside-modifying enzymes (AMEs), which alter their chemical structures, thus lowering their affinity for the bacterial ribosome. The quest for novel aminoglycosides able to escape AME inactivation has led to the development of a number of rationally designed semisynthetic compounds, and to the discovery of apramycin as natural compound, that intrinsically evades almost all AMEs. Apramycin is a structurally unusual aminoglycoside, which has shown promising bactericidal activity against carbapenem-resistant *Acinetobacter baumannii*, reduced renal accumulation and a safer profile in comparison with gentamicin. It has been suggested that the safety of apramycin may be ascribable to a higher specificity towards bacterial ribosomes. The aim of the study was to compare apramycin to gentamicin with respect to (i) the two known renal uptake systems for gentamicin, megalin and organic cation transport 2 (OCT2) and (ii) the electron transport chain.

Methods:

To study the interaction with megalin, the displacement of [³H]gentamicin as a function of the extracellular concentration of non-labelled gentamicin or apramycin was assessed in LLC-PK1 cells, which endogenously express functional megalin. To characterize the interaction between aminoglycosides and OCT2, the uptake of [³H]1-Methyl-4-phenylpyridinium iodide ([³H]MPP⁺), a prototypical OCT2 substrate, was measured in the presence or absence of non-labelled aminoglycosides in HEK293 cells stably expressing human OCT2. Transport activity in wild type HEK293 cells was used as baseline value. Redox activity of complex I, II-III, and IV was measured spectrophotometrically in mitochondria isolated from rat kidneys.

Results:

[³H]gentamicin binding to LLC-PK1 cells was inhibitable by co-incubation with non-labelled gentamicin, suggesting a protein-mediated mechanism. The displacement of [³H]gentamicin by non-labelled gentamicin as well as apramycin was dose-dependent. The calculated concentration inhibiting 50% of the binding (IC₅₀) was 12.8 μM (95% CI 7.5-22.0) for gentamicin, 50.2 μM (95% CI 38.4-65.6) for apramycin. OCT2 transport activity was inhibited by gentamicin (11.7 ± 1.5 pmol/mg of protein vs 8.5 ± 1.7 pmol/mg of protein, P=0.01) but not by apramycin (11.7 ± 1.5 pmol/mg of protein vs 11.1 ± 3.0 pmol/mg of protein, P=NS). Complex I and IV activity were only slightly affected either by gentamicin or by apramycin at any of the concentrations tested. Complex II/III activity was inhibited in a dose-dependent manner by gentamicin, whereas no inhibition was detected with co-incubation with apramycin at any of the concentrations tested.

Conclusion:

The differential renal accumulation and toxicity of apramycin in comparison with gentamicin observed in vivo appears to be of pleiotropic nature, as apramycin displays a weaker interaction with megalin and OCT2 than gentamicin, and it is not an inhibitor of the electron transport chain, at least in our experimental setting.

D. Rutishauser², S. Krackow², A. Batavia^{1, 2}, P. Schraml², N. Wey², H. Moch²

The Merge of Synoptic Reports and Molecular Data from Renal Cancer Clinical Cohort Studies

*ETH Zurich*¹, *University Hospital Zurich*²

Introduction:

VHL (Von Hippel-Lindau) gene inactivation is the genetic hallmark of clear cell renal cell carcinoma (ccRCC). However, 5-12% of ccRCC with intact VHL have been shown to be more aggressive, conferring a poorer prognosis and worse survival. Currently, prognosis is mainly determined using pathological characteristics such as tumour grade and stage, whereas molecular pathology or proteomics data is not routinely used to predict patient survival. In order to identify phenotypic characteristics and molecular changes between VHL intact and VHL inactivated ccRCC we assessed molecular data from over 400 ccRCC samples from the University Hospital Zurich Tissue Biobank using genetics (WES + Oncoscan), epigenetics (methylation) and proteomic (mass spectrometry).

Methods:

We collected all available information from clinical databases and generated structured pathological reports for correlation analysis from a subset of our patient cohort. These synoptic reports consist of essential reporting elements as defined by national or international expert panels. We then generate a compilation by aligning cohort data, synoptic reports and molecular data. The protein expression data of matched normal and tumour tissue of 60 ccRCC patients was acquired by DIA HRM-MS, generating a proteome-wide protein profile for each sample. From the abundance matrix of over 7000 proteins the expression changes from normal to tumour tissue were calculated. The resulting sample by protein identity matrix of abundances, the cohort data and the synoptic reports were aligned to compilation.

Results:

The Fc-differences per protein between normal and tumour tissue were taken for predictors of sample categories. Clinical outcome categories were predicted by the proteome expression changes. Selected proteins most important for discriminating categories were identified. We developed a user surface to perform statistical analysis and to visualize fold change difference sizes and significances. A direct link leads to proteins most influential in discriminating categories. Structured pathology reports from all ccRCC, including stage, grade and other parameters were combined with molecular and proteomics data. Through the merge of comprehensive and deep proteome profiles with synoptic reports we are able to describe the consequences of VHL inactivation in ccRCC. In addition to that we have the option to carry out statistical analysis and correlate dozens of biologically and clinically relevant parameters with molecular data in a click and go fashion.

Conclusion:

Synoptic reporting allows providing more complete data in comparison to the usual narrative pathology reports that are available. For research and interpretation of molecular data in large cohort studies, structured pathology reports facilitate combination of molecular and proteomics data with a large number of clinical and pathological parameters is crucial; potentially leading to better prognosis predictions and treatment decisions.

A. Bauer^{3, 10}, A. Eskat³, A. Ntekim⁸, C. Wong⁴, D. Eberle^{3, 9}, E. Hedayati^{5, 6}, F. Tay³, H. Yau⁴, L. Stockley¹, d. Maria³, S. Şen², S. Egert-Schwender⁷, Y. Üresin², R. Grossmann³

How COVID-19 changed clinical research strategies: a global survey

Cambridge Clinical Trials Unit, Cambridge University Hospitals NHS Foundation Trust, Cambridge, United Kingdom¹, Center of Excellence for Clinical Research, University of Istanbul, Istanbul, Turkey², Clinical Trials Center Zürich, University Hospital Zurich, Zurich, Switzerland³, Clinical Trials Centre, The University of Hong Kong, Hong Kong⁴, Department of Oncology-Pathology, Cancer Center Karolinska, Karolinska Institute, Stockholm, Sweden⁵, Medical Unit of Breast Cancer, Sarcoma, and Endocrine Tumours, Theme Cancer, Karolinska University Hospital, Stockholm, Sweden⁶, Muenchner Studienzentrum, School of Medicine, Technical University of Munich, Munich, Germany⁷, University of Ibadan / University College Hospital Ibadan, Ibadan, Nigeria⁸, University of Zurich, Department of Biomedicine, Zurich, Switzerland⁹, University of Zurich, Institute of Biomedical Ethics and History of Medicine, Zurich, Switzerland¹⁰

Introduction:

With the COVID-19 pandemic clinical research faced new challenges, leading to an excessive operational demand and overload of involved parties in the clinical research field. In this publication, we evaluate the impact of COVID-19 on clinical research strategies, we compare the different adaptations taken by regulatory bodies and academic research institutions in a global context and we explore what we can learn to prepare for possible future pandemics.

Methods:

We conducted a cross-sectional, non-anonymous online survey, which was developed by the International Clinical Trial Center Network (ICN). We identified and assessed different COVID-19-specific adaptations taken by academic research institutions and regulatory bodies (i.e. regulatory authorities, research ethics committees and governmental health departments) using standard descriptive methods. The study was conducted following the SRQR guidelines.

Results:

Nineteen ICN members and their associated academic research institutions from 14 different countries/jurisdictions on four continents participated in this survey. The questionnaire completion rate was 95%. All participating academic research institutions developed and followed similar strategies, including hygienic and preventive measures, redeployment of staff and manpower recruitment, as well as prioritization of COVID-19 projects. In contrast, centralized management or coordination (i.e. via central units within research institutions or regional/institutional COVID-19 decision boards) of COVID-19 projects was not implemented in all countries/jurisdictions/institutions. Approaches concerning financing and project selection were adopted differently. Additionally, regulatory bodies reacted similarly to the COVID-19 pandemic in regard to project approvals. This included the implementation of fast-track authorization procedures for COVID-19 projects and the development of guidance documents. The information and advice provided by regulatory bodies were perceived to be valuable by most respondents. However, some ICN members considered those guidance documents to be inconsistent or unclear.

Conclusion:

Both academic research institutions and regulatory bodies worldwide were able to cope with the challenging pandemic situation by developing similar strategies. Close collaboration between academic research institutions and regulatory bodies, flexible redeployment of research staff and adaptation of working environment (on-site and in home-office), as well as dynamic risk-assessment on ongoing research activities will improve performance and accelerate responses in possible future pandemics. Nevertheless, we identified some unique approaches that allow fast and efficient responses to the pandemic. Ethical concerns, however, should be addressed in any new decision making process.

M. Paolucci¹, N. Wullemin³, C. Arena³, Y. Wäckerle-Men¹, V. Homère¹, M. Träxler¹, Y. Severin², T. Kündig¹, D. Bieli³, T. Sonati³, P. Johansen¹

Allergen-specific profiling of serum antibodies from patients with peanut allergy

Department of Dermatology, University of Zurich and University Hospital Zurich, Zurich, Switzerland¹, Institute of Molecular Systems Biology, ETH, Zurich, Switzerland², Mabyon AG, Schlieren, Switzerland³

Introduction:

Peanut allergy is one of the most common IgE-mediated food allergies. While IgE describes the sensitisation, peanut-specific IgG may counteract the pathological properties of IgE. The IgE-IgG balance as well as peanut-protein specificity and IgG subclasses may determine whether the patient develops symptoms or not. Among 16 identified peanut allergens, Ara h 1, 2, 3, and 6 bind IgE in the majority of peanut-allergic patients. Sensitisation to Ara h 2 and Ara h 6 are associated with more severe allergic reactions, including anaphylaxis. Ara h 8 and Ara h 9 are considered minor allergens and associated with mild local reactions. Ara h 8 can cross-react to the homologous aeroallergen Bet v 1, whereas Ara h 9 is responsible for cross-reactivity with other non-specific lipid-transfer proteins found in pollen and fruit.

Methods:

We describe the serological profiling of a Swiss cohort of 101 male (54.5%) and female (45.5%) peanut allergic patients. Both adults and children were included. The sera were tested for reactivity against different peanut allergens by an in-house sandwich IgG ELISA and by Immuno-CAP to detect IgE. Multiparametric analysis of the antibodies profiling was performed.

Results:

The majority of patients were sensitized to multiple peanut allergens. Ara h 2 and Ara h 6 were the allergens with the highest IgE levels. Of 101 sera, 93 (92.1%) and 89 (88.1%) were IgE positive for Ara h 2 and Ara h 6, respectively. Fifty-nine patients (58.4%) were sensitized to Ara h 1, 43 (42.6%) to Ara h 3, 58 (57.4%) to Ara h 8, and 22 (21.8%) to Ara h 9. All patients were IgG positive for Ara h 3, 99 (98%) for Ara h 1, 96 (95%) for Ara h 2, and 94 (93%) for each Ara h 6 and Ara h 8. We identified three clusters of patients according to the IgE and IgG levels: patients with low levels of antibodies against major and minor allergens, patients with high antibodies levels against Ara h 1, Ara h 2, Ara h 3 and Ara h 6 and low seroconversion rate against Ara h 8 and Ara h 9 or vice versa. Moreover, we observed that elderly patients had significantly higher levels of Ara h 8-specific antibodies compared to younger study participants.

Conclusion:

Sensitisation to Ara h 2 and Ara h 6 may be predictive of peanut allergy, as the majority of the patients were sensitised to these proteins. Ara h 2 and Ara h 6 are moderately homologous proteins and we observed similar levels of Ara h 2 and Ara h 6-specific IgE antibodies in the analysed cohort. In patients sensitised to Ara h 8 and Ara h 9, low levels or absence of antibodies against peanut major allergens may suggest a concomitant sensitisation to fruit or pollen allergens, which can induce cross-reactions to peanuts. Peanut allergy is a risk factor in birch pollen allergy due to cross-reactivity.

Z. Marti¹, J. Ruder¹, R. Martin¹

Characterization of Antibody-Secreting Cells in Multiple Sclerosis Patients and Healthy Controls Using an In Vitro Expansion System

University Hospital Zurich¹

Introduction:

Multiple Sclerosis (MS) is a debilitating autoimmune disease of the central nervous system (CNS) that mainly starts in young adults between 20-40 years of age. Both autoreactive CD4⁺ T cells and memory B cells are considered important for the pathogenesis of MS (Jelcic et al., 2018). B cells could contribute by antibody formation, antigen presentation, secretion of proinflammatory cytokines and regulation of immune responses. In the present study, we were interested: a) to establish an in vitro testing system to examine antibody formation against candidate autoantigens, and b) using this methodology as a first step towards the identification of autoreactive B cells in order to analyze their antigen-presenting function.

Methods:

Following a method introduced by Pinna et al. in 2009, we use IL-2 (1000U/ml) and the Toll-like receptor 7/8 agonist Resiquimod (2.5ug/ml) as stimuli to selectively expand antibody-secreting cells (ASCs) from the B cell memory compartment within peripheral blood mononuclear cells (PBMC). We quantified the effects of our dual stimulation using light microscopy, flow cytometry, and enzyme-linked immunosorbent assays (ELISAs), thereby characterizing cell morphology, composition, and antibody secretion.

Results:

Cell cultures from both HCs and RRMS patients showed no significant differences in cellular composition before and after stimulation. Both cohorts reacted to the stimulation by a significant and selective expansion of ASCs within the CD27⁺ B cell compartment. The remaining B cell subsets as well as T cells distinctly contracted. Furthermore, the stimulation was accompanied by the formation of microscopic proliferation clusters that were absent in unstimulated controls, and to a marked increase in IgM and IgG production (mean: >100pg/cell IgG/M), which correlated with the number of ASCs (p<0.05).

Conclusion:

In line with the literature, RRMS patients and healthy controls showed no significant differences in the cellular composition of peripheral blood cells. Our data support the efficacy of a dual stimulation with IL-2 and Resiquimod in selectively stimulating and expanding CD27⁺ memory B cells to ASCs, which are capable of producing large amounts of antibodies. Thus, the stimulated culture supernatants provide a useful platform to examine antibody repertoires and to study potential autoantigen-specific memory B cells in MS.

D. Eberle¹

Patient and Public Involvement in Clinical Research – an Overview and Outlook for Switzerland

*Clinical Trials Center, University Hospital Zurich*¹

Introduction:

Historically, clinical research has been marked by a clear distinction between researchers as experts and the role of patients as trial participant. However, over recent years, clinical research has been undergoing a paradigm change and patients are increasingly considered experts, who can provide unique insights due to personal experience. Such active involvement of patients and the public that exceeds the role as trial participants is known as patient and public involvement (PPI). PPI is supported by a strong ethical rationale as well as potential improvement of research quality.

In Switzerland, the concept of PPI is only slowly gaining momentum and support offers are limited. The aim of this project was to firstly assess the status quo of PPI in clinical research in Switzerland to then draft recommendations tailored to the situation of PPI in Switzerland.

Methods:

A sequential explanatory mixed methods design was chosen to assess the status quo PPI in clinical research in Switzerland, consisting of an online survey for regulatory and funding bodies, academic research infrastructure (ARI), researchers as well as patients and public, followed by semi-structured interviews. The survey results were descriptively analyzed and interview contents were thematically grouped to detect gaps of PPI in Switzerland and to draft targeted recommendations.

Results:

The survey outcomes (n=123) showed that all stakeholders generally support the concept of PPI and that they are willing to actively contribute. In addition, some organizations and researchers are already conducting PPI activities or are establishing PPI initiatives. However, there is no established nationwide initiative in Switzerland to support and promote PPI on a large scale. The survey amongst *Regulatory and Funding Bodies* and *ARI* identified several challenges of PPI in Switzerland. The lack of funding possibilities for PPI was considered the greatest challenge. Further challenges were a general lack of awareness of the concept of PPI, lack of education for not only patients and the public about clinical research but also for researchers about PPI. Other difficulties to overcome are missing PPI regulations and best practices. The survey amongst *Researchers* and *Patients and Public* showed that *Patients and Public* were evenly ready to engage on a consultation, collaboration and leadership level, whereas the majority of *Researchers* preferred to only consult with patient representatives. Motivation for the involvement of or engagement as patient representative were diverse and differed between *Researchers* and *Patients and Public*. The overarching reason for both groups however was the promotion of patient relevant research. All interview partners (n=3) agreed on the importance of further developing PPI concepts, but indicated that a culture change in clinical research is needed to approach the public and clinical research. Interview partners uniformly emphasized the need to bundle forces and urged to implement more efficient and clear processes.

Conclusion:

In general, the Swiss framework for PPI is insufficient. Joint effort of all stakeholders is needed to catch up with international developments in order to match high level ethical and quality standards. For this, a basic framework for PPI in clinical research in Switzerland should be implemented, including regulations and guidelines for PPI as well as widespread information for patients, the public and researchers. Further needed are training opportunities in PPI concepts for clinical research as well as a sustainable source of funding for PPI.

A. Laure¹, A. Rigutto¹, M. Kirschner², S. Hiltbrunner¹, A. Curioni¹

Comparative transcriptomics of inVivo and exVivo Mesothelioma samples

*Department of Medical Oncology and Hematology, University Hospital Zurich, 8091 Zurich¹,
Department of Thoracic Surgery, University Hospital Zurich, 8091 Zurich²*

Introduction:

Cancer cell lines are commonly used to study cancer biology including drug testing but prior studies indicate differences in the transcriptome between primary tumors and commercial cell lines in cancer. Another preclinical approach relies on the use of mouse models, but, it is unknown if these models resemble the human disease and therefore knowledge about the expression of markers of interest in preclinical approaches is crucial. To understand the reliability of preclinical models for mesothelioma studies, we have compared whole transcriptomes from fresh frozen malignant pleural mesothelioma (MPM) tumors and the ones derived from the matching cell lines and commercial cell lines. Moreover, we have compared the transcriptome of the mesothelioma murine cell line RN5 and the corresponding subcutaneous (s.c.) tumor.

Methods:

Sequencing libraries were prepared for 7 commercial cell lines, 18 fresh frozen tumor and the 10 corresponding patient-derived cell lines. In addition, libraries from six mouse tumors were compared to the corresponding cell line. Patient-derived cell lines were generated from digested fresh tumor material and FibrOut™ medium supplement was used to prevent overgrowth of fibroblastic cells. After 10 passages, cell lines were evaluated for remaining contaminations by microscopy and RNA was isolated. Tumors were digested enzymatically and cancer cells isolated by negative MACS sorting for TER119, CD45 and CD31. Mouse exVivo tumors were collected from s.c. injection of RN5 mesothelioma cells into wt-B6 mice and processed the same way as human tumors. Whole mRNA sequencing was performed using the SmartSeq2-Picelli protocol due to the low mRNA input of the human samples. Mouse samples were sequenced using the TruSeq RNA protocol. QC and data analysis was performed in collaboration with the Functional Genomics Center Zurich using the SUSHI platform.

Results:

Differential gene expression analysis revealed that in hierarchical clustering, patient-derived cell lines cluster closer to the corresponding tumors and that the control cell line (SV-40 transduced, healthy mesothelium cell line MetT-5A) differs the most from all malignant cell lines. Gene Ontology (GO) terms related to translation, regulation of transcription, cell cycle, NF-κB signaling and regulation of canonical WNT signaling are upregulated in all cell lines compared to cells isolated from fresh tumors. GO terms related to regulation of transcription, RNA splicing, mRNA processing, cell-cell signaling, immune response and cytokine-mediated signaling are upregulated in tumors and downregulated in cell lines. Further analysis revealed that canonical WNT signaling genes are significantly different in commercial cell lines when compared to fresh tumors. WNT-agonists WNT2, WNT2B, and CCN4, WNT-antagonists FRZB, SERPINF1 and SFRP2/4, WNT-receptors FZD8 and LGR5 and CCND2 are significantly less transcribed in commercial cell lines. On the contrary, the expression of canonical WNT-pathway genes is conserved to a higher degree in patient-derived cell lines. On the mouse samples (tumors and matching cell line) these expression of some WNT-associated genes is opposite to the human samples.

Conclusion:

We have demonstrated that in MPM, the transcriptome of tumors is more similar to the ones from patient-derived cell lines compared to transcriptomes of commercial cell lines. These results are of major relevance for the scientific community to choose the most appropriate model for studies on mesothelioma biology and drug testing to avoid miss-leading results.

K. Akeret¹, R. Buzzi², B. Thomson¹, N. Schwendinger¹, D. Schaer², M. Hugelshofer¹

Multimodal spatiotemporal analysis identifies a dominant MyD88/TLR4 dependent role of the choroid plexus in intracerebral hemorrhage related neuroinflammation

Department of Neurosurgery, Clinical Neuroscience Center, UniversitätsSpital and University of Zurich, Zurich, Switzerland¹, Division of Internal Medicine, UniversitätsSpital and University of Zurich, Zurich, Switzerland²

Introduction:

Neurological outcomes after intracerebral hemorrhage (ICH) strongly depend on the occurrence of secondary brain injury (ICH-SBI) that usually evolves within a week after the bleeding. The focus of this study was to further define the temporal interplay between pathophysiological processes driving ICH-SBI in the first seven days following ICH. Specifically, we hypothesized that the choroid plexus (CP) constitutes a mediator of ICH-SBI by functioning as an interface between the central and peripheral immune system.

Methods:

ICH-SBI was modeled by stereotactic injection of whole blood into the right striatum of mice. First a series of experiments were designed to investigate the changes observed during the first seven days after whole blood injection by 7 Tesla magnetic resonance imaging (MRI), spatial RNA sequencing (spRNAseq), and immunohistology. In addition, ⁵⁸Fe-labeled whole blood was used to spatially track the injected iron using laser ablation inductively coupled plasma mass spectrometry (LA-ICP-MS). All temporal experiments were performed using 10-12 weeks old C57BL/6J mice (nMRI=10, nLA-ICP-MS/spRNAseq=14, nImmunohistology=21). Temporal findings regarding inflammatory CP response informed the timepoint for specific readouts in mice with knock out for MyD88 and TLR4, aiming to further mechanistically characterize the inflammatory plexus response. Therefore, we used 10-12 weeks old MyD88^{-/-} (n=8) and TLR4^{-/-} (n=6) knockout mice with wild-type littermate controls (nMyD88^{+/+}=16, nTLR4^{+/+}=12).

Results:

We deconvoluted the spatiotemporal dynamics of distinct pathophysiological processes during the first seven days after intracerebral whole blood injection, such as red blood cell toxin liberation, CP activation, and perilesional leukocyte invasion. Red blood cell toxin liberation and metabolization presented as a multiphasic process: first, an immediate short-lived accumulation in the CP, potentially acting as a local trigger; second, a delayed liberation from the hematoma in the extracellular space due to overwhelmed resident phagocytes; and third, a lesional containment through intracellular processing by invaded phagocytes. Within hours after injection, there was a pronounced MyD88/TLR4 dependent immunological activation of the CP. We identified a remarkable upregulation of ICAM-1 on the apical surface of the CP epithelium and increased choroidal expression of ICAM-1, VCAM-1, and MadCAM-1 with a peak 24 hours after intracerebral whole blood injection. This was paralleled by a marked increase in the number of Kolmer's epiplexus cells, increased blood CSF barrier permeability, and a pronounced leukocytosis in the CP stroma. In addition, the data indicated a reduced CSF clearance in MyD88^{-/-} and TLR4^{-/-} knockout mice, either through reduced absorption of CSF or decreased secretion from the choroid plexus.

Conclusion:

The results of our study enhance the pathophysiological understanding of the spatiotemporal dynamics in the first seven days after ICH. The observation of an early and pronounced immunological activation of the CP positions this organ as a potential mediator and therapeutic target in ICH-SBI.

L. Krattiger^{1, 2}, B. Simona³, M. Tibbitt¹, M. Ehrbar²

An in vitro model to study the recovery of therapeutically ablated vascular networks

Department of Mechanical and Process Engineering, ETH Zurich, Switzerland¹, Department of Obstetrics, University and University Hospital of Zurich, Zurich, Switzerland², Ectica Technologies, Zurich, Switzerland³

Introduction:

Cycles of vascular growth and regression can be observed in physiology as well as pathology. Angiogenic phases are intermitted by vessel regression in the menstrual or hair cycle and tumor-supplying vasculature can regrow after therapeutic intervention through anti-angiogenic therapies (AATs). While AATs based on limiting the availability of VEGF have been successfully used in the clinics, it has also long been established that their efficacy varies with tumor types and can lead to development of more aggressive and heavily vascularised phenotypes upon treatment termination. To this day, a multitude of in vitro angiogenesis assays have been described, however, in vitro systems for modelling the recovery of a vascular network are lacking. In this study, we establish and describe a platform to generate controlled yet complex vascular networks which are sensitive to treatment with bevacizumab and which can be replenished through the addition of new endothelial cells.

Methods:

Three-dimensional cultures were grown by seeding cells onto a commercially available 96 well-plate featuring pre-cast poly(ethylene glycol)-based hydrogels (3DProSeed, Ectica Technologies). Sequentially seeded bone marrow-derived mesenchymal stem/stromal cells (BM-MSCs) and human umbilical vein endothelial cells (HUVECs, GFP expressing) were allowed to assemble into vascular-like networks for four days in presence of 50 ng/mL FGF-2. Networks were characterized by quantifying total GFP-length and staining for extracellular matrix molecules fibronectin and laminin. Bevacizumab was supplied from the start of endothelial culture to study its influence on network formation or after the four-day formation-period to study its effect on the maintenance or ablation of vascular networks. Fresh RFP-expressing HUVECs were added to pre-formed networks and their relative localization and potential recovery of regressing GFP-HUVEC-structures was monitored.

Results:

After three days of BM-MSC pre-culture and four days of co-culture with GFP-HUVECs, tightly interconnected endothelial networks had formed. The two co-cultured cell types shared a basement membrane-like layer of fibronectin and laminin and could be maintained for several days of co-culture. Vascular network formation on this platform appears to be sensitive to bevacizumab, as low concentration of this compound (10 µg/mL) prevented this morphogenic process. Interestingly, pre-formed day four-networks were seen to degrade only in presence of high bevacizumab concentrations (100 µg/mL), while no change could be observed in presence of low concentrations (10 µg/mL) compared to control conditions for at least four more days of culture. When RFP-HUVECs were added to pre-formed day four-GFP networks, they were seen to integrate into the established GFP-structures and helped to extend the longevity of the total endothelial networks.

Conclusion:

Our results suggest that the herein established and characterized platform can be employed to study processes regarding both the formation and maintenance of vascular structures. Due to its easy-to-use nature, sequential seeding of cells is possible, which will be used to study if and how endothelial cells can recover an AAT-compromised or regressed vascular network.

M. Wipplinger⁴, A. Abukar⁴, A. Hariharan⁴, S. Sun⁴, M. Ronner⁴, M. Sculco⁴, A. Okonska⁴, J. Kresoja-Rakic^{2, 4}, H. Rehrauer³, W. Qi³, V. van Beusechem¹, E. Felley-Bosco⁴

Double-stranded RNA structural elements holding the key to translational regulation in cancer: the case of editing in RNA Binding Motif Protein 8A

Amsterdam UMC, Vrije Universiteit Amsterdam, Medical Oncology, Cancer Center Amsterdam, De Boelelaan 1117, Amsterdam, Netherlands¹, Department of Pediatrics, Section of Developmental Biology, School of Medicine University of Colorado, Anschutz Medical Campus, Aurora, Colorado, USA², Functional Genomics Center Zürich, ETH Zürich/University of Zürich, Zürich, Switzerland³, Laboratory of Molecular Oncology, Department of Thoracic Surgery, University Hospital Zürich, Zürich, Switzerland⁴

Introduction:

Malignant Pleural Mesothelioma (MPM) is a rare and aggressive cancer associated to asbestos exposure. Recent studies linked altered RNA related processes to the pathogenesis of this disease. RNA binding motif protein 8a (RBM8A) is an essential gene in BRCA-associated protein 1 proficient MPM and its mRNA editing increases upon asbestos exposure in a mouse model of mesothelioma development. The aim of this study was to further characterize the role of RBM8A in mesothelioma and the consequences of its mRNA editing.

Methods:

We performed PCR using primers that specifically target the regions inside the RBM8A 3'UTR, which contains the editing sites. Sanger sequencing (Mycrosynth) was performed and A-to-I editing was determined using ImageJ software. Small interfering RNA (siRNA) was used to silence ADAR1 and ADAR2 in mesothelioma cell lines and editing levels were measured. RBM8A 3'UTR sequence was inserted into a dual luciferase reporter vector to investigate stabilizing effect of A-I editing. RNA-Protein-pulldown was used to investigate interaction of edited/un-edited RBM8A 3'UTR with RNA binding proteins. mADAR2 was cloned into a pCi puro vector and normal mesothelial cells were transfected followed by measurement of RNA/Protein expression and RNA editing levels.

Results:

RBM8A protein expression was higher in mesothelioma compared to mesothelial cells. Silencing RBM8A changed splicing patterns in mesothelial and mesothelioma cells, but drastically reduced viability only in mesothelioma cells. In the tissues of asbestos exposed mice, editing of Rbm8a mRNA is associated with increased protein immunoreactivity with no significant change of mRNA levels indicating post-transcriptional processes. Increased Adenosine-deaminase-acting-on-dsRNA (ADAR)-dependent editing of inverted Alu elements in the RBM8A 3'UTR was observed in human MPM compared to mesothelial cells. RBM8A 3'UTR Alu-elements reporter assays revealed that editing stabilizes the reporter activity. Unedited RBM8A 3'UTR had a stronger interaction with the RNA binding protein Musashi (MSI) compared to edited form in RNA pull-down experiments. Silencing MSI2 resulted in increased RBM8A protein levels. The same outcome was obtained by overexpression of Adar2 in mesothelial cells, which also resulted in increased levels of RBM8A 3'UTR mRNA editing.

Conclusion:

Altogether, these data provide evidence that ADAR-dependent editing contributes in maintaining elevated RBM8A protein levels in MPM by counteracting MSI2-driven downregulation. The presence of similar structural elements in other transcripts opens the possibility of a wider implication of this mechanism for a large number of proteins where translational control explains the poor relationship between mRNA and protein expression, which is observed in several tissues and cancers.

B. Carrara¹, Q. Vallmajó Martín^{1,2}, P. Papageorgiou¹, M. Ehrbar¹

3D *in vivo* Bone Marrow Organoids to dissect Mesenchymal Stromal Cells Chaos

Department of Obstetrics, University Hospital Zürich, University of Zürich, Schmelzbergstr. 12, 8091, Zürich, Switzerland¹, Gene Expression Laboratory, Salk Institute for Biological Studies, La Jolla, CA 92037, USA²

Introduction:

The bone marrow (BM) is a dynamic organ whose main function is to support haematopoietic cells, which assure life-long production of blood. The haematopoietic compartment is supported by the stromal fraction of the BM that comprises mesenchymal stromal cells (MSCs), a heterogeneous cell population that undergoes osteogenic, chondrogenic, adipogenic differentiation. Following a tissue engineering approach, we combine the knowledge on BM-MSCs with biomaterials to dissect such cells heterogeneity and model BM biology. Our technology consists in encapsulating BM-MSCs in synthetic, biocompatible polyethylene glycole (PEG) hydrogels and following cells developmental potential *in vitro* and *in vivo*. We are currently focusing on the *in vivo* characterization of two murine BM-MSCs populations, Skeletal Stem Cells (SSCs) and Bone Cartilage Stromal Progenitors (BCSPs), aiming at generating new knowledge for bone and bone marrow regenerative strategies.

Methods:

SSCs and BCSPs were mechanically and enzymatically extracted from limbs and sternum of post-natal day3 (P3) GFP⁺-C57/BL6 mice and separated by FACS using the marker panels CD45-Ter119-Tie2-AlphaV⁺Thy6C3-CD105-CD200⁺ and CD45-Ter119-Tie2-AlphaV⁺Thy6C3-CD105⁺, respectively. Due to the high amount of cells needed for *in vivo* trials, both cell types were expanded under standard culture conditions for 7 days. Subsequently, the cells were encapsulated at different cell densities in PEG hydrogels with or without minimal amounts of BMP-2. Such scaffolds, whose size is around 0.5 cm in diameter, were subcutaneously implanted at the back of NMRI-Foxn1^{nu} immunocompromised mice and harvested after 8 weeks. Upon explantation, samples were macroscopically inspected, imaged and fixed. Bone formation was quantified through micro-CT analysis, followed by decalcification and histological characterization.

Results:

The subcutaneous implantation of the scaffolds allowed to visually monitor their localization within the 8 weeks of implantation. At explantation, all the scaffolds were found back with their initial size, confirming biomaterial stability. Distinct scenarios in terms of BM organoids (or *ossicles*) were observed based on the different combinations of cell densities and BMP-2. A first macroscopic evaluation showed SSCs being more performant as they induced the formation of stiffer ossicles with high degree of vascularization both with and without BMP-2, at different cell densities. BCSPs generated ossicles only when in combination with BMP-2. Still-ongoing Micro-CT and histological analysis will precisely determine whether there is a direct proportionality between cell density, BMP-2 concentration at implantation and bone formation or marrow morphological complexity. Also, the GFP-labelling of the implanted cells will aid tracing them back in the ossicles, giving further information on their role in the organoids onset, thus on their biological function.

Conclusion:

The results suggest that our technology can generate 3D *in vivo* BM organoids and so elegantly model such organ. Moreover, it proved to be a good instrument for investigating SSCs and BCSPs biological function *in vivo*, since even from a first macroscopical evaluation different outcomes from SSCs or BCSPs-loaded scaffolds were observed. Lastly, the biocompatibility of our biomaterial was demonstrated as most of the ossicles were found to be vascularized, thus suggesting their integration with the host vasculature and so the remodeling of the material by implanted or host cells.

L. Jingya¹, D. Abegg¹, L. Malinowska², M. Rudnik¹, O. Distler¹, P. Błyszczuk¹, P. Picotti², G. Kania¹

Protein conformational changes and functional alterations in dermal fibroblasts from patients with systemic sclerosis

Department of Rheumatology, Center of Experimental Rheumatology, University Hospital Zurich, University of Zurich, Zurich, Switzerland¹, Institute of Molecular Systems Biology, ETH Zurich, Zurich, Switzerland²

Introduction:

Despite intensive studies and clinical trials, there is still no available precise diagnostic tool and treatment of the patients affected by systemic sclerosis (SSc). Proteopathies are diseases characterized by the production of aberrant conformers of certain proteins that lead to a disturbance of their cellular functions and disease. It is believed that the structure of a protein is principally responsible for its function. By identifying altered protein structures on a proteome-wide scale, there is a possibility to detect protein functional changes. We aimed to screen for changes in the protein conformation and to correlate with cell function in SSc dermal fibroblasts compared to fibroblasts from healthy donors (HC) using a novel approach of limited proteolysis followed by functional assays.

Methods:

Diffuse cutaneous (dc)SSc and HC dermal fibroblasts were used for recently established Limited Proteolysis-coupled Mass-Spectrometry (LiP-MS) to examine protein structural alterations in a proteome-wide scale. Further, the responsive signalling targets in these cells, including the NF- κ B-dependent pathway and energy metabolism, were evaluated. Fibroblasts were stimulated with inflammatory cytokines, highly relevant in SSc, including TNF α , IL-1 β , TGF- β , IL-17A, and a combination of IL-17A and TGF- β . To examine the NF- κ B activity, cells were transduced with a pseudo-typed HIV-1-based lentiviral vector. The measurements of luciferase signal were analysed. RT-qPCR was used to assess the expression of NF- κ B-dependent genes for non-transduced cells. ATP measurements were analysed and presented as the amount of luminescent signal.

Results:

LiP-MS analysis detected 53263 common peptides in SSc and HC fibroblasts, of which 41 peptides showed conformational changes in SSc fibroblasts in comparison with HC fibroblasts. The 41 conformationally altered peptides showed significant enrichment in GO pathways for: biological processes (9), molecular function (7) and cellular components (21). SAE1, CTNND1, CDC37, and PPP1R13L were related to the NF- κ B-dependent pathways, while ATP5A1, GSTM1, PCK2, ANPEP, GM2A, GNS, CAD, ACOT2 were connected with metabolic processes. There was a tendency of lower levels of mRNA RELA, NFKBIA, MMP1 and TNC expression levels in untreated and stimulated SSc fibroblasts compared to HC fibroblasts. The assessment of the NF- κ B activity in untreated SSc fibroblasts showed a trend to lower fold change compared to HC fibroblasts (0.63 vs 1, SE 0.19, $p=0.07$). A statistically significant difference between SSc and HC fibroblasts was found in TGF- β stimulated fibroblasts (0.64 vs 1, SE 0.16, $p=0.046$). SSc fibroblasts showed a lower ATP level compared to HC fibroblasts in untreated condition (0.82 vs 1, SE 0.09, $p=0.07$), after stimulation with IL-1 β (0.85 vs 1, SE 0.08, $p=0.07$) and TGF- β (0.81 vs 1, SE 0.09, $p=0.05$). Of note, a statistically significant difference between SSc and HC fibroblasts was found in IL-17A stimulated cells (0.82 vs 1, SE 0.07, $p=0.02$).

Conclusion:

LiP-MS approach allowed for the identification of conformational changes in SSc fibroblast mainly related to signal transduction and metabolic pathways. Confirmatory functional studies showed deregulated NF- κ B activity and ATP levels in SSc fibroblasts. Therefore, LiP-MS approach may create a distinctive opportunity to discover new disease biomarkers and functionally transformed pathways. Furthermore, this method may advance therapeutical approaches, where only structurally altered proteins could be targeted, without interfering with non-changed proteins.

R. Odabası², L. Krattiger^{1, 2}, B. Emiroglu¹, M. Ehrbar², M. Tibbitt¹

Lymphatic endothelial cell vascular structure formation

Department of Mechanical and Process Engineering, ETH Zurich, Switzerland¹, Department of Obstetrics, University and University Hospital of Zurich, Zurich, Switzerland²

Introduction:

Therapeutic vascularization, meaning the promotion of vessel-formation through delivery of specific growth factors, proves to be both challenging to accomplish and pivotal for the generation of functional engineered tissues. While vascular angiogenesis has been studied using different scaffolds as well as in perfused microfluidic chip setups the lymphatic vascular (LV) system was deemed a secondary system because diseases of the blood vascular systems are a major contributor to mortalities in the developed world. With the discovery of lymphatic-specific markers only a few decades ago, the field of lymphatic research is still very young, more so the engineering of LVs. In vitro, lumen-forming lymphatic capillaries have been reportedly formed in fibrin and collagen-based hydrogel scaffolds. However, synthetic scaffolds hold promise as they provide a more controllable environment.

Methods:

In this study LV structure will be formed in Factor XIIIa crosslinked polyethylene glycol gels (PEG), as well as on gradient gels (3DProSeed, Ectica Technologies). To ensure the survival and proliferation of the lymphatic endothelial cells (LEC), LECs will be encapsulated in co-culture with bone-marrow-derived mesenchymal stem/stromal cells (BM-MSc). To generate LVs complex architecture, aspects ranging from cell densities, PEG stiffnesses and suitable growth factors will be assessed. Once the right parameters are established, triple co-cultures consisting of LECs, BM-MSCs and human umbilical vein endothelial cells (HUVEC) will be studied and immunologic assays will be performed to assess whether LECs retain or lose their lymphatic phenotype. Moreover, potential mutual influences, such as changes in ECM deposition will be investigated.

Results:

The HUVEC-BM-MSc co-culture conditions have been established and characterized. It could be shown that with increasing cell density and softer gel stiffness the cultures tend to span larger and more connected structures. Keeping the co-cultures stimulated with fibroblast growth factor 2 (FGF-2) showed larger structures than stimulation with vascular endothelial growth factor A (VEGF-A). At very high cell densities, structures could be formed even in the absence of supplemented growth factor.

Conclusion:

Finding the optimal culture conditions for LEC-BM-MSc co-cultures enables more sophisticated screening experiments. For example, various cancer cell lines could be introduced to the lymphatic endothelial co-cultures and the therapeutic effectiveness of known anti-cancer agents could be assessed and compared to blood endothelial co-cultures. A later step foresees the study of LECs on a microfluidic chip, with a newly designed layout with multiple channels.

K. Becker³, M. Gysin³, D. Verma¹, K. Haldimann³, N. Müller², M. Schuurmans², D. Ordway¹, B. Schulthess³, S. Hobbie³

Preclinical profiling of apramycin as a possible drug candidate for the treatment of mycobacterial lung infections

Colorado State University¹, University Hospital of Zurich², University of Zurich³

Introduction:

Pulmonary infections with nontuberculous mycobacteria (NTM) are notoriously difficult to treat. Therapeutic outcome is often poor despite elaborate multi-drug regimens, a phenomenon related to inherent resistance mechanisms in NTM. Amikacin, for instance, an important component of mycobacterial therapy, is reasonably efficacious against *Mycobacterium avium* complex (MAC) infections but has shown lower potency against *Mycobacterium abscessus*. We have previously identified apramycin as an aminoglycoside with excellent mycobacterial coverage including best-in-class in-vitro activity against *M. abscessus*.

Methods:

Here, we used antimicrobial susceptibility testing, sputum inhibition assays, synergy assays, and time-kill kinetic experiments to study the in-vitro activity of apramycin in comparison to amikacin and other standard-of-care drugs commonly used in the treatment of *M. abscessus* infections. The in-vivo efficacy of EBL-1003, a formulation prepared with crystalline apramycin free base, was assessed in two *M. abscessus* acute infection models using SCID and CFTR/CFTR mice.

Results:

Antimicrobial susceptibility testing with a panel of clinical *M. abscessus* isolates revealed apramycin MICs of 0.5–2 µg/mL and thus about 4 to 8-fold lower than for amikacin. Broth microdilution checkerboard assays demonstrated additive antibacterial activity of apramycin when combined with bedaquiline or other drugs. Antibacterial activity was slightly inhibited in patient sputum, to a degree comparable to that for amikacin and tobramycin. In-vitro time-kill kinetics suggested a higher bactericidal potency of apramycin than of amikacin. A dose as low as 16 mg/kg apramycin sq BID resulted in CFU reductions in both SCID and CFTR/CFTR mice. In comparison, treatment with 16 mg/kg of amikacin sq BID had no significant effect on the CFU counts in CFTR/CFTR mice relative to the vehicle group. A mid dose of 64 mg/kg apramycin resulted in >1-log CFU reductions in both the SCID and the CFTR/CFTR model relative to the start of treatment.

Conclusion:

The potent in-vitro activity of apramycin against *M. abscessus* described previously translated into a time-kill kinetic and a CFU reduction in mouse lungs and spleens that was found to be more potent than that of amikacin. Our findings warrant continued consideration of apramycin as a potential drug candidate for lower dose treatment of pulmonary NTM infections and higher drug safety.

C. Zhao⁵, A. Chirkova¹, R. Palma Villar³, S. Rosenborg², J. Lindberg³, L. Friberg⁵, S. Hobbie⁴

Apramycin first-in-human trial to determine population pharmacokinetics in plasma and urine to guide efficacious dose finding predictions

Juvabis AG¹, Karolinska University Hospital², RISE Research Institutes of Sweden³, University of Zurich⁴, Uppsala Universitet⁵

Introduction:

EBL-1003, a crystalline free base of apramycin, is under development for human use because it has repeatedly demonstrated high efficacy against a large variety of multidrug-resistant bacterial species in multiple animal infection models for a variety of disease indications. Both toxicity and cross-resistance, commonly encountered with other aminoglycoside antibiotics, appear relatively low, which has been attributed to its unusual chemical structure when compared to other aminoglycosides.

Methods:

A first-in-human Phase I study has been conducted with a population pharmacokinetic (PPK) analysis as one of its objectives. The drug was administered intravenously over 30 min in five dose ascending groups ranging from 0.3 to 30 mg/kg. Plasma and urine samples were collected from 30 healthy volunteers.

Results:

A mammillary four-compartment PK model, with linear elimination from the central compartment and a renal fractional excretion of 90%, described the data. Apramycin clearance was proportional to the absolute estimated glomerular filtration rate (absolute eGFR) as defined by the Chronic Kidney Disease Epidemiology Collaboration (CKD-EPI) formula and corrected by body surface area. All fixed effect parameters were allometrically scaled to total body weight (TBW). Clearance and steady-state volume of distribution were estimated to 5.5 L/h and 16 L, respectively, for a typical individual with absolute eGFR of 124 mL/min and TBW of 70 kg. Probability of pharmacodynamic target attainment (PTA) analyses demonstrated that the anticipated efficacious dose (30 mg/kg daily, 30-min intravenously infusion) reaches 95% for an area under concentration-time curve over minimum inhibitory concentration ratio (AUC/MIC) target ≤ 40 given an MIC of 8 mg/L in a virtual population with impaired renal function (absolute eGFR=80 ml/min, TBW=75 kg).

Conclusion:

The pharmacokinetic profile of apramycin after intravenous infusion of EBL-1003 resembles that of other aminoglycosides currently in clinical use. The results support further development of apramycin as a potential drug candidate for the treatment of critical bacterial infections.

L. Zurfluh¹, T. Hothorn², R. Zimmermann¹, C. Haslinger¹, A.P. Simões-Wüst¹

Study protocol: Bryophyllum pinnatum treatment of anxiety related to preterm labour – a randomized, double-blind, placebo-controlled trial, as IIT

Department of Obstetrics, University Hospital Zurich, Zurich, Switzerland¹, Epidemiology, Biostatistics and Prevention Institute, University of Zurich, Zurich, Switzerland²

Introduction:

Preterm birth is the leading cause of mortality and morbidity in newborns and is often caused by preterm contractions. Therapeutic options for the treatment of preterm contractions are still limited until today. The application of tocolytics achieves a 24-48 hours delivery delay in most cases, which provides time for foetal lung maturation by the administration of glucocorticoids to the mother and transportation in utero to a suitable perinatal centre. Due to considerable side effects and in the absence of benefit regarding pregnancy outcome, current guidelines do not support the use of tocolytics for more than 48 hours. During the last years, mothers' anxiety proved to play an important role in pregnancy outcomes, especially in the case of preterm labour. An option for a long-term therapy addressing not only myometrial contractions but also anxiety, is the herbal medicine *Bryophyllum pinnatum*. This perennial succulent plant has been used as a (frequently add-on) tocolytic therapy for many years, which is supported by various *in vitro* studies. Interestingly, *B. pinnatum* has also been used to treat anxiety and sleeping disorders. All clinical studies performed so far and data from pharmacovigilance reveal good tolerability and a high safety during pregnancy.

Methods:

To estimate the clinical effects of Bryophyllum 50% chewable tablets, a randomised, double-blind, placebo-controlled trial is currently being conducted at the University Hospital in Zurich. This exploratory study investigates the use of Bryophyllum 50% chewable tablets as a follow up therapy after the 48 hours standard tocolytics and focuses especially on its effect on maternal anxiety. After recruitment, patients are randomly assigned to two groups (Bryophyllum vs. placebo). In both groups, patients take study medication (verum or placebo) four times a day, each time two tablets. At day 1, 7, and 14, participants fill out three different questionnaires to assess anxiety levels and sleep quality (State-Trait-Anxiety Inventory, STAI; Pregnancy-related Anxiety Questionnaire Revised 2, PRAQ-R2; and Pittsburgh Sleep Quality Index, PSQI). Study participation continues until week 37 of pregnancy or – if birth takes place before – the birth of the child. Beside the anxiety and sleep quality questionnaires, study parameters include hospitalisation days after randomisation and gestational age at birth as well as adverse events.

Results:

The study protocol was submitted to the responsible committees and was approved by the ethics committee Zurich as well as by Swissmedic. The study is currently in the recruitment phase. Goal is the recruitment of 60 patients.

Conclusion:

The main purpose of this exploratory pilot-study is to find out whether *B. pinnatum* as a follow-up treatment to tocolysis helps to reduce anxiety. Whether it affects sleep quality, hospitalisations' duration before delivery and gestational age at birth will be investigated as well. The data will allow an estimate of the treatment effect and a power calculation for a later confirmatory study.

Trial Registration: ClinicalTrials.gov; NCT05110599

H.A. Bischoff-Ferrari^{4, 7, 18}, G. Freystätter^{4, 7, 18}, B. Vellas¹⁴, B. Dawson-Hughes¹⁵, R. Kressig¹⁹, J. Kanis³, W.C. Willett⁹, J. Manson¹⁰, R. Rizzoli¹², R. Theiler^{4, 7}, L. Hofbauer², G. Armbrecht¹⁶, J. da Silva⁵, M. Blauth⁶, C. de Godoi Rezende Costa Molino^{4, 7}, W. Lang^{4, 7}, U. Siebert^{1, 11, 17}, A. Egli^{4, 7}, E. Orav⁸, M. Wiczorek^{4, 7}, for the DO-HEALTH Research group¹³

Effects of vitamin D, omega-3 fatty acids and a simple home strength exercise program on fall prevention: the DO-HEALTH randomized clinical trial

Center for Health Decision Science, Departments of Epidemiology and Health Policy & Management, Harvard T.H. Chan School of Public Health, Boston, Massachusetts, USA¹, Centre for Healthy Aging, Department of Medicine III Dresden University Medical Centre, Dresden, Germany and Centre for Regenerative Therapies Dresden, Technische Universität Dresden, Dresden, Germany², Centre for Metabolic Diseases, University of Sheffield Medical School, Sheffield, United Kingdom and Mary MacKillop Institute for Health Research, Australian Catholic University, Melbourne, Victoria, Australia³, Centre on Aging and Mobility, University of Zurich and City Hospital Zurich, Waid Zurich, Switzerland⁴, Centro Hospitalar e Universitário de Coimbra, Coimbra, Portugal and Coimbra Institute for Clinical and Biomedical Research (iCBR), Faculty of Medicine, University of Coimbra, Coimbra, Portugal⁵, Department for Trauma Surgery, Medical University of Innsbruck, Innsbruck, Austria⁶, Department of Aging Medicine and Aging Research, University of Zurich and University Hospital, Zurich, Switzerland⁷, Department of Biostatistics, Harvard T.H. Chan School of Public Health, Boston, Massachusetts, USA⁸, Department of Epidemiology and Department of Nutrition, Harvard T H Chan School of Public Health, Boston, MA, USA⁹, Department of Medicine, Brigham and Women's Hospital, Harvard Medical School, Boston, Massachusetts, USA¹⁰, Department of Public Health, Health Services Research and Health Technology Assessment, UMIT - University for Health Sciences, Medical Informatics and Technology, Hall i.T., Austria¹¹, Division of Bone Diseases, Geneva University Hospitals and Faculty of Medicine, Geneva, Switzerland¹², DO-HEALTH Research group¹³, Gérontopôle de Toulouse, Institut du Vieillissement, Centre Hospitalo-Universitaire de Toulouse, Toulouse, France and UMR INSERM 1027, University of Toulouse III, Toulouse, France¹⁴, Jean Mayer USDA Human Nutrition Research Centre on Aging, Tufts University, Boston, Massachusetts, USA¹⁵, Klinik für Radiologie, Charité – Universitätsmedizin Berlin, corporate member of Freie Universität Berlin and Humboldt-Universität zu Berlin, Berlin, Germany¹⁶, Program on Cardiovascular Research, Institute for Technology Assessment and Department of Radiology, Massachusetts General Hospital, Harvard Medical School, Boston, Massachusetts, USA¹⁷, University Clinic for Aging Medicine, City Hospital Zurich, Waid, Zurich, Switzerland¹⁸, University Department of Geriatric Medicine FELIX PLATTER, and University of Basel, Basel, Switzerland¹⁹

Introduction:

The role of vitamin D, omega-3 fatty acids and home exercise in fall prevention among generally healthy and active older adults is unclear. Objective: To test the effect of daily supplemental vitamin D, marine omega-3s fatty acids and a simple home exercise program (SHEP), alone or in combination, on the incidence of total and injurious falls among generally healthy older adults.

Methods:

We performed a 2x2x2 factorial design randomized controlled trial among 2157 community-dwelling adults age 70 years and older, who had no major health events in the five years prior to enrolment, recruited from Switzerland, Germany, Austria, France, and Portugal between December 2012 and November 2014. Participants were randomly assigned to 2000 international units / day of vitamin D3 and/or 1 g/day of marine omega-3s, and/or a SHEP versus placebo and/or control exercise over three years. The primary endpoint for the present fall analysis was the incidence rate of total falls. The secondary fall endpoint was the incidence rate of injurious falls. Falls were recorded prospectively throughout the trial. Since there were no interactions between treatments, main effects are reported based on modified intent-to-treat.

Results:

Of 2157 randomized participants, 1900 (88%) completed the study. The mean age was 74.9 years, 61.7% were women, 40.7% had serum 25-hydroxyvitamin D concentration < 20 ng/ml, and 83% were at least moderately physically active. In total, 3333 falls including 2141 injurious falls were recorded over a median follow-up of 2.99 years. Vitamin D and SHEP had no benefit on total or injurious falls, whilst omega-3s compared to no omega-3s reduced total falls by 10% (incidence rate ratio IRR = 0.90, 95% CI [0.81, 1.00], p = 0.04), including more active participants (IRR=0.84, 95% CI [0.72, 0.97]). The omega-3 benefit did not reach significance for incidence rate of injurious falls overall (IRR = 0.91, 95% CI [0.81, 1.01]), but in more active older adults (IRR=0.81, 95% CI [0.70, 0.95]).

Conclusion:

Among generally healthy, active and vitamin D-replete older adults, supplemental omega-3s may have a modest benefit for fall prevention, whilst daily high-dose vitamin D or a simple home exercise program had no benefit.

E. Avilla-Royo^{3, 6}, L. Vonzun³, J. Monné Rodriguez⁷, M. Weisskopf^{1, 9}, F. Famos³, R. Zimmermann⁴, U. Ueli^{2, 5, 8}, N. Ochsenbein-Kölble^{4, 8}, M. Ehrbar^{4, 9}

Healing-triggering biomaterials for fetal membrane repair

Center of Surgical Research, University Hospital Zurich, Switzerland¹, Children's Research Center, University Children's Hospital of Zurich, University of Zurich, Switzerland², Department of Obstetrics, University and University Hospital of Zurich, Switzerland³, Department of Obstetrics, University and University Hospital of Zurich, Switzerland⁴, Department of Pediatric Surgery, University Children's Hospital Zurich, Switzerland⁵, Institute for Biomechanics, Swiss Federal Institute of Technology, Switzerland⁶, Laboratory for Animal Model Pathology, Institute of Veterinary Pathology, University of Zurich, Switzerland⁷, The Zurich Center for Fetal Diagnosis and Therapy, Switzerland⁸, University of Zurich, Switzerland⁹

Introduction:

Minimally-invasive prenatal interventions which aim to ameliorate fetal developmental defects have become a clinical reality and are currently performed for a variety of life-threatening complications. However, in up to 30% of the cases, the intervention translates into preterm birth and its associated negative consequences. The puncture created in the fetal membranes (FMs) during fetoscopy and their reported inability to heal might play a role in the risk for iPPROM. Despite promising, none of the investigated approaches has been clinically translated, and there is currently no clinical strategy to prevent iPPROM after a fetoscopic intervention. We have earlier shown that regeneration-inducing factors, such as platelet derived growth factor (PDGF)-BB can promote the migration and proliferation of FM cells when encapsulated in a biomaterial. Here, to elucidate the potential such biomaterial for FM repair in a clinically relevant setting, we investigated the healing-triggering capacity of such biomaterial in an ovine model.

Methods:

To investigate the effect of PDGF-BB to elicit a healing response of FMs, we established a FM defect model in pregnant sheep. In this novel in vivo model, we applied an umbrella-shaped nitinol implant loaded with our previously engineered poly(ethylene glycol) (TG-PEG) biomaterial that released PDGF-BB. At explantation, we performed macroscopic examinations as well as immunohistochemistry analysis of the implants.

Results:

The comparison of empty or growth factor-loaded implants shows that platelet-derived growth factor (PDGF-BB) promoted a healing response consisting of angiogenesis, immune cells, and migration, proliferation and ECM deposition in the implanted biomaterial.

Conclusion:

This study is a first proof-of-concept that TG-PEG hydrogels loaded with PDGF-BB, by triggering cell recruitment and proliferation from the myometrium and the vicinity of the FMs, might be able to heal FM defects. Longitudinal studies lasting until the time of delivery will be required to understand the long term healing response of the FMs.

V. Haunerding¹, J. Sarabia del Castillo², L. Pelkmans², M. Levesque¹

Trametinib selectively increases susceptibility to immune-mediated cell death in the M130219 melanoma cell line while having the opposite effect on M130429 cells

University Hospital Zurich, Department of Dermatology¹, University of Zurich, Institute for Molecular Life Sciences²

Introduction:

Immunotherapy in the form of immune checkpoint blockade (ICB) has drastically improved therapy outcomes for stage III and IV melanoma, but a large fraction of patients still fail to respond or develop resistance during treatment. The combination of ICB with targeted therapy such as MEK or BRAF inhibitors might expand treatment options for those patients.

Methods:

We used two cell lines generated from different metastatic sites from the same melanoma patient, M130219 and M130429, and co-cultured them with activated natural killer (NK) cells from peripheral blood of healthy donors. In addition, we used the MEK inhibitor trametinib in some co-culture conditions. We performed iterative indirect immunofluorescence imaging (4i) for markers of cell state, cell death and NK cell activation on these co-cultures and computationally identified the different cell types (segmentation). This allowed us to extract cellular features together with data on cell-cell interaction. The experiment was performed with NK cells from three healthy donors, each done in technical triplicates and at 5 different time points. The high throughput setup with a laser scanning microscope and an automated raw data processing pipeline allowed us to perform all measurements on a single 384 well plate to minimize experimental variation.

Results:

Each of the cell types in this assay could successfully be identified based on nuclear and cytoskeletal markers and CD45 staining. Co-culture of both tumor cell lines with activated NK cells resulted in increased cancer cell death in all conditions compared to control tumor cells cultured without NK cells. Interestingly, addition of trametinib increased susceptibility to immune-induced cell death in M130219 cells. In contrast, M13029 cells showed higher rates of cell death in co-culture with immune cells without the addition of trametinib.

Conclusion:

We could successfully expand the use of the 4i imaging technology to an immune-oncology setup, which resulted in a large, computationally annotated dataset with single cell information about cell state and interactions of cells with their neighboring cells. The results from this experimental setup showed that two cell lines from the same genetic background respond fundamentally opposite to immune cell-mediated killing in combination with trametinib. This platform can be further expanded to test drug libraries of small molecule inhibitors, but also to gain insight into the cellular events that confer resistance to target cell lysis from cytotoxic immune cells.

T. Look¹, E. Puca², R. De Luca², T. Hemmerle², P. Roth¹, D. Neri², M. Weller¹, T. Weiss¹

Lomustine and the immunocytokine L19TNF display promising anti-tumor activity against glioblastoma

Department of Neurology and Clinical Neuroscience Center, University Hospital Zurich and University of Zurich, Zurich, Switzerland¹, Philogen S.p.A., Siena, Italy²

Introduction:

Glioblastoma is the most common and most aggressive primary brain tumor in adults. We recently investigated the antibody-cytokine fusion protein L19TNF as a novel immunotherapeutic strategy against glioblastoma. L19 binds to a tumor-specific epitope that is conserved across species and enables a targeted delivery of tumor necrosis factor α (TNF) to the tumor site. This immunotherapy could be safely administered but only had limited anti-tumor activity. Here, we investigated different combination partners for L19TNF in preclinical glioma models and translated the most effective treatment combination to patients with recurrent glioblastoma after first-line therapy.

Methods:

We used immunocompetent orthotopic glioma mouse models to study L19TNF in combination with the immunocytokine L19IL2, immune checkpoint inhibition based on a blocking antibody against programmed cell death-1 (anti-PD1), the anti-angiogenic agent bevacizumab and the chemotherapeutic agent lomustine. Tumor growth was monitored with MRI. To investigate immune-dependent mechanisms we used different immunodeficient mouse models. To understand modes of actions and resistance, we used flow cytometry, immunofluorescence, ex vivo proteomics and single-cell RNA sequencing (scRNA-seq). Furthermore, we translated the most efficient combination therapy to patients with glioblastoma within a phase I/II clinical trial (NCT04573192).

Results:

In immunocompetent orthotopic glioma mouse models, the combination of lomustine and L19TNF demonstrated strong synergistic anti-tumor activity and cured a majority of tumor-bearing mice, whereas lomustine or L19TNF monotherapy only had only very limited anti-tumor activity. This effect was completely abrogated in immunodeficient mouse models. Ex vivo profiling of the tumors and tumor-infiltrating immune cells demonstrated an increase of tumor-infiltrating immune cells upon combination therapy and molecular effects of lomustine on the cancer cells and L19TNF on the tumor vasculature. Based on these encouraging results, we translated the combination of L19TNF and lomustine to patients with recurrent glioblastoma. For the first patients, the treatment with lomustine and L19TNF was well tolerated.

Conclusion:

L19TNF and lomustine demonstrate immune-dependent promising anti-glioma activity in orthotopic preclinical models and is currently studied in patients with recurrent glioblastoma.

P. Wendel-Garcia¹, R. Erlebach¹, D. Hofmaenner¹, G. Camen¹, R. Schuepbach¹, C. Jüngst¹, B. Müllhaupt¹, J. Bartussek¹, P. Buehler¹, S. David¹, R. Andermatt¹

Effect of long-term ketamine infusion on cholangiopathy in COVID-19 associated acute respiratory distress syndrome

University Hospital of Zurich¹

Introduction:

A higher-than-usual resistance to standard sedation regimens in COVID-19 patients suffering from acute respiratory distress syndrome (ARDS) has led to the frequent use of the second-line anaesthetic agent ketamine. Simultaneously, an increased incidence of cholangiopathies in mechanically ventilated patients receiving long-term infusion of high-dose ketamine has been noted. Therefore, the main objective of this study was to investigate a causal relationship between the long-term, high-dose infusion of ketamine and the occurrence of cholangiopathy in mechanically ventilated patients suffering from COVID-19 associated ARDS.

Methods:

Post-hoc analysis of a prospective observational cohort of patients suffering from COVID-19 associated ARDS between March 2020 and August 2021. A time-varying, multivariable adjusted, cumulative weighted exposure mixed-effects model was employed to analyse the exposure-effect relationship between ketamine infusion and total bilirubin levels.

Results:

Two-hundred forty-three critically ill patients were included into the analysis. Ketamine was infused to 170 (70%) patients at a rate of 1.4 [0.9–2.0] mg/kg/h for 9 [4–18] days. The mixed-effects model revealed a positively correlated infusion duration-effect as well as dose-effect relationship between ketamine infusion and rising bilirubin levels ($p < 0.0001$). In comparison, long-term infusion of propofol, even at high doses, was not associated with increasing bilirubin levels ($p = 0.352$). Patients having received ketamine infusion had a multivariable adjusted hazard of developing a cholangiopathy during their ICU stay of 3.2 [95% confidence interval, 1.4–7.2] ($p < 0.01$).

Conclusion:

A causally plausible, dose-effect relationship between long-term infusion of ketamine and rising total bilirubin levels, as well as an augmented, ketamine associated, hazard of cholangiopathy in critically ill COVID-19 patients could be shown. Ketamine should be refrained from whenever possible for the long-term analgo-sedation of mechanically ventilated COVID-19 patients. If however faced with the necessity to employ ketamine in this setting infusion should be limited for as few days as possible, bilirubin should be monitored daily and ketamine infusion should be halted as soon as elevated bilirubin levels become apparent.

Unplanned Re-visits of Seniors in the Emergency Department*Institut für Notfallmedizin¹***Introduction:**

Seniors have a high risk of re-visits to emergency departments (ED) varying between 12-20% within the first month and 19-33% within three months after ED discharge. The rate of ED re-visits within 72 hours is a key indicator for quality of care in emergency medicine and varies between 1-15%. Reasons for ED re-visits are the natural course of illness, misdiagnosis, lack of homecare and self-discharge against medical advice. However, risk factors for ED re-visits have not been fully investigated. Therefore, the aim was to analyse the incidence of ED re-visits and to identify risk factors for ED re-visits within 72 hours one and three months after ED discharge.

Methods:

In this retrospective study, seniors (≥ 70 yrs.) were consecutively enrolled if they presented with an Emergency Severity Index of 2 or 3 in a tertiary care ED in 2019, and were discharged after the ED visit. The frequencies of unplanned ED re-visits within 72 hours, one and three months after ED discharge as well as reasons and potential risk factors for ED re-visits were investigated by univariate and multivariable logistic regression models.

Results:

592 seniors were enrolled of whom 30 patients (5.1%) re-visited the ED significantly more often for gastrointestinal complaints (OR 2.9, 95% CI 1.04 – 8.2, $p=0.043$) such as vomiting and abdominal pain within 72 hours after ED discharge. Furthermore, discharge against medical advice (OR 5.6, 95% CI 1.7 – 18.1, $p=0.004$) and ED presentation during night shifts (OR 2.7, 95% CI 1.2 – 6.1, $p=0.014$) were significant risk factors for ED re-visits within 72 hours after discharge.

Sixty-six seniors (11.2%) re-visited the ED within one month after discharge and 79 patients (13.3%) within three months. Hospital stay in the preceding six months before the index ED presentation was a risk factor for ED re-visits within one (OR 2.0, 95% CI 1.2 – 3.4, $p=0.009$) and three months (OR 2.0, 95% CI 1.2 – 3.3, $p=0.005$) after ED discharge. Seniors who presented at the index ED visit with urogenital symptoms (OR 2.1, 95% CI 1.0 – 4.5, $p=0.050$), during night shifts (OR 1.9, 95% CI 1.1 – 3.4, $p=0.028$) or living alone (OR 1.9, 95% CI 1.04 – 3.5, $p=0.036$) had an increased risk for ED re-visits within three months after discharge.

Conclusion:

Although the frequencies of ED re-visits among seniors at 72 hours, one and three months after discharge tends to be low and most re-visits were illness-related, seniors need to be assessed for risk factors for ED re-visits. Discharge should be carefully evaluated in order to improve patient safety and in balance to ED overcrowding and health care costs.

M. Sun¹, M. Bialasek², M. Król², M. Weller¹, T. Weiss¹

A macrophage-based drug delivery platform for glioma treatment

Department of Neurology and Clinical Neuroscience Center, University Hospital and University of Zurich, Switzerland¹, Faculty of Veterinary Medicine, Warsaw University of Life Sciences, Poland²

Introduction:

Glioblastoma is the most common and aggressive primary brain tumor in adults with an urgent need for more effective treatment strategies. At present, even though various drugs have been developed and showed potent anti-tumor activity *in vitro*, their application *in vivo* is limited by ineffective delivery and systemic toxicity. Therefore, novel strategies to deliver these drugs effectively and safely to the tumor site are urgently needed. Here, we developed an adoptive transfer strategy against malignant brain tumors utilizing macrophages that are loaded with ferritin-protein cages containing drugs or other proteins and transfer these nanocarriers to cancer cells *in vitro* and *in vivo*.

Methods:

Live-time imaging, microscopy and flow cytometry were utilized to investigate the transfer efficiency of ferritin cages from loaded macrophages to human and mouse glioma cells. Co-cultures of glioma cells and macrophages loaded with ferritin-drug cages were used to study the anti-glioma activity *in vitro* and orthotopic immunocompetent mouse glioma models were used to study the anti-glioma activity *in vivo*. Affinity purification-mass spectrometry (AP-MS) was used to elucidate the mechanisms of transfer by characterizing the interactome of ferritin cages within macrophages and cancer cells.

Results:

Flow cytometry analysis showed that more than 95% of murine and human glioma cells were fluorescently labeled after 24 h of co-culture with murine/human macrophages loaded with fluorescently-labeled ferritin cages, indicating high transfer efficiency from macrophages to cancer cells. The transfer of ferritin-cages from macrophages into cancer cells was dependent on direct cell-to-cell contact. We also confirmed the transfer of ferritin cages from macrophages to glioma cells *in vivo*. For this, we treated orthotopic GL-261 glioma-bearing mice intravenously or intratumorally with macrophages that were loaded with fluorescently-labeled ferritin cages. *In vivo* imaging, confirmed a fluorescent signal above the tumor region and *ex vivo* microscopy confirmed the localization of ferritin-cages in cancer cells at the tumor site. To study the anti-glioma activity with therapeutic active payloads, we loaded murine/human macrophages with ferritin cages carrying monomethyl auristatin E (vcMMAE) and co-cultured these cells with murine and human glioma cells *in vitro*, respectively. This revealed a time- and concentration-dependent cytotoxicity to glioma cells. *In vivo*, intravenous or intratumoral administration of ferritin-vcMMAE protein cages conferred a survival benefit in two orthotopic murine glioma models (GL-261 and CT-2A) and intratumoral administration cured 50% (GL-261) - 75% (CT-2A) of glioma bearing mice. AP-MS revealed the interactome of ferritin-cage-binding proteins and suggests that phagocytic and cytoskeleton re-arrangement pathways are involved in the uptake and transfer of ferritin-cages from macrophages to glioma cells. Selected binding proteins are mechanistically studied in ongoing knockdown experiments.

Conclusion:

This study demonstrates the potential of a novel macrophage-based drug-delivery platform for glioma treatment and provides a rationale for clinical translation.

N. Lohaus^{2,4}, R. Reichen^{2,6}, R. Reimann⁵, I. Abela¹, I. Jelcic^{2,6}, M. Huellner³

A case of SARS-CoV-2-associated acute disseminated encephalomyelitis

Department of Infectious Diseases and Hospital Epidemiology, University Hospital Zurich, Zurich, Switzerland¹, Department of Neurology, University Hospital Zurich, Zurich, Switzerland², Department of Nuclear Medicine, University Hospital Zürich, Zürich, Switzerland³, Institute of Diagnostic and Interventional Radiology, University Hospital Zurich, Zurich, Switzerland⁴, Institute of Neuropathology, University Hospital Zurich, Zurich, Switzerland⁵, Neuroimmunology and Multiple Sclerosis Research Section, Department of Neurology, University Hospital Zurich, Zurich, Switzerland⁶

Introduction:

Severe acute respiratory syndrome coronavirus type 2 (SARS-CoV-2) is still spreading globally causing coronavirus disease 2019 (COVID-19) pandemic. Besides from respiratory symptoms and fever, several neurological disorders have been associated with SARS-CoV-2 infection, e.g. metabolic/hypoxic encephalopathy, stroke, seizure and Guillaine-Barré syndrome. Co-incidence is in the majority of cases the reason for association, i.e. association in time, but proof by cerebrospinal fluid (CSF) diagnostics is sparse. We here outline a case of central nervous system (CNS) autoimmune disease most likely caused by asymptomatic SARS-CoV-2 infection.

Methods:

Retrospective analysis of clinical, radiological and CSF findings, and case presentation.

Results:

Case Presentation: A 28-year-old female was admitted to our center with her first generalized seizure. Up to three weeks before she had suffered from attentional deficits and a constant headache that was worse in the morning or when bending her head down. MRI showed a left frontal mass with perifocal edema and patchy contrast enhancement, raising the suspicion of cerebral lymphoma. However, ¹⁸F-FET PET favored a nonneoplastic lesion. CSF analysis revealed only mononuclear pleocytosis of 14 cells/μl without cytological signs of malignancy. No evidence of lymphoma was found with immunophenotyping of CSF and blood. Albumin ratio, CSF total protein, Reibergram, glucose ratio and CSF lactate were normal, oligoclonal bands were negative. Acute disseminated encephalomyelitis (ADEM) was suspected and finally confirmed by histopathological results from brain biopsy. Re-questioning of the patient revealed no history of recent symptomatic infections or vaccinations, but a history of two high-risk contacts to COVID-19 patients, one four weeks and another five months ahead of the seizure. Consequently serological testing was performed which detected CSF and serum antibodies against four SARS-CoV-2-derived antigens and intrathecal production of IgG against two SARS-CoV-2 antigens using an in-house developed bead-based assay (ABCORA 2.0). PCR analysis of blood and CSF was negative for SARS-CoV-2. MRZ reaction and serum MOG- and AQP4-specific antibodies were negative. High-dose methylprednisolone therapy with subsequent tapering improved the symptoms rapidly.

Conclusion:

To conclude, the findings suggest SARS-CoV-2 infection without respiratory symptoms as the cause of ADEM in this case. Clinicians should be aware of atypical or asymptomatic SARS-CoV-2 infection as a potential trigger of post-infectious neurological disease with atypical clinical features.

D. Hofmaenner⁷, B. Seeliger⁶, M. Doebler¹, P. Wendel-Garcia⁷, R. Schuepbach⁷, J. Schmidt⁵, T. Welte⁶, M. Hoepfer⁶, H. Gillmann², C. Kuehn³, S. Ehrentraut¹, J. Schewe¹, C. Putensen¹, K. Stahl⁴, C. Bode¹, S. David⁷

Intracranial Hemorrhages on Extracorporeal Membrane Oxygenation: Differences Between COVID-19 and Other Viral Acute Respiratory Distress Syndrome

Department of Anesthesia and Intensive Care Medicine, University Hospital Bonn, Bonn, Germany¹, Department of Anesthesiology, Hannover Medical School, Hannover, Germany², Department of Cardiothoracic, Transplant and Vascular Surgery, Hannover Medical School, Hannover, Germany³, Department of Gastroenterology, Medical School Hannover, Hannover, Germany⁴, Department of Nephrology and Hypertension, Hannover Medical School, Hannover, Germany⁵, Department of Respiratory Medicine, Medical School Hannover and Member of the German Centre for Lung Research, Biomedical Research in End-stage and Obstructive Lung Disease Hannover (BREATH), Hannover, Germany⁶, Institute of Intensive Care Medicine, University Hospital Zurich, Zurich, Switzerland⁷

Introduction:

Extracorporeal membrane oxygenation (ECMO) is a potentially lifesaving procedure in acute respiratory distress syndrome (ARDS) due to COVID-19. Previous studies have suggested a high prevalence of clinically silent or manifest cerebral bleedings in patients with COVID-19. Based on this fact, together with the hemotrauma and the requirement of therapeutic anticoagulation on ECMO support, we hypothesized an increased risk of intracranial hemorrhages (ICH) in COVID-19 patients on ECMO. In this study, ICH occurrence rate, circumstances and clinical outcomes in patients receiving ECMO support due to COVID-19–induced ARDS were analyzed in comparison to a cohort of viral non-COVID-19–induced ARDS patients.

Methods:

In a multicentric, retrospective study from January 2010 to May 2021, conducted at three tertiary care ECMO centers in Germany and Switzerland, two-hundred ten ARDS patients on ECMO support (142 COVID-19 vs. 68 viral non-COVID patients) underwent analysis. Analyses included the occurrence of ICH, 90-day survival, extracranial bleeding events and mean doses of anticoagulants over the first 7 days of ECMO support. 90-day ICU survival was compared using Kaplan-Meier curves and hazard ratios were calculated via Cox proportional hazard modeling.

Results:

ICH of any severity occurred in 29 of 142 COVID-19 patients (20%) versus four of 68 patients in the control group (6%). 15 of 29 ICH events in the COVID-19 group were classified as major (52%) including nine fatal cases (9/29, 31%). In the control group, there was only 1 major ICH event (1/4, 25%). The adjusted subhazard ratio for the occurrence of ICH in the COVID-19 group was 5.82 (97.5% CI, 1.9–17.8; $p = 0.002$). The presence of ICH was an independent risk factor for mortality in the entire cohort (adjusted HR, 2.37; 95% CI, 1.4–4.0; $p = 0.001$). 90-day survival in the COVID-19 group was 38.7% versus 55.9% in the control group (adjusted HR, 1.03; 95% CI, 0.6–1.7; $p = 0.908$). The overall ICU mortality in the presence of ICH of any severity was 88%. Prior major extracranial bleeding events were associated with an increased risk for ICH (SHR, 2.28; 97.5% CI, 1.0–5.1; $p = 0.044$). The mean daily dose of unfractionated heparin over the first 7 days per kg bodyweight was higher in the COVID-19-group compared with controls (252 IU/kg [IQR, 186.7–351.9 IU/kg] vs 196.5 IU/kg [IQR, 108.4–332.4 IU/kg]; fold-change, 1.28) ($p = 0.017$).

Conclusion:

This large, multicenter analysis showed a six-fold increased adjusted risk for ICH and a 3.5-fold increased incidence of ICH in COVID-19 patients on ECMO compared to viral non-COVID-19–induced ARDS patients. Prospective studies are needed to confirm these observations and to evaluate whether the bleeding risk can be reduced by adjusting anticoagulation strategies without risking more thromboembolic events.

R. Erlebach⁴, L. Wild¹, B. Seeliger³, A. Rath², R. Andermatt⁴, D. Hofmaenner⁴, C. Ganter⁴, C. Putensen¹, T. Welte³, P. Wendel Garcia⁴, S. David⁴, C. Bode¹, K. Stahl²

Outcomes of patients with initial acute respiratory failure on venovenous extracorporeal membrane oxygenation (ECMO) requiring additional circulatory support by VVA-ECMO

Departement of Anaesthesiology and Intensive Care Medicine, University Hospital Bonn, Bonn, Germany¹, Department of Gastroenterology, Hepatology and Endocrinology, Hannover Medical School, Hannover, Germany², Department of Respiratory Medicine and German Centre of Lung Research (DZL), Hannover Medical School, Hannover, Germany³, Institute of Intensive Care Medicine, University Hospital Zurich, Zurich, Switzerland⁴

Introduction:

Veno-venous (VV) extracorporeal membrane oxygenation (ECMO) has increasingly been used to support patients with severe acute respiratory distress syndrome (ARDS). In case of additional cardio-circulatory failure of reversible origin, some experienced centers upgrade the VV-ECMO strategy with an additional arterial backflow cannula (termed VVA-ECMO). Here we analyzed short and long-term outcome together with potential predictors of mortality to help acknowledging futile situation at the time of VV-ECMO upgrade.

Methods:

Retrospective analysis from 2008-2021 at three ECMO referral centers of outcome in VV-ECMO patients with ARDS that received VVA upgrade due to acute cardio-circulatory deterioration.

Results:

We identified 73 VVA-ECMO patients that had either required an upgrade from VV to VVA (n=53) or were directly triple cannulated (n=20). Their age was 49 (28-57) years and SOFA score was 13 (11-16) at VV implantation. ECMO support was required over 12 (6-22) and ICU length of stay was 32 (16-46) days. Overall ICU mortality was 48% and hospital mortality 51%. Although 8 patients were lost to follow-up at two years, only two patients died after hospital discharge. A SOFA score > 14 at the day of VVA upgrade and higher lactate level were independent predictors of mortality in the multivariate regression analysis. The Survival function overall and stratified by SOFA score is presented in Figure 1.

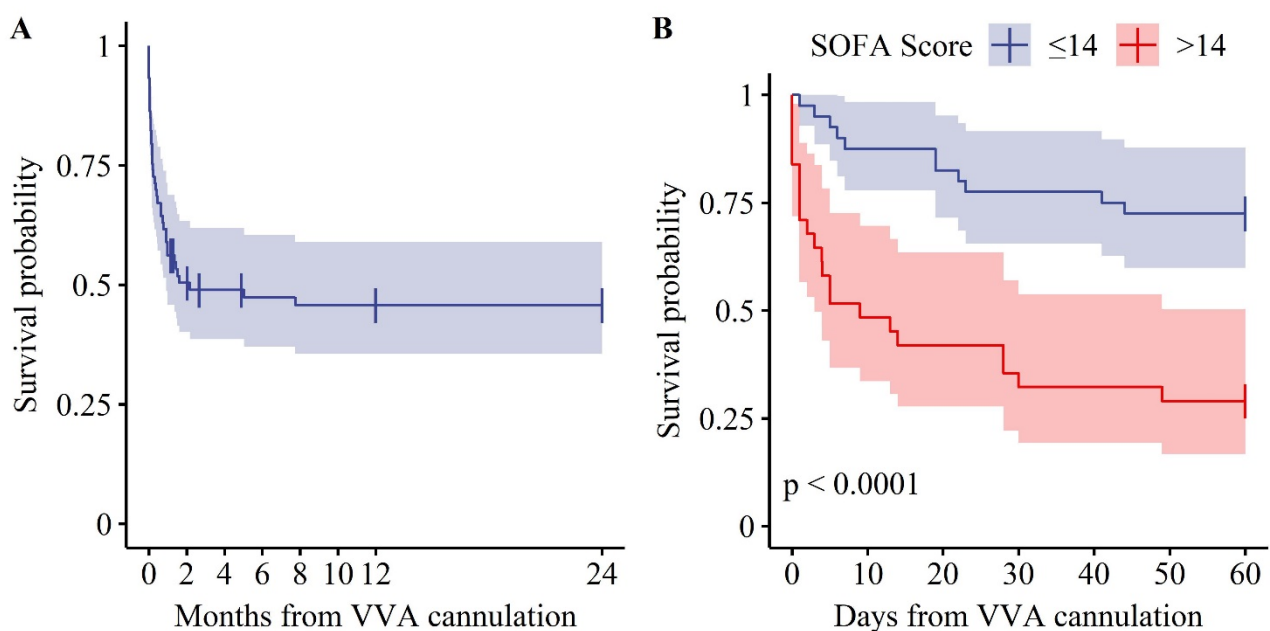


Figure 1: Survival function from VVA-ECMO cannulation. A) overall, B) stratified by SOFA score.

Conclusion:

This large analysis of VVA-ECMO patients with initial respiratory failure demonstrates that approximately every second triple cannulated VVA-ECMO patient survived hospital stay. This encouraging survival rate was preserved over a two-year follow up. A SOFA score >14 and elevated lactate levels at the day of VVA upgrade evaluation predicts unfavorable outcome.

E. Lattmann², T. Deng², M. Walser², P. Widmer², C. Rexha-Lambert², V. Prasad², O. Eichhoff¹, M. Daube², R. Dummer¹, M. Levesque¹, A. Hajnal¹

A DNA replication-independent function of pre-replication complex genes during cell invasion in *C. elegans*

Department of Dermatology, University Hospital Zurich, Switzerland¹, Department of Molecular Life Sciences, University of Zurich, Switzerland²

Introduction:

Cell invasion is an initiating event during tumor cell metastasis and an essential process during development.

Methods:

A screen of *C. elegans* orthologs of genes over-expressed in invasive human melanoma cells has identified several components of the conserved DNA pre-replication complex (pre-RC) as positive regulators of anchor cell (AC) invasion.

Results:

The pre-RC functions cell-autonomously in the G1-arrested AC to promote invasion, independently of its role in licensing DNA replication origins in proliferating cells. While the helicase activity of the pre-RC is necessary for AC invasion, the downstream acting DNA replication initiation factors are not required. The pre-RC promotes the invasive fate by regulating the expression of extracellular matrix genes and components of the PI3K signaling pathway. Increasing PI3K pathway activity partially suppressed the AC invasion defects caused by pre-RC depletion, suggesting that the PI3K pathway is one critical pre-RC target.

Conclusion:

We propose that the pre-RC acts in the non-proliferating AC as a transcriptional regulator that facilitates the switch to an invasive phenotype.

M. Spalinger¹, R. Sanchez Alvarez¹, C. Gottier¹, A. Montalban-Arquez¹, M. Schwarzfischer¹, A. Niechcial¹, S. Lang¹, M. Scharl¹

Loss of PTPN23 in the intestinal epithelium results in epithelial hyperproliferation and lethal diarrhea in a microbiota dependent manner

Department for Gastroenterology and Hepatology, University Hospital Zurich, Zurich, Switzerland¹

Introduction:

Protein tyrosine phosphatase non-receptor type 23 (PTPN23) plays a critical role in regulating epidermal growth factor (EGF) receptor signaling and its loss has been associated with aberrant cell proliferation and promotes onset of epithelial cancers. However, the role of PTPN23 in the intestinal epithelium has not been investigated yet. Here, we investigated how PTPN23 deletion in intestinal epithelial cells (IEC) affects intestinal homeostasis.

Methods:

To study the role of PTPN23 in the intestinal epithelium, we crossed mice with a LoxP flanked PTPN23 gene (PTPN23^{fl/fl} mice) to mice expressing the CreERT construct under the villin promoter (PTPN23-VilCreERT mice). PTPN23 was deleted in IEC in these mice by tamoxifen-injections on five consecutive days. PTPN23^{fl/fl} mice injected with tamoxifen served as control.

Results:

PTPN23 deletion in IEC resulted in drastic loss of weight starting around 10-14 days after the first tamoxifen injection, eventually leading to death within 3-5 weeks due to severe wasting disease with severe diarrhea. Histology revealed massive hyper-proliferation of the colonic epithelium accompanied with elevated immune cell infiltration. In line with previous reports on the function of PTPN23, we observed highly elevated levels of EGF receptor, possibly accounting for the massive epithelial hyper-proliferation and aberrant water secretion/defective water resorption in these mice. Furthermore, we observed bacterial translocation to the spleen and the liver, indicating defective anti-bacterial defense in the intestinal epithelium of PTPN23-VilCreERT mice. In line with this, 16S sequencing revealed significant differences in the intestinal microbiome with an overgrowth of bacteria that have been reported to be heavily coated with IgA. PTPN23-VilCreERT mice showed reduced apical presence of the poly Ig receptor, a receptor that transports IgA from the lamina propria through IEC into the gut lumen. Notably, while serum IgA levels were normal, its levels in the stool were reduced, confirming defective transport of IgA into the gut lumen. In addition, autophagy was significantly reduced in PTPN23-VilCreERT mice when compared to their littermates. Of interest, antibiotic treatment was sufficient to prevent epithelial hyper-proliferation, diarrhea and death in PTPN23-VilCreERT mice, indicating that this drastic phenotype was microbiota-dependent and likely the result of defects in bacterial handling.

Conclusion:

Our results demonstrate that PTPN23 is indispensable for normal IEC function and its loss renders the intestinal epithelium unable to cope with invading bacteria. This uncovers a novel, so far unknown role of PTPN23 for regulating pathways involved in bacterial handling.

M. Gassner^{1,2}, S. Tanadini-Lang², R. Braun², N. Andratschke², J. Barranco-García²

Interpretability-Guided Content-Based Image Retrieval in Dermatology Imaging

ETH Zürich¹, USZ Zürich²

Introduction:

Early detection of cancerous skin lesions, especially melanoma, is of utmost importance. The survival rate decreases significantly if the cancer grows and develops metastasis. Even though neural networks have been shown to outperform dermatologists in the classification of skin lesions, computer-aided diagnostics (CAD) have not transitioned from academia to clinical consultation in dermatology. The two main reasons for that are: (i) the lack of explainability on the neural network classifier (black box approach); and (ii) in dermatology a diagnosis is context dependent, and a lesion management approach is advised. A transition from manual or statistical image retrieval from the literature or datasets that are visually close to the ones of interest to a stochastically solution using convolutional neural networks (CNN) has been successfully achieved in the past. This unsupervised method, called content-based image retrieval (CBIR) only focuses on the image features and would propose several close cases helping to add some context into the diagnosis. Recently, Silva, et al. proposed a method which adds explainability and improves the retrieval quality by fine tuning their CNN with saliency maps. We evaluated this new Interpretability-guided content-based image retrieval (IG-CBIR) in our dermoscopic datasets.

Methods:

The IG-CBIR algorithm consists of four steps: (i) a CNN classifier; (ii) saliency map extraction; (iii) fine-tuning of the classifier with the help of the saliency maps; and (iv) the content-based image retrieval. Saliency maps are used to measure the spatial support of a particular class for each image. Diagnosticians can thus verify the decision of the neural network by a sanity check with these maps. Furthermore, the saliency maps are used for the fine-tuning of the classifier to add more bias on important regions. Silva, et al. showed that this improves the image retrieval qualitatively in the following step. The closest skin lesion images with respect to a query image are found by means of cosine similarity in the feature space of the last convolutional layer. These three outputs, the saliency map, the prediction, and the retrieved images are valuable tools for dermatologists in their decision process while adding explainability to the algorithm. The HAM10000 dataset, consisting of 10015 skin lesion images and of 7 classes, was used for the training and evaluation. Image retrieval in medical imaging requires both, a qualitative and a quantitative evaluation. The quantitative evaluation is carried out by taking solely the labels into account and not the clinical relevancy. The P@k metric is used, where the precision of k retrieved images is calculated for all classes and the AP@k score by taking the macro average over all classes.

Results:

For 1000 test images the AP@k score yields: 0.78 for k=1, 0.63 for k=4, and 0.58 for k=9. From a qualitative point of view, it was shown that most retrieved images are of clinical importance. Furthermore, the retrieved images for a query lesion with features that indicate cancer were mostly malignant lesions, even if they were of a benign type. This increases the sensitivity and helps users to not overlook malignant lesions.

Conclusion:

In dermatology imaging the ground truth is patient context dependent. By providing similar examples from a curated dataset IG-CBIR the image can be evaluated in a context thus helping in the diagnosis process.

K. Kostopanagiotou³, RA. Costa³, M. Kirschner³, A. Curioni¹, H. Moch², M. Rechsteiner², I. Opitz³

Technical aspects of selective pulmonary vein plasma sampling in liquid biopsy for lung cancer in translational research.

USZ - Department of Oncology¹, USZ - Department of Pathology², USZ - Department of Thoracic Surgery³

Introduction:

Genomic profiling from tissue-based biopsies of solid lung tumors are invasive, lack repeatability and provide limited heterogeneity information. Liquid biopsy from peripheral blood overcomes these disadvantages but suffers from circulating biomarkers paucity. In translational research, the tumor-draining vein selective sampling technique is a way to increase the biomarker's concentration. This increases the extracted circulating tumors DNA concentration (ctDNA) but limited technical details exist for the technique itself. Obtained plasma volumes for genomic analysis remain non-estimated making a project preparation difficult. This study estimates sampled volumes aiding researchers in designing a liquid biopsy project.

Methods:

Observational study in a series of lung cancer patients undergoing anatomical lung resection. Tumor-draining pulmonary veins were ex-vivo venipunctured, immediately post-resection. Obtained plasma volume values after processing (cellular elements and debris removal) were recorded and analyzed for relation with demographic, tumor, procedure and anatomical factors through 'Mann-Whitney U' and 'Kruskal-Wallis' tests.

Results:

Tumor-draining vein samples from 58 subjects (mean age 65.5, male 57%, median BMI 25) provide median plasma volume 2.3mls per sampling. (IQR 0.98-5.0mls, range 0.2-9.4mls) Between resection types, pneumonectomy provides more volume than lobectomy or segmentectomy. ($p=0.04$) Thoracotomy (all pneumonectomies) provide more than minimally invasive approaches. ($p=0.01$) Robotic resections provide less than VATS ($p=0.006$) or thoracotomy. ($p=0.002$) VATS is indifferent to thoracotomy. ($p=0.126$) Lobar or segmental sampling is also indifferent. ($p=0.361$) Lower lobes have more segments than upper ones, still all lobes provide statistically non-different blood volumes. ($p=0.58$)

Conclusion:

A minimum plasma volume is required for ctDNA examination in various genomic profiling techniques. Researchers expect more plasma volume when sampling tumor-draining veins from pneumonectomy specimens (as expected) and from VATS or open resections versus robotics. Volumes are statistically indifferent between lobectomies versus segmentectomies and between upper versus lower lobes.

S. Kakava^{1,2}, E. Schlumpf¹, A. von Eckardstein^{1,2}, J. Robert¹

Differential trafficking of high-density lipoproteins containing or lacking apolipoprotein E in brain endothelial cells

University hospital Zurich (Switzerland)¹, University of Zurich (Switzerland)²

Introduction:

Alzheimer's disease (AD) is the leading cause of senile dementia in elderly people with over 50 million affected individuals worldwide. Apart from the well-known neuropathological hallmarks (beta-amyloid and tangles accumulations), the pathogenic importance of cerebrovascular dysfunction is increasingly recognized in the development of AD. Epidemiological evidence showed that cerebrovascular damage precedes neuropathological pathologies. Interestingly, high-density lipoprotein (HDL), a blood lipid transporter, possesses several vasoprotective functions and epidemiological studies showed associations of HDL-cholesterol levels with the risk of AD. We previously reported that HDL reduces beta-amyloid deposition within the vasculature and inhibits vascular inflammation. Interestingly a small subpopulation of HDL particles containing apoE (HDLE+) were more effective than those lacking apoE (HDLE-). However, HDL being in the blood must interact with brain endothelial cells (EC) to display its anti-AD properties, a process that remains poorly understood.

Methods:

HDL was isolated from plasma of healthy donors by ultracentrifugation and then further fractionated using an apoE immunoaffinity column to generate total HDL, HDLE+ and HDLE-. Fluorescent or 125I-radio labeled HDL were used to measure binding (4°C), association or transport (37°C) through primary human brain EC or the cell line hCMEC/D3.

Results:

We confirmed that HDL is bound and internalized by brain EC. RNA interference and pharmacological inhibitions showed that HDL binding and association were dependent of scavenger receptor BI (SR-BI) and endothelial lipase whereas low density lipoprotein receptor (LDLR) and ATP binding cassette G1 (ABCG1) knockdown only reduced HDL association. Finally, although HDL was transported through brain EC independently of apoE status, we found that HDLE+ did not co-localize with HDLE- suggesting independent trafficking pathways.

Conclusion:

Our findings support distinct trafficking pathways of HDLE+ and HDLE- through brain EC's that might imply different HDL cerebrovascular functions relevant to AD.

S. Changkhong^{1,2}, P. Lithanatudom¹, I. Opitz², M. Meerang²

Role of CD147 (Basigin) in Malignant Pleural Mesothelioma

Department of Biology, Faculty of Science, Chiang Mai University, Chiang Mai, Thailand¹, Department of Thoracic Surgery, University Hospital Zurich, Zurich, Switzerland²

Introduction:

We aim to identify novel therapeutic targets for malignant pleural mesothelioma (MPM), an aggressive cancer caused primarily by asbestos exposure. In this study, we focus on the role of CD147 that has been shown to almost exclusively expressed in MPM tumor tissues compared to mesothelial reactive cells. CD147 or Basigin (BSG), a transmembrane glycoprotein, is an immunoglobulin superfamily that plays a role in various cellular processes. CD147 also overexpressed in a wide range of cancers eg. hepatocellular carcinoma, breast cancer, and promoted their malignant and chemoresistant properties.

Methods:

We evaluated the expression of CD147 compared to other cancers using the publically available TCGA database. We next measured gene expression level of CD147 in USZ MPM patient cohort compared to non-MPM tissues, using quantitative real time RT-qPCR (qPCR). Protein levels of CD147 in cell lines were analyzed by western blot. Transient knockdown of CD147 was achieved by using Dicer-substrate siRNAs (DsiRNAs).

Results:

Employing TCGA database, we identified mesothelioma (MESO) as one of the top eight cancer patient cohorts that express high CD147 transcripts. We further confirmed that CD147 is upregulated in MPM tumors (n=49), compared to non-MPM tissues (n=18; collected from patients suspected with MPM but the diagnosis was benign) in the USZ patient cohort (p=0.0016). From a total of 10 MPM established cell lines, 7 showed upregulation of CD147 gene compared to non-MPM cell line. Western blot in a subset of MPM cells showed that CD147 in MPM cells are highly glycosylated. The quantification of western blot showed positive correlation between gene and protein expression (p=0.019, r=0.89, n=6). We identified 3 DsiRNA sequences that showed >85% CD147 knockdown efficiency. Using these siRNAs, we will further investigate effects of CD147 knockdown in MPM cells.

Conclusion:

A large subset of MPM tumors and cell lines overexpressed CD147. Thus, investigating the role of CD147 upregulation may further lead to the discovery of a novel players in MPM progression and therapeutic target.

Targeting lung cancer by CD26/DPP4 inhibition in combination with an immune-checkpoint inhibitor

Thoracic Surgery Department, University Hospital Zürich¹

Introduction:

Lung cancer is the leading cause of death among all cancer patients. Immune checkpoint inhibitor (ICI) gained an attention as cancer therapeutics. Clinical trials employing ICI showed an improved survival in cancer patients. However, the limited response rate and resistance of ICI became a rising issue in immunotherapy.

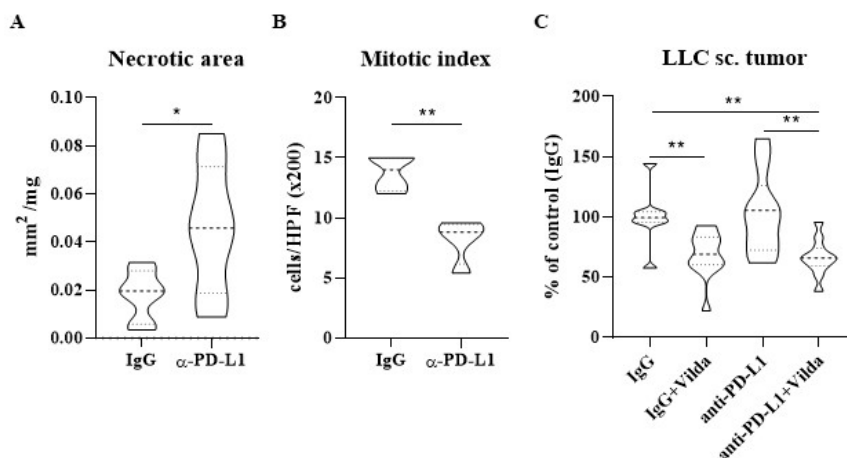
CD26/DPP4 is constitutively expressed on lung cells playing a role in the growth of tumors. Previously, we showed that the inhibition of CD26/DPP4 reduced size of lung tumors along with enhanced tumor-infiltrating NK cells. In spite of enhanced NK cells, total elimination of the tumor was not achieved due to increased expression of PD-L1. We therefore aimed at establishing a novel synergistically acting therapeutics of CD26/DPP4 inhibition in combination with an immune checkpoint inhibitor to against lung cancer.

Methods:

By subcutaneous injection of mouse lung cancer cell line (LLC), an orthotopic lung tumor model was established. Pilot experiments were performed to select the best performing ICI including antibodies anti-PD-L1, anti-PD-1, and anti-CTLA4 against LLC. Tumor growth was evaluated by wet weight of tumor mass at 2 weeks after injection. Intra-tumor necrosis and mitosis were analyzed by histological assessment. The CD26/DPP4-inhibitor Vildagliptin was given to mice in drinking water of 50 mg/kg daily dose.

Results:

The pilot test of ICIs against LLC showed that anti-PD-L1 therapy showed the best anti-cancer effect with significantly higher tumor necrosis (Fig. A) and lower mitosis (Fig. B) compared to non-specific IgG treated control group, although wet weight of tumor was not significantly reduced by antibody treatment. The combination of anti-PD-L1 and Vildagliptin showed a significantly reduced tumor size compared to the control group and anti-PD-L1 treated group (Fig. C). Vildagliptin and control IgG treated group showed significantly reduced tumor size. N=9, *p<0.05, **p<0.01



Conclusion:

These preliminary data show that the combination of an ICI with a CD26/DPP4-inhibitor has synergistic anti-tumor effects in lung cancer.

M. Meerang¹, J. Kreienbühl¹, V. Orlowski¹, S. Müller¹, M. Kirschner¹, I. Opitz¹

Importance of Cullin4 Ubiquitin Ligase in Malignant Pleural Mesothelioma

Department of Thoracic Surgery, University Hospital Zurich, Zurich, Switzerland¹

Introduction:

Malignant pleural mesothelioma (MPM) is primarily driven by loss of tumor suppressor genes. In this study, we explored importance of cullin4 (CUL4; 2 paralogs, CUL4A and CUL4B), a member of the cullin protein family that have been shown to be dysregulated in MPM as a consequence of tumor suppressor gene NF2 loss. We also evaluated the efficacy of the cullin inhibition by pevonedistat, a small molecule inhibiting cullin neddylation.

Methods:

We assessed the expression of CUL4A and CUL4B in tissues using immunohistochemistry (IHC) and quantitative real time PCR. We tested the efficacy of pevonedistat in 13 MPM cell lines in 2D and 3D culture compared to non-malignant mesothelial cells. Four groups of severe combined immunodeficiency SCID mice (n=8/group) bearing intraperitoneal (ip.) pevonedistat sensitive (MSTO211H) or resistant (ACC-Meso1) cell lines were treated with pevonedistat (50 mg/kg; ip.) on a 5day on/5day off schedule for 3 cycles. Treatment efficacy was assessed by means of overall survival. To evaluate the mechanism of treatment, additional groups of mice (n=5/group) were treated for one cycle followed by tissue collection and analysis.

Results:

Gene expression of CUL4A and CUL4B were upregulated in MPM tumor specimens compared to non-malignant pleural tissues. Data from the TCGA MPM cohort revealed that high CUL4B gene expression was associated with short disease free survival. Accordingly, using IHC on tissue microarray, we demonstrated that high CUL4B protein expression was associated with short progression free survival of MPM patients. Five MPM cell lines (38%) were highly sensitive to cullins inhibition by pevonedistat (IC₅₀<0.5 μM). This remained true in 3D spheroid culture. The treatment induced S/G2 cell cycle arrest and accumulation of cells undergoing DNA rereplication (containing >4N DNA content) more predominantly in the sensitive cell lines. DNA rereplication is known to be mediated by CDT1 accumulation and indeed the accumulation of CDT1 was detected after the treatment. Nevertheless, there was no difference in the extent of CDT1 accumulation comparing between sensitive and resistant cell lines. In vivo, pevonedistat treatment significantly prolonged survival of mice bearing both sensitive (MSTO211H) and resistant (ACC-Meso-1) MPM tumors. Pevonedistat treatment reduced growth in pevonedistat sensitive tumor but increased apoptosis in pevonedistat resistant tumor. Thus, we analyzed cells associated with tumor microenvironment including mouse macrophage (F4/80+) and vessel formation (CD31+) that may explain the efficacy of pevonedistat in the resistant model. The treatment significantly reduced numbers of tumor associated macrophage in resistant tumors, while it showed no effect in sensitive tumors. The treatment did not alter polarization of macrophage as shown by no change in the expression of Arginase1, a marker of immunosuppressive M2 macrophage, after treatment. There was no effect on blood vessel formation in both tumor models at this time point.

Conclusion:

High CUL4B expression may play a role in MPM progression. Inhibition of cullins by pevonedistat induced growth arrest and DNA re-replication in a subset of MPM. Pevonedistat showed favorable effect for MPM treatment in vivo, even for a resistant tumor model. This effect may be mediated by reduced tumor-associated macrophage infiltration.

E. De Cecco¹

CRISPR screen to identify modulators of prion transfer

*University Hospital Zurich*¹

Introduction:

Protein aggregation disorders affect millions of people and are essentially incurable. Protein aggregates “jump” from one neuron to another, thereby infecting the entire brain and causing neurodegeneration. Here I propose to enumerate all genetic modifiers of transcellular transfer, using prion disorders as a prototypic model. Prions, the causative agent of Transmissible Spongiform Encephalopathies, transfer from cell to cell in many ways, potentially including nanotubes, trafficking within exosomes, GPI-painting and transport in microvesicles. However, the genetic landscape of interactors and regulators remains largely unknown. Several potential receptors for prion uptake have been investigated, but their role remains unclear and to date there is no evidence for a receptor specific for prions.

Methods:

I will utilize two novel, powerful tools developed in the lab: single-gene CRISPR-cut and CRISPR-activator libraries spanning the entire human genome and a highly prion-susceptible human cell line in which the gene encoding for the prion protein was replaced by its ovine homologue. For biosafety reasons, I am using synthetic ovine prions produced from in vitro shaking of the recombinant monomeric protein. The advantage of synthetic PrP^{Sc} aggregates is their high purity, which allows an easier manipulation and a selective labelling with commercially available fluorescent probes. Cells expressing the genetic transactivator dCas9-VPR will be genetically perturbed with our CRISPR-activator pooled library and then challenged with labelled prions directly in the culture medium. Prion-positive cells will be isolated by FACS sorting and their genomic DNA will be subjected to next-generation sequencing to identify the enriched/depleted 4sgRNA guides and their corresponding genes.

Results:

I stably expressed dCas9-VPR in two human cell lines and successfully tested the knock-out efficiency in both the parental polyclonal line and in selected monoclones. Thanks to the multiplexing of 4 distinct sgRNA guides against one single gene, our CRISPR libraries outperformed all commercial ones, and hold great potential to identify previously overlooked candidates. In addition, I tested various commercial fluorophores to label prions, and optimized the labeling protocol to increase the efficiency of the reaction. Prions showed to be actively internalized by most cells within 24 hours and the uptake is strictly dependent on aggregates' concentration and on their sonication, which results in particles of smaller size. Prion-positive cells could be reliably detected and quantified both by flow cytometry and widefield microscopy, with the latter being an alternative detection method in case of issues. In parallel, I am developing a genetically encoded reporter system to detect non-labelled transferred prions, which I plan to use in the subsequent step of hit validation.

Conclusion:

My project would represent the first genome-wide genetic analysis in a fully human background ever performed in the field of prion diseases. This is particularly relevant as a major problem in the identification of druggable targets in prion diseases is the difficulty of recapitulating in human models the results obtained in rodents. The simultaneous interrogation of the whole genome is the most powerful way to identify all genes regulating this process and could pave the way for the application of personalized medicine also in the field of prion diseases.

A. Lakkaraju¹, A. Aguzzi¹

Gpr133 ablation delays onset of prion disease

Institute of Neuropathology, University Hospital of Zurich¹

Introduction:

Prion diseases are protein misfolding and aggregating disorders (PMA) implicated in Creutzfeldt-Jakob disease (CJD) and several transmissible spongiform encephalopathies of humans and animals. PrPC is highly expressed in the CNS albeit its physiological role there is yet to be clearly elucidated. We have previously discovered that PrPC activates Gpr126, an adhesion GPCR expressed on Schwann cells. We also interrogated other adhesion GPCRs for their ability to bind and elicit signaling response to FT. All studied receptors were unreactive except Gpr133 (also called Adgrd1). Gpr133 is expressed in the CNS and in other tissues; its endogenous agonists and the signal transduction pathways are unknown. Gpr133 resembles Gpr126 in that it contains PTX and CUB domains and is autoproteolytically processed. A large number of SNPs have been reported for Gpr133, some of which seem to affect its surface expression and signaling activity. PrPC overexpression accelerates prion diseases, whereas its ablation prevents the disease. This suggests a gain of toxic functions by prions, possibly resulting from inappropriate modulation of brain-resident GPCRs. We sought to investigate and characterize the molecular details associated with the interaction of PrPC to Gpr133 and whether Gpr133 plays any role in the manifestation of prion disease.

Methods:

To characterize Gpr133, we used animal models (mice ablated of Gpr133), organotypic slice cultures and cell lines. Techniques such as immunohistochemistry, flow cytometry, ELISA and in vitro biochemical assays were utilized in all these model systems to characterize the binding to the receptor and the activity of the receptor. Prion infected mice models were used to assess time course of progression of the disease.

Results:

Gpr133 is predominantly expressed in a subset of neurons in mice brain. Overexpression of Gpr133 in cell lines results in increased intracellular cAMP, yet treatment of Gpr133-overexpressing cells with N-terminus of PrPC (FT: flexible tail) resulted in dramatic dampening of cAMP production. Mapping for interaction domains revealed that proximal charged 5 amino acids of FT (KKRPK) sufficed to bind to the PTX domain on the extracellular region of Gpr133. Presence of positive charge in FT sufficed to facilitate this binding to Gpr133. Interestingly, treatment with FT also averted cellular toxicity associated with cAMP accumulation in Gpr133 expressing cells. Furthermore, unlike Gpr126, Gpr133 activity was not regulated by binding of other extracellular matrix proteins such as Collagen IV. Importantly, mice ablated of PrPC revealed a significant decrease in the expression of Gpr133 suggesting an association / regulation between both the proteins. Treatment of cerebellar organotypic cultured slices from the brains of Gpr133 ablated mice resisted neuronal loss upon treatment with prions and prion mimetics (POM1 antibody). Prion infection of Gpr133 ablated mice although did not prevent the disease itself, a significant delay in the onset of disease symptoms was observed.

Conclusion:

Our results here suggest that Gpr133 activity is strongly suppressed by binding of PrPC in physiological conditions. Furthermore, similar to Gpr126 binding on Gpr133 is mediated via its PTX domain to which the positively charged domain of FT binds. Our results further highlight that absence of Gpr133 prevents neuronal loss in organotypic cultured slices treated with prions and delays the onset of prion disease in mice suggesting an important role for the receptor in manifestation of prion disease. Overall our study highlights Gpr133 as a novel receptor for prion protein in health and disease.

G. Forgo¹⁰, N. Kucher¹⁰, S. Barco¹⁰, E. Micieli¹⁰, W. Ageno¹³, L. Castellucci⁷, G. Gabriela⁴, H. Ddungu⁹, V. Erich¹², M. Dumantepe¹⁴, M. Guillermo Esposito³, S. Konstantinides¹¹, C. McLintock⁶, F. Ní Áinle⁵, A. Spyropoulos¹, T. Urano², B. Hunt⁸

An update on the global use of risk assessment models and thromboprophylaxis in hospitalized patients with medical illnesses from the World Thrombosis Day steering committee: systematic review and meta-analysis

Feinstein Institutes for Medical Research and the Zucker School of Medicine at Hofstra/Northwell¹, Graduate University of Public Health, Shizuoka, Japan², Hospital de Clinicas Facultad de Medicina³, Instituto Nacional de Cancerología⁴, Mater Misericordiae University Hospital and Rotunda Hospital⁵, National Women's Health Auckland City Hospital⁶, Ottawa Hospital Research Institute, University of Ottawa⁷, Thrombosis & Haemophilia Centre, Guys & St Thomas' NHS Foundation Trust⁸, Uganda Cancer Institute⁹, University Hospital of Zurich¹⁰, University Medical Center Mainz¹¹, University of Campinas¹², University of Insubria¹³, Uskudar University School of Medicine¹⁴

Introduction:

Venous thromboembolism (VTE) is a leading cause of cardiovascular morbidity and mortality. The majority of VTE events are hospital-associated. In 2008, the ENDORSE multinational survey reported that only around 40% of medical patients at risk of VTE received adequate thromboprophylaxis.

Methods:

In our systematic review and meta-analysis, we aimed at providing updated figures concerning the use of thromboprophylaxis globally. We focused on: (i) the frequency of patients with an indication to thromboprophylaxis according with individual models; (ii) the use of adequate thromboprophylaxis; (iii) reported contraindications to thromboprophylaxis. Observational non-randomized studies or surveys focusing on medically ill patients were considered eligible.

Results:

After screening, we included 27 studies from 20 countries for a total of 137,288 patients. Overall, 50.5% (95%CI: 41.9%-59.1%, I² 99%) of patients had an indication to thromboprophylaxis: of these, 54.5% (95%CI: 46.2%-62.6%, I² 99%) received adequate thromboprophylaxis. The use of adequate thromboprophylaxis was 66.8% in Europe (95%CI: 50.7% to 81.1%; I² 98%), 44.9% in Africa (95%CI: 31.8% to 58.4% I² 96%), 37.6% in Asia (95%CI: 25.7%-50.3%, I² 97%), 58.3% in South America (95%CI 31.1%-83.1%, I² 99%), and 68.6% in North America (95%CI 64.9%-72.6%, I² 96%). No major differences in adequate thromboprophylaxis use were found across risk assessment models. Bleeding, thrombocytopenia, and renal/hepatic failure were the most frequently reported contraindications to thromboprophylaxis.

Conclusion:

The use of anticoagulants for VTE prevention has been proven effective and safe, but thromboprophylaxis prescriptions are still unsatisfactory among hospitalized medically ill patients around the globe with marked geographical differences.

A. Hariharan⁴, W. Qi², H. Rehrauer², M. Ronner⁴, M. Wipplinger⁴, J. Kresoja-Rakic⁴, S. Sun⁴, M. Sculco⁴, L. Oton-Gonzalez⁴, JH. Rüschoff³, I. Schmitt-Opitz¹, E. Felley-Bosco⁴

RNA editing landscape in mesothelioma and the role of editing enzyme ADAR2 in growth, chemotherapy response and interferon signaling

Department of Thoracic Surgery, University Hospital Zurich¹, Functional Genomics Center, ETH Zurich, University of Zurich², Institute for Pathology and Molecular Pathology, University Hospital Zurich³, Laboratory of Molecular Oncology, Department of Thoracic Surgery, University Hospital Zurich⁴

Introduction:

Pleural mesothelioma (PM) is a rare and aggressive cancer associated with asbestos exposure. It is mainly driven by loss of function of tumor suppressor genes, with the most frequent being BRCA1-associated-protein-1 (BAP1), which is mutated in about 50% of PM. In a mouse model (Nf2+/-) of asbestos-induced mesothelioma development, increased levels of A-to-I (read as G) changes in RNA by the activity of adenosine deaminases acting on double-stranded RNA (ADARs) were observed. ADAR expression levels also increased upon asbestos exposure, particularly ADAR2 expression which increased only upon tumor formation. The aim of this study was to characterize ADAR-dependent RNA editing in human samples and assess its role in tumor.

Methods:

Levels of A-to-I RNA editing were determined from RNA sequencing data from The Cancer Genome Atlas (TCGA) and Bueno's cohort. ADAR2 expression levels and BAP1 mutational status were also extracted. ADAR2 knockout (KO) in mouse RN5 and human Mero95 cells were generated using CRISPR/Cas9 system. Wild-type ADAR2 was stably transfected into the KO cells to obtain the rescue cells. Proliferation of cells was measured using MTT assay. Viability of spheroids after treatment with pemetrexed was measured using Cell Titer Glo assay. Protein expression of enzymes involved in folate metabolism and interferon-stimulated genes was determined by western blotting.

Results:

In human TCGA and Bueno datasets, tumours were found to have higher ADAR-mediated A-to-I RNA editing compared to mesothelial precursors. In these datasets, ADAR2 expression levels were higher in BAP1 wild-type tumours, with corresponding increase in A-to-I RNA editing in transcripts. In addition, heterogeneity in ADAR2 expression was observed between mesothelial and mesothelioma cells, compared to ADAR1 expression. To investigate the role of ADAR2, ADAR2-deficient mouse and human mesothelioma cell lines were generated. Using these models, it was found that ADAR2 loss resulted in reduced cell proliferation as well as increased sensitivity to pemetrexed, an anti-folate used as first-line chemotherapy for mesothelioma patients. This can be attributed to a decrease in expression of dihydrofolate reductase and thymidylate synthase, key players in folate metabolism and DNA synthesis as well as targets of ADAR-mediated editing, that we observed in ADAR2-deficient cells. dsRNAs are identified and destabilised by ADARs, thereby dampening the interferon-induced inflammatory response. In the absence of ADAR2, upregulation of interferon signalling was observed. The phenotypes observed in the ADAR2-deficient cells were all rescued by ADAR2 overexpression.

Conclusion:

Altogether, these observations indicate an important role of RNA editing in mesothelioma, especially RNA editing enzyme ADAR2. Higher ADAR2 expression was associated with wild-type BAP1 expression. The expression of ADAR2 regulates growth, chemotherapy response, and inflammatory response downstream of dsRNA, in mesothelioma.

S. Ambrosini², F. Montecucco³, D. Koljin⁴, A. Akhmedov², S. Mohammed², G. Liuzzo⁵, A. Beltrami⁷, F. Crea⁵, F. Ruschitzka⁶, T. Lüscher^{1,2}, N. Hamdani⁴, S. Costantino², F. Paneni^{2,6}

The methyltransferase SETD7 drives myocardial ischemic injury by modulating the Hippo pathway: a study in mice and humans

Cardiology, Royal Brompton & Harefield Hospital Trust and Imperial College London, London SW3 6NP, United Kingdom¹, Center for Molecular Cardiology, University of Zürich², First Clinic of Internal Medicine, Department of Internal Medicine and Centre of Excellence for Biomedical Research (CEBR), University of Genoa³, Institute of Physiology, Ruhr University, Bochum, Germany⁴, Polyclinic Agostino Gemelli, Catholic University of the Sacred Heart, Rome, Italy⁵, University Heart Center, Cardiology, University Hospital Zurich, Switzerland⁶, University of Udine, Italy⁷

Introduction:

Ischemic heart disease is a leading cause of death worldwide. Although revascularization strategies significantly reduce mortality after acute myocardial infarction (MI), a significant number of MI patients develop heart failure. Protein methylation is emerging as a key biological signal implicated in the pathophysiology of cardiovascular (CV) disease. In this regard, the methyltransferase SETD7 was recently shown to methylate proteins relevant to CV homeostasis. The present study aims to investigate the role of SETD7 in myocardial ischemia-reperfusion (I/R) injury.

Methods:

Experiments were performed in neonatal rat ventricular myocytes (NRVM), SETD7 knockout mice (SETD7^{-/-}) undergoing myocardial I/R injury, myocardial samples from patients with and without ischemic heart failure as well as peripheral blood mononuclear cells from patients with ST elevation MI (STEMI, n=25) and age-matched healthy controls (n=20).

Results:

Glucose deprivation (GD) in NRVM led to upregulation of SETD7 and direct mono-methylation of the Hippo signaling effector YAP. SETD7-dependent methylation of YAP led to its cytosolic retention thus impeding YAP binding to the promoter of pro-survival genes. Selective pharmacological inhibition of SETD7 by (R)-PFI-2 blunted YAP mono-methylation thereby restoring its nuclear retention. We show that YAP binds the promoter of antioxidant genes catalase and superoxide dismutase, thus preventing GD-induced mitochondrial oxidative stress, organelle swelling and apoptosis. Consistently, infarct size, myocardial oxidative stress and left ventricular dysfunction were reduced in SETD7^{-/-} mice undergoing I/R as compared to wild-type littermates. Of clinical relevance, in cardiomyocytes isolated from I/R mice and patients with ischemic heart failure (R)-PFI-2 prevented mtROS accumulation while improving Ca²⁺-activated tension. Finally, SETD7 was upregulated in PBMCs from STEMI patients and negatively correlated with MnSOD and CAT

Conclusion:

We demonstrate that SETD7-dependent methylation of YAP is an important mechanism underpinning myocardial oxidative stress, mitochondrial damage and apoptosis during ischemia. Pharmacological modulation of SETD7 by (R)-PFI-2 may represent a potential therapeutic approach to prevent myocardial ischemic damage through modulation of the Hippo pathway.

I. Martinez Lopez¹, M. Haberecker², M. Kirschner¹, F. Schläpfer¹, V. Orłowski¹, J. Rüschoff², I. Opitz¹

Analysis of surgery-derived specimens and primary cell cultures for the study of Chronic Thromboembolic Pulmonary Hypertension

Department of Thoracic Surgery, University Hospital Zurich¹, Institute of Pathology and Molecular Pathology, University Hospital Zurich²

Introduction:

Chronic Thromboembolic Pulmonary Hypertension (CTEPH) is a rare, chronic, debilitating disease characterized by bilateral pathological changes of the pulmonary arteries (PAs). The latter are thought to originate from overgrowth of endothelial (ECs) or vascular smooth muscle (VSMCs) cells. However, the proportion of these cells in our Pulmonary Endarterectomy (PEA)-derived tissues has been smaller than expected. We therefore investigate this further through molecular and pathological characterization of surgical specimens and primary cell cultures.

Methods:

For primary culture, peripheral fibrotic obstructive material, intima and media tissues removed during PEAs were digested, plated and cultured. Along their corresponding FFPE tissues, successfully growing primary cells were characterized using hematoxylin and eosin, and Immunohistochemical stainings, including endothelial (Pan-cytokeratin), smooth muscle (Smooth Muscle Actin (SMA), Caldesmon, Smoothelin, Smooth Muscle Myosin Heavy Chain (SMM1)), mesenchymal (Vimentin), and proliferation (Ki-67) markers.

Results:

We established primary cells from 31 fibrotic tissues, 27 intima and 3 media samples derived from 31 patients. Cultured cells show unique morphologies, great diversity in growth rate and distribution patterns. The described Immunohistochemical panel on a set of cells, allowed the identification of different types of fibroblasts: normal fibroblasts (Vim+/PanCK,SMA,Smooth-), myofibroblasts (Vim,SMA,SMM1+/PanCK,Cald,Smooth-), epithelioid fibroblasts (Vim,PanCK+/SMA,Cald-), and some co-cultures.

Interestingly on gross examination, the fibrotic tissue showed either white or yellow nodules. FFPE stainings revealed white nodules with an unusual histology of neo-vascularization within the intima and varying degrees of fibrotic changes, while the yellow nodules had inflammatory cells and foamy macrophages, the latter indicating the presence of atherosclerotic changes. We are currently evaluating a possible correlation between the type of fibroblasts from primary culture and the macroscopic nodules.

Conclusion:

Our findings in this initial sample subset show that CTEPH lesions could be the result of a fibrotic process rather than overgrowing ECs or VSMCs. We are currently preparing all cell blocks and tissues for staining and molecular analysis.

M. Gagesch^{2,3}, M. Wiecek^{2,3}, B. Vellas⁷, R. Kressig¹¹, R. Rizzoli⁹, J. Kanis^{1,8}, W. Willett^{5,6}, A. Egli^{2,3}, W. Lang^{2,3}, E. Orav⁴, h. Bischoff-Ferrari^{2,3,10}

Effects of vitamin D, omega-3 fatty acids and a simple home exercise program on pre-frailty prevention among generally healthy and robust adults age 70 and older: The DO-HEALTH randomized clinical trial

Centre for Metabolic Bone Diseases, University of Sheffield Medical School, Sheffield, UK¹, Centre on Aging and Mobility, University Hospital Zurich and University of Zurich, Zurich, Switzerland², Department of Aging Medicine, University Hospital Zurich, Zurich, Switzerland³, Department of Biostatistics, Harvard T. H. Chan School of Public Health, Boston, USA⁴, Department of Epidemiology, Harvard T. H. Chan School of Public Health, Boston, USA⁵, Department of Nutrition, Harvard T. H. Chan School of Public Health, Boston, USA⁶, Gérontopôle, Toulouse University Hospital, University of Toulouse, UMR INSERM 1295, Toulouse, France⁷, Mary McKillop Institute for Health Research, Australian Catholic University, Melbourne, Australia⁸, Service of Bone Diseases, Geneva University Hospitals and Faculty of Medicine, Geneva, Switzerland⁹, University Clinic for Aging Medicine, City Hospital Zurich, Zurich, Switzerland¹⁰, University Department of Geriatric Medicine FELIX PLATTER, Basel, Switzerland¹¹

Introduction:

The benefits of supplemental vitamin D, marine omega-3 fatty acids, and a simple home exercise program (SHEP) on frailty prevention in generally healthy community-dwelling older adults are unclear. To test the effect of vitamin D, omega-3s, and a SHEP, alone or in combination on incident pre-frailty and frailty in robust older adults over a follow-up of 36 months.

Methods:

DO-HEALTH is a multi-center, double-blind, placebo-controlled, 2x2x2 factorial randomized clinical trial among generally healthy European adults aged 70 years or older, who had no major health events in the 5 years prior to enrollment, sufficient mobility and intact cognitive function. As a secondary outcome of the DO-HEALTH trial, among the subset of participants who were robust at baseline, we tested the individual and combined benefits of supplemental 2,000 IU/day of vitamin D3, 1 g/day of marine omega-3s, and a SHEP on the odds of being pre-frail and frail over 3 years of follow up.

Results:

At baseline 1,137 out of 2,157 participants were robust (mean age, 74.3 years; 56.5% women, mean gait speed 1.18 m/s). Over a median follow-up of 2.99 years, 696 (61.2%) became pre-frail and 29 (2.6%) frail. Odds ratios (OR) (95% CI) for becoming pre-frail were 0.81 (0.62-1.07; p=0.13) for vitamin D3 compared to no vitamin D3, 0.84 (0.64-1.11; p=0.22) for omega-3s compared to no omega-3s, 0.89 (0.67-1.16; p=0.38) for SHEP compared to control exercise, and 0.61 (0.38-0.98; p=0.04) for all 3 treatments combined compared to control (placebo for the supplements and control exercise). None of the individual treatments or their combination significantly reduced the odds of becoming frail.

Conclusion:

Robust, generally healthy and active older adults without major comorbidities, may benefit by a combination of high-dose supplemental vitamin D3, marine omega-3s, and SHEP with regard to the risk of becoming pre-frail over 3 years.

H. Bischoff-Ferrari^{2, 4, 13}, W. Willett⁶, J. Manson⁷, B. Dawson-Hughes¹¹, M. Manz⁸, R. Theiler^{2, 4}, K. Brändle^{2, 4}, B. Vellas¹⁰, R. Rizzo⁹, R. Kressig¹⁴, H. Staehelin¹⁴, J. da Silva³, G. Armbrecht¹², A. Egli^{2, 4}, J. Kanis¹, E. Orav⁵, S. Gängler^{2, 4}

Combined Vitamin D, omega-3 fatty acids and a simple home strength exercise program may reduce cancer risk among active adults age 70 and older: a randomized clinical trial

Center for Metabolic Diseases, University of Sheffield Medical School, Sheffield, United Kingdom and Mary MacKillop Institute for Health Research, Australian Catholic University, Melbourne, Victoria, Australia¹, Center on Aging and Mobility, University Hospital Zurich, City Hospital Waid&Triemli and University of Zurich, Zurich, Switzerland², Centro Hospitalar e Universitário de Coimbra, Coimbra, Portugal and Coimbra Institute for Clinical and Biomedical Research (iCBR), Faculty of Medicine, University of Coimbra, Coimbra, Portugal³, Department of Aging Medicine and Aging Research, University Hospital Zurich and University of Zurich, Zurich, Switzerland⁴, Department of Biostatistics, Harvard T.H. Chan School of Public Health, Boston, Massachusetts, USA⁵, Department of Epidemiology and Department of Nutrition, Harvard T H Chan School of Public Health, Boston, MA, USA⁶, Department of Medicine, Brigham and Women's Hospital, Harvard Medical School, Boston, Massachusetts, USA⁷, Dept. of Medical Oncology and Hematology, University and University Hospital Zurich, Zurich, Switzerland⁸, Division of Bone Diseases, Geneva University Hospitals and Faculty of Medicine, Geneva, Switzerland⁹, Gérontopôle de Toulouse, Institut du Vieillissement, Center Hospitalo-Universitaire de Toulouse, Toulouse, France and UMR INSERM 1027, University of Toulouse III, Toulouse, France¹⁰, Jean Mayer USDA Human Nutrition Research Center on Aging, Tufts University, Boston, Massachusetts, USA¹¹, Klinik für Radiologie, Charité – Universitätsmedizin Berlin, corporate member of Freie Universität Berlin and Humboldt-Universität zu Berlin, Berlin, Germany¹², University Clinic for Aging Medicine, City Hospital Zurich, Switzerland¹³, University Department of Geriatric Medicine FELIX PLATTER, and University of Basel, Basel, Switzerland¹⁴

Introduction:

The role of vitamin D, omega-3 fatty acids and home exercise as prevention strategies for the risk of any invasive cancer is unclear. Therefore, the objective of this study was to test the individual and combined benefit of vitamin D, omega-3 and a simple home strength exercise program on the risk of any invasive cancer.

Methods:

The DO-HEALTH trial is a three-year, multi-centre, 2x2x2 factorial design double-blind randomized-controlled trial to test the individual and combined benefit of three public health interventions. The trial was conducted between December 2012 and December 2017 in five European countries. Participants were generally healthy community-dwelling adults ≥ 70 years. The interventions were supplemental 2000 IU/day of vitamin D3, and/or 1 g/day of marine omega-3s, and / or a simple home strength exercise (SHEP) programme compared to placebo and control exercise. In this pre-defined exploratory analysis, time-to-development of any verified invasive cancer was the primary outcome in an intent-to-treat analysis. Adjustments included age, sex, prior fall, body mass index, study site, and cancer history. ClinicalTrials.gov Identifier: NCT01745263

Results:

2157 participants (mean age 74.9 years; 61.7% women; 40.7% with 25-OH vitamin D below 20 ng/mL, 83% at least moderately physically active) were randomized. Over a median follow-up of 2.99 years, 81 invasive cancer cases were diagnosed and verified. For the three individual treatments, adjusted hazard ratios (HR, 95% CI, cases intervention versus control) were 0.76 (0.49-1.18; 36 vs 45) for vitamin D3, 0.70 (0.44-1.09, 32 vs 49) for omega-3s, and 0.74 (0.48-1.15, 35 vs 46) for SHEP compared to control. For combinations of two treatments, adjusted HR were 0.53 (0.28-1.00; 15 vs 28 cases) for omega-3s plus vitamin D3, 0.56 (0.30-1.04; 11 vs 21) for vitamin D3 plus SHEP, and 0.52 (0.28-0.97; 12 vs 26 cases) for omega-3s plus SHEP. For all three treatments combined compared to placebo, the adjusted HR was 0.39 (0.18-0.85; 4 vs 12 cases).

Conclusion:

Supplementation with daily high-dose vitamin D3 plus omega-3s, combined with a simple home exercise program showed a cumulative reduction in cancer risk in generally healthy and active, and largely vitamin D replete adults ≥ 70 years.

K. Gegenschatz-Schmid², S. Buzzi⁵, J. Grossmann³, B. Roschitzki⁴, R. Urbanet², R. Heuberger⁶, D. Glück¹, A. Zucker⁵, M. Ehrbar²

A surface treatment of nitinol implants reduces blood activation by altered protein adsorption

Blood Transfusion Service SRC, Zurich, Switzerland¹, Department of Obstetrics, University and University Hospital of Zurich, Zurich, Switzerland², Functional Genomics Center Zurich, University of Zurich/ETH Zurich, Zurich Switzerland; SIB Swiss Institute of Bioinformatics, Lausanne, Switzerland³, Functional Genomics Center Zurich, University of Zurich/ETH Zurich, Zurich, Switzerland⁴, Qvanteq AG, Zurich, Switzerland⁵, RMS Foundation, Bettlach, Switzerland⁶

Introduction:

Due to their favorable elastic properties, corrosion resistance and biocompatibility blood-contacting Nitinol is the material of choice for devices to treat cardiovascular diseases. A major drawback however is their strong thrombogenicity, making the use of systemic anticoagulation inevitable. Therefore, there is an urgent clinical need for reducing the thrombogenicity of Nitinol. We describe a simple surface treatment including the removal of surface contaminations and functionalizing the surface with phosphate ions. This treatment rendered commercially available Nitinol highly hydrophilic and anti-thrombotic. We investigate here the efficacy and mechanism of this treatment by comparing standard and surface treated Nitinol samples in terms of blood contact activation, cell adhesion, protein adsorption and endothelialization.

Methods:

Nitinol discs and braids were tested. Discs were electropolished and passivated whereas the braids were thermally oxidized after electropolishing. These Standard (S) samples were washed with 0.9% NaCl prior to usage. Treated (T) samples were additionally treated with oxygen plasma, functionalized with KH₂PO₄, sealed with trehalose and washed with Hanks prior to usage. The surface chemistry was analyzed by X-ray photoelectron spectroscopy (XPS) and its wettability by water contact angle measurements. To investigate blood activation and clot formation, T and S braids were incubated statically and dynamically for 1h in fresh, minimally heparinized whole human blood. Blood activation was quantified by measuring thrombin-antithrombin complex (TAT) and β -Thromboglobulin (β -TG) concentrations in the blood plasma. Adherent human blood components were visualized by immunofluorescence and by scanning electron microscopy. Blood plasma proteins adsorbed on S and T disks were analyzed by a standard proteomic work flow. To study the mechanism of blood activation, S and T braids were pre-coated with 50 nM and 200 nM active FX (FXa) and inactive FX for 1 h in Hanks prior to static blood incubation tests. In whole human blood FX and FXII were inhibited by addition of Rivaroxaban (1-25 μ g/ml) and FXII900 (1-100 μ M), respectively. Endothelialization on S and T disks was evaluated by observing cell coverage of GFP-expressing HUVECs over 4 days and quantifying the fluorescence signal.

Results:

T surfaces show significantly lower water contact angles ($\leq 10^\circ$) than S surfaces (70° - 90°). XPS measurements revealed increased amounts of phosphate, calcium, and magnesium ions on T. Static and dynamic blood incubation tests showed a drastic reduction of thrombus formation, decreased TAT and β -TG concentrations, and reduced fibrin fiber deposition on T devices. Proteomic analysis of adsorbed proteins showed reduced protein abundance on T compared to S surfaces, including proteins of the complement pathway. Interestingly, the treatment increased the adsorption of calcium-binding vitamin K-dependent proteins including FX. Static blood incubation tests with FXa precoated braids resulted in blood activation on T surfaces while Rivaroxaban and FXII900 inhibited blood activation on S surfaces. The endothelialization was not altered upon surface treatment.

Conclusion:

The herein presented treatment made Nitinol surface ultra-hydrophilic and anti-thrombotic. We propose that the strong hydrophilicity and the presence of phosphate and calcium ions steer the adsorption, conformation, and activation of blood proteins. We propose that this surface treatment might be applicable to all titanium alloys.

M. Kirschner², Y. Zhang¹, F. Schläpfer², V. Orlowski², M. Meerang², I. Opitz²

MicroRNAs contribute to the chemotherapy response of malignant pleural mesothelioma

Department of Thoracic Surgery, the 2nd Hospital of Jilin University, China¹, Department of Thoracic Surgery, University Hospital Zurich, Switzerland²

Introduction:

Although platinum-pemetrexed chemotherapy remains the gold-standard for treatment of malignant pleural mesothelioma (MPM), to date we are still lacking predictive biomarkers able to identify patients who truly respond to chemotherapy. Aiming to overcome this problem, we previously performed microRNA expression profiling in tumour tissue of responders and non-responders to induction chemotherapy, which identified candidate predictive microRNAs. Candidates from this profiling are now investigated in vitro for their potential to alter the response of MPM cell lines to cisplatin and pemetrexed.

Methods:

Commercially available MPM cell lines MSTO-211H, H28, Meso1 and Mero82, and the non-malignant transformed mesothelial cell line MeT-5A were reverse transfected with mimics of microRNAs showing differential expression in responders and non-responders. In a first step, we assessed the effect of microRNA overexpression on cell growth without drug treatment. Next, 24h post transfection, cells were treated with increasing concentrations of cisplatin or pemetrexed for 5 days, at which point IC50s were determined. Finally, transfected cells were treated with the combination of cisplatin and pemetrexed at the concentration of the respective IC50s.

Results:

Initial analyses of five candidate microRNAs revealed that overexpression frequently resulted in reduced cell growth of MPM cell lines, but not in MeT-5A. Specifically, overexpression of miR-380-5p resulted in at least 40% growth inhibition, overexpression of miR-221-3p or miR-30a in at least 30% growth inhibition in MPM lines. Investigating the effect on cisplatin response, we observed that in a subset of cell lines, overexpression of miR-380-5p and miR-221-3p resulted in increased sensitivity to the drug. This effect was most pronounced for miR-221-3p, for which we saw significantly lower IC50 values in MSTO-211H (17.59 vs 2.65, $p < 0.001$) and Meso1 (21.59 vs 5.54, $p < 0.001$). Furthermore, in Meso1 cells, overexpression of miR-380-5p, also resulted in a significant increase in sensitivity to cisplatin (21.59 vs 10.36, $p = 0.045$). However, neither of these microRNAs induced strong sensitisation to pemetrexed. In contrast, overexpression of miR-221-3p, the microRNA with the strongest sensitising effect towards cisplatin, appears to induce increased resistance against pemetrexed. Evaluating the effect of microRNA overexpression on the sensitivity to the cisplatin-pemetrexed doublet then showed that although cells are not sensitised to pemetrexed, the sensitising effect on cisplatin is strong enough to result in significantly reduced cell growth 5 days after treatment when compared to the drug-treatment without microRNA overexpression. For both miR-221-3p and miR-380-5p overexpression, transfected cells treated with the combination showed 50-75% lower cell growth than cells without microRNA overexpression.

Conclusion:

First in vitro investigations suggest that overexpression of microRNAs previously linked to chemotherapy-response has the potential to increase the sensitivity to cisplatin. Interestingly, current data for pemetrexed suggest that some microRNAs might render cells more resistant to this drug. However, when treated with the cisplatin-pemetrexed doublet, the sensitising effect on cisplatin seems to be the dominant mechanism, resulting in increased response to the doublet in microRNA overexpressing cells.

S. Sun³, W. Qi², M. Ronner³, A. Hariharan³, M. Wipplinger³, I. Opitz¹, H. Rehrauer², E. Felley-Bosco³

Endogenous Retrovirus expression and type-I interferon signaling in human mesothelioma

Dept Thoracic Surgery, Zurich University Hospital¹, Functional Genomics Center Zurich, ETH Zurich, University of Zurich², Laboratory of Molecular Oncology, Dept Thoracic Surgery, Zurich University Hospital³

Introduction:

Pleural mesothelioma (PM) is a rapidly fatal tumor. The Cancer Genome Atlas (TCGA) investigation of PM revealed that patients with activated type-I interferon (IFN) pathway have a better clinical outcome. We recently demonstrated that the expression of endogenous retroviruses (ERV) due to promoter demethylation contributes to dsRNA formation and activation of type-I IFN signaling in an experimental mouse model of mesothelioma development. The aim of this study is to investigate ERV and type-I IFN activation in human PM.

Methods:

ERV's expression was determined from TCGA and Bueno's cohorts RNA-seq data, as well as Colunga's mesothelial precursors RNA-seq data as normal control. ERV's expression was confirmed by qPCR. Methylation of genomic DNA was assessed after treatment with sodium bisulfite followed by quantitative methylation specific PCR. DNA demethylation was induced in human mesothelial cells by demethylating agent 5-Aza-2'-deoxycytidine (5-Aza-CdR) treatment. To block the type-I IFN signaling, cells were treated with JAK inhibitor Ruxolitinib. IFN stimulated genes (ISGs) expression upon 5-Aza-CdR or Ruxolitinib treatment was determined by qPCR and Western Blot (WB). Flow cytometry using J2 antibody in the presence or absence of RNase III digestion and J2 pull-down were used to verify the presence of dsRNA.

Results:

Long-terminal-repeats (LTR) represent the most abundant transposable elements (TE) upregulated in PM patients datasets compared to mesothelial precursors. 86% of LTR and 14% of long interspersed nuclear elements represent more than two fold upregulated TE in both datasets. Within LTR, we identified three representative ERVs which are specifically enriched in PM and we further analyzed the most abundant one "Candidate-HERV-1". Its expression was lower in normal mesothelial cells compared to mesothelioma cells. Its levels were significantly increased by 5-Aza-CdR treatment. We determined 5-Aza-CdR induced "Candidate-HERV-1" promoter demethylation. Its promoter was more demethylated in mesothelioma tissue compared to non-tumor tissue. 5-Aza-CdR treatment of mesothelial cells was also accompanied by increased levels of ISGs. Basal ISGs expression was higher in mesothelioma cells compared to mesothelial cells with intact IFN gene and it was significantly decreased by treatment with Ruxolitinib. We confirmed the presence of dsRNA by Flow cytometry and verified "Candidate-HERV-1" is part of the dsRNA by J2 pull-down.

Conclusion:

Immunotherapy has been recently approved as first-line treatment for unresectable PM and best response is predicted in tumors with an activated basal immune response. We may provide tools for patients' stratification.

C. Trevisan¹

Arrayed CRISPR activation screening of human transcription factors to identify modifiers of PrPC

*Institut für Neuropathologie*¹

Introduction:

The cellular prion protein (PrPC) is a cell-surface glycoprotein, responsible for the pathogenesis of prion diseases, fatal neurodegenerative disorders that affect humans and a large variety of animals. The biosynthesis of PrPC is a prerequisite for PrP^{Sc} formation, an abnormally folded isoform of the cellular prion protein, which lead to a severe and progressive neuronal death through yet poorly defined pathways. Since the physiological role of PrPC is still not completely clear, different effort were performed in our group to find regulators of its expression through genome-wide screens. The following project aims to perform a CRISPR arrayed screen on a human glioblastoma cell line, using in-house human activation library. Such study will hopefully unravel new genes playing a role in PrPC activity and therefore it will contribute to broaden the spectrum of available pharmacological targets, which can be considered for therapies against prion.

Methods:

We performed an arrayed CRISPRa screens, in a 384 well plate format, using the entire set of human transcription factors (1636 genes), packaged in lentiviruses. The advantage of activate the expression of the TFs with CRISPRa may exceed the limitation of previous study: indeed through siRNAs and CRISPRi it was not possible to identify any transcription factors specifically controlling PrPC expression, perhaps because transcriptional gene regulation relies on redundant factors. A stable expressing dCas9-VPR human glioblastoma cell line (U251-MG) was used as a cellular model. As screen readout, we relied on the FRET-based biochemical assay, to detect the effect of the different genes activation on PrPC expression.

Results:

The identification of transcription factors regulating PrPC expression is ongoing. The validation of the candidate genes, to exclude cell-line specific hits, will be performed on a second cell line, possibly on iPSC-derived neurons.

Conclusion:

The only strong genetic risk factor for prion disease has remained PRNP, the human gene encoding for the prion protein. Thanks to the recent generation of the human CRISPRa arrayed libraries in our lab, it will be possible to search for other novel genes driving PrPC expression. This is the fundamental reason why the proposed work focuses on a genetic screen: the founding of new modifiers could provide unexpected regulatory pathway, which involve PrPC expression.

S. Sellitto¹

Investigate the genetic and molecular landscape of the hnRNP K cellular essentiality by performing unbiased CRISPR screens

Institute of Neuropathology¹

Introduction:

The heterogeneous nuclear ribonucleoprotein K (hnRNP K) is an essential gene encoding an RNA Binding Protein (RBP) belonging to the multifunctional family of the heterogeneous nuclear ribonucleoproteins (hnRNPs). hnRNP K primarily regulates the pre-RNA and RNA metabolism on different levels within the cell and it has been extensively identified as a central target of multiple types of malignancies (AML, CML, breast and prostate cancer). Recently, hnRNP K has been reported to have functional roles also in neurodevelopmental processes (CNS myelination, synaptic plasticity and axogenesis) and neurological disorders like SCA10, ALS, FTD and Au-Kline syndrome. Also, very recently, our lab describes a role of this protein in prion diseases. Considering this, hnRNP K is emerging as an interesting protein in neurophysiology and neuropathology. A better understanding of these functions, with particular focus on prion diseases, will be of remarkable importance. In addition, a deeper characterization of the two faces of hnRNP K in cancer and neuropathology could be seminal to elucidate shared mechanisms of genetic and molecular abnormalities. On this line, genome-wide screens offer a great opportunity to dissect the different cellular roles of hnRNP K by identifying synthetic viable interactions and functional essential domains of this protein.

Methods:

The project is organized in two experimental screens: 1) a whole genome screen to identify genes whose perturbation suppresses the low cellular fitness induced by the hnRNP K loss-of-function; 2) a domain-dependency screen to assess the functional essentiality of single hnRNP K's domains and their internal components. For the first goal, we used the Brunello library to perform a whole genome pooled CRISPR knockout screen. Two human glioblastoma cell lines (LN-229 and U251-MG) knockout for the hnRNP K gene and expressing the Cas9 enzyme were used as cellular models. For the second screen, we combined the exogenous expression of seven different hnRNP K deleted variants with a set of eight intronic sgRNAs knocking out the endogenous hnRNP K gene only. The LN-229 and U-251MG cells were used as cellular models and the viability assessed by CellTiterGlo recording.

Results:

In the first screen, we identified 763 and 37 significantly enriched and depleted genes respectively. The enriched genes were ranked based on the statistics, the fold change and the number of guides enriched and further clustered for functional interactions using the STRING database. We finally generated two lists of potential hits based on the related cellular fitness resulting from their single knockout and validated some of them individually. In the second screen, we identified 3 indispensable and 4 dispensable hnRNPK's domains in the LN-229 and U-251MG cells.

Conclusion:

Investigating the genetic and molecular landscape of hnRNP K essentiality in an unbiased and comprehensive way will highlight the mechanistical underpinnings of its cellular indispensability. Moreover, the biological understanding of how hnRNP K exerts its fundamental role inside the cell may provide insights into the complex biology of this protein and it could potentially track unknown pathways at the intersections between cancer, neurodevelopment and neurodegeneration.

S. La Cioppa^{1,2}, L. Krattiger^{1,2}, B. Emiroglu¹, L. Moser², J. Kartenbender¹, M. Tibbitt¹, M. Ehrbar²

A microfluidic osteogenesis-on-a-chip device

Department of Mechanical and Process Engineering, ETH Zurich¹, Department of Obstetrics, University and University Hospital of Zurich²

Introduction:

Bone defects are either caused by trauma, aging, or diseases like osteoporosis or cancer. Hence, microfluidic devices are of great interest for bone regeneration strategies as well as disease modeling. These structural and functional models of human tissue enable research at high throughput within small volumes. In addition, microfluidic PDMS chips can replace or complement classical 2D cell cultures by better mimicking the 3D environment of native tissue. Bone for example, is a highly dynamic, strongly vascularized 3D tissue system. Thereby, on-chip cultures show the potential of 3D environments to elicit a more physiological state for bone cell cultures. Moreover, as a target organ for many drugs, a more precise replica of bone tissue would facilitate the investigation of a plethora of therapeutics. However, most current 3D cell culture models are based on natural-derived materials, which give rise to unpredictability, which are a huge drawback for pharmaceutical research. The herein described approach, on the other hand, uses 3D scaffolds produced out of synthetic PEG NB (8-arm) microgels, which allow the independent tuning of material stiffness and pore size. Therefore, microgel-seeded chips create macroporous substrates for advanced cell cultures since they enable cells to infiltrate more efficiently and provide better nutrient and gaseous exchange. Additionally, different modes of perfusion can further support on-chip osteogenesis by simulating fluid flow of native vascularized bone tissue.

Methods:

To build the scaffold, human bone marrow-derived mesenchymal stem/stromal cells (BM-MSCs) were seeded into PDMS chips together with microgels. Different injection methods were compared by microscopic evaluation of cell distribution and viability. In addition, immunostainings and subsequent imaging were performed to detect the extracellular matrix components collagen and fibronectin. For the induction of osteogenesis, cell-seeded chips were cultured in presence of bone morphogenetic protein 2 (BMP2) for 14 days.

Results:

Successful microgel entrapment and optimal distribution of cells within the substrate has been established. Furthermore, BM-MSCs proliferation and maintenance were monitored over extended time periods (up to seven days). Additionally, cell spreading and an increase of extracellular matrix (ECM) components like collagen type I and fibronectin was shown over time. Moreover, alkaline phosphatase (ALP) staining confirmed enhanced ALP activity for BMP2 supplemented samples compared to controls.

Conclusion:

In summary, protocols for the generation of on-chip osteogenic cultures have been established. Future experiments will investigate the influence of microgel stiffness and pore size on osteodifferentiation. Finally, the established protocols will be integrated into more complex systems, specifically perfusable vascularized culture systems containing cancer cells.

D. Werner¹, W. Faigle¹, J. Ruder¹, V. Kana¹, R. Martin¹

Assessing the antioxidative and immunomodulatory capacity of hydroxytyrosol in lymphocytes

Neuroimmunology and MS Research, Neurology Clinic, University Hospital Zurich, University of Zurich, Zurich 8091, Switzerland¹

Introduction:

Autoimmune inflammation leading to demyelination and neuronal damage is the main pathomechanism in multiple sclerosis (MS). Metabolic changes in both neurons and immune cells, particularly oxidative stress-mediated processes, result in neurodegeneration and lead to clinical disability. So far, no antioxidative/neuroprotective therapy is approved in MS, and demonstrating neuroprotective efficacy in MS remains challenging. Hydroxytyrosol (HT), the major phenolic compound found in olive fruits and leaves, is one of the most potent, naturally occurring antioxidants. Due to its oral availability, rapid and active transport into the brain, and its excellent safety profile, it appears promising as a possible neuroprotective treatment in MS. While previous data point to HT inducing neuroprotective pathways in neurons, its effect on immune cells is not known. Here, we aimed to assess the immunomodulatory effect of HT by testing its capacity to reduce reactive oxygen species (ROS) levels in immune cells.

Methods:

Peripheral blood mononuclear cells (PBMCs) from healthy donors were treated for 24h with different HT compounds (synthetic pure, naturally derived purified HT), incubated with the ROS inducer tert-butyl hydroperoxide (TBHP), and analyzed by flow cytometry. ROS levels were assessed using the CellRox reagent in CD19+ B cells, CD3+ T cells CD14+ monocytes.

Results:

HT treatment reduced basic ROS production in cultured PBMCs. Upon ROS induction with TBHP, HT reduced ROS production in PBMCs in a dose dependent manner, particularly in CD19+ B cells.

Conclusion:

These findings reveal interesting effects of HT in PBMCs and important immune cells that may be beneficial in MS and other autoimmune conditions. Ongoing studies focus on elucidating HT-induced gene expression changes and effects on PBMC, in particular B cell activation, but also immune cell aging. HT-induced effects could be employed to prevent radical-mediated cell toxicity, which is at the core of many steps of tissue damage in MS.

J. Freij¹, N. Jarzebska¹, A. Reichmuth¹, M. Mellett¹, S. Pascolo¹

Synthetic mRNA platform

Department of Dermatology, University Hospital Zurich (USZ)¹

Introduction:

Synthetic messenger RNA (mRNA) molecules are the active pharmaceutical ingredient in two approved and globally used anti-COVID19 vaccines: Comirnaty from BioNTech/Pfizer and Spikevax from Moderna. In addition, synthetic mRNAs are being developed as drugs to prevent or treat cancer (vaccines and therapies) and a large panel of diseases ranging from autoimmunity, infections, degenerative and hereditary diseases. Synthetic mRNA is produced in vitro by transcription of a DNA Matrix. Inclusion of optimized necessary features (Cap and poly-A tail) can be achieved co-transcriptionally or post-transcriptionally. In addition, sequences that enhance the function of ivt mRNA including its translation or stability can be incorporated. Our goal is to continuously optimize synthetic mRNA and formulations in order to provide the scientific community with the best mRNA tools for their research. These modifications, for example, will improve the stability of mRNA formulations, an important aspect for cold chain supply. Other modifications will improve site-specific tissue expression or in the case of cancer vaccination, tumor-homing.

Methods:

We use in vitro transcription to produce synthetic mRNA containing established features (i.e. 5' cap, untranslated regions "UTRs", coding sequence) and original aspects (e.g. base modifications) that are tested in vitro in transformed (mouse and human tumor cells) and primary (murine and human immune cells) cells for mRNA expression, for example of mRNA coding luminescent or fluorescent reporter proteins. Concurrently, we test in vitro and in vivo (in mice) available RNA transfection reagents as well as formulations (polyplexes and lipoplexes) that we develop in-house in order to define the best methods to transfect different cell types or organs. In that case reporter genes (firefly luciferase) or immunogens (e.g. ovalbumin or SARS-CoV-2 Spike) are encoded by the synthetic mRNA.

Results:

In 2017, we implemented an academic mRNA-production and formulation platform at the University Hospital of Zurich (<https://www.cancer.uzh.ch/en/Research/mRNA-Platform.html>). Through this platform we have (i) optimized design, production and purification of synthetic mRNA and (ii) tested commercially available as well as homemade delivery formulations for use in vitro and in vivo. We defined the conditions to get efficient production of optimized mRNA and identified formulations that can be used for mRNA delivery in vivo in order to perform therapies or vaccination. We have the capacity to produce milligrams of optimized synthetic mRNA yearly.

Conclusion:

Through our mRNA platform, we provide researchers with optimized mRNA coding their proteins of interest as well as adequate formulations for in vitro or in vivo utilization of synthetic mRNA. This platform aims at fostering mRNA-based research, innovation and clinical developments in Zurich to improve tools for research projects and for clinical vaccines and therapeutics.

D. Müller Vizentini³, T. Haider¹, M. Cavusoglu², G. Pathare^{4,5}, I. Sudano¹, J. Loffing⁴, C. Wagner⁵, D. Schmidt¹, P. Suter³, C. Rossi²

The impact of 3 days dietary salt load on skin sodium content, intravascular volume and blood pressure in healthy men

Department of Cardiology, University Hospital Zurich¹, Department of Diagnostic and Interventional Radiology, University Hospital Zurich², Department of Internal Medicine, University Hospital Zurich³, Institute of Anatomy, University of Zurich⁴, Institute of Physiology, University of Zurich⁵

Introduction:

The maintenance of extracellular sodium balance is important for the control of extracellular fluid volume and blood pressure. Excessive dietary sodium consumption can lead to arterial hypertension. While the kidney is well known to play a central role in the maintenance of sodium homeostasis, the skin was recently proposed to be crucially involved by buffering extracellular sodium non-osmotically to negatively loaded proteoglycans. Despite the functional importance of sodium balance for the cardiovascular system, relatively little is known about the regulatory interplay between the skin and other organs to control fluid volume balance and blood pressure.

Methods:

We assessed body weight, blood pressure and sodium concentration in plasma, 24-hour urine and in the skin via sodium magnetic resonance imaging (²³Na-MRI) in 18 healthy young men, aged 21 to 44 years before and after 3 consecutive days of high dietary salt load (6 grams of salt tablets per day) on top of their usual diet in an observational within-subject study. Blood volume (BV) and BV-related parameters (plasma volume, red blood cell volume, hemoglobin mass) were measured via the optimized carbon monoxide (CO)-rebreathing (OpCO) technique. Additionally, the urinary abundance of the renal thiazide-sensitive NaCl cotransporter (NCC), plasma aldosterone and MR-proANP concentrations were assessed. The data is presented as mean changes ± SD and a two-tailed p-value < 0.05 was considered as statistical significant.

Results:

After 3 days of high dietary salt load, body weight (1.3 ± 1.6 kg, N=16, p= 0.006), skin sodium content and urinary sodium/chloride excretion were increased (Na_{skin} : 9.3 ± 2.7 mmol/l, N= 12, p< 0.001; Na_{urine} : 77.9 ± 60.9 mmol/24h, N= 16, p< 0.001, Cl_{urine} : 77.3 ± 58.4 mmol/24h, N=16, p< 0.001) while plasma sodium ($\text{Na}_{\text{plasma}}$: 0.0 ± 1.5 mmol/l, N=16, p= 1.000) and blood pressure ($\text{BP}_{\text{systemic}}$: -3.6 ± 8.8 mmHg, N= 16, p=0.125; $\text{BP}_{\text{diastolic}}$: -3.8 ± 7.1 , N= 16, p=0.580) remained unchanged. Blood volume (BV: 44.1 ± 323.1 ml, N= 14, p= 0.618), red blood cell volume (RBCV: -77.4 ± 199.3 ml, N= 14, p= 0.170) and hemoglobin mass (Hbmass: -24.0 ± 54.0 g, N= 14, p= 0.121) did not change while plasma volume (PV: 121.5 ± 200.8 ml, N= 14, p= 0.041) increased and relative hemoglobin mass decreased (Hbmass/kg: -0.53 ± 0.70 g/kg, N= 14, p= 0.014). Furthermore, plasma aldosterone levels decreased (-27.5 ± 50.4 ng/l, N=16, p=0.023) and plasma MR-proANP increased (4.9 ± 7.0 pmol/l, N=16, p=0.020). The urinary excretion of total and phosphorylated NCC was decreased suggesting a compensatory downregulation of renal sodium retention.

Conclusion:

Short-term controlled sodium load in healthy male subjects did not alter blood pressure but primarily lead to an increase in body fluid volume as indicated by an increase in body weight and plasma volume, which was accompanied by a modulation of volume-regulatory hormones and an altered interplay between the skin and the kidney to counterbalance the dietary sodium excess. A better understanding of the mobilization of non-osmotic salt storage in the skin may contribute to improved treatment of hypertension and body fluid imbalance as frequently observed in heart failure and chronic kidney disease.

H. Bischoff-Ferrari¹, S. Gängler², T. Muenzer³, B. Dawson-Hughes⁴, W. Lang², R. Theiler², A. Egli², G. Freystätter¹

Effects of transdermal testosterone and/or monthly vitamin D on fall risk in pre-frail hypogonadal men age 65 and older: a double blind 2x2 factorial design randomized placebo-controlled trial

(1) Center on Aging and Mobility, University Hospital Zurich, City Hospital Waid&Triemli and University of Zurich (2) Department of Aging Medicine and Aging Research, University Hospital Zurich and University of Zurich (3) University Clinic for Aging Medicine, City Hospital Zurich, Switzerland¹, (1) Center on Aging and Mobility, University Hospital Zurich, City Hospital Waid&Triemli and University of Zurich, Zurich, Switzerland (2) Department of Aging Medicine and Aging Research, University Hospital Zurich and University of Zurich, Zurich, Switzerland², Geriatriische Klinik, St. Gallen, Switzerland³, Jean Mayer USDA Human Nutrition Research Center on Aging, Tufts University, Boston, Massachusetts, USA⁴

Introduction:

Background: Low testosterone blood levels have been associated with an increased risk of falling in older men, however evidence from randomized controlled trials is lacking. Also, combined benefits with vitamin D supplementation are unknown.

Methods:

To test whether transdermal testosterone at a dose of 75 mg per day and/or 24'000 IU Vitamin D once per month reduce the fall risk in community dwelling men age 65 and older with low total testosterone levels (<11.30 nmol/l) and fulfilling at least 1 criteria of Fried-based frailty criteria. The primary outcomes were number of persons who fell and the rate of falls, assessed prospectively at two follow-up clinical visits (6 and 12 months) and four follow-up phone calls (2, 4, 8, and 10 months). Analyses adjusted for age, fall history, person-time and the baseline measures of BMI, 25-(OH)D, total testosterone level, and short physical performance test battery score (SPPB). As there were no significant interactions between treatments, main effects are presented.

Results:

553 of 1126 men met the pre-screening inclusion criteria, and of those only 91 men met the blood level targets to be enrolled in the trial (mean age: 72.2± 5.9 years, baseline mean total testosterone blood levels: 10.8 ±3.0 mmol/L, mean 25(OH)D concentration: 26.8±7.6 ng/ml (20.9% below 20 ng/ml)). Over 12 months, 38 participants had 74 falls. The odds of falling was not significantly influenced by testosterone versus no testosterone (OR = 0.62 (0.23, 1.68)), but participants who received monthly vitamin D versus no monthly vitamin D had a 2.6-fold increased odds of falling (OR = 2.69 (1.05, 6.89)). The rate of falls was neither influenced by testosterone (IRR = 0.62 (0.32, 1.23)), nor by vitamin D (IRR = 1.52 (0.76, 3.03)), significantly. Only men treated with testosterone and achieving the highest quartile of total testosterone levels at follow-up had a reduced rate of falls (IRR = 0.15 (0.02, 0.97)).

Conclusion:

Transdermal testosterone did not reduce the odds or the rate of falling significantly, although a benefit among those achieving the highest testosterone blood levels cannot be excluded. Conversely, monthly vitamin D increased the odds of falling independent of testosterone supplementation.

N. Schwendinger², B. Thomson², H. Richter¹, J. Fierstra², M. Hugelshofer²

Near-Infrared Spectroscopy Based Bedside Monitoring for Cerebrovascular Disease

Clinic for Diagnostic Imaging, Departement of Clinical Diagnostics and Services, Vetsuisse Faculty, University of Zurich,¹, Departement of Neurosurgery, University Hospital Zurich²

Introduction:

Cerebral blood flow (CBF) is a parameter that is strictly regulated to maintain a steady supply of oxygen and nutrients to the brain. Cerebrovascular reactivity (CVR) describes the capacity of a vessel to dilate or constrict in response to a vasoactive stimulus. It is an indicator for cerebrovascular reserve and is used as a marker of cerebrovascular health.

Near-Infrared Spectroscopy-CVR

Near-Infrared Spectroscopy (NIRS) is a technique, that is based upon light absorption in tissue. As opposed to visible light, tissue and bone are almost transparent in the near-infrared spectrum (700-1100nm). This allows near-infrared light to penetrate several centimeters under the skin. The primary light-absorbing molecules in the near-infrared spectrum in tissue are metal complex chromophores like hemoglobin. Deoxyhemoglobin and oxyhemoglobin are known to have different absorption spectra. Thus, they can be distinguished using NIRS. A change in CBF is represented by the washout of deoxyhemoglobin (DHbO), caused by inflow of oxygenated Hemoglobin (HbO). Cerebrovascular reactivity can be measured by applying a vasoactive stimulus and measuring the consecutive increase in cerebral blood flow per magnitude of the vasoactive stimulus. The most established stimulus is a standardized hypercapnic (CO₂) challenge.

Methods:

To validate the concept of measuring cerebrovascular reactivity with Near-Infrared Spectroscopy our group established a sheep model. The idea was to compare BOLD MRI measurements of cerebrovascular reactivity with NIRS measurements. The sheep were put under general anesthesia and intubated. A hypercapnic challenge was used as a vasoactive stimulus. After an initial 120 seconds baseline, PetCO₂ was increased by 15mmHg for 240 seconds. Sequential BOLD MRI scans or NIRS Measurements were performed to measure cerebrovascular reactivity.

Results:

This study showed that Near-Infrared Spectroscopy is able to measure changes in CVR, similar to CVR changes measured with BOLD MRI. Figure 1 shows the NIRS signal response in comparison to the BOLD signal response. The application of a vasoactive stimulus led to an increase in cerebral blood flow and changes the ratio of DHbO and HbO.

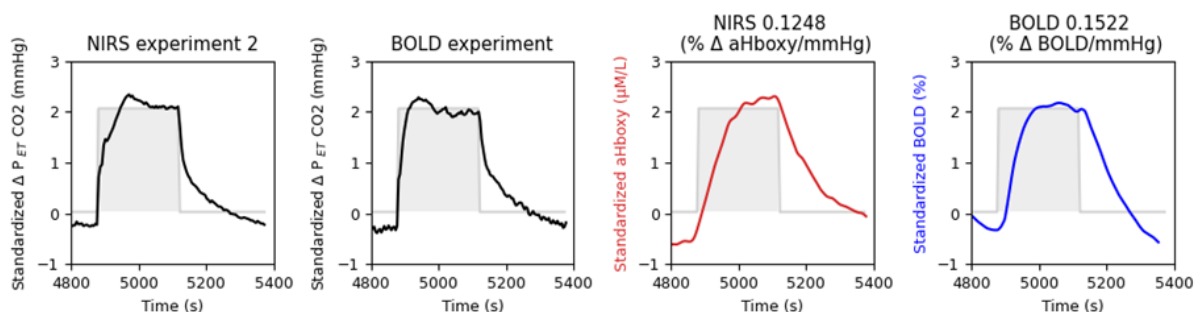


Figure 1: NIRS response compared to BOLD response. From left to right: standardized CO₂ pulse before NIRS experiment standardized CO₂ pulse during the BOLD experiment, standardized NIRS response, and the standardized BOLD response. Titles of the two most right figures present the calculated CVR values. Curves have been standardized to give an impression of the signal without comparing absolute values.

Conclusion:

Although NIRS and NIRS-CVR have been mentioned repeatedly in the literature, they have failed to be implemented as a diagnostic tool in clinical practice. NIRS CVR measurements would allow for prolonged bedside monitoring, potentially including critically ill patients on the intensive care unit, and thereby reduce the need to transport critically ill neurosurgical patients to the radiology department. Further, it would allow continuous measurement of CBF during neurosurgical procedures. We envision NIRS with the application CVR measurements as a comprehensive tool to measure cerebral blood flow at the bedside.

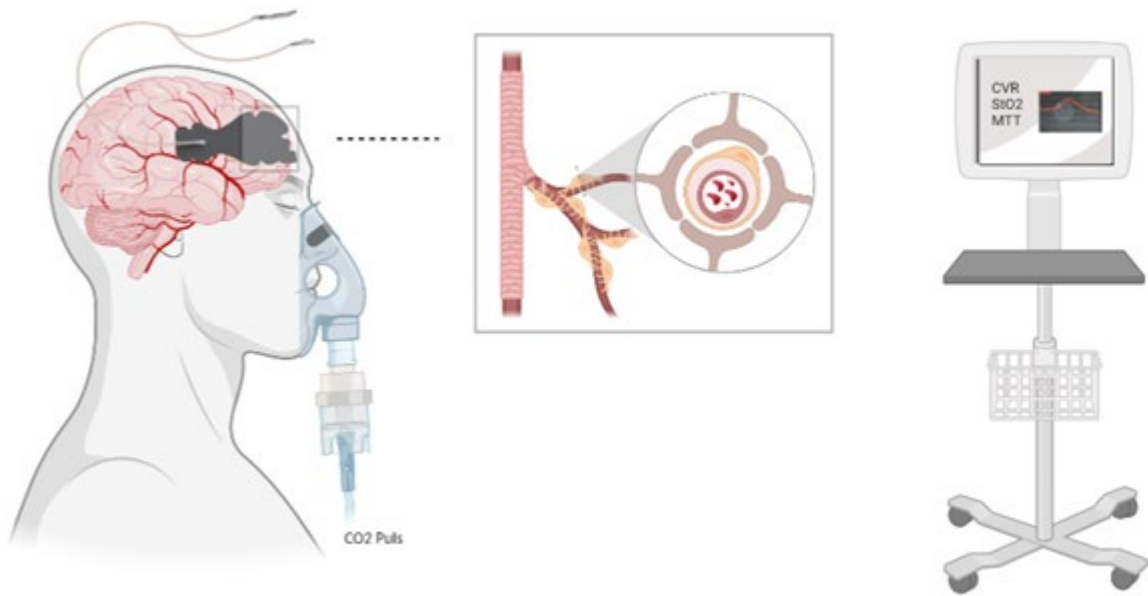


Figure 2: It depicts the non-invasive NIRS measurement with a Patch (Luciole Medical) as well as the hypercapnic stimulus to induce alterations in cerebral blood flow as we envision for our non-invasive bedside monitoring.

M. Paolucci¹, V. Homère¹, N. Wuillemin², D. Bieli², Y. Wäckerle-Men¹, T. Kündig¹, N. Pengo², T. Sonati², A. Barberis², P. Johansen¹

Pre-clinical evaluation of fully human anti-peanut monoclonal antibodies: protection against anaphylaxis in mice

Department of Dermatology, University of Zurich and University Hospital Zurich, Zurich, Switzerland¹, Mabylon AG, Schlieren, Switzerland²

Introduction:

Peanut (PN) allergy with anaphylaxis is a type I hypersensitivity immune reaction mediated by the binding of PN allergens to IgE-FcεRI complexes on the surface of mast cells and basophils and the cellular degranulation of these cells. We are currently seeking to gain better insight into a passive allergy immunotherapy (AIT) based on PN-specific monoclonal anti-PN antibodies (mAbs). The allergen-specific mAbs can compete for the binding of the peanut allergen to IgE and could have a potential role in binding the Fcγ receptors (FcγR) on the surface of the effector cells.

Methods:

Human anti-PN mAbs were developed by screening sera from PN allergic patients for PN-specific IgG. B cells were selected and mAbs recombinantly cloned. C3H mice were sensitized by intraperitoneal (i.p.) injections of low-dose PN allergens and aluminium hydroxide consecutively for four weeks. Prior to testing the mAbs *in vivo*, competition ELISA was performed to evaluate the potential of different combination of anti-PN IgG1 mAbs to compete with allergen-specific IgE from PN-sensitized C3H mice. To test human anti-PN mAbs efficacy *in vivo*, sensitized mice were treated by intravenous injection of human IgG1, IgG4 or Fcγ mutated mAbs. Finally, the mice were challenged with a high PN dose (i.p), which induces hypothermia in allergic mice. The body temperature as well as clinical signs were monitored as a measure for anaphylaxis.

Results:

After *in vitro* assessment of mAbs combination efficacy by competition ELISA, passive immunotherapy of PN-sensitized mice with anti-PN IgG1 or IgG4 mAbs was associated with a significant reduction or an absence of anaphylactic reactions after PN-challenge. The prevention of anaphylaxis was dose-dependent with IgG4 being slightly more effective than IgG1. Despite the species mismatch, therapeutic effect could also be observed two weeks post immunotherapy. To test if part of the immunotherapeutic effect was mediated by inhibitory FcγR signalling, allergic mice were treated with mutated mAbs unable to bind Fcγ receptors on mast cells or basophils; especially IgG4 is known to have higher affinity to FcγRs that induce tolerance signals. Interestingly, the Fcγ mutated mAbs also prevented PN-specific anaphylaxis in mice dose-dependently and was not inferior to Fcγ-binding anti-PN mAbs.

Conclusion:

Applying a PN allergy mouse model that we developed for evaluation of therapeutic candidates, we could show that anti-PN antibodies cloned from PN-allergic individuals can prevent allergic anaphylaxis in mice. The therapeutic effect in mice is likely based on allergen neutralisation and independent of the potentially inhibitory Fcγ receptor signalling and is dose-dependent. Passive allergy immunotherapy may represent a promising treatment option of PN-allergic patients.

J. Tschumi^{4, 9}, L. Jörimann^{4, 9}, A. Ciuffi⁸, J. Fellay^{2, 8}, M. Battegay⁵, E. Bernasconi³, A. Calmy⁷, M. Cavassini⁸, A. Rauch⁶, S. Kuster¹, T. Klimkait⁵, RD. Kouyos^{4, 9}, H. Günthard^{4, 9}, K. Metzner^{4, 9}, . SHCS⁴

No Evidence of Low-Level Replication in 40 HIV-1 Infected Individuals on Suppressive Antiretroviral Therapy

Cantonal Hospital of St. Gallen¹, EPFL², Regional Hospital Lugano³, University Hospital Zurich, Division of Infectious Diseases and Hospital Epidemiology⁴, University of Basel⁵, University of Bern⁶, University of Geneva⁷, University of Lausanne⁸, University of Zurich, Institute of Medical Virology⁹

Introduction:

Infection with human immunodeficiency virus type 1 (HIV-1) leads to the integration of the viral genome into the host genome and establishes a latent reservoir that cannot be eradicated by antiretroviral therapy (ART) and is the major obstacle for HIV cure. In our study that enrolled over 1'000 HIV-1 infected individuals from the Swiss HIV Cohort Study, the HIV-1 reservoir was found to be decaying on a population level, but increasing in >25% of individuals over a time period of ~5.4 years after initiation of ART. The mechanisms for the stability and persistence of the HIV-1 reservoir in individuals receiving suppressive ART are debated, with low-level replication and clonal expansion of latently infected cells being the two most commonly discussed mechanisms. Additionally, the role of intermittent viremia in the maintenance of the HIV-1 reservoir remains unclear. In this study, ongoing low-level replication was investigated as a potential driving force for the HIV-1 reservoir stability. If low-level replication was responsible for the stability of the HIV-1 reservoir, we would expect increases in genetic distances and genetic diversity of proviruses, especially in those individuals showing an increase of the HIV-1 reservoir in the presence of intermittent viremia.

Methods:

We characterized the HIV-1 reservoir in four different groups of HIV-1 infected individuals, presenting either an increase or a decrease of the HIV-1 reservoir and experiencing or not experiencing episodes of intermittent viremia over a time period of >10 years on suppressive ART. In total, 40 individuals were included, 10 per group, and four longitudinal PBMC samples were collected for each individual. Sequence analysis of near full-length HIV-1 proviruses in those samples were performed as follows: An average pairwise diversity score was calculated as measure for genetic diversity of proviruses, phylogenetic analysis was performed on consensus sequences, and the presence of drug resistance mutations was investigated.

Results:

Genetic distances of individuals' consensus sequences did not increase over time in any of the four groups. Similarly, we found that the proviral sequence diversity did not increase in any group over time, neither in full-length sequences nor in pol. However, average pairwise diversity was found to be significantly higher in individuals experiencing episodes of intermittent viremia. The total gain of drug resistant mutations in proviruses over time was not significantly different among the four groups.

Conclusion:

Our results show no evidence of evolution, i.e., no ongoing low-level replication, in any group of HIV-1 infected individuals and suggest that another mechanism, e.g., clonal expansion, must be mainly responsible for the persistence of the HIV-1 reservoir in individuals receiving suppressive ART, largely independent of episodes of intermittent viremia.

L. Jörimann^{2,4}, J. Tschumi^{2,4}, C. Leemann², C. Schenkel¹, S. Chaudron³, M. Zeeb^{2,4}, K. Neumann², H. Kuster², D. Braun², C. Grube², R. Kouyos^{2,4}, K. Metzner^{2,4}, H. Günthard^{2,4}, SHCS²

Absence of HIV-1 Evolution in early treated patients switching to DTG monotherapy for 48 weeks

Roche Zurich¹, University Hospital Zurich, Infectious Diseases², University of Oxford³, University Zurich⁴

Introduction:

We have recently shown in a randomized trial (CID, 2019;69(9):1489–97) that simplification to Dolutegravir monotherapy was non-inferior to continued combination antiretroviral therapy (ART) in patients who started treatment during primary HIV-1 Infection. Here, in a subset of patients, we investigated whether differences in HIV-1 evolution, as indirect measure of undetected, low-level HIV-1 replication, between the two study arms could be observed.

Methods:

The early simplified study (ES) is a randomized trial within the Zurich Primary HIV Infection Study (ZPHI), where 101 early treated and suppressed patients were assigned 2:1 to either Dolutegravir monotherapy or continued triple therapy (NCT02551523). In general, early treated patients show lower reservoir diversity, facilitating assessment of viral evolution as a marker for low-level replication. Near full-length HIV-1 proviral PCR and next generation sequencing were established and applied to longitudinal patients' PBMC samples one year after ART start, and at weeks 0 and 48 of ES. Differences in reservoir persistence between the two treatment groups was assessed through HIV-1 proviral sequence analysis along with phylogenetic analysis. Average pairwise diversity score of each sequence was calculated based on ambiguous nucleotides as a measure for diversity of the sequence. Additionally, total number of INSTI drug resistance mutations per sample were compared between the two treatment groups. Furthermore, quantification of intracellular HIV-1 RNA forms by qPCR was performed.

Results:

All patients had undetectable viral load (<50 copies/ml) and in general low levels of HIV proviral DNA during the whole study period (CID,2019:69(9):1489-97). Nevertheless, near full-length sequencing followed by stringent quality control for time points (all three timepoints needed to be available) and sequence completeness (near full length) was successful for 34 (15 monotherapy, 19 triple therapy) out of 101 patients. Mean genetic distance of the patients' HIV-1 proviral sequences measured from week 0 to week 48 was not significantly different with 0.0527 substitution/nt in the monotherapy (n=15) and 0.0323 in the triple therapy group (n=19) (p=0.46). Mean average pairwise diversity within the sequences did not change significantly over 48 weeks from 0.005 to 0.002 in the monotherapy and from 0.004 to 0.003 in the triple therapy group (p=0.632). No new major drug resistance mutation appeared in the integrase gene in the monotherapy group. Additionally, no intracellular viral RNA was detected in qPCR assays with a detection limit of 12 copies/106 GAPDH copies.

Conclusion:

Longitudinal sequence analysis of 15 patients from the monotherapy group showed no signs of HIV-1 evolution over 48 weeks. In addition, no difference between the monotherapy and the triple therapy group was found regarding viral diversity, genetic distances or intracellular viral RNA. In conclusion, no discernable viral evolution through potential low-level replication was found in this group of early treated patients with two different treatment regimens over 48 weeks.

S. Saeedi Saravi^{1,2}, G. Karsai³, P. Lee^{1,2}, J. Beer^{1,2}

Acetate reverses the gut microbiota metabolite phenylacetyl glutamine (PAG)-induced endothelial senescence by epigenetic and SASP modulation

Center for Molecular Cardiology, University of Zurich, 8952 Schlieren, Switzerland¹, Department of Internal Medicine, Cantonal Hospital Baden, 5404 Baden, Switzerland², Institute of Clinical Chemistry, University Hospital Zurich, 8952 Schlieren, Switzerland³

Introduction:

The gut microbiota metabolite PAG is clinically linked to CAD and arterial thrombosis. Yet, very little is known about the role and mechanisms of PAG in vascular cells. We sought to investigate 1) effects of PAG on metabolic/epigenetic state and senescence-associated secretory phenotype (SASP) in ECs; 2) reversal effects of acetate on PAG-induced endothelial senescence and dysfunction.

Methods:

We examined the effects of PAG (100 μ M; according to our preliminary studies) with or without acetate (3 μ M) on cellular senescence (via SA- β -galactosidase staining) and function (via ex vivo and in vitro angiogenesis and migration assays), and epigenetic and SASP characterization in proliferating human aortic EC (PEC; passage 5) and aortas from young mice.

Results:

We found that PAG increases mitochondrial ROS production accompanied by downregulated isocitrate dehydrogenase-2 (Idh2), a marker of mitochondrial function. PAG-treated cells revealed a significant reduction in angiogenesis and cell migration accompanied by decreased phosphorylation of eNOSS1177 and AMPKT172 and activation of acetyl-coA carboxylase (ACC) that leads to the loss of acetyl-coA, leading to decreased histone 3 (H3) acetylation ($p < 0.001$, $n = 6$). Importantly, PAG significantly induced senescence, as represented by increased SA- β -gal-positive cells ($p < 0.01$), and upregulated SASP (TNF- α and VCAM-1; $p < 0.001$). Conversely, acetate intriguingly increased phosphorylation of AMPKT172 and eNOSS1177 and H3 acetylation accompanied by reduced SA- β -gal-positive cells, downregulated SASP, and improved mitochondrial function. Additionally, acetate restored angiogenesis and migration in PAG-treated aortic rings and endothelial cells to the magnitude seen in young aortas or PEC.

Conclusion:

We conclude that PAG causes endothelial dysfunction via metabolic/epigenetic and SASP modulation and that acetate represents new possibilities for rejuvenating senescent ECs and preventing aging-related CVD.

Y. Trinh^{1,3}, S. Frank², E. Schlumpf¹, J. Robert¹, A. von Eckardstein^{1,3}

Endothelial lipase and its endogenous inhibitor Angiopoietin-like protein 3 regulate binding and uptake of both low and high-density lipoproteins by aortic endothelial cells

University Hospital of Zurich¹, University of Graz², University of Zurich³

Introduction:

Atherosclerosis is characterized by the accumulation of low-density lipoprotein (LDL) in the arterial wall, a process requiring LDL to pass the endothelial barrier. Likewise, the removal of cholesterol from atherosclerotic lesions by high-density lipoproteins (HDL) even requires two passages through endothelial cells to enter and leave the arterial wall. Several studies suggest that trans-endothelium transit of lipoproteins is an active process regulated by proteins that limit the binding to, the internalization by and the transport through endothelial cells (EC). Endothelial lipase (EL), a phospholipase expressed by EC, binds to LDL in circulation and regulates LDL plasma level. While EL is known to regulate trans-endothelial transport of HDL, its role in LDL trans-endothelial transport remains unknown. Angiopoietin-like protein 3 (ANGPTL3) is a natural inhibitor of EL and its pharmacological inhibition is under clinical investigation with the aim to reduce plasma LDL levels in patients suffering of homozygous familial hypercholesterolemia. However if EL promotes transport of HDL and LDL through EC, disinhibition of ANGPTL3 and the subsequent increase in EL activity might determine the risk of atherosclerosis beyond their plasma levels.

Methods:

Here we transfected human primary aortic EC (hAEC) with either siRNA against EL or adenoviruses encoding for catalytically active or inactive EL. We measured binding (4°C) and cell association (37°C) of ¹²⁵I-LDL and ¹²⁵I-HDL. Finally, we investigated whether inhibition of EL by drugs or ANGPTL3 reduces the cell association of radioiodinated lipoproteins.

Results:

After RNA interference against EL, binding and association of LDL were significantly reduced by 21% and 30%, respectively, compared to 36% and 27%, respectively for HDL. Conversely, binding and association of LDL were increased after overexpression of catalytically active EL by 175% and 294%, respectively, as well as inactive EL by 185% and 214%, respectively. Pharmacological inhibition of EL using orlistat or XEN445 also reduced cell association of LDL by 50% and 19%, respectively. Finally, addition of ANGPTL3 to EL-overexpressing cells reduced cell association of LDL to a similar degree as the EL-specific inhibitor XEN445.

Conclusion:

Together our results demonstrate that EL and its endogenous inhibitor ANGPTL3 regulate binding and cell association of both HDL and LDL. Further research has to unravel the implications of ANGPTL3 inhibition for transendothelial transport of lipoproteins, the deposition and removal of cholesterol in the vascular wall, and ultimately atherosclerosis.

A. Kraft^{1,2}, M. Meerang², M. Kirschner², V. Boeva^{1,3,4}, I. Opitz²

Screening for extracellular vesicle-derived biomarkers for early detection of malignant pleural mesothelioma

Computational Genetics and Epigenetics of Cancer Group, Department of Computer Science, Institute for Machine Learning, ETH Zurich, Zurich, Switzerland¹, Department of Thoracic Surgery, University Hospital Zurich, Zurich, Switzerland², INSERM, U1016, Cochin Institute, CNRS UMR8104, Paris Descartes University, Paris, France³, Swiss Institute of Bioinformatics (SIB), Zurich, Switzerland⁴

Introduction:

Malignant pleural mesothelioma (MPM) is an aggressive cancer of the mesothelial layer of pleura. Environmental and occupational exposure to asbestos is considered the main cause of MPM so far, but recent studies suggest exposure to carbon nanotubes, erionite fibers and therapeutic ionizing radiation may also be risk factors. The number of MPM cases worldwide is rising and is expected to peak between 2020-2025. Most cases are detected at a late stage and have very poor survival (6-12 months). Late diagnosis is a consequence of a long latency period (average 44 years) and non-specific symptoms. Imaging scans are insufficient for diagnosis and invasive tissue biopsies are not suitable for all patients. The standard treatment based on pemetrexed and cisplatin is relatively ineffective at increasing patients' survival. Early detection of the disease would likely increase treatment options and improve clinical outcomes. MiRNAs and RNAs encapsulated in extracellular vesicles have been shown to be relatively stable in the circulation, therefore can serve as potential blood-based diagnostic biomarkers. Our project is aimed at the identification of extracellular vesicle-derived biomarkers that could be used in blood-based diagnostic tests for early detection of MPM.

Methods:

We established primary cell cultures from pleural effusion of 4 MPM and 3 non-MPM patients. Extracellular vesicles from cell culture supernatants were extracted using Qiagen Exoeasy Maxi kit. RNA was extracted using the mirVana PARIS kit followed by transcriptome and small RNA sequencing. Small RNA and transcriptomic data was processed using exceRpt and Trimmomatic, respectively. Reads were mapped on the GRCh38 reference genome and gene counts were calculated using exceRpt and Kallisto. Transcriptomic counts were normalized using TMM normalization from edgeR and small RNA counts were normalized using rlog transformation from DESeq2. Differential gene expression analysis was performed on both datasets using edgeR and DESeq2. Genes with FDR <0.05 and log₂ fold change >1 were selected as candidate MPM-biomarkers, which were then compared with TCGA MPM and ExoRBase data.

Results:

We identified 32 genes upregulated in MPM compared to non-MPM samples, including 16 protein coding genes, 10 lncRNAs and 3 miRNAs. All of the candidate biomarkers have been previously detected in exosomes from normal samples and breast, colorectal and pancreatic cancers. lncRNAs SCARNA10, SNHG17 and SNHG20 were already linked with higher exosomal expression in these cancers. SNHG15 was previously linked with worse overall survival in mesothelioma, while SNHG17 was associated with cell cycle progression and proliferation in a pan cancer study. SCARNA10, SNHG15, MAGEA3, MAGEA1, TAF1D, EIF4A2 and SNGH20 were upregulated in some of the MPM samples in the TCGA cohort. Our miRNA-biomarker candidate, hsa-miR-3648, was previously shown to be overexpressed in MPM. Moreover, we identified hsa-miR-30a-5p to be upregulated in MPM. Previous studies have reported miR-30 family to be one of the most enriched miRNA families in mesothelioma, with miR-30e-5p significantly associated with poorest survival.

Conclusion:

We identified extracellular vesicle-derived candidate biomarkers for MPM using primary cell cultures. More primary cells will be subjected to screening in the next months. We will further evaluate the level of candidate biomarkers using qPCR applied to matched plasma and tissue samples of already profiled samples. In further steps, we will validate our findings using additional patients' plasma samples.

A. Joachimbauer², C. Gil-Cruz², K. Frischmann², R. Büchel³, D. Schmidt¹, F. Ruschitzka¹, B. Ludewig²

Investigating the immunologic pathways involved in the progression of acute myocarditis to inflammatory cardiomyopathy

Cardiology, University Hospital Zurich¹, Cardiology, University Hospital Zurich / Immunology, Kantonsspital St. Gallen², Nuclear Medicine³

Introduction:

Inflammatory cardiomyopathy is the most common cause of non-ischemic heart failure and is the long-term consequence of non-recovered myocarditis. In the majority of patients, acute myocarditis resolves entirely, but approximately 30% of individuals do not fully recover and progress to inflammatory cardiomyopathy. The persistent immune activation of the myocardium is fostering adverse cardiac remodelling and left ventricular dysfunction, which cause cardiomyopathy and finally heart failure. The main driver for the progression of acute to chronic myocardial inflammation are cardiac-specific autoimmune responses against the protein myosin heavy chain 6 (MYH6). However, the underlying immunologic mechanisms responsible for the induction of autoimmune responses against myocardial proteins remained elusive for a long time. Recently, our group has shown in a preclinical model that the progression of myocarditis depends on autoimmune CD4⁺ T cells cross-reacting with bacteria in the intestinal microbiome. Hence, it is plausible that similar mechanisms are involved in myocardial inflammatory processes in patients suffering from acute myocarditis and inflammatory cardiomyopathy. Therefore, we further investigate the association of cardiac-reactive CD4⁺ and microbiota-reactive CD4⁺ T cells during the development of acute and chronic myocardial inflammation in a translational study.

Methods:

Establishment of a prospective study including patients with acute myocarditis and inflammatory cardiomyopathy. Analysis of the immunologic landscape by using high-dimensional flow cytometry, ELISA or commercial assays. Determination of the microbiota composition using 16S rRNA gene sequencing. Integrative analysis of clinical data including cardiac imaging with high-dimensional immunologic analysis will be performed.

Results:

This study was approved by the ethics commission of the Canton Zurich and we recently started the recruitment of the study cohorts.

Conclusion:

The ImmpathCarditis study will provide a deeper insight in the underlying immunologic mechanisms involved in the development and progression of myocarditis. This project is expected to identify myosin-specific cross-reactive CD4⁺ T cells as one of the immunologic key mechanisms involved in the progression of acute myocarditis to inflammatory cardiomyopathy in humans. In particular, we expect that myocarditis patients expressing the same HLA DQ/B1*03 haplotype and sharing a specific microbial composition will present with higher levels of cross-reactive T cells and antibodies sensitive for microbial and cardiac antigens.

Targeting Mitochondria: A Link between Prostate Cancer Metabolism and Novel Therapeutic Approaches*Departement of Urology¹***Introduction:**

In castration resistance, prostate cancer (PCa) cells rewire their metabolism to meet new anabolic needs. The increased bioenergetic demands require a large amount of energy (ATP), which is mainly produced from mitochondrial oxidative phosphorylation (OXPHOS) and glycolysis. Mitochondria play a central role in energy metabolism and tumorigenesis in PCa cells. Mitophagy is an important mitochondrial quality control system that selectively degrades excessive or damaged mitochondria by autophagic processes. Therefore, our goal is to investigate changes in metabolic pathways in different PCa cells. Furthermore, we aim to manipulate mitophagy in order to increase cancer cell death and drug sensitivity.

Methods:

Human PCa cell lines PNT1A, LNCaP and PC-3 were cultured in androgen-deprived medium. Cells were treated with mitophagy inhibitor Mdivi-1 (20-50 μ M). Cell proliferation was assessed by WST-1 assay after 1, 4 and 7 days. Mitochondrial membrane potential (MMP) and reactive oxygen species (ROS) was measured. Mdivi-1 treated PCa were assessed for mitochondrial respiration and substrate utilisation by extracellular flux Seahorse assay and colorimetric Mitoplate assay.

Results:

Cell proliferation was significantly decreased in LNCaP after 4 days of treatment with 20 μ M Mdivi-1 (54.65 ± 4.580 SEM, $P=0.0003$) compared to vehicle control (100%). Active mitochondrial fission protein DRP1 was significantly reduced in all cell lines upon Mdivi-1 treatment. Extracellular flux analysis revealed higher oxygen consumption rate (OCR) in LNCaP cells compared to benign PNT1A and androgen-independent PC-3. Mdivi-1 treated LNCaP exhibited significantly reduced basal OCR (-0.9900 ± 0.2972 SEM, $P=0.0291$) but had no significant impact on PNT1A and PC3 cells. Extracellular acidification rate (ECAR) was elevated in PC-3 cells only, indicating a glycolytic phenotype. Mitoplate assay showed reduced substrate utilisation of tricarboxylic acid cycle intermediates such as pyruvate, succinate and fumarate upon inhibition of mitochondrial fission in all PCa cells most prominently in LNCaP cells. Treatment with 50 μ M Mdivi-1 for 24 h significantly increased ROS production in LNCaP (2.823 ± 0.6151 , fold change, SEM $P=0.0101$), compared to control. No significant ROS production was observed in PNT1A and PC-3 cells. Furthermore, MMP was significantly decreased in LNCaP compared to untreated control, indicating mitochondrial dysfunction.

Conclusion:

Here we show that during tumorigenesis prostate cancer cells change their metabolic pathway towards OXPHOS in androgen-sensitive cells but not in androgen-independent PC-3 cells. Our data demonstrates that this metabolic reprogramming can be exploited by blocking mitophagy, which reduces OXPHOS and has a strong antitumor effect.

I. Krizanovic-Grgic^{1,2}, S. Anwer², C. Spengler¹, A. Breitenstein², F. Tanner²

3D Atrial Strain for Prediction of Atrial Fibrillation Recurrence

ETH Zurich¹, University Hospital Zurich²

Introduction:

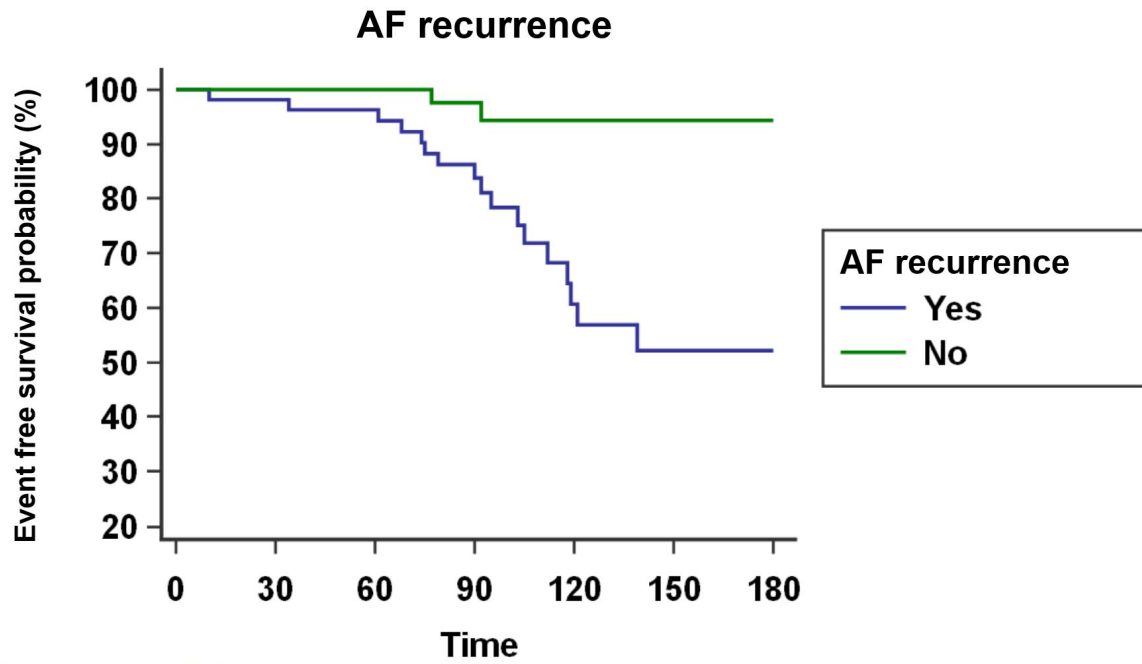
Atrial fibrillation (AF) is one of the most common arrhythmias worldwide. Treatment options apart from medication include pulmonary vein isolation (PVI). There are yet insufficient parameters for outcome prediction of this intervention.

Methods:

127 AF patients were prospectively recruited from December 2018 until October 2021. All patients underwent a pre-procedural echocardiography with acquisition of 3D volumes for left atrial (LA) 3-dimensional strain (LAS) using Canon Aplio i900 followed by radiofrequency ablation including a 3-dimensional electro-anatomical voltage mapping (EAVM) (CARTO3). Low voltage corresponding to scar areas (local amplitude <0.5 mV) was measured with the measurement tool of the CARTO3 system. Patients were followed-up until January 2021. The primary endpoint of the study was early recurrence of AF within first year.

Results:

During follow-up, 22 out of 113 patients (19.5%, AF-Group) experienced recurrence of AF. No differences were found in baseline characteristics between the AF-Group and the Non-AF-Group. However, in the AF-Group, LAS was significantly impaired (median -3.7, IQR [-5.5 to -3.2]) when compared to the Non-AF-Group (-6.7 [-10.1 to -1.6], $p=0.021$), while LA EAVM-% ($p=0.687$) as well as EAVM-area ($p=0.800$) did not differ between the two groups. No significant correlations were found between LAS and EAVM parameters (EAVM-%: $r=0.1$, $p=0.200$; EAVM-area: $r=0.1$, $p=0.276$). A cut-off of -6.12% for LAS showed good sensitivity and reasonable specificity (ROC: sens. 91%, spec. 55%, AUC=0.7, $p=0.002$) to differentiate between the groups. Kaplan-Meier analysis (Figure) based on this LAS cut-off showed a significant difference in event-free survival between the AF-Group and the Non-AF-Group ($p=0.004$). LAS was associated with an increased risk of early AF recurrence (HR 1.12, IQR [1.01-1.24], $p=0.025$), while EAVM parameters were not (EAVM-%: $p=0.494$; EAVM-area: $p=0.742$).



Number at risk

Group: Yes

54 53 48 32 16 9 5

Group: No

47 46 45 30 15 9 5

Conclusion:

3-dimensional LAS was associated with early recurrence of AF after PVI, while EAVM-% and EAVM-area were not.

M. Mirrahimi¹, K. Klein¹, M. Houtman¹, M. Frank-Bertoncelj¹, M. Macukiewicz¹, O. Distler¹, C. Ospelt¹

Homeobox D transcription factors shape differential joint environment between anterior finger joints and thumb

Center of Experimental Rheumatology, Department of Rheumatology, University Hospital Zurich, University of Zurich, Zurich, Switzerland¹

Introduction:

The expression of embryonic Homeobox (HOX) genes is tightly regulated based on anatomic location in human adult dermal and synovial fibroblasts. Previously, we showed that HOX-D10,-D11 and -D13 are higher expressed in synovial fibroblasts from small distal joints from the hands and feet, in particular in digits II-V and wrists compared to thumb and that this expression pattern is epigenetically imprinted¹. The consequences of the tightly restricted expression of these transcription factors are largely unknown.

Methods:

Synovial tissues were isolated from paws of naïve C57BL/6 mice (n=8), from patients with rheumatoid arthritis (RA), osteoarthritis (OA) and from healthy controls. Synovial fibroblasts were cultured and transfected with GapmeR to silence HOXD10, -D11, and -D13, respectively or with control GapmeR. RNA sequencing was performed on the NovaSeq platform and pathway analysis was done using R packages and web-based tools (GSEA, EnrichR, Cytoscape). HOXD target gene expression was measured by qPCR (n=3-6).

Results:

To confirm and further analyze the distinctive expression pattern of HOXD genes, we measured their expression in healthy synovial tissues of different joints of human feet and mouse paws. Similar to what we had found in hands, HOXD10, -D11 and -D13 were less abundant in the joints of the first digit of human feet compared to digits II-V (n=3-4 in each joint). Measurements in joints of mouse paws showed lower expression of HoxD10, -D11 and -D13 in distal interphalangeal joints compared to proximal interphalangeal joints and metacarpophalangeal (MCP) joints, respectively. Silencing of HOXD10, -D11 and -D13, affected the expression of 5333, 2217 and 7347 genes, respectively, in cultured RA synovial fibroblasts from human wrists (n=3). There were more transcripts equally regulated by HOXD10 and -D13 (40% of all HOXD10 and 31% of all HOXD13 regulated transcripts), than by HOXD11 and either -D10 or -D13 (18% of all HOXD10 regulated genes and 16% of all HOXD13 regulated genes), suggesting most redundancy between HOXD10 and -D13 (Fig.1). Among genes differentially expressed in SF isolated from MCP II-V versus thumb joints, 19%, 4% and 33% were regulated by HOXD10, -D11 or -D13, respectively, supporting a role for HOXD13 in particular in shaping the joint specific environment. All three HOXD transcription factors regulated genes involved in cell cycle progression, demonstrating dependence of synovial fibroblasts on these HOX genes for cell division. Other enriched pathways were primary cilia assembly, integrin-signaling pathways, regulation of unsaturated fatty acid synthesis and extra-cellular matrix protein organization.

Conclusion:

The expression of HOXD10, -D11 and -D13 in synovial fibroblasts and tissues strikingly overlaps with predilection sites for RA. Silencing experiments suggested that these embryonic HOX transcription factors have a crucial role in regulating fibroblast functions and might shape a joint specific environment that modulates the development and course of RA in specific joints.

F. Haslbeck¹, L. Schmidli¹, M. Adams¹, H. Bucher¹, D. Bassler¹, G. Natalucci¹

Creative music therapy and long-term neurodevelopmental outcomes in preterm infants at age two and five years: Results of a controlled, feasibility trial

Newborn Research Zurich, Department of Neonatology¹

Introduction:

The primary goal of Creative Music Therapy (CMT) is to relax, stabilize, stimulate, and support preterm infants and their parents by providing nurturing infant-directed singing accompanied with the monochord, e.g., during kangaroo-care. We aimed to test feasibility in preparation for a randomized controlled trial and explore whether CMT would harm long-term neurodevelopment in extremely preterm infants (EPTs).

Methods:

We conducted a controlled, prospective, longitudinal, feasibility trial to test the impact of CMT on neurodevelopmental outcome in EPTs born < 29 weeks' gestation at two and five years of age. Of 47 EPTs born at the University Hospital Zurich in 2013-2014, 13 consecutively recruited EPTs received CMT 2-3 times per week by a specially trained music therapist. The remaining 34 EPTs received the standard treatment of the neonatal intensive care unit. Neonatal data was extracted from the national database of the Swiss Neonatal Network. Socio-demographic data and perinatal complications were analyzed and compared between groups as risk factors. These neurodevelopmental risk factors entail socio-economic status (SES), gestational age, birth weight, male gender, intraventricular hemorrhage, leukomalacia, ventricular dilatation, sepsis, bronchopulmonary dysplasia, retinopathy of prematurity, chorioamnionitis and intubation. Following neurodevelopmental outcomes were analyzed using Mann-Whitney U tests: cognitive, language, and motor indices of the Bayley Scales of Infant and Toddler Development, 3rd edition at the 2-year follow-up (FU2) and KABC-II - Kaufman Assessment Battery for Children at the 5-year follow-up (FU5).

Results:

Among the 47 participants, 39 (83%) EPT were examined at two (FU2) and 29 (62%) at five years (FU5) of age, respectively. The rate of neurodevelopmental risk factors at birth between the two groups were similar or higher in the CMT group, except for a higher prevalence of ventricular dilatation and intraventricular hemorrhage in the standard treatment group. While there was no difference in the FU2 measures between the two groups, the Fluid-Crystallized Index of the KABC-II was significantly higher in the CMT than the standard treatment group ($p < 0.05$).

Conclusion:

In this sample, while CMT was associated with better cognitive outcomes at five years of age and no treatment harm, the present findings must be interpreted with caution due to the small sample size and the non-randomized design of this study. Long-term neurocognitive follow-up trials with larger controlled randomized cohorts receiving CMT are recommended.

H. Gabrys³, L. Basler³, S. Burgermeister³, S. Hogan¹, M. Ahmadsei³, M. Pavic³, M. Bogowicz³, D. Vuong³, S. Tanadini-Lang³, R. Förster³, K. Kudura², M. Huellner², R. Dummer¹, M. Guckenberger³, M. Levesque¹

PET/CT radiomics for prediction of hyperprogression in metastatic melanoma patients treated with immune checkpoint inhibition

Department of Dermatology, University Hospital Zurich¹, Department of Nuclear Medicine, University Hospital Zurich², Department of Radiation Oncology, University Hospital Zurich³

Introduction:

This study evaluated pre-treatment FDG-PET/CT-based radiomic signatures for early prediction of hyperprogression in metastatic melanoma patients treated with immune-checkpoint inhibition (ICI).

Methods:

56 consecutive metastatic melanoma patients treated with immune checkpoint inhibition and available imaging were included in our study and a total of 330 lesions were individually segmented on pre-treatment CT and 2[18F]fluoro-2-deoxy-D-glucose (FDG)-PET imaging. Hyperprogression on a lesion level (HPL) was defined as progression according to RECIST 1.1 and doubling of tumor growth rate, whereas hyperprogression on a patient level (HPD) was defined as patient progression according to RECIST 1.1 and at least one HPL. PET/CT-based radiomic signatures from baseline were used to build a model predicting hyperprogression three months after start of treatment. The model was internally validated with the hold-out method.

Results:

Median follow-up duration was 32 months. Using the RECIST criteria for treatment response, 69 (20.9%) of all lesions were identified as progressing at 3 months. 29 lesions were classified as hyperprogressive, thereby showing a HPL rate of 8.8% in 8/56 (14.3%) patients. HPD patients constituted 57.1% of all progressing patients. HPD was a high-risk factor with HR=8.5 (95%CI 3.5-20.9). Furthermore, patients with HPD showed significantly shorter survival compared to non-HPD patients (7 months vs. "not reached", $p < 0.005$). The HPL model achieved AUC = 0.80 (95%CI 0.63-0.91) in the test set. The model had extra-trees architecture and relied mostly on grey level run length matrix (GLRLM) and neighborhood grey tone difference matrix (NGTDM) CT texture features.

Conclusion:

FDG-PET/CT-based radiomic signatures yield potential for pre-treatment prediction of hyperprogression, thereby serving as rapid non-invasive biomarkers. Such biomarkers could support clinical decision making in allowing to avoid additional toxicity and delayed treatment adaptation in metastatic melanoma patients treated with immune checkpoint inhibition.

N. Winkler¹, A. Shehab¹, F. Tanner¹

Right and left ventricular strain for outcome prediction in severe aortic stenosis

Department of Cardiology, University Heart Center, University Hospital Zurich, Zurich, Switzerland¹

Introduction:

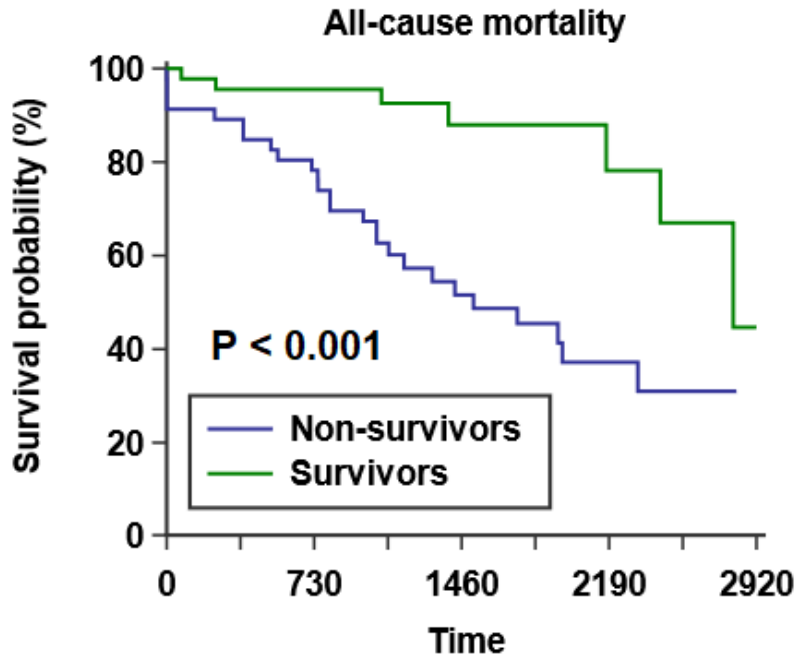
Speckle-tracking echocardiography plays an increasingly important role in the evaluation of aortic stenosis (AS). Global longitudinal strain (GLS) contributes to outcome prediction in various cardiovascular diseases. Left (LV) and right ventricular (RV) GLS have been studied separately in AS patients undergoing trans-catheter aortic valve implantation (TAVI). We aim to study if combining LV and RV GLS improves their association with all-cause mortality post-TAVI.

Methods:

A total of 91 patients undergoing TAVI for severe AS were included. LV GLS and RV GLS were determined by speckle tracking echocardiography within three months pre-TAVI. During post-TAVI follow-up, all-cause mortality was defined as primary endpoint. Combined ventricular strain was defined as the sum of LV+RV GLS.

Results:

RV GLS was significantly impaired among non-survivors (N=57, median -13.93, $p=0.001$) compared to survivors (-17.19, $p=0.001$), while LV GLS was not (-11.53 versus -10.42, $p=0.25$). Survivors exhibited a lower combined ventricular strain compared to non-survivors ($p=0.008$). A cut-off value of pre-TAVI RV GLS above -16.62% differentiated survivors from non-survivors with good sensitivity and specificity (sens. 77%, spec. 65%, AUC 71%, $p<0.001$). This cut-off value was used for Kaplan-Meier survival analysis, which revealed a significant difference between survivors and non-survivors ($p<0.001$) (Fig. 1). LV GLS and left ventricular ejection fraction (LVEF) did not differentiate significantly between survivors and non-survivors. RV GLS was associated with an increased risk of all-cause mortality (HR 1.10, $p=0.017$), also when adjusted to LV GLS (HR 1.10, $p=0.028$), while LV GLS alone was not (HR 1.04, $p=0.39$). Similar to RV GLS, combined ventricular strain revealed an association with all-cause mortality (HR 1.05, $p=0.038$).



Number at risk

Group: Non-survivors

45 41 36 25 18 14 7 5 0

Group: Survivors

45 43 43 30 18 10 8 3 2

Conclusion:

In this study, right ventricular strain as well as combined left and right ventricular strain was associated with all-cause mortality post-TAVI, while LV GLS and LVEF were not.

R. Fritze^{1, 2, 4}, M. Hilty², C. Ganter², R. Schüpbach², J. Bartussek^{2, 3}

Can we trust what we measure? Analysis of blood oxygenation levels obtained by fingertip sensors and arterial blood gas using classical statistics and machine learning techniques.

Department of Anaesthesia and Intensive Care Medicine, Karl Landsteiner University Krems & University Hospital of Krems, Austria¹, Department of Intensive Care Medicine, University of Zurich & University Hospital Zurich², Department of Quantitative Biomedicine, University of Zurich³, Research Group Data Mining, Faculty of Computer Science, University of Vienna, Austria⁴

Introduction:

State-of-the-art ICU respirators are being equipped with sophisticated algorithms that are able to adjust the ventilation support automatically in order to enable the patient to breathe autonomously as fast as possible. These algorithms rely on correct input measured by the sensors attached to the machine. Especially, a correct measurement of the blood oxygen saturation (SpO₂) is of crucial importance. We therefore compared the SpO₂ values measured noninvasively by fingertip sensors and with blood oxygen saturation in blood samples (sO₂) taken from patients admitted to the Department of Intensive Care Medicine at University Hospital of Zurich.

Methods:

We extracted data from historic blood gas samples from patients admitted to the ICUs of the University hospital Zurich between 2018 and 2021 from our electronic patient data management system (PDMS). Patients aged 18 years or less and patients with partially missing blood gas data were excluded. The remaining 197121 blood gas samples from 4490 patients were included in this trial. The data was joined with other information from the PDMS. The information retrieved encompassed the corresponding SpO₂ measurements and other biometric data, lab data, vital parameters, diagnoses, artificial ventilation data (if applicable). We analyzed the difference between arterial sO₂ and simultaneously registered fingertip sensor SpO₂ values with a maximum acceptable difference of +/-3%. The selection of this threshold was driven by clinical considerations. We further used two different approaches to identify the cause of large differences between SpO₂ and sO₂: (1) We used classical statistics (Fisher's exact test for binomial variables and Mood median test for continuous variables). (2) We trained Random Forest Trees to predict if the difference SpO₂-sO₂ will be less than -3%, within the range of -3% and 3% or larger than 3%.

Results:

- (1) SpO₂ from the two tested fingertip sensors showed very similar values. The smaller the saturation was, the larger became the variance of the difference of the two measured saturation values.
- (2) There was a considerable drift of the measured SpO₂ sensor data. The smaller the saturation in the arterial blood sample (sO₂) was, the larger became the mean difference SpO₂-sO₂.
- (3) We found that approximately 1% of all blood gas samples labeled as "arterial" are likely to be obtained from venous blood.
- (4) With classical statistics, we were able to show that several parameters were associated with significantly higher probability to have an absolute SpO₂-sO₂ difference larger than 3%.
- (5) The Random Forest Trees also allowed us to identify several parameters that were associated with a SpO₂-sO₂ difference larger than 3%. Some parameters deemed important by the Random Forest Classifier were also identified by classical statistics.

Conclusion:

A missing reliable labelling of the source of the blood gas samples had turned out to be a hard obstacle for the subsequent data analysis. Blood samples with SpO₂-sO₂ larger than 3% were suspected to be falsely labeled venous or central venous blood samples. Nevertheless, we were able to identify several variables that were associated with a significant larger gap. The results of this trial should be validated by further prospective randomized controlled trials.

Z. Kotkowska^{1,3}, Y. Waeckerle-Men¹, A. Duda¹, I. Kolm¹, A. Høgset⁵, T. Kündig¹, C. Halin³, P. Sander^{2,4}, P. Johansen¹

Photochemically-delivered antigens of *Mycobacterium bovis* BCG induce strong T-cell response in mice

Department of Dermatology, University of Zurich and University Hospital Zurich, Zurich, Switzerland¹, Institute of Medical Microbiology, University of Zurich, Zurich, Switzerland², Institute of Pharmaceutical Sciences, ETH Zurich, Zurich, Switzerland³, National Center for Mycobacteria, University of Zurich, Zurich, Switzerland⁴, PCI Biotech Holding ASA, Oslo, Norway⁵

Introduction:

Vaccination against extracellular pathogens is very efficient and results in production of pathogen-specific antibodies. However, infections caused by intracellular pathogens, such as *Mycobacterium tuberculosis*, are not easily treated by vaccination due to inaccessibility for extracellular antibodies and poor stimulation of cytotoxic T-cell responses by the vaccine. Photochemical internalization (PCI) is a method that has shown potential in delivery of live bacterial vaccine and photosensitizer to antigen-presenting cells (APCs), stimulating MHC class I-restricted response of CD8 T-cells. Aim of this study was to develop PCI as a method for delivery of BCG in order to trigger response of CD8 T cells.

Methods:

Mice received intradermal injections of live *Mycobacterium bovis* BCG and photosensitizer TPCS2a. The photosensitizer was activated by administration of light 18 hours later. BCG-specific CD4 and CD8 T-cell responses were measured in blood, spleen, and lymph nodes by flow cytometry, ELISA, and ELISPOT. Early inflammatory reactions were analysed in the skin by histology and immunohistochemistry.

Results:

PCI improved BCG-specific response of CD4 and CD8 T-cells, characterized by the proliferation and production of IFN- γ , TNF- α , IL-2, and IL-17. Intradermal vaccination allowed for stronger and more long-lasting response of T cells compared to intravenous vaccination. Furthermore, PCI improved antigen presentation by causing upregulation of MHC and costimulatory molecules on APCs. Histology of the skin showed local inflammation at the site of vaccination with strong involvement of neutrophils. Light-activation of the photosensitizer was necessary for the improvement of APC- and T-cell- response.

Conclusion:

These results demonstrate that PCI-based vaccination can be applied to live bacteria for targeted delivery of antigen to the cytosol of APCs. PCI enabled cross-presentation of the antigens for stimulation of antigen-specific CD8 T-cells, facilitating their proliferation and activation, improving the overall immunogenicity of *Mycobacterium bovis* BCG. In the future PCI may be important for the prevention of intracellular pathogens, such as tested here *Mycobacterium bovis*, and also potentially be applied as an immunotherapeutic treatment for such pathogens.

E. Cannizzaro¹, G. Forestieri², A. Brusca², M. Roncador¹, D. Rossi², T. Zenz¹

Liquid biopsy for genomic profiling of circulating tumor DNA (ctDNA) in lymphoma through CAPP-seq.

Department of Medical Oncology and Hematology - USZ¹, Institute of Oncology Research (IOR), Bellinzona²

Introduction:

B-cell Non-Hodgkin lymphomas (B-NHL) are heterogeneous tumors with a vast diversity of the underlying genetics and clinical presentation. While 60% of B-NHL are cured with chemo-immunotherapy, early detection of relapse is crucial for the management of the remaining cases. Interim monitoring and follow up surveillance are currently based on imaging scans (PET-CT) which lack the sensitivity to detect minimal residual disease (MRD) and clonal evolution of the tumor. Genomic profiling, however, requires invasive tissue biopsies which are limited to site accessibility. Through liquid biopsy of peripheral blood, circulating fragmented DNA (cfDNA) derived from cell apoptosis, can be isolated from plasma of lymphoma patients for detection and profiling of its tumor fraction (ctDNA). ctDNA sequencing is a valuable biomarker in lymphoma that can overcome the limitations of current diagnostic methods thereby enhancing the sensitivity of disease detection. Although several methods have been established for ctDNA profiling in lymphomas, the most successfully used is a targeted hybrid capture sequencing approach via CAPPseq (CAncer Personalized Profiling by deep Sequencing).

Methods:

To set up our CAPPseq approach we have selected a group of B-NHL patients currently in care at USZ undergoing different types of treatment (chemotherapy, immunotherapy, radiotherapy, CART19 therapy and allogeneic HSCT) for first diagnosed or relapsed disease. Patients are monitored over a minimum time period of 3 to 12 months. Liquid biopsy is performed by collecting peripheral blood samples at longitudinal time points. Paired samples of peripheral blood for isolation of both PBMCs and plasma are acquired to provide germinal (non-tumoral) control DNA for our analysis. Illumina based libraries of both genomic and circulating DNA are prepared using the KAPA HyperCap workflow (Roche). All samples, individually identified by molecular barcoding, are captured on a probes panel including coding regions recurrently mutated as well as non-coding regions commonly targeted by aberrant somatic hypermutations (aSHM) in B-NHL. Bioinformatic analysis of deep sequenced captured libraries selects tumor-specific variants in the cfDNA by exclusion of common variants found in both gDNA and cfDNA, therefore enabling detection of circulating tumour DNA (ctDNA) in plasma samples. Available diagnostic sequencing of tumor biopsies is used for CAPPseq findings validation.

Results:

In our first CAPPseq experiment we analysed single time point plasma samples from patients affected by different B-NHL entities (DLBCL, Burkitt's Lymphoma, Follicular Lymphoma, MALT Lymphoma, Post-Transplant Lymphoproliferative Disorder). Our results were consistent with available NGS data from tumor targeted sequencing. Specifically, CAPPseq detected mutations in driver genes reported in FoundationOne Heme performed on tumor biopsies of two DLBCL (*CARD11, PIM1, BCL2*), one PTLD (*CARD11, STAT3*) and one Burkitt's Lymphoma (*MYC, TP53, ID3*) samples. Where we could not validate our findings with tumor sequencing data, we observed that the mutational pattern captured by CAPPseq recapitulated the B-NHL subtype signature: variants in chromatin regulation and immune response related genes were found in the Follicular and MALT Lymphoma samples (*CREBBP, KMT2D, TET2, TNFRSF124*). Additionally, variants in genes commonly targeted by aSHM (*BCL6, IGLL5*) were found across all lymphoma subtypes.

Conclusion:

We have assessed the ability of this approach to reliably inform on the mutational pattern of B-NHL subtypes and we have now established a functional system of samples acquisition and processing between the clinics and the laboratory settings for the development of ctDNA sequencing as an experimental diagnostic tool at USZ. With this approach, we aim at demonstrating the ability of this method to improve early prediction of response to therapy and risk stratification of B-NHL patients while implementing a minimal invasive test.

P. Brasier-Lutz¹, M. De Marco Zompit¹, S. Adam³, D. Durocher^{2,3}, M. Stucki¹

Targeting CIP2A as a potential alternative or complementary treatment strategy to PARP Inhibitor therapy

Department of Gynecology, University Hospital and University of Zurich, Schlieren, Switzerland¹, Department of Molecular Genetics, University of Toronto, Toronto, Ontario, Canada², Lunenfeld-Tanenbaum Research Institute, Mount Sinai Hospital, Toronto, Ontario, Canada³

Introduction:

Germline mutations of BRCA1 and BRCA 2 predispose women to early-onset breast- and ovarian cancer, especially to the most aggressive forms the triple negative breast cancer and the high-grade serous ovarian carcinoma. Poly-(ADP-Ribose)-Polymerase (PARP) inhibitors have improved the maintenance therapy of BRCA mutated epithelial ovarian cancers and are increasingly also used in metastatic breast cancer. Unfortunately, the development of PARP inhibitor resistance is common and thus, alternative treatment options or combination strategies are urgently needed to improve patient outcome.

The expression level of cancerous inhibitor of protein phosphatase 2A (CIP2A) was shown to correlate with serous ovarian cancer and breast cancer aggressiveness as well as with reduced survival in serous ovarian cancer. Comparable to PARP, the loss of CIP2A was recently shown to be lethal in BRCA 1 and BRCA 2 deficient cells. CIP2A might therefore be a therapeutic target in BRCA1/2 mutated cancers. Mechanistically, CIP2A forms a complex with the DNA repair factor TOPBP1 and recruits it to DNA lesions during mitosis, where they form filamentous assemblies of unknown function. Interestingly, disruption of the CIP2A-TOPBP1 interaction is lethal in BRCA 1/2 deficient but not in BRCA 1/2 proficient cells. In this study, we investigate CIP2A and TOPBP1 localization in various BRCA deficient and proficient breast- and ovarian cancer cell lines to explore the potential clinical relevance of CIP2A.

Methods:

CIP2A-TOPBP1 mitotic structures were compared between various BRCA 1 deficient and BRCA 1 proficient breast- and ovarian cancer cell lines. CIP2A-TOPBP1 complexes and the interaction of CIP2A and TOPBP1 were investigated by immunofluorescence (IF) staining and by proximity ligation assay (PLA). Cells were visualized on a confocal laser scanning microscope.

Results:

CIP2A and TOPBP1 interact only during mitosis but not in interphase, underlining the mitotic function of CIP2A-TOPBP1. CIP2A-TOPBP1 filaments are found to a higher extend in BRCA 1 deficient as compared to BRCA 1 proficient cancer cells.

Conclusion:

CIP2A and TOPBP1 selectively interact during mitosis and form filamentous assemblies in breast- and ovarian cancer cells. The increased formation of filamentous structures in BRCA 1 mutated cancer cells combined with the inability of BRCA deficient cells to tolerate loss of CIP2A, might indicate an important role of this complex in stabilizing DNA lesions in mitosis that are inherited from the previous S-phase. Further research is needed to evaluate CIP2A's full potential as a novel drug target in breast- and ovarian cancer. Strategies to target CIP2A by small-molecule inhibitors need to be developed.

M. Jacobs², O. Krupkova¹, A. Barbero¹, M. Ehrbar²

Development of a bioinspired engineered ovary to restore fertility in cancer patients

*Department of Biomedicine, University and University Hospital Basel, Basel, Switzerland¹,
Department of Obstetrics, University and University Hospital of Zurich, Zurich, Switzerland²*

Introduction:

A major drawback of most chemo- and radiotherapeutic cancer treatments is their toxicity to the ovaries, meaning they may affect fertility and/or endocrine function of female patients. The state-of-the-art method nowadays is the cryopreservation of the ovaries. However, with transplantation of ovarian tissue after the end of cancer treatment there is always the risk to also transfer malignant cells back into the patient which could lead to disease recurrence. A safe alternative to restore fertility in female cancer patients could be to develop a bioengineered ovary using different biomaterials, which would be used as a safe, temporary environment for the patient's follicles. Like the natural ovary, it would contain the patient's follicles, ensure its survival, and support its growth. In this study, we develop 3D scaffolds consisting of different biomaterials to culture cells for several days. We will evaluate cell viability, morphology, and proliferation in response to the different hydrogel formulations.

Methods:

Scaffolds for cell culture were fabricated using a combination of the synthetic polymer polyethylene glycol (PEG) and the natural biomaterial collagen type I. Collagen type I was incorporated into the hydrogels to enable cell adhesion within the bioinert PEG hydrogels. Another approach to promote cell adhesion is to incorporate RGD into the hydrogels, which was investigated as well. Different concentrations of collagen were used, and the hydrogels were either supplemented with RGD, or not. In a first approach, hydrogels were seeded with human bone marrow-derived mesenchymal stromal cells (BM-MSCs) at two different concentrations. Cell morphology, proliferation and viability were evaluated over seven days using brightfield imaging, and by quantifying the DNA content of hydrogels directly after fabrication and after one week of culture.

Results:

With the help of established protocols to seed PEG hydrogels with BM-MSCs, it was possible to successfully seed cells in PEG-collagen composite hydrogels. Using brightfield imaging it was observed that BM-MSCs start to spread faster in hydrogels containing collagen, compared to those fabricated without. This observation was the same for hydrogels prepared with or without RGD and for both cell seeding densities. Cells proliferated in all hydrogel compositions during seven days of culture, and no difference in proliferation between hydrogels prepared with and without collagen, using the higher cell concentrations, could be detected.

Conclusion:

To conclude, a protocol has been established to seed BM-MSCs into PEG-collagen hydrogels with different concentrations of collagen. Future experiments will be carried out incorporating other ECM components into the hydrogels and using fetal membrane cells as more sensitive cells to test for differences in cell proliferation and viability depending on the hydrogel composition. In addition, matrix deposition of cells will be detected using immunofluorescence staining for fibronectin and subsequent imaging. The morphology of the cells within the hydrogel scaffolds will be evaluated by staining actin and cell nuclei. The stability of hydrogel composition will be evaluated by measuring the collagen content after different number of days in culture.

S. Nussbaum¹, S. Anwer¹, L. Erhart¹, D. Zurcher¹, A. Walther¹, G. Tsiourantani¹, F. Tanner¹

Association of left ventricular myocardial work with all-cause mortality after transcatheter aortic valve implantation

University Heart Center - Zurich¹

Introduction:

Echocardiography is an important modality for peri-interventional assessment of patients undergoing transcatheter aortic valve implantation (TAVI). Left ventricular (LV) global longitudinal strain measures ventricular deformation at end-systole, while myocardial work parameters determine LV deformation throughout the cardiac cycle and correct for afterload. This study aims at evaluating LV deformation by myocardial global work efficiency (GWE) and index (GWI) in early post-TAVI echocardiography and explore its association with all-cause mortality.

Methods:

We analyzed 144 patients with severe aortic stenosis and an echocardiography study within two weeks after TAVI. All echocardiographic analyses were performed using GE EchoPac v2.6. Follow-up data was obtained from medical records until September 2021. All-cause mortality was the primary endpoint.

Results:

During a median follow-up duration of 625 [IQR: 511.0 – 769.8] days, 25 (17.5%) patients died. No significant differences in the baseline characteristics were found between non-survivors and survivors. GWE (Figure 1-A) and GWI (Figure 1-B) were significantly lower among non-survivors than survivors. Both myocardial work parameters differentiated non-survivors from survivors with a cut-off value of -85% for GWE and 990 mmHg% for MWI (Figure 2; both $p < 0.001$).

Conclusion:

In this study, GWE and GWI were lower among non-survivors than survivors and were associated with an increased risk of all-cause mortality after TAVI.

S. Anwer¹, F. Guastafierro¹, L. Erhart¹, S. Costa¹, D. Akdis¹, M. Schuermann¹, S. Hosseini¹, N. Kuzo¹, A. Gasperetti¹, C. Brunckhorst¹, F. Duru¹, A. Saguner¹, F. Tanner¹

Right atrial strain and cardiovascular outcome in arrhythmogenic right ventricular cardiomyopathy

University Heart Center - Zurich¹

Introduction:

Arrhythmogenic right ventricular cardiomyopathy (ARVC) is characterized by progressive fibro-fatty infiltration of the myocardium and associated with adverse cardiovascular (CV) events. This study aims to examine right atrial (RA) deformation in ARVC and understand its association with cardiovascular outcomes.

Methods:

RA strain was determined in 50 patients with definite ARVC diagnosed according to the 2010 taskforce criteria. They were compared to a matched control group of 50 healthy individuals. Association with outcome was analysed over a median follow-up duration of 5 years. A subgroup of 30 ARVC patients with normal RA volume (ARVC-N) was compared to 30 matched controls (Control-N) and outcome analysed separately.

Results:

RA reservoir, conduit, and pump strain were significantly impaired in ARVC versus control. Similar observations were made in the N-ARVC subgroup. Reservoir strain was associated with increased risk of atrial arrhythmia (AA) [HR 0.88, P <0.01] and CV events [HR 0.92, P <0.01]. Conduit strain also predicted AA [HR 1.02, P <0.01], while pump strain predicted CV events [HR 1.09, P=0.02]. Reservoir strain improved the fitness of bivariable models for association of RVEDAI, RVFAC, and global longitudinal strain (RVGLS) with CV events.

Conclusion:

ARVC patients display impaired RA strain even when RA volume is normal. Reservoir and pump strain are associated with an increased risk of CV events. Reservoir strain improved model fitness for association of RVGLS and other echocardiographic parameters with CV events.

T. Ziswiler⁷, M. Luciani^{3, 7}, C. Vanetta¹⁶, A. Springer^{1, 2}, T. Diteepeng³, A. von Eckardstein¹¹, D. Müller¹¹, M. Barbagallo⁹, D. Conen¹⁴, C.E. Aubert^{6, 12}, N. Rodondi^{6, 12}, T. Sinnecker^{8, 13}, G. Moschovitis⁵, A. Auricchio⁴, S. Osswald^{1, 2}, M. Kühne^{1, 2}, L.H. Bonati^{8, 15}, J. Beer^{3, 7, 10}, on behalf of the Swiss-AF Investigators

Association of Trimethylamine N-Oxide with Impaired Cognitive Function in Patients with Atrial Fibrillation: A Swiss-AF Cohort Study

Cardiology Division, University Hospital Basel, Basel, Switzerland¹, Cardiovascular Research Institute Basel, University Hospital Basel, Basel, Switzerland², Center for Molecular Cardiology, University of Zurich, Schlieren, Switzerland³, Department of Cardiology, Istituto Cardiocentro Ticino, Lugano, Switzerland⁴, Department of Cardiology, Regional Hospital of Lugano (EOC), Lugano, Switzerland⁵, Department of General Internal Medicine, Inselspital, Bern University Hospital, University of Bern, Switzerland⁶, Department of Internal Medicine, Cantonal Hospital of Baden, Baden, Switzerland⁷, Department of Neurology and Stroke Center, University Hospital Basel, University of Basel, Switzerland⁸, Department of Neurology, University Hospital of Zurich, Zurich, Switzerland⁹, Faculty of Medicine, University of Zurich, Zurich Switzerland¹⁰, Institute of Clinical Chemistry, University Hospital of Zurich, Zurich, Switzerland¹¹, Institute of Primary Health Care (BIHAM), University of Bern, Switzerland¹², Medical Image Analysis Center (MIAC AG), Basel, Switzerland¹³, Population Health Research Institute, McMaster University, Hamilton, Canada¹⁴, Research Department, Reha Rheinfelden, Rheinfelden, Switzerland¹⁵, Seminar for Statistics, ETH Zurich, Zurich, Switzerland¹⁶

Introduction:

As patients with atrial fibrillation (AF) are predisposed to suffer from major adverse cerebrovascular events (MACE), they are also more likely to suffer MACE linked sequelae such as cognitive impairment. We hypothesized that the gut microbiome derivate trimethylamine N-oxide (TMAO) may amplify this pathomechanism through its hypercoagulative, proinflammatory and proatherogenic effects.

Methods:

Patients of the Swiss-AF cohort with determined TMAO plasma levels, cognitive testing (n = 2'379) and cerebral magnetic resonance imaging (cMRI) (n = 1'722) at baseline were included. Neurocognitive testing and blood samples at baseline were both obtained on the different study sites during the first patient visit. Overall cognitive performance was indicated by the Cognitive Construct (CoCo) score, which is a factor score reflecting different cognitive functions measured by four validated neuropsychological assessments within the Swiss-AF cohort: the Montreal Cognitive Assessment (MoCA), Trail Making Test (parts TMT-A and TMT-B), Semantic Fluency Test (SFT) and Digital Symbol Substitution Test (DSST). All cognitive test scores obtained were correlated with quartiles of patients' TMAO plasma levels (Q1: 0.6-4, Q2: 4-5.8, Q3: 5.8-9.1, Q4: 9.1-164µmol/l). The relevance of co-existence of stroke in cMRI (i.e., clinically overt, silent, or no stroke) and high TMAO plasma levels was evaluated. Linear effect models with multiple TMAO- (overall meat consumption >3 times per week, physical activity, glomerular filtration rate, presence of diabetes mellitus) and cognition-relevant (EQ-5D-5L score, geriatric depression scale, education level) covariate adjustment were employed.

Results:

In our preliminary analysis, AF patients within the highest TMAO quartile consumed more meat, had a more sedentary lifestyle and were more likely to suffer from metabolic syndrome. After multivariable adjustment, patients in the highest quartile of TMAO levels was associated with significant poorer cognitive performance according to the global cognitive score (CoCo: estimate -0.11, 95% CI [-0.17, -0.49], p<0.001) and the well-established MoCA test (-0.53, 95% [-0.93, -0.12], p = 0.011) compared to patients in the lowest quartile. This was observed accordingly in the SFT, DSST, TMT-A and TMT-B. In the subgroup analysis, lower CoCo score and MoCA scores were significantly associated with overt (-0.18, 95% [-0.33,-0.04], p=0.012) or silent (-0.126, 95% [-0.25,0.002], p=0.053) strokes. Furthermore, high TMAO levels and silent strokes were associated with lower MoCA scores (-1.03, 95% CI [-1.91,-0.15], p=0.023).

Conclusion:

This analysis shows an association between elevated TMAO plasma levels and cognitive impairment in AF patients. This association seemed especially in patients with previous cryptogenic strokes. More longitudinal data is necessary to clarify the causality and dynamics between TMAO and cognitive impairment in patients with AF.

E. Breuer¹, D. Birrer¹, S. Da Silva Guerra¹, A. Gupta¹, P.-A. Clavien¹, B. Humar¹

Division of tasks in the regenerating liver: proliferation, hypertrophy & metabolic functions

Department of Surgery and Transplantation, Swiss HPB Center, University Hospital Zurich, Switzerland¹

Introduction:

The liver has the unique ability to regenerate after tissue loss, however after too extensive resection patients are at risk of developing post-hepatectomy liver-failure (PHLF). Until now there is no causal treatment option. The exact causes of PHLF are still unclear, but one possible explanation is that the small remnant fails to regenerate because it is overwhelmed with its vital metabolic tasks. After surgical resection, the regenerating liver orchestrates proliferation and metabolism via the spatial separation of the hepatocytes within the liver lobule, according to the blood flow from the portal to the central vein. Although extensive research has been performed on zonation in the adult liver, the distribution of these metabolic functions and its correlation with cell proliferation following hepatectomy remains poorly understood.

Methods:

Male wild-type mice (C57Bl/6) were subjected to sham surgery, standard (68%) and extended (86%, eventually leading to PHLF) hepatectomies and mice were harvested at different timepoints ranging from 8 hours to 1 week after hepatectomy. Liver regeneration was assessed by the liver weight to body weight (LW/BW) ratio, serum samples were obtained from the inferior vena cava before organ harvesting. The liver tissue was paraffin-embedded and analyzed by immunohistochemistry. Hepatocyte area, number and size of nuclei and the location in relation to the PP-PV-axis were assessed on histology under exclusion of lipid droplets and vessels. For selected targets, a multiplexed immunofluorescence method was used to achieve spatial information using known zonation markers. Hepatocytes were isolated by a two-step collagenase perfusion method and analyzed by flow-cytometry. The results were correlated with genome-wide transcriptome data using RNAseq.

Results:

We provide an overview of proliferating and metabolically active hepatocytes during liver regeneration. While proliferation originates in midlobular hepatocytes, the pericentral area displays a marked hypertrophy between at 32h and 48h. Hypertrophic hepatocytes present with nuclear upregulation of p27^{Kip1} and increased nuclear size or number, both possibly indicating cell-cycle arrest after S-phase and/or endoreplication. In addition, there is a positive correlation between metabolic function, e.g. upregulation of targets involved in beta-oxidation like HADHB, and cell size. Furthermore, using isolated hepatocytes, we note a zonally varying increase in cellular and nuclear ploidy, focused on the midlobular hepatocytes.

Conclusion:

With the goal to obtain insights into the division of tasks within the regenerating liver, we observe spatially and temporally dynamic patterns of hypertrophy, proliferation and cell ploidy. The zoned patterns of several relevant metabolic pathways, mostly concerning beta-oxidation and gluconeogenesis, are diminished after hepatectomy. PHLF samples show a disturbed cell-cycle progression with a marked increase in p27^{Kip1}, a cyclin-dependent kinase inhibitor, and marker for hypertrophy, as well as an increase in cell size. In addition, a relevant number of hepatocytes appear to be stuck at the G2/M checkpoint. This is underlined by transcriptomics data, which identified the ATM Pathway (G2_M checkpoint arrest) to be the most differentially activated pathway.

K. Valkova², L. Matter², T. Schachtner², M. Huellner¹, D. Mueller⁴, V. Luyckx³, T. Mueller²

Development of a protocol for the dynamic measurement of renal functional reserve

Department of Nuclear Medicine, University Hospital of Zurich (USZ)¹, Division of Nephrology, University Hospital of Zurich (USZ)², Division of Nephrology, Children's Hospital of Zurich³, Institute of Clinical Chemistry, University Hospital of Zurich (USZ)⁴

Introduction:

Kidneys have an intrinsic reserve capacity to respond to a higher workload by increasing filtration in their nephrons, called renal functional reserve (RFR). The degree of RFR becomes particularly important when the number of functioning nephrons is reduced. Despite the high clinical relevance of RFR, the necessary dynamic measurements are rarely done in the clinical routine, due to time- and workload as well as lack of standardized protocols.

Methods:

We developed a novel RFR protocol using 99mTc-DTPA (DTPA CI), Creatinine (Crea CI) and Iohexol (Io CI) Clearance before and after an oral protein load performed in an outpatient clinical setting within one day. Baseline glomerular filtration rate was measured (mGFR) after pre-hydration with 10ml water per kg body weight orally to achieve fluid steady state. Thereafter, baseline DTPA- and Io CI was determined after a single DTPA and Iohexol i.v. injection. Next, an oral protein load, consisting of a standardized L-arginine rich beef protein shake, with 1.5 g protein per kg body weight was given to the participants over 15minutes. 30mins later a second DTPA and Iohexol dose was injected. GFR was measured in regular intervals starting 60 minutes after protein meal to determine the peak mGFR. We defined RFR as the difference of post-protein stimulation peak mGFR to baseline mGFR in fasting state. The results were compared to simultaneously measured Crea CI. For Io CI determination new protocol and a mathematical 2-compartment model formula was developed in cooperation with the Institute of Clinical Chemistry.

Results:

In a first step, we measured the RFR in 7 healthy subjects (age range 30 to 61 yrs, 3 male, 4 female). The results showed a high heterogeneity of post-stimulation mGFRs (range 78 to 109 ml/min/1.73 m² mGFR (DTPA CI) at 210 min and 93-217 ml/min/1.73 m² mGFR (Crea CI) at 180 mins after protein load). In particular, we saw in 3 study subjects a drop in GFR compared to the pre-stimulation baseline GFR, indicating a paradox loss of RFR. As the study subjects were healthy, no medical morbidities were known and the results showed a high heterogeneity we modified the study protocol by extending the time of measurements to 330 min post-stimulation and increasing the frequency of measurements to every 30 mins. So far, we measured RFR with the novel extended protocol in 13 healthy volunteers (age range 23 to 70 yrs, 9male, 4 female). The time point modification manifested high, inter-individual time differences in reaching the peak GFR values post-protein load. This extension allowed a robust detection of the peak GFR, which occurred between 150 to 240 mins after the protein meal and ranged between 82 – 122 ml/min/1.73m² measured by DTPA CI and 101 to 279 ml/min/1.73m² measured by Crea CI. RFR was detected in 6 of 13 participants with both DTPA CI und Crea CI method compared to 3 participants, who had no RFR. The remaining 4 participants had contradictory RFR outcomes in DTPA and Crea CI method. The mean RFR (\pm SD) was 13 (\pm 15) ml/min/1.73m² corresponding to 14 (\pm 16) % post-stimulation increase in DTPA CI and 30 (\pm 44) ml/min/1.73m² corresponding to 25 (\pm 34)% increase in Crea CI. Iohexol CI data are pending (exp. March 2022).

Conclusion:

The measurement of RFR with a simplified stimulation by oral protein load is possible. However, to detect the RFR frequent and extended measurements of GFR post-stimulation are essential due to the high inter-individual differences in reaching the hyperfiltration peak. A short post-stimulation measurement period, a too low protein load and too long measurement intervals might not detect the true functional renal response.

O. Evrova¹, E. Müller¹, L. Fabbella¹, M. Hartmann¹, I. Dedes², P. Imesch², J. Metzler², G. Schär², M. Shilaih¹, V. Vongrad¹, B. Leeners¹

Isolation and characterization of primary human cells from eutopic and ectopic endometrium and endometriosis associated adhesions.

Department of Reproductive Endocrinology¹, Department of Gynecology²

Introduction:

Endometriosis is a chronic disease that affects 6-10% of women in reproductive age globally and is associated with severe pelvic pain and infertility. The development of new treatments requires further investigation into the etiology and pathogenesis of the disease on representative tissue. Usually, in vitro endometriotic models include immortalized cell lines, but often research into new treatments requires the establishment of their efficacy on primary cells of various donors, thus requiring isolation and culturing of primary endometriotic cells from lesions. Common to all endometriotic lesions is repetitive tissue injury and repair which leads to highly collagenous and fibrotic samples that are difficult to convert to single-cells for further assays. Current standards in sample processing relies on a complex concoction of enzymes and inhibitors which may have an effect on assays (e.g. phenotyping, pathway analysis). We therefore tested 2 different cell isolation methods for ectopic endometrial tissue: enzymatic tissue digestion and cell migration. We then characterized the stromal fibroblasts by the expression of several cell markers in these cells.

Methods:

Human eutopic and ectopic endometrial tissue were collected from women undergoing surgery due to endometriosis or uterine leiomyoma. Signed informed consent was obtained from each patient (BASEC 2020-02117). Primary human endometriotic cells were isolated from endometriosis tissue (including adhesions) using enzymatic digestion or cell migration method. For the enzymatic digestion, tissues were digested using collagenase I (or IV), DNase I and Rock inhibitor for 40 min - 1 hour at 37°C. The cell suspension was passed through a cell strainer and the flow-through fraction (mainly stromal cells) was plated onto cell culture flasks, while the backflush fraction plated onto Matrigel coated wells. For the cell migration method, the tissue was cut into small pieces (approx. 1.5 mm²), placed into culture plates and allowed to adhere by drying (10-15 min), after which cell culture medium was added. Plates were not moved and the culture medium was not changed for 5 days, after which initial migrating cells out of the tissue pieces were observed. Cells were collected and passaged after 20 days. Cells from eutopic endometrium were isolated only with the enzymatic digestion method, where the stromal cell component was collected in the flow-through fraction, while the epithelial cells in the back-flush fraction. All primary cell populations were characterized by bright field microscopy, immunofluorescence or flow cytometry for different epithelial and stromal endometrial cell markers, including EpCAM, CD90, CD44, CD45, vimentin, ki67, and α -SMA.

Results:

Endometriotic cells were isolated by both methods, but not as efficient when compared to cell isolation from eutopic endometrium. The cell migration method was primarily successful for cell isolation from endometriosis associated adhesions, only few cells migrated out from the non-adhesion endometriosis tissue. The endometriotic cells were determined to be CD90+, CD44+, CD45-, EpCAM- via flow cytometry, and positive for vimentin and ki67 via immunofluorescence, similar to the eutopic stromal fraction, but with increased α -SMA expression.

Conclusion:

Cell migration was successfully established as a cell isolation method for cells from endometriotic adhesions. Additionally, it was determined that endometriotic cells express similar markers as eutopic stromal endometrial cells, but have increased α SMA expression, suggesting they have pro-fibrotic, myofibroblast phenotype.

H. Lakshminarayanan², D. Rutishauser², S. Pfammatter¹, P. Schraml², H. Bolck², H. Moch²

Liquid biopsy-based protein biomarkers as a tool for disease monitoring in clear cell renal cell carcinoma

Functional Genomics Centre Zurich¹, Institute for Pathology and Molecular Pathology²

Introduction:

Clear cell renal cell carcinoma (ccRCC) is the most lethal urological malignancy. Currently, disease prognosis is mainly defined by pathological characteristics such as tumor grade and stage using the gold standard tissue biopsies. However, these often cannot correctly predict patient survival, which variably ranges from less than 6 months to over 5 years, where 30% of the patients are diagnosed with metastasis and further 30% develop metastatic progressive disease. To aid the clinical management of ccRCC patients, liquid biopsy could be a powerful tool since it enables the surveying of patients' biological fluids for molecular tumor biomarkers with minimal invasion. In this study, we seek to investigate patient plasma as a potential source of protein biomarkers for ccRCC monitoring in clinics.

Methods:

36 plasma samples from seven consenting ccRCC patients, with and without metastasis, were used in this study. Plasma samples collected before surgery, after surgery, and at several follow-up time points were subject to tryptic cleavage following an SP3 assisted on-bead digestion protocol and the cleaved peptides were investigated by LC-MS/MS, using Water ACQUITY UPLC System and Thermo Scientific™ Q Exactive™ HF mass analyzer, following a Data Independent (DIA) method. Data processing was carried out using Spectronaut™ and Rv4.1.1. Further data analysis was carried out using publically available bioinformatics tools.

Results:

The acquired data was searched against Uniprot Homo Sapien database limited to 1% FDR. In total, 523 protein groups and 789 proteins were identified. A broad dynamic range of proteins was covered and representation of lower abundant proteins that could be associated with disease pathology was observed. Further, pathway and enrichment analysis revealed proteins involved in several oncogenic mechanisms involved in ccRCC.

Conclusion:

DIA MS-based proteomic analysis of plasma samples from ccRCC patients can help identify proteins potentially associated with disease progression, thereby acting as circulating biomarkers. Further analysis will reveal the correlation of these markers with clinical and pathological features, further defining the role of liquid biopsy in the clinical management of ccRCC.

E. Breuer¹, L. Roth¹, L. Russo¹, V. Kepenekian², G. Passot², P. Gertsch¹, O. Glehen², K. Lehmann¹

Hematogenous, but not locoregional recurrence is controlled by systemic chemotherapy following cytoreductive surgery & HIPEC for colorectal cancer

Department of Visceral and Transplant Surgery, University Hospital Zurich, Switzerland¹, University Hospital of Lyon, Lyon, France²

Introduction:

Cytoreductive surgery (CRS) and hyperthermic intraperitoneal chemotherapy (HIPEC) can improve cancer specific survival in patients with peritoneal metastasis of colorectal origin. Despite the obvious advance in the field of medical oncology, the impact of systemic treatment on the prognosis of peritoneal metastasis remains unclear. We therefore aimed to assess the unknown effect of systemic chemotherapy on cancer specific outcomes after CRS/HIPEC.

Methods:

The present study is a retrospective cohort analysis from two European tertiary centers between 2005-2017. Patients received standard perioperative chemotherapy. HIPEC was indicated after radical cytoreduction (CC-score 0, no visible tumor) and conducted at 42°C for 90 minutes with mitomycin C/doxorubicin ($\geq 15\text{mg/m}^2$) or 43°C for 30 minutes with oxaliplatin (300-400 mg/m^2). Follow-up included clinical exams, tumor markers and CT scan every six months. Statistical analyses were performed with R-Studio (V3.4.1). Kaplan Meier curves and Mantel-Cox Log Rank test were used to test for differences in survival. Uni- and multivariable analyses were performed with Cox regression analysis.

Results:

Overall, 732 patient with peritoneal metastasis from colorectal cancer with a median peritoneal cancer index of 6 (IQR: 3-11) were included. The median age was 59 (IQR: 51-66) years. 95% received pre- or postoperative chemotherapy. Two thirds received FOLFOX/FOLFIRI and 12% a triplet therapy. Half of all patients had additional targeted therapies. The number of preoperative cycles was 6.2 (± 3.2) and postoperative 6.8 (± 3.5). Multimodal treatment including CRS/HIPEC resulted in a median OS of 51 months, and a DFS of 12 months. Addition of targeted (EGFR or VEGF antibody) therapy to FOLFOX or FOLFIRI did not improve survival. Recurrence occurred in 73.5% of patients and was diagnosed in the peritoneum (26.3%), hematogenous (30.0%) or mixed (14.0%). Peritoneal recurrence after CRS/HIPEC resulted in poor survival compared to patients with isolated hematogenous recurrence (36m vs 51m, $p=0.002$). In conclusion, patients with hematogenous recurrence demonstrated improved survival with more aggressive chemotherapy (43m vs 89m, HR 2.05, $p=0.018$), while systemic treatment did not reduce the occurrence of peritoneal recurrence (32m vs 40m, HR:1.32, $p=0.138$).

Conclusion:

This study including patients after radical surgery demonstrates that recurrence to the peritoneum has a dismal prognosis. In addition, peritoneal metastasis is less sensitive to systemic chemotherapy compared to hematogenous disease in liver and/or lung. This finding is novel and highly relevant. Today, treatment recommendations do not differ between the type of metastasis, and many RCTs assessing novel systemic regimens include only few patients with PM. Therefore, treatment recommendations are based on data from patients with hematogenous metastasis, not reflecting the local biology and distinct tumor environment of peritoneal metastasis. Patients with peritoneal metastasis have a dramatically poorer survival compared to hematogenous metastasis. In addition, intensive systemic chemotherapy improves outcomes of hematogenous metastasis, but fails to control peritoneal disease. This data highlights the different biologic behavior and responsiveness to systemic treatment of peritoneal metastasis in contrast to liver or lung metastasis.

I. Moneke¹, M. Haberecker², J. Jang³, E. Faccioli³, I. Opitz³, W. Jungraithmayr^{1, 3}

CD26-inhibition correlates with the absence of Chronic Lung Allograft Dysfunction and decreases fibroblast activity in vitro

Klinik für Thoraxchirurgie, Universitätsklinikum Freiburg¹, Pathology Department, University Hospital Zürich², Thoracic Surgery Department, University Hospital Zürich³

Introduction:

Chronic lung allograft dysfunction (CLAD) limits the survival after lung transplantation (Tx). CLAD is characterized by progressive fibrosis of small airways and lung parenchyma. No effective therapy is available that reverses or prevents CLAD. CD26 is a molecule with enzymatic activity also playing a key role in the progression of fibrotic diseases. Here, we analyzed the inhibitory effect of CD26 on fibroblast activity in vitro and the role of CD26-inhibition on allograft rejection in lung transplant patients.

Methods:

Profibrogenic mRNA and protein levels were analyzed in vitro on the CD26-expressing fibroblast cell line Wi-38 using RT-qPCR and Western blot. CD26 was inhibited by Vildagliptin. Migration and proliferation activity of activated fibroblasts was analyzed by Incucyte® and Celltiter-Glo®. Characteristics of patients undergoing lung Tx between 2004 and 2021 were reviewed. Lung biopsies were analyzed by immunohistochemistry (IHC) for CD26.

Results:

In vitro, the expression profibrogenic genes (α SMA, FAP α , IGFBP7, Collagen 3 and Fibronectin) was significantly reduced in activated lung fibroblasts by Vildagliptin treatment. Also, migration and proliferation activity were attenuated by Vildagliptin. In 221 patients analyzed, CLAD was absent in 34 patients treated with the CD26-inhibitor Sitagliptin vs. an incidence of 18% in patients without Sitagliptin intake ($p=0.02$). Five-year survival in patients on Sitagliptin was significantly improved vs. patients without CD26-inhibitor intake (80% vs. 58%, $p=0.006$). Likewise, the incidence of acute cellular rejection (ACR) was significantly reduced in patients on Sitagliptin (7% vs. 35%, $p=0.01$). IHC of patient lung biopsies showed CD26 to be expressed in perifibrotic areas of CLAD lesions. Additional clinical data from University Hospital Zurich and from University Hospital Padua confirmed the finding that Sitagliptin intake correlated with the absence of acute and chronic allograft rejection.

Conclusion:

CD26-inhibition attenuates key pro-fibrotic mediators and fibroblast activity in vitro. Impressively, patients on CD26-inhibitor did not show any CLAD. Moreover, ACR was significantly reduced. Gliptins which are in routine clinical use for the treatment of type II diabetes thus seem to have great potential to repurpose for a novel clinical application against lung allograft rejection.

Z. Khodabakhshi¹, P. Wallimann¹, H. Gabrys¹, M. Guckenberger¹, N. Andratschke¹, S. Tanadini-Lang¹

The Impact of Image Preprocessing and Harmonization Methods on Magnetic Resonance Image Radiomic Features Stability

University Hospital Zurich¹

Introduction:

Radiomics analysis is actively being explored for diagnostic and prognostic modeling in brain tumors and metastases. Multicenter studies provide generalizable models for clinical applications. However, robustness of radiomics models are challenged by issues of non-biological variations on radiomics features introduced by different scanners/ scanner settings (acquisition and reconstruction). These confounders can severely hamper multicenter studies. This study aims to investigate the effect of image preprocessing (gray level discretization) and harmonization methods (image and feature level harmonization) on the stability of MRI radiomic features.

Methods:

We enrolled 25 patients, who underwent 2 contrast-enhanced T1 MRI studies of brain metastases within 2 months. The volume of interest (VOI) were delineated by an expert radiation oncologist. Prior to feature extraction, isotropic resampling to $0.6 \times 0.6 \times 0.6$ mm³ was performed and then all MR image intensities were discretized using fixed numbers of bins (32,64,128 and 256) and fixed bin size (VOI intensity range divided by 32,64,128 and 256). We implemented three MR normalization methods including z-score, Nyul, and white-stripe methods and ComBat feature harmonization. Altogether, 165 IBSI based radiomics features including first-order, second-order, and higher-order texture features were extracted from each VOI. In addition, we extracted 616 radiomic features by using wavelet (LLL, LHL, LLH and HLL) preprocessing. Intraclass correlation coefficients (ICC) were calculated to determine feature stability before and after normalization/harmonization. Features with $ICC \geq 0.8$ were considered as stable.

Results:

Discretization based on fixed number of bins could effectively improve the stability of radiomic features in comparison with fixed bin size. For all cases increasing the number of bins or decreasing the size of bins resulted in higher number of stable features for both normalized and non-normalized images. The results show that ComBat harmonization can improve the stability of features for all four image sets. Images discretized with 256 bin number and normalized with Nyul method followed by ComBat harmonization achieved the highest number of stable features (32% of all features). The same configuration with non-normalized feature yielded 30% stable features.

Conclusion:

Different non-biological variants arising from scanner type, image acquisition, and reconstruction settings can significantly impact on images which results in high variability in radiomics features. In the current study, we could address some of the challenges by using normalization and harmonization methods and recommend using ComBat harmonization in multicenter studies to improve radiomic feature stability.

I. Jelcic³, A. Müller², M. Hilty³, I. Reichen³, K. Jordan¹, N. Wolfensberger², J. Ruder³, B. Vlad³, S. Ferrer³, K. Ritter², M. Foege³, L. Andreas³, U. Schanz², R. Martin³

Efficacy and safety of autologous hematopoietic stem cell transplantation in multiple sclerosis (aHSCT-in-MS) in Zurich

Department of Consultation-Liaison Psychiatry and Psychosomatic Medicine, University Hospital and University of Zurich, Zurich, Switzerland¹, Department of Medical Oncology and Hematology, University Hospital and University of Zurich, Zurich, Switzerland², Neuroimmunology and Multiple Sclerosis Research Section, Department of Neurology, University Hospital and University of Zurich, Zurich, Switzerland³

Introduction:

Multiple Sclerosis (MS) is among the most common causes of persistent neurological disability among young adults and is caused chronic autoimmune process leading to demyelination and neurodegeneration in the central nervous system. Autologous hematopoietic stem cell transplantation (aHSCT) is used for the treatment of highly inflammatory and aggressive relapsing-remitting or progressive MS patients since 1995. Based on robust data with regard to efficacy and improved safety of aHSCT in MS, the Swiss Federal Office of Public Health (FOPH) granted approval in June 2018 with the requirement that patients participate in a prospective registry at our center ("aHSCT-in-MS"). We here present the first safety and efficacy data for aHSCT-in-MS in Switzerland.

Methods:

MS patients received aHSCT according to the BEAM-ATG protocol, because they had experienced inflammatory breakthrough activity and/or progression of MS despite highly effective disease-modifying therapy (DMT). We prospectively monitored adverse events (AE) and efficacy outcomes such as "no evidence of disease activity (NEDA)", i.e. absence of relapses, new or contrast-enhancing MRI lesions and clinical progression, defined as sustained progressive worsening of expanded disability status scale (EDSS). Safety was analyzed in the first 35 patients, and efficacy in 27 patients, who had >12 months of follow-up.

Results:

At baseline, median age was 40 years (range 25-54), median disease duration 9.1 years (range 1.6-19.7) and median EDSS 4.0 (1.5-6.5). 16 (45.7%) patients had relapsing-remitting MS, 10 (28.6%) had secondary progressive MS and 9 (25.7%) had primary progressive MS. Indication for aHSCT was set because of relapses in 15 (42.9%) patients, radiological activity in 21 (60%) of patients and clinical progression in 18 (51.4%), which occurred despite treatment with ocrelizumab in 11 (31.4%) patients, rituximab in 11 (31.4%) patients, fingolimod in 11 (31.4%) patients and natalizumab in 4 (11.4%) patients. Median post-aHSCT follow-up was 23.8 months (range 6.0-62.3). Most patients developed mucotoxic and infectious AE, most frequently mucositis and/or enteritis (82.9%), then upper airway infections (45.7%) and urinary tract infections (28.6%), usually in the first 20 days after transplantation. Serious AE occurred in 22/35 (62.9%) patients with consecutive good recovery. 2 patients with secondary progressive MS committed assisted suicide 19 and 23 months post-aHSCT because of subjective perception of progression, although NEDA was confirmed in both cases. NEDA status was achieved in 22/27 (81.5%) patients 1 year after aHSCT and in 11/16 (68.8%) 2 years after aHSCT. Until last follow-up, we observed sustained EDSS improvement in 20/35 (57.1%) patients, stable EDSS in 8/35 (22.9%) and EDSS-relevant progression in 7/35 (20%) patients.

Conclusion:

In summary, safety of aHSCT-in-MS is acceptable, and efficacy outcomes are similar to other aHSCT studies and better than approved DMT. However, aHSCT-in-MS requires thorough psychiatric screening and follow-up, vigilant monitoring especially regarding infectious AE and antimicrobial prophylaxis.

M. Hänsel², K. Steigmiller¹, A. Lufft², C. Gebhard³, U. Held¹, S. Wegener²

10-year trends in cardiovascular risk factors in Switzerland: non-traditional risk factors are on the rise in women more than in men

Department of Biostatistics at Epidemiology, Biostatistics and Prevention Institute, University of Zurich, Switzerland¹, Department of Neurology and Clinical Neuroscience Center, University Hospital Zurich and University of Zurich, Switzerland², Department of Nuclear Medicine, University Hospital Zurich and University of Zurich, Switzerland³

Introduction:

Effective control of cardiovascular risk factors is the prerequisite to prevent cardiovascular disease. It is increasingly clear that non-traditional cardiovascular risk factors (nt-cvrf) such as stress significantly add to cardiovascular risk arising from traditional cardiovascular risk factors (t-cvrf). To determine sex-specific changes and 10-year trends in prevalence of t-cvrf and nt-cvrf in Switzerland. Effective control of cardiovascular risk factors is the prerequisite to prevent cardiovascular disease. It is increasingly clear that non-traditional cardiovascular risk factors (nt-cvrf) such as stress significantly add to cardiovascular risk arising from traditional cardiovascular risk factors (t-cvrf). To determine sex-specific changes and 10-year trends in prevalence of t-cvrf and nt-cvrf in Switzerland.

Methods:

We obtained anonymized data from 22'134 participants (51% women) of the governmental Swiss Health Survey, performed every five years (2007, 2012, and 2017). Epidemiological parameters, t-cvrf and nt-cvrf were analyzed in a cross-sectional approach and observational study design. Temporal trends in epidemiological parameters, t-cvrf (e.g. hypertension, diabetes, hypercholesterolemia, alcohol/nicotine consumption, physical activity, smoking), and nt-cvrf (e.g. stress at work, feeling exhausted at work, working despite illness, locus of control, energy and vitality, sleep disorders, major depression) were matched by sex.

Results:

Over the observation period, the number of women having full-time jobs increased considerably (2007: 38%, 2012: 39%, 2017: 44%). This was accompanied by a substantial rise in the prevalence of nt-cvrf including stress at work (2007: not available, 2012: 59%, 2017: 66%), reduced feeling of energy and vitality (2007: not available, 2012: 23%, 2017: 29%), and sleep disorders (2007: 26%, 2012: 24%, 2017: 29%) in women. This trend was less pronounced in men. Amongst t-cvrf, only the prevalence of obesity and hypercholesterolemia increased over time in both sexes, while other t-cvrf remained stable (hypertension [27%], diabetes [5%]) or decreased (smoking [9.4 cigarettes/day]).

Conclusion:

A rise in women's economic participation alongside a pronounced increase in nt-cvrf in the female Swiss population emphasizes the need to improve cardiovascular risk stratification and implement effective preventive measures for neuro- and cardiovascular disease.

P. Baumgartner², M. Zahn², H. Handelsmann², K. Geier², S. Petrus², M. Hänsel², A. Luft^{1, 2}, S. Wegener²

Optic Nerve Sonography to monitor Intracranial pressure after large vessel ischemic stroke – The ONSITE Study

Cereneo Center for Neurology and Rehabilitation, Vitznau, Switzerland¹, Department of Neurology and Clinical Neuroscience Center, University Hospital Zurich and University of Zurich, Switzerland²

Introduction:

Malignant middle cerebral artery (MCA) infarction due to extensive, space-occupying brain edema is one of the most feared complications of a large stroke in the MCA territory. Patients at risk are monitored based on clinical symptoms, which can be complicated by comorbidities such as delirium or systemic infections. Readily available, non-invasive methods to monitor intracranial pressure in stroke patients could facilitate treatment decisions such as hemicraniectomy. We are investigating whether optic nerve sonography (ONS) can detect brain edema early after stroke.

Methods:

We repeatedly measured the optic nerve sheath diameter (ONSD) through transorbital ultrasound in 60 stroke patients up to 120h after stroke. In addition, we performed ONS once in 30 non-stroke control subjects to derive normal ONSD values. Brain edema was assessed with neuroimaging (CT/MRI). Stroke patients were grouped by severity of edema (no edema, sulcal effacement, ventricle compression and midline shift >3mm, or requiring hemicraniectomy).

Results:

Mean ONSD was increased on the ipsi- as well as the contralateral side in all patients after stroke compared to controls (6.6 ± 0.7 mm on ipsilateral side and 6.5 ± 0.7 mm on contralateral side vs. $6.1 \text{ mm} \pm 0.5 \text{ mm}$ in controls, $p < 0.01$ for each side vs. control). Highest ONSD values were found in patients who developed large brain edema with midline shifts >3mm. Strikingly, the largest ONSD values in these patients were found early after stroke, within 12 hours after symptom onset (7.4 ± 0.7 mm in midline shift group vs. 6.4 ± 0.6 mm in stroke patients without edema, $p < 0.01$).

Conclusion:

Ultrasound assessment of the ONSD is able to identify patients at risk of developing malignant MCA infarction within 12h of stroke. After showing the feasibility of the method, we now plan to find an ONSD threshold for prospectively predicting the development of a malignant course of MCA infarcts.

M. Zahn², B. Lafci^{4, 5}, A. Steiner², P. Baumgartner², F. Fierz³, J. Gunzinger³, A. Luft^{1, 2}, A. Boss⁶, D. Razansky^{4, 5}, S. Wegener²

Multispectral optoacoustic imaging of cerebrovascular disease

Cereneo Center for Neurology and Rehabilitation, Vitznau, Switzerland¹, Department of Neurology and Clinical Neuroscience Center, University Hospital Zurich and University of Zurich, Switzerland², Department of Ophthalmology, University Hospital Zurich, University of Zurich, Zurich, Switzerland³, Institute for Biomedical Engineering and Institute of Pharmacology and Toxicology, University of Zurich, Zurich, Switzerland⁴, Institute for Biomedical Engineering, Department of Information Technology and Electrical Engineering, ETH Zurich, Zurich, Switzerland⁵, Institute of Diagnostic and Interventional Radiology, University Hospital Zurich, Zurich, Switzerland⁶

Introduction:

Atherosclerosis and inflammatory changes of the neck and brain arteries could lead to ischemic stroke. Treatment guidelines focus on stenosis degree and vessel morphology based on duplex sonography, which only provides a limited characterization of the plaque and the associated vessel wall. We tested the potential of multispectral optoacoustic tomography (MSOT) to characterize plaques and inflammatory vessel wall changes in patients with cardiovascular disease.

Methods:

To this end, 20 stroke patients and 7 patients with suspicion of giant cell arteritis (GCA) have been included in the study. Affected arteries, either carotid or superficial temporal artery (STA), were examined with MSOT. The method relies on detection of acoustic echoes generated by light absorption in biological tissues, thus enabling high-resolution imaging of disease specific biomarkers with optical contrast. We concentrated on the assessment of lipid content and oxygenation state to find markers for the type (atherosclerotic vs inflammatory) and severity of cerebrovascular disease.

Results:

Preliminary findings in the affected STA of patients with GCA indicate that an inflamed vessel exhibits elevated levels of total haemoglobin (HbT = 0,6275 a.u. versus 0,243 a.u. in the normal wall) along with reduced oxygenation levels ($HbO/[HbO+Hb] = 0.45$ versus 0.72). Analysis of the lipid content in carotid plaques is ongoing and will be presented at the conference.

Conclusion:

Our preliminary results indicate that MSOT may serve as a non-invasive method to characterize cerebrovascular disease with haemoglobin (Hb) being a new marker for severity of inflammation in the effected vessel wall. More patients will be included to validate the results.

Information

Wann

Donnerstag, 19. Mai 2022
8.15 – 17.45 Uhr

Kontakt

Universitätsspital Zürich
Direktion Forschung und Lehre
Rämistrasse 100
8091 Zürich

+41 43 253 01 10
df1@usz.ch
www.usz.ch

Veranstalter

Universitätsspital Zürich
Direktion Forschung und Lehre

Anmeldung und Teilnahme

Es ist keine Anmeldung nötig.
Die Teilnahme ist kostenlos.
Die Veranstaltung findet vor Ort statt.
Die Beiträge von 8.15 – 12.20 Uhr werden
live übertragen und im Anschluss an die
Veranstaltung online aufgeschaltet.

Programm und Abstracts

[Link](#)

Online-Teilnahme

[Link](#)



Folgen Sie dem USZ unter



Titelbild: Wir bedanken uns bei Prof. Dr. Roberto Speck,
für das Bild eines Sphäroids aus MB-MDA-231 Zellen,
das mit Makrophagen infiltriert wird.